NOTE TO USERS

University of Alberta

A Role for RHAMM in Mitosis and Multiple Myeloma

by

Christopher A. Maxwell 

A thesis submitted to the Faculty of Graduate Studies and Research in partial fulfillment

of the requirements for the degree of Doctor of Philosophy

in

Medical Sciences-Oncology

Edmonton, Alberta

Fall, 2004

Your file Votre référence
ISBN: 0-612-95980-5
Our file Notre référence
ISBN: 0-612-95980-5

University of Alberta

Library Release Form

Name of Author: Christopher A. Maxwell

Title of Thesis: A role for RHAMM in mitosis and multiple myeloma

Degree: Doctor of Philosophy

Year this Degree Granted: 2004

#2 7525 116 St

Edmonton, AB T6G 1P4

04 August 2004

ACKNOWLEDGEMENTS

This thesis is the result of the cumulative efforts, both scientific and personal, of many wonderful people. First, I must acknowledge Linda Pilarski, Ph.D. for providing me with the means and opportunity to investigate a project that has resulted in immeasurable professional and personal growth. Linda helms a scientific environment that is both supportive and challenging. I will be forever grateful for the encouragement and respect that she has provided me and for the people that, thanks to her, have surrounded me within her lab. Drs. Andrew Belch, M.D. and Tony Reiman, M.D. provide a passion and purpose to the research ongoing under Linda's supervision; Tony also made seminal observations of the prognostic significance of RHAMM^{-exon4} expression. .Mary Crainie, Ph.D. initiated the RHAMM isoform project and cloned these species. Jonathan Keats has been an amazing friend and colleague. In addition to invaluable personal support, he assisted in the creation of RHAMM deletion mutants and quantitative RT-PCR experiments. Drs. John Shaughnessey Jr., Ph.D. and Bart Barlogie, M.D., along with their contemporaries at the Myeloma Institute for Research and Therapy, collaborated extensively by providing data regarding RHAMM expression and myeloma disease. I have also benefited from the insights and direction of my supervisory committee, Kevin Kane, Ph.D. and Michael Hendzel, Ph.D. Michael's personal support and his knowledge of cytoskeletal networks and, along with Xuejun Sun, Ph.D., confocal microscopy have benefited me greatly. Moreover, Ellen Shibuya, Ph.D. and Gordon Chan, Ph.D. have been essential resources in the world of mitosis; Ellen provided much needed insights into *Xenopus* biology and Gordon, along with performing microinjection experiments and providing various reagents, was an invaluable resource for many challenges. I am also

grateful to V. Assmann, Ph.D., D. Compton, Ph.D., and Oliver Gruss, Ph.D for providing various reagents.

I have been extraordinarily fortunate to benefit from the generousity and support of friends and family through many challenging times. As important as the scientific contributions of the aforementioned were, this thesis is the result of the strength and understanding provided by my loved ones. To them I am forever indebted and devoted.

TABLE OF CONTENTS

LIST OF TABLES

LIST OF FIGURES

LIST OF ABBREVIATIONS

aa	amino acid
Aik	aurora/Ipl1 kinase
AML	acute myeloid leukemia
APC	adenomatous polyposis coli
AurA	Aurora A kinase
AurB	Aurora B kinase
B2M	β 2 microglobin
Bim	bipolar in mitosis
BM	bone marrow
BMMC	bone marrow mononuclear cells
BRCA	breast cancer (gene)
BX_7B	basic $(X)_7$ basic
BZIP	basic leucine zipper
CA	cytogenetic abnormalities
CaM	calmodulin
cdc	cell division control
cdk	cyclin dependent kinase
CDR	complementarity-determining region
CENP	centromere protein

CI	confidence interval
CIN	chromosomal instability
CK2	casein kinase II
CML	chronic myeloid leukemia
CT	cancer/testis
D-	drosophila
DAPI	4',6-Diamidino-2-phenylindole
DNA	deoxyribonucleic acid
ELISA	enzyme-linked immunosorbent assay
EN	engrailed
ER	endoplasmic reticulum
ERK	extracellular regulated kinase
EtOH	ethanol
FACS	fluorescence activated cell sort
FAK	focal adhesion kinase
FCE	fluorescence capillary electrophoresis
FISH	fluorescence in situ hybridization
FGFR	fibroblast growth factor receptor
FRAP	fluorescence recovery after photobleaching

GAP	GTPase activating protein
γTuRC	γ-tubulin ring complexes
GEP	gene expression profiling
GFP	green fluorescence protein
GPI	glycosylphosphatidylinositol
GTP	guanosine-triphosphate
H-	human
HA	hyaluronan
HARC	hyaluronan receptor complex
HABP	hyaluronan binding protein
Hgb	hemoglobin
HR	hazard ratio
IgH	Immunoglobulin Heavy chain
IHABP	intracellular HA binding protein
INCENP	inner centromere protein
IP	immunoprecipitation
K-fibers	kinetochore fibers
KLP	kinesin like protein
LDH	lactate dehydrogenase

M	mitosis
mAb	monoclonal antibody
MAP	microtubule associated protein
MAPK	mitogen activated protein kinase
MEK	mapk-erk kinase
MEN	mitotic exit network
MeOH	methanol
MGUS	Monoclonal gammopathy of undetermined significance
MM	multiple myeloma
MMSET	multiple myeloma SET containing protein
MPF	maturation promoting factor
M-protein	monoclonal protein
MRI	magnetic resonance imaging
MSI	microsatellite instable
Msps	mini-spindles
MSV	murine sarcoma virus
NuMA	nuclear protein of the mitotic apparatus/ nuclear mitotic apparatus protein
pAb	polyclonal antibody
PB	prebleed
PBMC	peripheral blood mononuclear cells

PC	plasma cells
PCLI	plasma cell labeling index
PCM	pericentriolar material
PO_4	phoshate
qRT-PCR	quantitative RT-PCR
RCC1	regulator of chromosome condensation
RHAMM	Receptor for hyaluronan mediated motility
RFU	relative fluorescence units
RNA	ribonucleic acid
RNAi	RNA inhibition
ROI	region of interest
RT-PCR	reverse transcriptase polymerase chain reaction
S.E.	standard error
SEREX	serological identification of antigens by recombinant expression
SET	Su(var), Enhancer of zeste, Trithorax
Spd	spindle defective
SRD	serine rich domain
TACC	transforming acidic coiled coil
TOGp	tumor overexpressed gene product

TPX2	targeting protein for Xklp2
us	unsynchronized
ut	untransfected
X-	xenopus

Introductory Chapter

I.1.1: Receptor for Hyaluronan (HA) Mediated Motility (RHAMM): murine isoforms and functions

The Receptor for Hyaluronan (HA) Mediated Motility (RHAMM) was initially identified by Hardwick *et al.*, 1992 as a constituent of a novel HA receptor complex (HARC). HARC, first identified in 1982 (Turley, 1982), was purified from the supernatants of murine NIH-3T3, and murine sarcoma virus (MSV) transformed 3T3, and resolved into three major HA binding protein (HABP) bands of estimated molecular weight 70K, 66K and 56K (Turley *et al.*, 1987). HA and HARC regulated the *ras*-promoted locomotion of murine cell lines (Turley *et al.*, 1991); *ras* induction elevated HA production and a neutralizing monoclonal antibody (mAb) targeting the 56 K HABP, 3T3.5, blocked HA induced locomotion (Turley *et al.*, 1991). 3T3.5, and the non-blocking 3T3-7, were raised against purified HABPs, affinity purified and shown to be neutralized by addition of HABPs (Turley *et al.*, 1991); these antibodies specifically immunoprecipitate ~56K protein bands, with additional detection of a non-glycosylated 48-49K band and, in response to *ras*-induction, a >200 K HARC band (Turley *et al.*, 1991) (Turley *et al.*, 1993a). Initial cloning identified RHAMM (designated RHAMM2) as a ~50- 60 K protein encoded by 340 amino acids (aa), with an internal repetitive sequence of 5 x 21 aa (Hardwick *et al.*, 1992). mAb and pAb, raised against a 19mer murine RHAMM2 (mRHAMM2) peptide (nt sequence 804-864, aa 268-288) corresponding to human RHAMM (hRHAMM) aa 503-522 (~68% identity), immunofluorescence demonstrated cell surface localization and these antibodies inhibited *ras*-regulated locomotion (Hardwick *et al.*, 1992). RHAMM2 expression was regulated

by *ras*-induction and *in vitro* binding assays demonstrated that a recombinant RHAMM2 species bound to biotinylated-HA (Hardwick *et al.*, 1992). Antibody blocking experiments further demonstrated that RHAMM2 mediated TGF-β-induced locomotion (Samuel *et al.*, 1993) and RHAMM2, but not CD44, facilitated HA dependent motility within *ras*-transformed cells (Turley *et al.*, 1993a).

RHAMM, unlike CD44 and other link module based HABPs (in which HA binding utilizes tandem repeat loops with homology to the cartilage link protein), utilizes a 35-aa COOH-terminal region to interact with HA (Yang *et al.*, 1993). This region can be further subdivided into two HA binding motifs, of 10 and 11 aa respectively (Yang *et al.*, 1993). The *in vitro* interaction between RHAMM and HA is largely ionic, as determined by 68% inhibition with increasing [NaCl] (150mM vs 500mM) (Yang *et al.*, 1993). The HA binding domains of RHAMM, corresponding to hRHAMM aa 636-646 and aa 658-667, are highly basic (~50% Lysine or Arginine) (Yang *et al.*, 1993); these basic residues are essential for the interaction (Yang *et al.*, 1994b) and the motif has become known as Basic (B) $(X)_7$ Basic (B X_7 B) motifs (Yang *et al.*, 1993; Yang *et al.*, 1994b). Indeed, this same domain binds to heparin, in an ionic manner and with a slightly muted affinity compared to HA (Yang *et al.*, 1994a).

In addition to a role in the motility of sperm (Kornovski *et al.*, 1994), astrocyte and microglial cells (Turley *et al.*, 1994), bovine aortic smooth muscle cells (Savani *et al.*, 1995) and human malignant B cells (Turley *et al.*, 1993b), occupation of RHAMM2 initiated signaling events. HA induced locomotion, mediated through RHAMM2 and

induced by RHAMM antibodies (aa 443-463), initiated tyrosine phosporylation events targeting pp125^{FAK} which led to focal adhesion turnover (Hall *et al.*, 1994).

Additional RHAMM NH_2-terminal sequence was isolated and characterized within 3T3 murine fibroblasts (Entwistle *et al.*, 1995) and localized to murine chromosome 11 and human chromosome 5q33.2-qter (Spicer *et al.*, 1995). RHAMM1, the major form (70K) lacking an exon, and RHAMM1v4, a minor variant (73K), are predominantly hydrophilic proteins with predicted helical structure (Entwistle *et al.*, 1995). To remain consistent with the human isoforms (to be described below), the coding region of RHAMM2 contains exons that correspond to hRHAMM^{FL} exon 10-18 with 5 repetitive stretches of a segment of exon 12. RHAMM1v4, the minor variant, contains exons that correspond to hRHAMM^{FL} exon 6-18, with repetition of a segment of exon 12, while RHAMM1, the major variant, lacks hRHAMM^{FL} exon 8. PredictProtein analysis (Rost, 1996) of hRHAMM^{FL} identified two putative phosphorylation sites, a casein kinase II (S^{229}ETE) and a protein kinase C (T^{231}EK), within exon 8 but, to date, no other specific functions have been attributed to this segment of the protein.

In a seminal manuscript, Hall *et al.*, 1995 demonstrated that RHAMM is important in initiating and maintaining *ras* transformation. Overexpression of genomic RHAMM clone (corresponding to hRHAMM exons 8-18) or RHAMM1v4 cDNA induced transformation, as measured by foci formation, high nuclear overlap index, anchorage independent growth in agar and tumor formation in mice, and increased random locomotion (Hall *et al.*, 1995). Overexpression of a mutated RHAMM1v4

variant, in which basic residues within the COOH terminal B $(X)_7$ B domain were augmented resulting in an inability to bind HA (Yang *et al.*, 1994b), had no such effect (Hall *et al.*, 1995). Indeed, ras-transformed fibroblasts were reverted with a dominant negative suppressor mutant of RHAMM (Hall *et al.*, 1995). The suppressor mutant was augmented in the B $(X)_7$ B HA binding domain by replacement of five basic aa with three acidic (glutamic acid) and two neutral (asparagine and tryptophan) aa and insertion of one leucine (Hall *et al.*, 1995). Clones expressing this mutant displayed flattened cell shape, low nuclear overlap ratios and did not develop tumors *in vivo* despite exhibiting higher than control levels of $p21^{ras}$ (Hall *et al.*, 1995). These clones were also unable to transiently phosphorylate FAK and signal to focal adhesions. These results suggest that focal adhesion signaling is involved in the maintenance of *ras* transformation (Hall *et al.*, 1995).

In another important manuscript, soluble RHAMM1 inhibited cell cycle progression of H-*ras*-transformed fibrosarcoma cells (Mohapatra *et al.*, 1996). Interestingly, 48-55% of transformed cells arrested in G_2/M while non-transformed cells completely ablated growth (Mohapatra *et al.*, 1996). Soluble RHAMM1 also suppressed Cdc2 kinase and Cyclin B1 expression with absolute loss by 48 hours post treatment (Mohapatra *et al.*, 1996); the effect was not immediate, however, as no significant reduction of Cdc2 levels was observed at 24 hours post incubation (Mohapatra *et al.*, 1996). Interestingly, suppression of RHAMM, with a dominant suppressor RHAMM mutant, confers resistance to *ras*-transformation (Hall *et al.*, 1995) and results in similar reduction in Cdc2 levels (Mohapatra *et al.*, 1996). Addition of soluble RHAMM1 prior to

intervenous injection of *ras*-transformed fibrosarcoma cells significantly attenuated their tumorigenic and metastatic potential (Mohapatra *et al.*, 1996). Also important to note is that Cyclin A levels, indicative of S phase progression, were unaffected by soluble RHAMM treatment (Mohapatra *et al.*, 1996). These results suggest that HA occupancy of RHAMM, or inhibition of RHAMM occupancy (by addition of soluble RHAMM), significantly alters signaling pathways upstream of *ras* activation with consequent affects on FAK signaling, cell motility and cell cycle progression.

RHAMM appears to act upstream of signaling pathways that target, or regulate, *ras* and *FAK*, and this activity is dependent upon the function of the tyrosine kinase $pp60^{src}$ (*src*) (Hall *et al.*, 1996). A dominant negative *src* ablates the effect of RHAMM1v4 overexpression and v-*src*-transformed cells demonstrate RHAMM-independent motility (Hall *et al.*, 1996). Indeed, a small cellular fraction (2%) of RHAMM co-precipitates src (this RHAMM species occurs as a 125 K protein possibly due to alternate splicing or glycosylation events) while the reciprocal co-precipitation does not occur (Hall *et al.*, 1996). It was suggested that RHAMM, as a glycophophatidyl inostitol (GPI)-linked cell surface receptor, colocalizes with src at caveolae and activation of RHAMM, through HA, triggers a transient increase in src kinase activity resulting in ras activation and focal adhesion signaling with consequent actin reorganization and cell locomotion (Hall *et al.*, 1996). In a subsequent examination, RHAMM1v4 was identified as a cell surface and intracellular protein (Zhang *et al.*, 1998); inhibition of cell surface RHAMM1v4, with an antisense construct, deters the ability of cells to respond to platelet derived growth factor (PDGF) and activate ERK (Zhang *et al.*, 1998). Indeed, RHAMM is required for ERK

activation by mutant active ras (Zhang *et al.*, 1998). Within RHAMM1v4 transfected cells, RHAMM coimmunoprecipitates ERK1 and MEK and vice versa (Zhang *et al.*, 1998). However, this reciprocal interaction does not occur in dominant mutated RHAMM-transfected cells suggesting that the COOH-terminal basic domain facilitates the RHAMM1v4-ERK interaction (Zhang *et al.*, 1998).

Fieber *et al.*, 1999 identified an additional 523 bp of RHAMM cDNA at the NH_2-terminus of the protein; the full length protein was detectable as a ~100 K protein (Hofmann *et al.*, 1998). While the presence of an AP-1 binding site at pos.-191 to -197 suggested that RHAMM may be inducible by *ras*, examination of ras-induced RHAMM expression revealed no stimulation of message or protein levels within a rat embryonic fibroblast line (Fieber *et al.*, 1999). RT-PCR analysis revealed that RHAMM expression was detected in all murine tissues examined with elevated expression in the testis and lymphatic tissues (spleen and thymus) (Fieber *et al.*, 1999). The authors also demonstrated that while RHAMM interacts with HA, but in their hands not heparin or chondroitin sulphate, it localized to the intracellular compartment and was not shed into conditioned media (Hofmann *et al.*, 1998). The authors suggested that the protein be renamed intracellular hyaluronic acid binding protein (IHABP) (Hofmann *et al.*, 1998); for the remainder of this thesis, however, the protein will be referred to as RHAMM.

I.1.2: RHAMM: human isoforms and functions

Human RHAMM was isolated and identified from a human breast cDNA library as a 725 aa, predicted 84 K protein encoded by 18 exons (termed $RHAMM^{FL}$) with conservation of the COOH-terminal HA-binding domains (Wang *et al.*, 1996). hRHAMM contained only one copy of the 21mer sequence (exon 12) repeated 5 times in mRHAMM (Wang *et al.*, 1996). hRHAMM, in combination with β1-integrins, participates in thymocyte motility (Gares *et al.*, 1998) and is negatively regulated by β1-integrin occupancy (Gares and Pilarski, 1999). However, no splice variants of exon 8, similar to mRHAMM1v4, have yet been identified for hRHAMM. Independent laboratories have identified two alternative splice variants of RHAMM. First, Wang *et al.* 1998, identified a variant of RHAMM lacking exon 13 [termed RHAMM(-E9), referred to as $RHAMM^{-exon13}$ for remainder of thesis] within breast carcinoma samples. Both isoforms and total RHAMM, as determined by qualitative RT-PCR and immunostaining, significantly correlated with tumor progression (Wang *et al.*, 1998). Interestingly, RHAMM immunostaining demonstrated significant subcellular heterogeneity with cytoplasmic and nuclear staining (Wang *et al.*, 1998). Next, a RHAMM splice variant of exon4 [termed RHAMM B, referred to as $RHAMM^{-exon4}$ for remainder of thesis] was identified from breast cancer cell lines (Assmann *et al.*, 1998). Both $RHAMM^{FL}$ and $RHAMM^{-exon4}$ were present in all examined breast cancer lines (Assmann *et al.*, 1998). Subcellular fractionation and immunofluorescence revealed that RHAMM was an intracellular protein (Assmann *et al.*, 1998).

In 1999, Crainie *et al.* and Assmann *et al.* published seminal manuscripts describing hRHAMM isoforms. Crainie *et al.*, 1999 identified $RHAMM^{FL}$, $RHAMM^{-exon4}$ and $RHAMM^{-exon13}$ transcripts within the malignant clone of multiple myeloma (MM) B-lineage cells. Of particular note, RHAMM transcripts were rarely detected in the peripheral blood of normal controls while 66^{+}/-9% of MM plasma cells and 56^{+}/-5% of circulating CD19+ MM B cells were RHAMM-positive by FACS analysis (Crainie *et al.*, 1999). $RHAMM^{FL}$ and $RHAMM^{-exon4}$ transcripts were common while $RHAMM^{-exon13}$ transcripts were very rare (Crainie *et al.*, 1999). Identification of products from RT-PCR amplification of $RHAMM^{-exon13}$ transcripts required very sensitive detection methods (Crainie *et al.*, 1999). Assmann *et al.*, 1999 demonstrated that $RHAMM^{FL}$ and $RHAMM^{-exon13}$ are able to associate with microtubules *in vitro* and *in vivo*. $RHAMM^{-exon4}$, however, does not associate with interphase microtubules (Assmann *et al.*, 1999). GFP constructs of $RHAMM^{FL}$ and $RHAMM^{-exon13}$ colocalized with interphase microtubules while $RHAMM^{-exon4}$ targeted the nucleus (Assmann *et al.*, 1999). All RHAMM isoforms localized to the mitotic spindle (Assmann *et al.*, 1999) (see Chapter 1). Secondary structure prediction demonstrated a high probability of coiled-coil structure from aa 69 through aa 681 and deletion constructs localized a Ca^{2+}-dependent calmodulin binding domain to aa 574-602 (Assmann *et al.*, 1999). The calmodulin binding potential of RHAMM was later confirmed in rat brain extracts and subcellular fractionation and immunofluorescence identified RHAMM as a mitochondrial associated protein (Lynn *et al.*, 2001). Moreover, RHAMM colocalized with actin filaments *in vivo* and cosedimented with polymerized actin *in vitro* (Assmann *et al.*, 1999).

I.1.3:RHAMM and cancer

The relationship between RHAMM expression and malignant phenotypes was initially described in malignant B lymphocytes (Turley *et al.*, 1993b). RHAMM expression was found predominantly on malignant late stage B cells and plasma cells (Turley *et al.*, 1993b). Further characterization demonstrated that clonotypic B lineage cells from MM patients were motile in a RHAMM-dependent manner (Masellis-Smith *et al.*, 1996). Conversely, MM plasma cells were sessile; interestingly, while MM B cells expressed cell surface RHAMM, MM plasma cells internalized RHAMM upon HA contact (Masellis-Smith *et al.*, 1996). mAb experiments confirmed that RHAMM antibodies, but not CD44 antibodies, inhibited the motility of MM B cells (Masellis-Smith *et al.*, 1996). These observations were duplicated in chronic lymphocytic leukemia cells stimulated with IL-8 (Till *et al.*, 1999). Within these cells, RHAMM, but not CD44, mediated IL-8-induced motility (Till *et al.*, 1999). The discovery of disease-specific expression of alternate RHAMM isoforms within MM patient samples (Crainie *et al.*, 1999) promoted speculation that RHAMM isoforms may affect oncogenesis through differential subcellular localization and functions.

In addition to its association with hematological malignancies, RHAMM expression is intimately associated with tumors of epithelial origin. As previously mentioned, hRHAMM, and its isoforms, was initially cloned from breast cancer samples and cell lines (Wang *et al.*, 1996; Assmann *et al.*, 1998; Wang *et al.*, 1998). Moreover, RHAMM expression and intracellular localization is strongly associated with invasive behaviour (Assmann *et al.*, 2001), overall survival (Assmann *et al.*, 2001) (Wang *et al.*,

1998) and progression (Wang *et al.*, 1998) of mammary carcinomas. Additionally, RHAMM expression is correlated with progression and survival in stomach (Li *et al.*, 2000), pancreatic (Rein *et al.*, 2003) and colon cancer (Yamada *et al.*, 1999) while genetic deletion of RHAMM attenuates the formation of aggressive fibromatosis as initiated by a targeted mutation of the adenomatous polyposis coli (APC) gene (Tolg *et al.*, 2003).

I.1.4: RHAMM as a tumor associated antigen

Serological identification of antigens by recombinant expression cloning (SEREX) allows the identification of antigenic proteins in cancer (Sahin *et al.*, 1995). SEREX involves screening cancer patients' sera against a tumor-derived cDNA expression library allowing for the identification of gene products that have induced antibody production within the patient examined. SEREX antigens can arise from normal differentiation antigens, cancer-testis antigens, overexpressed antigens, mutated genes, translocation products or potentially tumor specific splice variants (Line *et al.*, 2002). RHAMM has recently been identified by SEREX as a tumor associated antigen in colon (Line *et al.*, 2002), melanoma, renal cell carcinoma, breast cancer, ovarian carcinoma, AML and CML (Greiner *et al.*, 2002). Some (Line *et al.*, 2002) but not others (Greiner *et al.*, 2002) identified postitive serological results from healthy volunteers. Interestingly, whereas mRHAMM appears to be expressed in all tissues examined (Fieber *et al.*, 1999), consistent detection of hRHAMM expression appears to be limited to the testis (Line *et al.*, 2002) (Greiner *et al.*, 2002). Reports of RHAMM expression have identified the testis, spleen, colon, and stomach (Line *et al.*, 2002), the testis, placenta and thymus

(Greiner *et al.*, 2002) and the testis, placenta, lung, and pancreas (Greiner *et al.*, 2004) as RHAMM positive tissues (in decreasing orders, respectively). RHAMM expression is rare in normal peripheral blood (PB) (Greiner *et al.*, 2002) (Line *et al.*, 2002) (Crainie *et al.*, 1999) and purified $CD19^+$ (Crainie *et al.*, 1999) or $CD34^+$ peripheral blood mononuclear cells (PBMC) (Greiner *et al.*, 2004); however, RHAMM expression has been demonstrated, at the protein level, within mobilized (from PBMC) and steady state (from bone marrow) $CD34^+$ hematopoietic stem cells (Pilarski *et al.*, 1999). These results suggest that tumors may be overproducing disease-specific variants, consistent with reports by Crainie *et al.*, 1999, that are eliciting immune responses; alternatively, RHAMM may be an intracellular MAP that, when overexpressed in tumors, is aberrantly, or increasingly, presented within the context of MHC and elicits an immune response.

I.2.1: Microtubules and motility

The association between RHAMM, motility and microtubules appear to be in diametric opposition. However, the regulation of microtubule dynamics and coordination of microtubule/actin interactions are essential to the dynamic establishment of the cellular asymmetries inherent in processes like cell motility, wound healing and division (Rodriguez et al., 2003). Microtubules, dynamic polymers of α and β tubulin, have inherent polarity. The minus ends of microtubules are nucleated at the centrosome while the plus ends extend throughout the cytoplasm. Microtubules transit between two states. They are prone to 'catastrophe', rapid shortening towards their minus ends, and 'rescue', extension of their plus ends. At the leading edge of adherent cells, the balance of microtubule polymerization/ depolymerization regulates signaling molecules that initiate

membrane ruffling and lamellipodial protrusions (Waterman-Storer and Salmon, 1999). At the trailing edge, and within the uropod of thymocytes, microtubule targeting promotes the relaxation of substrate contacts allowing for detachment and motility (Waterman-Storer and Salmon, 1999). Additional to these "regulatory" microtubule/actin interactions, "structural" interactions exist between these cytoskeletal systems (Rodriguez *et* al., 2003). Cytoskeletal crosslinkers, like plectin and BPAG1a/b, may mediate spatiotemporal regulation of focal contacts and guide cell motility (Rodriguez *et* al., 2003); it is interesting to note that while RHAMM is physically much smaller than other plakins (200-600 kD), RHAMM shares significant antigenic similarity to plectin. Indeed a monoclonal antibody targeting plectin cross-reacts with 70 and 85 kD variants of RHAMM (Zhou *et* al., 2002). Identification of MAPs that regulate microtubule dynamics may provide insight into novel regulatory mechanisms controlling the motility of non-adherent cells. The primary microtubule stabilizing MAP in *Xenopus* is XMAP215, a 228 kD protein that antagonizes the activity of microtubule destabilizers, or catastrophe factors, and regulates the Ran-GTP-induced assembly of microtubules (Popov *et al.*, 2001). XMAP215 related proteins include *Minispindles* (Msps) in *Drosophila* and colonic and hepatic tumor over-expressed protein (TOG) in humans. Regulators of microtubule dynamics, like TOG, molecular motors and other MAPs play an essential role in another process that is dependent on dramatic, dynamic and precise reorganization of the microtubule cytoskeleton: mitosis.

I.2.2: Mitosis: Centrosomes and G_2/M transition

The centrosome is a non-membrane enclosed organelle that is postioned centrally in the cell and nucleates and organizes microtubule arrays. Centrosomal defects have been implicated in a number of diseases with particular emphasis on a putative role in the development of chromosomal instability and oncogenesis; abnormal centrosomes, characterized by expression of various centrosomal proteins, elevated centrosome number and volume, have been implicated in the formation of tri-polar or multipolar spindles, chromosomal missegregation, aneuploidy and carcinogenic progression within prostate, pancreatic, and breast carcinoma (Pihan *et al.*, 1998) (Pihan *et al.*, 2001) (Lingle *et al.*, 1998) (Sato *et al.*, 2001). The centrosome is a tripartite structure consisting of core centrioles (tubulin polymers), a matrix of pericentriolar material (PCM) and microtubule nucleating sites (Salisbury, 2003). To identify essential componenets of the PCM, Hamill *et al.*, 2002 screened conditional *C. elegans* mutants for defective spindle function. Several defined centrosomal gene products were identified along with a novel gene, entitled *spindle defecetive-5 (spd-5)*. Spd-5 is a 135 K, multiple coiled coil protein that acts as a PCM scaffold and is responsible for the centrosomal localization of gamma-tubulin, *X*MAP215 and Aurora A kinase family members (see section *I.2.5*) (Hamill *et al.*, 2002). Interestingly, SPD-5 also interacts with dynein (Hamill *et al.*, 2002); in this way, SPD-5 may represent a prototypic PCM component which, like pericentrin, ninein,and CEP135, is extensively coiled coil (Salisbury, 2003) and targeted to microtubule minus ends by the dynein motor complex (Zimmerman and Doxsey, 2000) (Young *et al.*, 2000).

To maintain genetic fidelity, duplication of the interphase centrosome must occur once during each cell cycle; failure to duplicate may result in a monopolar spindle, mitotic failure and a polyploid phenotype while multiple duplication cycles may result in multipolar spindle architecture, chromosomal missegregation and aneuploidy. Thus centrosome duplication is a tightly regulated process that occurs concurrently with DNA replication (Hinchcliffe and Sluder, 2001). Centrin, a ubiquitous Ca^{2+}-binding protein of centrosomes, plays an essential role in centrosome structure and centriole duplication potentially through a Ca^{2+} responsive contractile complex with another centrosomal protein (Salisbury, 2004); this hypothesis may explain the calcium/calmodulin dependence of centrosome duplication in *Xenopus* extracts (Matsumoto and Maller, 2002). Indeed, PCM coiled coil components like pericentrin B/kendrin, myosin V, and AKAP450 contain calmodulin-binding domains (Moisoi *et al.*, 2002); drug disruption of microtubules releases calmodulin-containing 'star-like' structures from the centrosomal matrix (Moisoi *et al.*, 2002).

PCM components may be loaded onto centrosomes, in a microtubule-dependent or independent manner, at all stages of the cell cycle but mitotic entry initiates a dramatic increase in centrosomal volume, termed centrosomal maturation (Blagden and Glover, 2003). Centrosomal maturation, loading factors such as nuclear/mitotic apparatus protein (NuMA), Aurora A kinase, targeting protein for Xklp2 (TPX2), TOG, and transforming acidic coiled coil (TACC) proteins to sites of microtubule nucleation, is vital to subsequent spindle assembly (see below).

I.2.3: Mitosis: spindle assembly

Formation of a bipolar spindle is essential to the proper segregation of replicated chromosomes and the maintenance of genetic stability within the two resulting daughter cells. The process of spindle morphogenesis and chromosome segregation is highly dynamic, coordinated and strictly monitored. The pathways and proteins responsible for monitoring chromosomal segregation (i.e. the spindle assembly checkpoint mediated by Bub family members, Mad family members, ROD, Zw10 and kinetochore proteins) and mitotic exit (best described in *S. cerevisiae* and mediated by Mitotic Exit Network (MEN) proteins) will not be reviewed in this thesis. Instead, this thesis will highlight the pathways and proteins responsible for the initiation, establishment, integrity and disassembly of a bipolar mitotic spindle.

I.2.3a: Mitosis: Xenopus spindle assembly

Within vertebrate somatic cells, the process of spindle morphogenesis has been described by the plus-end search and capture model proposed by Kirschner and Mitchison (1986). Briefly, dynamic microtubules, nucleated from duplicated polar centrosomes, radiate towards and capture chromosomes through kinetochore attachment sites (Mitchison *et al.*, 1986). However, a centrosome independent pathway exists in some organisms and cell types, including in female germ-cell meiosis (Karsenti and Vernos, 2001). In frog egg extracts, chromosome-induced microtubule nucleation and organization is induced in a Ran-GTP dependent manner (Carazo-Salas *et al.*, 1999) (Kalab *et al.*, 1999) (Ohba *et al.*, 1999) (Wilde and Zheng, 1999). The efficiency of Ran, a Ras family GTPase, is regulated through the concerted activities of Ran-GAP, a GTPase

activating protein, and its cofactors RanBP1 and RanBP2 as well as the guanine nucleotide-exchange factor RCC1. The presence of RCC1 promotes the accumulation of Ran-GTP, the active form of Ran (Carazo-Salas *et al.*, 1999); as RCC1 associates with chromosomes while Ran-GAP and RanBP1 remain soluble, a gradient of Ran-GTP is established with a local enrichment proximal to chromosomes (Kalab *et al.*, 2002) (Moore *et al.*, 2002). Enrichment of active Ran promotes microtubule nucleation through downstream effector proteins such as TPX2 and NuMA (Gruss *et al.*, 2001) (Nachury *et al.*, 2001) (Wiese *et al.*, 2001). Ran-GTP, for example, has been shown to deplete importin-B, a nuclear pore protein that binds NuMA and TPX2 and inhibits aster formation (Nachury *et al.*, 2001) (Wiese *et al.*, 2001).

I.2.3b: Mitosis: mammalian spindle assembly

Evidence for chromosome-induced microtubule assembly within mammalian cells was provided recently with the demonstration that spindle morphogenesis could be inhibited by RNA interference targeting TPX2 (Gruss *et al.*, 2002). Moreover, direct observations of monostral-induced monopolar spindles demonstrated that kinetochore microtubule fibers (K-fibers) form without direct connection to centrosomes, are integrated into the spindle and recruited to centrosomes through the actions of NuMA and complexed proteins, possibly dynein (Khodjakov *et al.*, 2003). Thus, evidence exists for the plus-end and minus-end capture of microtubules that emanate from the centrosomes and kinetochores, respectively. Currently, the major effector proteins for chromosome-induced microtubule polymerization and focusing appear to be TPX2, Aurora A and NuMA.

I.2.4: Hklp2 (Kinesin like 7) and TPX2 (repp86, p100, Ki-S2)

Xenopus kinesin-like protein 2 (Xklp2) was first cloned by Boleti *et al.*,1996 and described as a plus end directed molecular motor that localizes to centrosomes and is targeted to spindle poles through its COOH-terminal domain. Xklp2 was identified as an important determinant of centrosome separation and spindle bipolarity (Boleti *et al.*, 1996). Later it was determined that a COOH-terminal basic leucine zipper motif targeted Xklp2 to microtubule minus ends through the cumulative action of the dynein-dynactin motor complex and a 100 K microtubule associated protein (MAP) termed targeting protein for Xklp2 (TPX2)(Wittmann *et al.*, 1998). TPX2 was described as a basic ~82.5 K protein that is nuclear during interphase and phosphorylated at mitosis during which time it localizes to the mitotic spindle pole through the action of dynein/dynactin (Wittmann *et al.*, 2000). In *Xenopus*, augmentation of TPX2 function, through immunodepletion and addition of excess TPX2, disrupted the organization of spindle poles (Wittmann *et al.*, 2000). Gruss *et al.*, 2001 first linked TPX2 function to Ran by demonstrating that *Xenopus* TPX2 is required for Ran-GTP and chromosome-induced microtubule polymerization in M phase extracts. Importin-α, a nuclear transport factor, binds and inhibits TPX2 (Gruss *et al.*, 2001) (Schatz *et al.*, 2003). Importin mediated inhibition is relieved proximal to chromatin by Ran-GTP induced displacement (Gruss *et al.*, 2001) which facilitates TPX2 dependent microtubule nucleation (Schatz *et al.*, 2003). Indeed, Ran-GTP stimulates an interaction between TPX2 and Aurora A (AurA) kinase, leading to the phosphorylation and activation of AurA in a microtubule dependent manner (Tsai *et al.*, 2003). The direct interaction of TPX2 with AurA 'locks' the active confirmation of Aurora A (Bayliss *et al.*, 2003) and is specific for AurA but not AurB,

due to a single amino acid in the kinase catalytic domain of AurA (Bayliss *et al.*, 2004); binding of TPX2 to AurA blocks the ability of p53 to inhibit AurA (Eyers and Maller, 2004). The above mentioned experiments were performed within *Xenopus* extracts. Consistent with the *Xenopus* data, human TPX2 (hTPX2) is required for AurA targeting through a direct interaction (Kufer *et al.*, 2002). The role of TPX2 in spindle assembly, however, has been questioned in the mammalian context. RNA inhibition of TPX2, by some groups (Gruss *et al.*, 2002) but not others (Garrett *et al.*, 2002), impairs the formation of a bipolar spindle in HeLa cells. Gruss *et al.*, 2002 demonstrated that RNA interference led to an accumulation of prometaphase-like phenotypes with separated centrosomes nucleating microtubule asters but with few, or no, chromosome contacting spindle microtubules. Garrett *et al.*, 2002, however, demonstrated that hTPX2 RNA interference arrested cells in a metaphase phenotype albeit with multipolar spindle architecture. Thus, it is currently unclear if TPX2 mediated activation of AurA leads to chromosome induced microtubule polymerization in mammalian cells or, alternatively, TPX2 functions as an important determinant of spindle integrity and not spindle assembly.

Interestingly, TPX2 was independently identified by Heidebrecht *et al.*, 1997 as p100, and later repp86. P100 was identified as a nuclear phosphoprotein that was exclusively expressed from G_1/S until the end of cytokinesis. A mAb that recognized p100/rebb86, termed Ki-S2, was shown to be a more specific marker of cell proliferation than Ki-67 (Heidebrecht *et al.*, 1997) and its expression is strongly related to telomerase activity in endometrioid carcinomas (Bonatz *et al.*, 2001). Moreover, a repp86 labeling

index (RI) was a significant determinant of adverse prognosis and the most important predictor of event-free and disease specific survival in neuroblastoma (Krams *et al.*, 2003).

I.2.5: Aurora kinases

Aurora kinases (AurA, AurB, Aur C) are key regulators of cell cycle progression; AurA regulates centrosome and spindle function (Andrews *et al.*, 2003), AurB functions in chromosome segregation and cytokinesis (Andrews *et al.*, 2003) while little is known of AurC, a testis specific kinase (Tseng *et al.*, 1998). As this thesis focuses on AurA rather than AurB and AurC, only a brief description of AurB mitotic function will be reviewed (for a complete review see (Andrews *et al.*, 2003)).

Originally identified in *S. cerevisiae* as Increased in ploidy1 (Ipl1) (Chan and Botstein, 1993), related to Aurora in *Drosophila* (Glover *et al.*, 1995) (Shevelyov, 1993), and cloned as Aurora/Ipl1 related kinase (Aik) in *H. sapiens* (Kimura *et al.*, 1997), the nomenclature surrounding aurora kinases is complex. AurA [aka HsAIRK1, BTAK (breast tumor activated kinase), Aik, ARK1, aurora2, gene name *STK6, STK15*], is a serine/threonine kinase that localizes to the centrosome and spindle pole, is encoded at human chromosome 20q13.2-q13.3 and is related to *Xenopus* Eg2 (aka *Xenopus* AurA) (reviewed in (Giet and Prigent, 1999)).

In elucidating AurA function, several species have been studied with various inhibition of function assays. Within all species examined AurA is a ~40-45 K

phosphoprotein that localizes to centrosomes and mitotic spindle poles and is optimally expressed at G_2/M transition. In *Xenopus*, inhibition of Eg2 function, through a catalytically inactive variant incapable of autophosphorylation, led to the formation of monopolar spindles (Roghi *et al.*, 1998). In *Drosophila*, mutation, resulting in a kinase inhibited variant, or RNA interference (RNAi) disruption of AurA function leads to a metaphase arrest with aberrant spindles, characterized by short spindles and reduced astral microtubules (Giet *et al.*, 2002). Moreover, disruption of AurA function impairs the spindle pole targeting of *Drosophila* transforming acidic coiled coil (D-TACC) protein (Giet *et al.*, 2002). In *C. elegans* embryos, RNAi disruption of AurA function leads to aneuploidy resulting from severely disorganized bipolar spindle poles (Schumacher *et al.*, 1998); others, however, have used RNAi to show that AurA is essential for the integrity and maturation [i.e. loading of pericentriolar material (PCM) components like γ-tubulin] of mitotic centrosomes (Hannak *et al.*, 2001). In human HeLa cells, incomplete inhibition of AurA function, with antibody microinjection and RNA interference, demonstrates that AurA is critical for multiple mitotic progression events including G_2/M transition, centrosomes separation, spindle assembly, chromosome alignment and cytokinesis (Marumoto *et al.*, 2003). Complete inhibition of AurA, and its partner protein AJUBA, led to an accumulation of transfected cells in late G_2, with accumulation of cyclin B1 but decreased cyclin B1 kinase activity (Hirota *et al.*, 2003). Incomplete inhibition of AurA, with RNAi, resulted in an increase in the proportion of cells within early mitotic stages (i.e. prophase, prometaphase, metaphase) and an increase in apoptotic cells at early timepoints (48 hour post transfection) (Marumoto *et al.*, 2003). The majority of mitotic cells demonstrated bipolar spindle architecture with misaligned chromosomes,

characterized by $MAD2^{+}$ kinetochores (indicative of non-microtubule attached kinetochores), suggestive of loose connections between microtubules and kinetochores in early mitosis (Marumoto *et al.*, 2003). AurA inhibition by RNAi also resulted in elevated levels of multinucleated cells suggestive of a defect in cytokinesis; these RNAi induced results were confirmed by antibody microinjection experiments which also resulted in the formation of multipolar spindle architecture (Marumoto *et al.*, 2003). Given the importance of AurA to mitotic events, it is not surprising that its biology has been fervently studied in the last three years leading to the discovery of a wide variety of partner proteins and downstream phosphorylation targets. In addition to activation complexes with TPX2 (Bayliss *et al.*, 2004) (Bayliss *et al.*, 2003) (Eyers and Maller, 2004) (Kufer *et al.*, 2002) (Kufer *et al.*, 2003) (Eyers *et al.*, 2003) (Tsai *et al.*, 2003) and Ajuba (Hirota *et al.*, 2003), Aurora A complexes with TACC1-TOG (Conte *et al.*, 2003), phosphorylates Histone H3 (Crosio *et al.*, 2002), CENP-A (Kunitoku *et al.*, 2003), BRCA1 (Ouchi *et al.*, 2004), and p53 leading to mdm2-mediated degradation of p53 (Katayama *et al.*, 2004), and regulates telomerase activity through c-myc (Yang *et al.*, 2004).

STK6 (aka *stk15)* maps to chromosome 20q13.2, a region commonly amplified in epithelial tumors (Reichardt *et al.*, 2003) (Collins *et al.*, 2001) (Hidaka *et al.*, 2000), and AurA is amplified in a variety of tumors including breast, colorectal, ovarian, bladder and hepatocellular carcinoma(Tanaka *et al.*, 1999) (Bischoff *et al.*, 1998) (Gritsko *et al.*, 2003) (Sen *et al.*, 2002) (Jeng *et al.*, 2004). Indeed, overexpression of AurA overrides the

mitotic spindle assembly checkpoint leading to chromosomal missegregation, despite Mad2+ kinetochores, failure of cytokinesis and multinucleation (Anand *et al.*, 2003); additionally, AurA overexpression endows cells with taxol resistance due to the defective spindle assembly checkpoint (Anand *et al.*, 2003). Taken together, these data support targeting Aurora kinases in cancer therapies; initial trials are underway with a potent Aurora inhibitor VX-680 (Harrington *et al.*, 2004).

AurB is a chromosome passenger protein that localizes to kinetochores from prophase to metaphase transitioning to the spindle midzone at anaphase and the cleavage furrow at cytokinesis (Adams *et al.*, 2001). AurB targeting is mediated by INCENP, a chromosome passenger protein, and Survivin, an inhibitor of apoptosis (IAP)-like protein (Adams *et al.*, 2001) (Romano *et al.*, 2003). In mammalian cells, AurB regulates chromosome alignment and segregation; loss of AurB function, by microinjection of antibodies, abrogates the mitotic spindle checkpoint leading to premature exit from metaphase (Kallio *et al.*, 2002). Many studies have demonstrated that the AurB complex, AurB-INCENP-Survivin, is essential to cytokinesis; the complex performs a combination of functions including the regulation of microtubule dynamics through regulation of Rho, bundling of anti-parallel microtubules, phosphorylation and regulation of intermediate filaments and myosin II (Andrews *et al.*, 2003). Additionally, AurB regulates chromotin structure through the phosphorylation of chromosome proteins, including the nucleosome component Histone H3, a centromere component CENP-A, DNA topoisomerase II and a chromatin remodeling protein (Andrews *et al.*, 2003). In turn, the regulation of AurB is complex, spatial and dynamic; *in vitro* experiments demonstrate that AurB kinase activity

is augmented by complexing with Survivin and INCENP while fluorescence recovery after photobleaching experiments highlight two mitotic populations of AurB with differential *in vivo* dynamics dependent on mitotic stage (Andrews *et al.*, 2003).

I.2.6: NuMA

Nuclear/Mitotic apparatus protein (NuMA) is a ~238 K phospoprotein that accumulates at mitotic spindle poles and demonstrates nuclear localization during interphase. Like RHAMM, NuMA is an α-helical, highly coiled coil protein with a short proline rich NH_2 terminal head and a longer COOH terminal tail; the COOH tail contains the nuclear localization signal and microtubule binding domains (Zeng, 2000) (Haren and Merdes, 2002). Also similar to RHAMM, the NuMA protein has been identified as multiple sized molecular masses ranging from 180-240 K by immunoblot analysis (Zeng, 2000). Indeed, Tang *et al.*, 1994 identified two shorter variants of NuMA (termed NuMA-s and NuMa-m) that demonstrated centrosomal localization during interphase presumably through their different COOH-terminal domains. Given the fact that immuolocalization of endogenous NuMA fails to demarcate interphase centrosomes, it is likely that these variants are very low abundance (Tang *et al.*, 1994). Although NuMA is a prominent component of interphase nucleii of most cell types examined, with the exception of non-proliferative, highly differentiated cell types (Taimen *et al.*, 2000), little is known about its role in the nucleus. Therefore, this section will focus on the more established functions of NuMA during mitosis. NuMA is concentrated at spindle poles, where it is considered to be the principal crosslinker of microtubule minus ends, through an association with the dynein/dynactin complex (Gaglio *et al.*, 1996) (Merdes *et al.*,

1996). NuMA may function in microtubule sliding and spindle stability by complexing with the dynein/dynactin motor complex and anchoring one microtubule relative to another sliding microtubule (Gaglio *et al.*, 1996) (Merdes *et al.*, 1996). As NuMA immunoblocking does not totally abolish mitotic centrosomal nucleation (Gordon *et al.*, 2001), it is likely that other MAPs contribute to the crosslinking of microtubule minus ends at spindle poles. NuMA is required for mitotic spindle stability until the onset of anaphase (Zeng, 2000) at which point it is dephosphorylated and released from spindle poles, and the dynein/dynactin motor complex, in a Cyclin B degradation-dependent manner (Gehmlich *et al.*, 2004).

In a seminal paper for mammalian spindle assembly, Khodjakov *et al.*, 2003 demonstrated that NuMA-dynein/dynactin complexes functioned in spindle morphogenesis. Live cell imaging, following induction of monopolar spindles with a reversible small molecule inhibitor of a mitotic kinesin, demonstrated that bundles of microtubules extended from the centromeric region of chromosomes (termed kinetochore (K)-fibers) to the cellular periphery (Khodjakov *et al.*, 2003). These bundles did not contact centrosomes and would extend to a distance of ~10μm in length prior to looping back and recontacting monopolar spindle microtubules (Khodjakov *et al.*, 2003). Washout experiments demonstrated that monopolar spindles could form bipolar spindles through the capture and incorporation of K-fibers by separated centrosomal microtubules (Khodjakov *et al.*, 2003). Microinjection of NuMA antibodies inhibited microtubule fiber looping within monopolar spindles and NuMA was consistently associated with the minus-ends (non-chromosome associated) of K-fibers (Khodjakov *et al.*, 2003). These

data highlight that, in a mammalian context, kinetochore microtubules form without contacting centrosomes and these K-fibers are incorporated into the spindle by minus-end capture and recruitment in a NuMA dependent manner (Khodjakov *et al.*, 2003).

I.2.7: Mitosis: Spindle integrity

The biology of mitotic spindle structure and dynamics, and the supportive role of molecular motors, has been elegantly reviewed within several prominent journals (Heald, 2000) (Wittmann *et al.*, 2001) (Sharp *et al.*, 2000) (Karsenti and Vernos, 2001). Mammalian spindle assembly appears to incorporate centrosome-dependent and centrosomes-independent microtubule nucleation and polymerization (Gruss *et al.*, 2002) (Khodjakov *et al.*, 2003) (Khodjakov *et al.*, 2000); once these fibers form, they must contact chromosomes, or align into bipolar arrays, position and equivalently segregated chromosomes into two daughter cells. The basis of this alignment and segregation are dynamic molecular machinery driven by directional microtubule motors. Balance of these motor forces is essential for spindle function and integrity. In simplistic terms, molecular motors function in three broad categories. First, bipolar molecular motors are responsible for establishing anti-parallel microtubule arrays that initially form the bipolar spindle. These motors, like Bipolar in mitosis-C (Bim-C), and motor complexes (like NuMA-dynein/dynactin) can cross-link and slide anti-parallel microtubules (for clarity, anti-parallel refers to the polarity of microtubules within the spindle; the microtubules are organized in a parallel manner but, as they orginate, or terminate, at opposing poles, with differing polarities) to establish spindle bipolarity. Secondly, chromosome associated motors, like chromokinesin and CENP-E, assemble at kinetochores, monitor

microtubule attachment and generate molecular forces responsible for alignment and segregation of chromosomes. Finally, the forces generated at the chromosomes, along with those generated throughout the spindle/developing spindle body, must be stabilized at the spindle pole. The principle cross-linker of microtubule minus ends appears to be NuMA-dynein complexes although other molecular complexes including TPX2, TACC, TOG and the kinesin HSET have been implicated in the maintenance of spindle integrity.

I.2.8: Mitosis: Cytokinesis

The end of the mitotic cycle involves the division of the two daughter cells. This division initiates shortly after anaphase with an invagination in the plasma membrane termed the cleavage furrow. The cleavage furrow is an actomyosin-based structure and its formation is dependent upon large scale microtubule organizational changes including the assembly of a central spindle. While the mechanisms and proteins involved in central spindle assembly, and mitotic spindle disassembly, have not been elucidated to the extent of spindle assembly, insights into these processes have been drawn from experiments in *C. elegans* and *Drosophila.* The role of the MAP PRC1 and the centralspindlin complex, a Rho-GAP and kinesin-like protein complex, in establishing the central spindle and initiating the cleavage furrow has recently been reviewed (Glotzer, 2003). As mentioned earlier, AurB is required for many of the elucidated processes of cytokinesis, including centralspindlin localization and furrow initiation (Glotzer, 2003). Interestingly, recent experimentation has revealed an important role for spindle assembly proteins, like TPX2 and TOG, in spindle disassembly. TPX2 and TOG appear to be major targets of the AAA-ATPase Cdc48/p97 that is essential for spindle disassembly (Cao *et al.*, 2003).

AAA-ATPase proteins utilize their ATPase activity to catalyze a variety of cellular processes including proteolysis, disassembly of protein complexes and unfolding of proteins (Cao *et al.*, 2003; Cheeseman and Desai, 2004). Cdc48, a conserved AAA-ATPase, forms a trimeric complex that is important for targeting proteins to the 26S proteosome (Bays and Hampton, 2002). Cao *et al.*, 2003 demonstrated that inhibition of this trimeric complex disregulated spindle disassembly despite normal degradation of Cyclin B and loss of histone H1 kinase activity (indicating that cells had exited metaphase). One component of the trimeric complex, Ufd1, associates with the *Xenopus* TPX2 and TOG proteins during anaphase/late mitosis (Cao *et al.*, 2003); inhibition of this association, through a dominant negative form of Cdc48, led to an increase association of TPX2 and TOG with microtubules during late mitosis (Cao *et al.*, 2003). Thus, disassociation of TPX2 and TOG from spindle microtubules appears to be an important step in spindle disassembly.

I.3.1: Myeloma: clinical features

Multiple myeloma (MM) is a malignancy of B-lineage cells symptomatically characterized by accumulation of plasma cells in the bone marrow (BM) and an elevated monoclonal (M) serum protein. MM accounts for ~15% of hematological malignancies and ~1% of all cancers in Canada (National Cancer Institute of Canada, 2003). In 2003, it is estimated that 1800 (1000 male, 800 female) newly diagnosed MM cases occurred in Canada (125, 65 male, 60 female, in Alberta) with 1250 deaths resulting from the disease (National Cancer Institute of Canada, 2003). The median survival for MM patients is roughly 2.5-3 years and MM accounts for ~2% of all cancer deaths in Canada (National

Cancer Institute of Canada, 2003). Minimal criteria for the diagnosis of multiple myeloma include the presence of at least 10% abnormal plasma cells (PC) in the BM with one of the following conditions: monoclonal serum protein (usually greater than 3 g/dL), monoclonal protein in the urine, or osteolytic lesions (Kyle, 1992). MM is symptomatically characterized by skeletal symptoms (i.e. bone pain, lytic lesions), due to the release of osteoclast stimulating factors by MM plasma cells and the accumulation of osteoclast cells in the BM, hypercalcemia in the blood, due to calcium release from the bones, anemia, due in part to heavy BM infiltration, infections, due to reduced white blood cell counts resulting from the disease or as an iatrogenic (treatment induced) consequence, and renal problems, due to elevated protein levels in the blood. Monoclonal gammopathy of undetermined significance (MGUS) is considered a premalignant, or possibly a malignancy under control, plasma cell tumor that may be a precursor disease for MM. Approximately 20-25% of MGUS patients progress to overt MM at a rate of 0.5-3% a year (reviewed in (Fonseca *et al.*, 2004)).

MGUS is defined as an expansion of plasma cells that does not exceed 10% of the BM and a M-protein that is <3 g/dL (Fonseca *et al.*, 2004). MGUS and MM share two very important characteristics: translocations involving the isotype switch region of the immunoglobulin heavy-chain (IgH) locus (human chromosome 14q32) and aneuploidy/chromosomal instability.

I.3.2: Myeloma: Immunoglobulin Heavy Chain (IgH) translocations

IgH switch translocations are speculated to be seminal events in myelomagenesis (Bergsagel and Kuehl, 2001) (Kuehl and Bergsagel, 2002). The incidence of IgH translocations increases with stage of disease (Bergsagel and Kuehl, 2001) (Fonseca *et al.*, 2004). Fluorescence in situ hybridization (FISH) detects IgH translocations in 50% of MGUS, 55-70% of intramedullary (localized) MM tumors, 70-80% in extramedullary MM and ~90% of MM cell lines (Bergsagel and Kuehl, 2001) (Fonseca *et al.*, 2004). It is currently postulated that switch translocations may initiate CIN within the malignant cell leading to an evolution of genetic events that permits the selection and propogation of more aggressive malignant clones (Bergsagel and Kuehl, 2001) (Kuehl and Bergsagel, 2002). This hypothesis has led to the classification of IgH translocations as primary versus secondary translocations. Primary translocations are thought to precede CIN whilst secondary translocations are thought to be progression events. Unlike other B-cell tumors that are characterized by a single Ig translocations, MM patients demonstrate diversity in primary IgH translocations partner chromosomes. Four loci have been identified as recurrent targets: 11q13 (~15% of patients), 4p16.3 (~15%), 16q23 (~6%), and 6p21 (~4%). While somewhat controversial, the target oncogenes of these translocations have been defined as *cyclin D1* (11q13), *FGFR3* and *MMSET* (4p16.3), *c-maf* (16q23) and *cyclin D3* (6p21). Complicating matters is the fact that 20-30% of MM tumors have IgH translocations that involve other partner chromosomes, including but not excluded to 20q11 (*maf-B*) and 6p25 (*IRF-4/MUM-1*), that occur at a prevalence of 1% or less (Fonseca *et al.*, 2004). Additionally, translocations at 8q24, targeting *c-myc*, are thought to be late secondary events in myeloma progression. Given the heterogeneity of

the disease's genetics and the diverse mechanisms of the putative oncogene's actions, a common mechanism for myeloma initiation has yet to be defined although it is speculated that overexpression of *cyclin D* genes may link all MM tumors (Fonseca *et al.*, 2004); it is interesting, however, that the highest expressers of *cyclin D1*, $t(11;14)^{+}$ MM patients, have good prognosis (Fonseca *et al.*, 2003) and cyclin D1 overexpression does not initiate CIN (Spruck *et al.*, 1999).

Based upon global gene expression profiling, MM patients have been classified into four distinct groups, MM 1-4 each with elucidated prognostic characteristics (Zhan *et al.*, 2002). MM4 most closely cosegregate with MM cell lines, overexpressing various proliferation gene products, while MM1 was most similar to MGUS and normal plasma cell expression patterns (Zhan *et al.*, 2002).

I.3.3: Myeloma: chromosomal instability (CIN)

In addition to the varying IgH partner chromosomes, the frequent occurrence of CIN, characterized by aneuploidy, within MM malignant cells is unique among hematological malignancies. Numerical chromosomal abnormalities are observed in approximately 80-90% of MM patients (Ho *et al.*, 2002); the most common being monosomies 13, 14, 16 and 22 and trisomies 3,5,7,9,11,15,19 and 21 (Fonseca *et al.*, 2004). Interestingly, the percentage of PCs, within a patient at any given time, harboring trisomies is variable and reflective of ongoing genetic instability (Fonseca *et al.*, 2004). The degree of aneuploidy is variable, no specific abnormalitiy is constant and the prevalence of aneuploidy is independent of stage (Fonseca *et al.*, 2004). MM patients do,

however, segregate into two broad categories: hyperdiploid and non-hyperdiploid myeloma. Hyperdiploid MM is defined as between 46/47 chromosomes while non-hyperdiploid MM can be further subdivided into hypodiploid (<45 chromosomes), pseudodiploid (44/45 to 46/47 chromosomes) and near-tetraploid (75 or more chromosomes) (Fonseca *et al.*, 2004). Non-hyperdiploid myelomas are often accompanied by recurrent IgH translocations, with emphasis on partner chromosomes 4p16.3, 11q13, and 16q23 (Fonseca *et al.*, 2004); the prevalence of IgH translocations in non-hyperdiploid MM (>85%) is statistically greater than within hyperdiploid MM (<30%) (Fonseca *et al.*, 2004). Moreover, the prevalence of monosomy 13, a recurrent abnormality identified in ~50% of MM patients, is more common in nonhyperdiploid MM patients (Fonseca *et al.*, 2004). While certain IgH translocations (t(4;14)) and monosomy 13 are associated with an adverse prognosis, DNA ploidy, as determined by DNA content analysis, has failed to be prognostically informative (Fonseca *et al.*, 2004) possibly due to its inability to discriminate between hypodiploid and pseudodiploid MM.

This thesis will investigate the biological function of RHAMM in order to elucidate it's association, if any, with myelomagenesis. The work presented herein is an extension of the observation of Crainie *et al.*, 1999 in which RHAMM, and two splice variants, were defined as qualitatively overexpressed within the myeloma malignant clone. **The overall hypothesis of this investigation is that expression of RHAMM, and its isoforms, is functionally related to the generation of aggressive myeloma clones.**

References:

Adams, R.R., Maiato, H., Earnshaw, W.C., and Carmena, M. (2001). Essential roles of Drosophila inner centromere protein (INCENP) and aurora B in histone H3 phosphorylation, metaphase chromosome alignment, kinetochore disjunction, and chromosome segregation. J Cell Biol *153*, 865-880.

Anand, S., Penrhyn-Lowe, S., and Venkitaraman, A.R. (2003). AURORA-A amplification overrides the mitotic spindle assembly checkpoint, inducing resistance to Taxol. Cancer Cell *3*, 51-62.

Andrews, P.D., Knatko, E., Moore, W.J., and Swedlow, J.R. (2003). Mitotic mechanics: the auroras come into view. Curr Opin Cell Biol *15*, 672-683.

Assmann, V., Gillett, C.E., Poulsom, R., Ryder, K., Hart, I.R., and Hanby, A.M. (2001). The pattern of expression of the microtubule-binding protein RHAMM/IHABP in mammary carcinoma suggests a role in the invasive behaviour of tumour cells. J Pathol *195*, 191-196.

Assmann, V., Jenkinson, D., Marshall, J.F., and Hart, I.R. (1999). The intracellular hyaluronan receptor RHAMM/IHABP interacts with microtubules and actin filaments. J Cell Sci *112 (Pt 22)*, 3943-3954.

Assmann, V., Marshall, J.F., Fieber, C., Hofmann, M., and Hart, I.R. (1998). The human hyaluronan receptor RHAMM is expressed as an intracellular protein in breast cancer cells. J Cell Sci *111 (Pt 12)*, 1685-1694.

Bayliss, R., Sardon, T., Ebert, J., Lindner, D., Vernos, I., and Conti, E. (2004). Determinants for Aurora-A Activation and Aurora-B Discrimination by TPX2. Cell Cycle *3*, 404-407.

Bayliss, R., Sardon, T., Vernos, I., and Conti, E. (2003). Structural basis of Aurora-A activation by TPX2 at the mitotic spindle. Mol Cell *12*, 851-862.

Bays, N.W., and Hampton, R.Y. (2002). Cdc48-Ufd1-Npl4: stuck in the middle with Ub. Curr Biol *12*, R366-371.

Bergsagel, P.L., and Kuehl, W.M. (2001). Chromosome translocations in multiple myeloma. Oncogene *20*, 5611-5622.

Bischoff, J.R., Anderson, L., Zhu, Y., Mossie, K., Ng, L., Souza, B., Schryver, B., Flanagan, P., Clairvoyant, F., Ginther, C., Chan, C.S., Novotny, M., Slamon, D.J., and Plowman, G.D. (1998). A homologue of Drosophila aurora kinase is oncogenic and amplified in human colorectal cancers. Embo J *17*, 3052-3065.

Blagden, S.P., and Glover, D.M. (2003). Polar expeditions--provisioning the centrosome for mitosis. Nat Cell Biol *5*, 505-511.

Boleti, H., Karsenti, E., and Vernos, I. (1996). Xklp2, a novel Xenopus centrosomal kinesin-like protein required for centrosome separation during mitosis. Cell *84*, 49-59.

Bonatz, G., Frahm, S.O., Klapper, W., Helfenstein, A., Heidorn, K., Jonat, W., Krupp, G., Parwaresch, R., and Rudolph, P. (2001). High telomerase activity is associated with cell cycle deregulation and rapid progression in endometrioid adenocarcinoma of the uterus. Hum Pathol *32*, 605-614.

National Cancer Institute of Canada. (2003). Canadian Cancer Statistics 2003, Toronto, Canada.

Cao, K., Nakajima, R., Meyer, H.H., and Zheng, Y. (2003). The AAA-ATPase Cdc48/p97 regulates spindle disassembly at the end of mitosis. Cell *115*, 355-367.

Carazo-Salas, R.E., Guarguaglini, G., Gruss, O.J., Segref, A., Karsenti, E., and Mattaj, I.W. (1999). Generation of GTP-bound Ran by RCC1 is required for chromatin-induced mitotic spindle formation. Nature *400*, 178-181.

Chan, C.S., and Botstein, D. (1993). Isolation and characterization of chromosome-gain and increase-in-ploidy mutants in yeast. Genetics *135*, 677-691.

Cheeseman, I.M., and Desai, A. (2004). Cell division: AAAtacking the mitotic spindle. Curr Biol *14*, R70-72.

Collins, C., Volik, S., Kowbel, D., Ginzinger, D., Ylstra, B., Cloutier, T., Hawkins, T., Predki, P., Martin, C., Wernick, M., Kuo, W.L., Alberts, A., and Gray, J.W. (2001). Comprehensive genome sequence analysis of a breast cancer amplicon. Genome Res *11*, 1034-1042.

Conte, N., Delaval, B., Ginestier, C., Ferrand, A., Isnardon, D., Larroque, C., Prigent, C., Seraphin, B., Jacquemier, J., and Birnbaum, D. (2003). TACC1-chTOG-Aurora A protein complex in breast cancer. Oncogene *22*, 8102-8116.

Crainie, M., Belch, A.R., Mant, M.J., and Pilarski, L.M. (1999). Overexpression of the receptor for hyaluronan-mediated motility (RHAMM) characterizes the malignant clone in multiple myeloma: identification of three distinct RHAMM variants. Blood *93*, 1684-1696.

Crosio, C., Fimia, G.M., Loury, R., Kimura, M., Okano, Y., Zhou, H., Sen, S., Allis, C.D., and Sassone-Corsi, P. (2002). Mitotic phosphorylation of histone H3: spatio-temporal regulation by mammalian Aurora kinases. Mol Cell Biol *22*, 874-885.

Entwistle, J., Zhang, S., Yang, B., Wong, C., Li, Q., Hall, C.L., A, J., Mowat, M., Greenberg, A.H., and Turley, E.A. (1995). Characterization of the murine gene encoding the hyaluronan receptor RHAMM. Gene *163*, 233-238.

Eyers, P.A., Erikson, E., Chen, L.G., and Maller, J.L. (2003). A novel mechanism for activation of the protein kinase Aurora A. Curr Biol *13*, 691-697.

Eyers, P.A., and Maller, J.L. (2004). Regulation of Xenopus Aurora A activation by TPX2. J Biol Chem *279*, 9008-9015.

Fieber, C., Plug, R., Sleeman, J., Dall, P., Ponta, H., and Hofmann, M. (1999). Characterisation of the murine gene encoding the intracellular hyaluronan receptor IHABP (RHAMM). Gene *226*, 41-50.

Fonseca, R., Barlogie, B., Bataille, R., Bastard, C., Bergsagel, P.L., Chesi, M., Davies, F.E., Drach, J., Greipp, P.R., Kirsch, I.R., Kuehl, W.M., Hernandez, J.M., Minvielle, S., Pilarski, L.M., Shaughnessy, J.D., Jr., Stewart, A.K., and Avet-Loiseau, H. (2004). Genetics and cytogenetics of multiple myeloma: a workshop report. Cancer Res *64*, 1546-1558.

Fonseca, R., Blood, E., Rue, M., Harrington, D., Oken, M.M., Kyle, R.A., Dewald, G.W., Van Ness, B., Van Wier, S.A., Henderson, K.J., Bailey, R.J., and Greipp, P.R. (2003). Clinical and biologic implications of recurrent genomic aberrations in myeloma. Blood *101*, 4569-4575.

Gaglio, T., Saredi, A., Bingham, J.B., Hasbani, M.J., Gill, S.R., Schroer, T.A., and Compton, D.A. (1996). Opposing motor activities are required for the organization of the mammalian mitotic spindle pole. J Cell Biol *135*, 399-414.

Gares, S.L., Giannakopoulos, N., MacNeil, D., Faull, R.J., and Pilarski, L.M. (1998). During human thymic development, beta 1 integrins regulate adhesion, motility, and the outcome of RHAMM/hyaluronan engagement. J Leukoc Biol *64*, 781-790.

Gares, S.L., and Pilarski, L.M. (1999). Beta1-integrins control spontaneous adhesion and motility of human progenitor thymocytes and regulate differentiation-dependent expression of the receptor for hyaluronan-mediated motility. Scand J Immunol *50*, 626-634.

Garrett, S., Auer, K., Compton, D.A., and Kapoor, T.M. (2002). hTPX2 is required for normal spindle morphology and centrosome integrity during vertebrate cell division. Curr Biol *12*, 2055-2059.

Gehmlich, K., Haren, L., and Merdes, A. (2004). Cyclin B degradation leads to NuMA release from dynein/dynactin and from spindle poles. EMBO Rep *5*, 97-103.

Giet, R., McLean, D., Descamps, S., Lee, M.J., Raff, J.W., Prigent, C., and Glover, D.M. (2002). Drosophila Aurora A kinase is required to localize D-TACC to centrosomes and to regulate astral microtubules. J Cell Biol *156*, 437-451.

Giet, R., and Prigent, C. (1999). Aurora/Ipl1p-related kinases, a new oncogenic family of mitotic serine-threonine kinases. J Cell Sci *112 (Pt 21)*, 3591-3601.

Glotzer, M. (2003). Cytokinesis: progress on all fronts. Curr Opin Cell Biol *15*, 684-690.

Glover, D.M., Leibowitz, M.H., McLean, D.A., and Parry, H. (1995). Mutations in aurora prevent centrosome separation leading to the formation of monopolar spindles. Cell *81*, 95-105.

Gordon, M.B., Howard, L., and Compton, D.A. (2001). Chromosome movement in mitosis requires microtubule anchorage at spindle poles. J Cell Biol *152*, 425-434.

Greiner, J., Ringhoffer, M., Taniguchi, M., Li, L., Schmitt, A., Shiku, H., Dohner, H., and Schmitt, M. (2004). mRNA expression of leukemia-associated antigens in patients with acute myeloid leukemia for the development of specific immunotherapies. Int J Cancer *108*, 704-711.

Greiner, J., Ringhoffer, M., Taniguchi, M., Schmitt, A., Kirchner, D., Krahn, G., Heilmann, V., Gschwend, J., Bergmann, L., Dohner, H., and Schmitt, M. (2002). Receptor for hyaluronan acid-mediated motility (RHAMM) is a new immunogenic leukemia-associated antigen in acute and chronic myeloid leukemia. Exp Hematol *30*, 1029-1035.

Gritsko, T.M., Coppola, D., Paciga, J.E., Yang, L., Sun, M., Shelley, S.A., Fiorica, J.V., Nicosia, S.V., and Cheng, J.Q. (2003). Activation and overexpression of centrosome kinase BTAK/Aurora-A in human ovarian cancer. Clin Cancer Res *9*, 1420-1426.

Gruss, O.J., Carazo-Salas, R.E., Schatz, C.A., Guarguaglini, G., Kast, J., Wilm, M., Le Bot, N., Vernos, I., Karsenti, E., and Mattaj, I.W. (2001). Ran induces spindle assembly by reversing the inhibitory effect of importin alpha on TPX2 activity. Cell *104*, 83-93.

Gruss, O.J., Wittmann, M., Yokoyama, H., Pepperkok, R., Kufer, T., Sillje, H., Karsenti, E., Mattaj, I.W., and Vernos, I. (2002). Chromosome-induced microtubule assembly mediated by TPX2 is required for spindle formation in HeLa cells. Nat Cell Biol *4*, 871-879.

Hall, C.L., Lange, L.A., Prober, D.A., Zhang, S., and Turley, E.A. (1996). pp60(c-src) is required for cell locomotion regulated by the hyaluronanreceptor RHAMM. Oncogene *13*, 2213-2224.

Hall, C.L., Wang, C., Lange, L.A., and Turley, E.A. (1994). Hyaluronan and the hyaluronan receptor RHAMM promote focal adhesion turnover and transient tyrosine kinase activity. J Cell Biol *126*, 575-588.

Hall, C.L., Yang, B., Yang, X., Zhang, S., Turley, M., Samuel, S., Lange, L.A., Wang, C., Curpen, G.D., Savani, R.C., and et al. (1995). Overexpression of the hyaluronan receptor RHAMM is transforming and is also required for H-ras transformation. Cell *82*, 19-26.

Hamill, D.R., Severson, A.F., Carter, J.C., and Bowerman, B. (2002). Centrosome maturation and mitotic spindle assembly in C. elegans require SPD-5, a protein with multiple coiled-coil domains. Dev Cell *3*, 673-684.

Hannak, E., Kirkham, M., Hyman, A.A., and Oegema, K. (2001). Aurora-A kinase is required for centrosome maturation in Caenorhabditis elegans. J Cell Biol *155*, 1109-1116.

Hardwick, C., Hoare, K., Owens, R., Hohn, H.P., Hook, M., Moore, D., Cripps, V., Austen, L., Nance, D.M., and Turley, E.A. (1992). Molecular cloning of a novel hyaluronan receptor that mediates tumor cell motility. J Cell Biol *117*, 1343-1350.

Haren, L., and Merdes, A. (2002). Direct binding of NuMA to tubulin is mediated by a novel sequence motif in the tail domain that bundles and stabilizes microtubules. J Cell Sci *115*, 1815-1824.

Harrington, E.A., Bebbington, D., Moore, J., Rasmussen, R.K., Ajose-Adeogun, A.O., Nakayama, T., Graham, J.A., Demur, C., Hercend, T., Diu-Hercend, A., Su, M., Golec, J.M., and Miller, K.M. (2004). VX-680, a potent and selective small-molecule inhibitor of the Aurora kinases, suppresses tumor growth in vivo. Nat Med *10*, 262-267.

Heald, R. (2000). Motor function in the mitotic spindle. Cell *102*, 399-402.

Heidebrecht, H.J., Buck, F., Steinmann, J., Sprenger, R., Wacker, H.H., and Parwaresch, R. (1997). p100: a novel proliferation-associated nuclear protein specifically restricted to cell cycle phases S, G2, and M. Blood *90*, 226-233.

Hidaka, S., Yasutake, T., Takeshita, H., Kondo, M., Tsuji, T., Nanashima, A., Sawai, T., Yamaguchi, H., Nakagoe, T., Ayabe, H., and Tagawa, Y. (2000). Differences in 20q13.2 copy number between colorectal cancers with and without liver metastasis. Clin Cancer Res *6*, 2712-2717.

Hinchcliffe, E.H., and Sluder, G. (2001). "It takes two to tango": understanding how centrosome duplication is regulated throughout the cell cycle. Genes Dev *15*, 1167-1181.

Hirota, T., Kunitoku, N., Sasayama, T., Marumoto, T., Zhang, D., Nitta, M., Hatakeyama, K., and Saya, H. (2003). Aurora-A and an interacting activator, the LIM protein Ajuba, are required for mitotic commitment in human cells. Cell *114*, 585-598.

Ho, P.J., Campbell, L.J., Gibson, J., Brown, R., and Joshua, D. (2002). The biology and cytogenetics of multiple myeloma. Rev Clin Exp Hematol *6*, 276-300.

Hofmann, M., Fieber, C., Assmann, V., Gottlicher, M., Sleeman, J., Plug, R., Howells, N., von Stein, O., Ponta, H., and Herrlich, P. (1998). Identification of IHABP, a 95 kDa intracellular hyaluronate binding protein. J Cell Sci *111 (Pt 12)*, 1673-1684.

Jeng, Y.M., Peng, S.Y., Lin, C.Y., and Hsu, H.C. (2004). Overexpression and amplification of Aurora-A in hepatocellular carcinoma. Clin Cancer Res *10*, 2065-2071.

Kalab, P., Pu, R.T., and Dasso, M. (1999). The ran GTPase regulates mitotic spindle assembly. Curr Biol *9*, 481-484.

Kalab, P., Weis, K., and Heald, R. (2002). Visualization of a Ran-GTP gradient in interphase and mitotic Xenopus egg extracts. Science *295*, 2452-2456.

Kallio, M.J., McCleland, M.L., Stukenberg, P.T., and Gorbsky, G.J. (2002). Inhibition of aurora B kinase blocks chromosome segregation, overrides the spindle checkpoint, and perturbs microtubule dynamics in mitosis. Curr Biol *12*, 900-905.

Karsenti, E., and Vernos, I. (2001). The mitotic spindle: a self-made machine. Science *294*, 543-547.

Katayama, H., Sasai, K., Kawai, H., Yuan, Z.M., Bondaruk, J., Suzuki, F., Fujii, S., Arlinghaus, R.B., Czerniak, B.A., and Sen, S. (2004). Phosphorylation by aurora kinase A induces Mdm2-mediated destabilization and inhibition of p53. Nat Genet *36*, 55-62.

Khodjakov, A., Cole, R.W., Oakley, B.R., and Rieder, C.L. (2000). Centrosome-independent mitotic spindle formation in vertebrates. Curr Biol *10*, 59-67.

Khodjakov, A., Copenagle, L., Gordon, M.B., Compton, D.A., and Kapoor, T.M. (2003). Minus-end capture of preformed kinetochore fibers contributes to spindle morphogenesis. J Cell Biol *160*, 671-683.

Kimura, M., Kotani, S., Hattori, T., Sumi, N., Yoshioka, T., Todokoro, K., and Okano, Y. (1997). Cell cycle-dependent expression and spindle pole localization of a novel human protein kinase, Aik, related to Aurora of Drosophila and yeast Ipl1. J Biol Chem *272*, 13766-13771.

Kornovski, B.S., McCoshen, J., Kredentser, J., and Turley, E. (1994). The regulation of sperm motility by a novel hyaluronan receptor. Fertil Steril *61*, 935-940.

Krams, M., Heidebrecht, H.J., Hero, B., Berthold, F., Harms, D., Parwaresch, R., and Rudolph, P. (2003). Repp86 expression and outcome in patients with neuroblastoma. J Clin Oncol *21*, 1810-1818.

Kuehl, W.M., and Bergsagel, P.L. (2002). Multiple myeloma: evolving genetic events and host interactions. Nat Rev Cancer *2*, 175-187.

Kufer, T.A., Nigg, E.A., and Sillje, H.H. (2003). Regulation of Aurora-A kinase on the mitotic spindle. Chromosoma *112*, 159-163.

Kufer, T.A., Sillje, H.H., Korner, R., Gruss, O.J., Meraldi, P., and Nigg, E.A. (2002). Human TPX2 is required for targeting Aurora-A kinase to the spindle. J Cell Biol *158*, 617-623.

Kunitoku, N., Sasayama, T., Marumoto, T., Zhang, D., Honda, S., Kobayashi, O., Hatakeyama, K., Ushio, Y., Saya, H., and Hirota, T. (2003). CENP-A phosphorylation by Aurora-A in prophase is required for enrichment of Aurora-B at inner centromeres and for kinetochore function. Dev Cell *5*, 853-864.

Kyle, R.A. (1992). Diagnostic criteria of multiple myeloma. Hematol Oncol Clin North Am *6*, 347-358.

Li, H., Guo, L., Li, J.W., Liu, N., Qi, R., and Liu, J. (2000). Expression of hyaluronan receptors CD44 and RHAMM in stomach cancers: relevance with tumor progression. Int J Oncol *17*, 927-932.

Line, A., Slucka, Z., Stengrevics, A., Silina, K., Li, G., and Rees, R.C. (2002). Characterisation of tumour-associated antigens in colon cancer. Cancer Immunol Immunother *51*, 574-582.

Lingle, W.L., Lutz, W.H., Ingle, J.N., Maihle, N.J., and Salisbury, J.L. (1998). Centrosome hypertrophy in human breast tumors: implications for genomic stability and cell polarity. Proc Natl Acad Sci U S A *95*, 2950-2955.

Lynn, B.D., Turley, E.A., and Nagy, J.I. (2001). Subcellular distribution, calmodulin interaction, and mitochondrial association of the hyaluronan-binding protein RHAMM in rat brain. J Neurosci Res *65*, 6-16.

Marumoto, T., Honda, S., Hara, T., Nitta, M., Hirota, T., Kohmura, E., and Saya, H. (2003). Aurora-A kinase maintains the fidelity of early and late mitotic events in HeLa cells. J Biol Chem *278*, 51786-51795.

Masellis-Smith, A., Belch, A.R., Mant, M.J., Turley, E.A., and Pilarski, L.M. (1996). Hyaluronan-dependent motility of B cells and leukemic plasma cells in blood, but not of bone marrow plasma cells, in multiple myeloma: alternate use of receptor for hyaluronan-mediated motility (RHAMM) and CD44. Blood *87*, 1891-1899.

Matsumoto, Y., and Maller, J.L. (2002). Calcium, calmodulin, and CaMKII requirement for initiation of centrosome duplication in Xenopus egg extracts. Science *295*, 499-502.

Merdes, A., Ramyar, K., Vechio, J.D., and Cleveland, D.W. (1996). A complex of NuMA and cytoplasmic dynein is essential for mitotic spindle assembly. Cell *87*, 447-458.

Mitchison, T., Evans, L., Schulze, E., and Kirschner, M. (1986). Sites of microtubule assembly and disassembly in the mitotic spindle. Cell *45*, 515-527.

Mohapatra, S., Yang, X., Wright, J.A., Turley, E.A., and Greenberg, A.H. (1996). Soluble hyaluronan receptor RHAMM induces mitotic arrest by suppressing Cdc2 and cyclin B1 expression. J Exp Med *183*, 1663-1668.

Moisoi, N., Erent, M., Whyte, S., Martin, S., and Bayley, P.M. (2002). Calmodulin-containing substructures of the centrosomal matrix released by microtubule perturbation. J Cell Sci *115*, 2367-2379.

Moore, W., Zhang, C., and Clarke, P.R. (2002). Targeting of RCC1 to chromosomes is required for proper mitotic spindle assembly in human cells. Curr Biol *12*, 1442-1447.

Nachury, M.V., Maresca, T.J., Salmon, W.C., Waterman-Storer, C.M., Heald, R., and Weis, K. (2001). Importin beta is a mitotic target of the small GTPase Ran in spindle assembly. Cell *104*, 95-106.

Ohba, T., Nakamura, M., Nishitani, H., and Nishimoto, T. (1999). Self-organization of microtubule asters induced in Xenopus egg extracts by GTP-bound Ran. Science *284*, 1356-1358.

Ouchi, M., Fujiuchi, N., Sasai, K., Katayama, H., Minamishima, Y.A., Ongusaha, P.P., Deng, C., Sen, S., Lee, S.W., and Ouchi, T. (2004). BRCA1 Phosphorylation by Aurora-A in the Regulation of G2 to M Transition. J Biol Chem *279*, 19643-19648.

Pihan, G.A., Purohit, A., Wallace, J., Knecht, H., Woda, B., Quesenberry, P., and Doxsey, S.J. (1998). Centrosome defects and genetic instability in malignant tumors. Cancer Res *58*, 3974-3985.

Pihan, G.A., Purohit, A., Wallace, J., Malhotra, R., Liotta, L., and Doxsey, S.J. (2001). Centrosome defects can account for cellular and genetic changes that characterize prostate cancer progression. Cancer Res *61*, 2212-2219.

Pilarski, L.M., Pruski, E., Wizniak, J., Paine, D., Seeberger, K., Mant, M.J., Brown, C.B., Belch, A.R. (1999) Potential role of hyaluronan and the hyaluronan receptor RHAMM in mobilization and trafficking of hematopoietic progenitor cells. Blood *93*, 2918-27

Popov, A.V., Pozniakovsky, A., Arnal, I., Antony, C., Ashford, A.J., Kinoshita, K., Tournebize, R., Hyman, A.A., and Karsenti, E. (2001). XMAP215 regulates microtubule dynamics through two distinct domains. Embo J *20*, 397-410.

Reichardt, W., Jung, V., Brunner, C., Klein, A., Wemmert, S., Romeike, B.F., Zang, K.D., and Urbschat, S. (2003). The putative serine/threonine kinase gene STK15 on chromosome 20q13.2 is amplified in human gliomas. Oncol Rep *10*, 1275-1279.

Rein, D.T., Roehrig, K., Schondorf, T., Lazar, A., Fleisch, M., Niederacher, D., Bender, H.G., and Dall, P. (2003). Expression of the hyaluronan receptor RHAMM in endometrial carcinomas suggests a role in tumour progression and metastasis. J Cancer Res Clin Oncol *129*, 161-164.

Rodriguez OC, Schaefer AW, Mandato CA, Forscher P, Bement WM, Waterman-Storer CM. Conserved microtubule-actin interactions in cell movement and morphogenesis. Nat Cell Biol. 2003;5:599-609.

Roghi, C., Giet, R., Uzbekov, R., Morin, N., Chartrain, I., Le Guellec, R., Couturier, A., Doree, M., Philippe, M., and Prigent, C. (1998). The Xenopus protein kinase pEg2 associates with the centrosome in a cell cycle-dependent manner, binds to the spindle microtubules and is involved in bipolar mitotic spindle assembly. J Cell Sci *111 (Pt 5)*, 557-572.

Romano, A., Guse, A., Krascenicova, I., Schnabel, H., Schnabel, R., and Glotzer, M. (2003). CSC-1: a subunit of the Aurora B kinase complex that binds to the survivin-like protein BIR-1 and the incenp-like protein ICP-1. J Cell Biol *161*, 229-236.

Rost, B. (1996). PHD: predicting one-dimensional protein structure by profile based neural networks. Methods in Enzymology *266*, 525-539.

Sahin, U., Tureci, O., Schmitt, H., Cochlovius, B., Johannes, T., Schmits, R., Stenner, F., Luo, G., Schobert, I., and Pfreundschuh, M. (1995). Human neoplasms elicit multiple specific immune responses in the autologous host. Proc Natl Acad Sci U S A *92*, 11810-11813.

Salisbury, J.L. (2003). Centrosomes: coiled-coils organize the cell center. Curr Biol *13*, R88-90.

Salisbury, J.L. (2004). Centrosomes: Sfi1p and centrin unravel a structural riddle. Curr Biol *14*, R27-29.

Samuel, S.K., Hurta, R.A., Spearman, M.A., Wright, J.A., Turley, E.A., and Greenberg, A.H. (1993). TGF-beta 1 stimulation of cell locomotion utilizes the hyaluronan receptor RHAMM and hyaluronan. J Cell Biol *123*, 749-758.

Sato, N., Mizumoto, K., Nakamura, M., Maehara, N., Minamishima, Y.A., Nishio, S., Nagai, E., and Tanaka, M. (2001). Correlation between centrosome abnormalities and chromosomal instability in human pancreatic cancer cells. Cancer Genet Cytogenet *126*, 13-19.

Savani, R.C., Wang, C., Yang, B., Zhang, S., Kinsella, M.G., Wight, T.N., Stern, R., Nance, D.M., and Turley, E.A. (1995). Migration of bovine aortic smooth muscle cells after wounding injury. The role of hyaluronan and RHAMM. J Clin Invest *95*, 1158-1168.

Schatz, C.A., Santarella, R., Hoenger, A., Karsenti, E., Mattaj, I.W., Gruss, O.J., and Carazo-Salas, R.E. (2003). Importin alpha-regulated nucleation of microtubules by TPX2. Embo J *22*, 2060-2070.

Schumacher, J.M., Golden, A., and Donovan, P.J. (1998). AIR-2: An Aurora/Ipl1-related protein kinase associated with chromosomes and midbody microtubules is required for polar body extrusion and cytokinesis in Caenorhabditis elegans embryos. J Cell Biol *143*, 1635-1646.

Sen, S., Zhou, H., Zhang, R.D., Yoon, D.S., Vakar-Lopez, F., Ito, S., Jiang, F., Johnston, D., Grossman, H.B., Ruifrok, A.C., Katz, R.L., Brinkley, W., and Czerniak, B. (2002). Amplification/overexpression of a mitotic kinase gene in human bladder cancer. J Natl Cancer Inst *94*, 1320-1329.

Sharp, D.J., Rogers, G.C., and Scholey, J.M. (2000). Microtubule motors in mitosis. Nature *407*, 41-47.

Shevelyov, Y.Y. (1993). Aurora, a non-mobile retrotransposon in Drosophila melanogaster heterochromatin. Mol Gen Genet *239*, 205-208.

Spicer, A.P., Roller, M.L., Camper, S.A., McPherson, J.D., Wasmuth, J.J., Hakim, S., Wang, C., Turley, E.A., and McDonald, J.A. (1995). The human and mouse receptors for hyaluronan-mediated motility, RHAMM, genes (HMMR) map to human chromosome 5q33.2-qter and mouse chromosome 11. Genomics *30*, 115-117.

Spruck, C.H., Won, K.A., and Reed, S.I. (1999). Deregulated cyclin E induces chromosome instability. Nature *401*, 297-300.

Taimen, P., Viljamaa, M., and Kallajoki, M. (2000). Preferential expression of NuMA in the nuclei of proliferating cells. Exp Cell Res *256*, 140-149.

Tanaka, T., Kimura, M., Matsunaga, K., Fukada, D., Mori, H., and Okano, Y. (1999). Centrosomal kinase AIK1 is overexpressed in invasive ductal carcinoma of the breast. Cancer Res *59*, 2041-2044.

Tang, T.K., Tang, C.J., Chao, Y.J., and Wu, C.W. (1994). Nuclear mitotic apparatus protein (NuMA): spindle association, nuclear targeting and differential subcellular localization of various NuMA isoforms. J Cell Sci *107 (Pt 6)*, 1389-1402.

Till, K.J., Zuzel, M., and Cawley, J.C. (1999). The role of hyaluronan and interleukin 8 in the migration of chronic lymphocytic leukemia cells within lymphoreticular tissues. Cancer Res *59*, 4419-4426.

Tolg, C., Poon, R., Fodde, R., Turley, E.A., and Alman, B.A. (2003). Genetic deletion of receptor for hyaluronan-mediated motility (Rhamm) attenuates the formation of aggressive fibromatosis (desmoid tumor). Oncogene *22*, 6873-6882.

Tsai, M.Y., Wiese, C., Cao, K., Martin, O., Donovan, P., Ruderman, J., Prigent, C., and Zheng, Y. (2003). A Ran signalling pathway mediated by the mitotic kinase Aurora A in spindle assembly. Nat Cell Biol *5*, 242-248.

Tseng, T.C., Chen, S.H., Hsu, Y.P., and Tang, T.K. (1998). Protein kinase profile of sperm and eggs: cloning and characterization of two novel testis-specific protein kinases (AIE1, AIE2) related to yeast and fly chromosome segregation regulators. DNA Cell Biol *17*, 823-833.

Turley, E.A. (1982). Purification of a hyaluronate-binding protein fraction that modifies cell social behavior. Biochem Biophys Res Commun *108*, 1016-1024.

Turley, E.A., Austen, L., Moore, D., and Hoare, K. (1993a). Ras-transformed cells express both CD44 and RHAMM hyaluronan receptors: only RHAMM is essential for hyaluronan-promoted locomotion. Exp Cell Res *207*, 277-282.

Turley, E.A., Austen, L., Vandeligt, K., and Clary, C. (1991). Hyaluronan and a cell-associated hyaluronan binding protein regulate the locomotion of ras-transformed cells. J Cell Biol *112*, 1041-1047.

Turley, E.A., Belch, A.J., Poppema, S., and Pilarski, L.M. (1993b). Expression and function of a receptor for hyaluronan-mediated motility on normal and malignant B lymphocytes. Blood *81*, 446-453.

Turley, E.A., Hossain, M.Z., Sorokan, T., Jordan, L.M., and Nagy, J.I. (1994). Astrocyte and microglial motility in vitro is functionally dependent on the hyaluronan receptor RHAMM. Glia *12*, 68-80.

Turley, E.A., Moore, D., and Hayden, L.J. (1987). Characterization of hyaluronate binding proteins isolated from 3T3 and murine sarcoma virus transformed 3T3 cells. Biochemistry *26*, 2997-3005.

Wang, C., Entwistle, J., Hou, G., Li, Q., and Turley, E.A. (1996). The characterization of a human RHAMM cDNA: conservation of the hyaluronan-binding domains. Gene *174*, 299-306.

Wang, C., Thor, A.D., Moore, D.H., 2nd, Zhao, Y., Kerschmann, R., Stern, R., Watson, P.H., and Turley, E.A. (1998). The overexpression of RHAMM, a hyaluronan-binding protein that regulates ras signaling, correlates with overexpression of mitogen-activated protein kinase and is a significant parameter in breast cancer progression. Clin Cancer Res *4*, 567-576.

Waterman-Storer, C.M., and Salmon, E. (1999). Positive feedback interactions between microtubule and actin dynamics during cell motility. Curr Opin Cell Biol *11*, 61-67.

Wiese, C., Wilde, A., Moore, M.S., Adam, S.A., Merdes, A., and Zheng, Y. (2001). Role of importin-beta in coupling Ran to downstream targets in microtubule assembly. Science *291*, 653-656.

Wilde, A., and Zheng, Y. (1999). Stimulation of microtubule aster formation and spindle assembly by the small GTPase Ran. Science *284*, 1359-1362.

Wittmann, T., Boleti, H., Antony, C., Karsenti, E., and Vernos, I. (1998). Localization of the kinesin-like protein Xklp2 to spindle poles requires a leucine zipper, a microtubule-associated protein, and dynein. J Cell Biol *143*, 673-685.

Wittmann, T., Hyman, A., and Desai, A. (2001). The spindle: a dynamic assembly of microtubules and motors. Nat Cell Biol *3*, E28-34.

Wittmann, T., Wilm, M., Karsenti, E., and Vernos, I. (2000). TPX2, A novel xenopus MAP involved in spindle pole organization. J Cell Biol *149*, 1405-1418.

Yamada, Y., Itano, N., Narimatsu, H., Kudo, T., Hirohashi, S., Ochiai, A., Niimi, A., Ueda, M., and Kimata, K. (1999). Receptor for hyaluronan-mediated motility and CD44 expressions in colon cancer assessed by quantitative analysis using real-time reverse transcriptase-polymerase chain reaction. Jpn J Cancer Res *90*, 987-992.

Yang, B., Hall, C.L., Yang, B.L., Savani, R.C., and Turley, E.A. (1994a). Identification of a novel heparin binding domain in RHAMM and evidence that it modifies HA mediated locomotion of ras-transformed cells. J Cell Biochem *56*, 455-468.

Yang, B., Yang, B.L., Savani, R.C., and Turley, E.A. (1994b). Identification of a common hyaluronan binding motif in the hyaluronan binding proteins RHAMM, CD44 and link protein. Embo J *13*, 286-296.

Yang, B., Zhang, L., and Turley, E.A. (1993). Identification of two hyaluronan-binding domains in the hyaluronan receptor RHAMM. J Biol Chem *268*, 8617-8623.

Yang, H., Ou, C.C., Feldman, R.I., Nicosia, S.V., Kruk, P.A., and Cheng, J.Q. (2004). Aurora-A kinase regulates telomerase activity through c-Myc in human ovarian and breast epithelial cells. Cancer Res *64*, 463-467.

Young, A., Dictenberg, J.B., Purohit, A., Tuft, R., and Doxsey, S.J. (2000). Cytoplasmic dynein-mediated assembly of pericentrin and gamma tubulin onto centrosomes. Mol Biol Cell *11*, 2047-2056.

Zeng, C. (2000). NuMA: a nuclear protein involved in mitotic centrosome function. Microsc Res Tech *49*, 467-477.

Zhan, F., Hardin, J., Kordsmeier, B., Bumm, K., Zheng, M., Tian, E., Sanderson, R., Yang, Y., Wilson, C., Zangari, M., Anaissie, E., Morris, C., Muwalla, F., van Rhee, F., Fassas, A., Crowley, J., Tricot, G., Barlogie, B., and Shaughnessy, J., Jr. (2002). Global gene expression profiling of multiple myeloma, monoclonal gammopathy of undetermined significance, and normal bone marrow plasma cells. Blood *99*, 1745-1757.

Zhang, S., Chang, M.C., Zylka, D., Turley, S., Harrison, R., and Turley, E.A. (1998). The hyaluronan receptor RHAMM regulates extracellular-regulated kinase. J Biol Chem *273*, 11342-11348.

Zhou R, Wu X, Skalli O. The hyaluronan receptor RHAMM/IHABP in astrocytoma cells: expression of a tumor-specific variant and association with microtubules. J Neurooncol. 2002;59:15-26.

Zimmerman, W., and Doxsey, S.J. (2000). Construction of centrosomes and spindle poles by molecular motor-driven assembly of protein particles. Traffic *1*, 927-934.

Chapter 1: RHAMM is a centrosomal protein that interacts with dynein and stabilizes spindle poles

This research was originally published in *Molecular Biology of the Cell.*

Reprinted from *Molecular Biology of the Cell* (Maxwell, C.A., Keats, J.J., Crainie, M., Sun, X., Yen, T., Shibuya, E., Hendzel, M., Chan, G., Pilarski, L.M. Mol.Biol. Cell 2003 14: 2262-76) with permission by the American Society for Cell Biology.

Introduction

The Receptor for Hyaluronan (HA) Mediated Motility (RHAMM, Intracellular Hyaluronan Binding Protein (IHABP), CD168), first described by Turley and colleagues (Turley, 1992; Turley et al., 1985, 1987, 1991), is a multifaceted protein with both intracellular and extracellular functions (Hardwick et al., 1992) ,(Assmann et al., 1999),(Pilarski et al., 2001). RHAMM mediates the HA-specific motility of a variety of cell types, including transformed cell lines and ex vivo malignant leukocytes (Masellis-Smith et al., 1996),(Pilarski et al., 2001). RHAMM is the founding member of the $B(X)_7B$ hyaladherin protein family and interacts with HA through basic (B) 9-11 amino acids (aa) $B(X)_7B$ motifs (Yang et al., 1994). Encoded by 18 exons, *RHAMM* localizes to chromosome 5q33.2-qter (Spicer et al., 1995) and encodes an 85 kDa protein with extensive coiled-coil structure and a basic amino-terminal globular domain (Hardwick et al., 1992),(Assmann et al., 1999). In addition to its role in cell migration, RHAMM expression, and overexpression, has been linked to ras transformation, tumor progression and metastasis (Hall et al., 1995). Moreover, RHAMM has been identified as a microtubule associated protein that also interacts with the actin cytoskeleton (Assmann et al., 1999). Overexpression of RHAMM in B lymphoid malignancies, and other cancers, suggests that it may play a role in human oncogenesis and disease progression (Crainie et al., 1999),(Wang et al., 1998). Two RHAMM splice variants, $RHAMM^{-exon\ 4}$ and $RHAMM^{-exon13}$, have been identified in myeloma patients and cancer cell lines (Crainie et al., 1999), (Assmann et al., 1999); all variants localize to the mitotic spindle although loss of exon 4 inhibits interaction with interphase microtubules (Assmann et al., 1999). The localization of RHAMM isoforms at the mitotic spindle provides a putative mechanism

through which RHAMM expression regulates mitotic integrity, ploidy and, possibly, carcinogenesis.

In animal cells, the duplication of centrosomes, and their subsequent polar separation, initiates the establishment of a bipolar microtubule array. Many centrosomal and non-centrosomal proteins, including microtubule motor complexes, coordinate early mitotic events. Kinesin-like protein 2 family members (Xklp2, Hklp2, KRP180) are essential for centrosomal separation and the maintenance of spindle bipolarity (Boleti et al., 1996). The carboxy-terminal leucine zipper of Xklp2 is required for its centrosomal and spindle pole localization, via an interaction with Targeting Protein for Xklp2 (TPX2) and the dynein/dynactin motor complex (Wittmann et al., 1998). TPX2 has recently been shown to mediate Ran-GTP dependent microtubule assembly and to target Aurora A kinase to the spindle pole (Gruss et al., 2002) (Kufer et al., 2002). A recurring mechanism in spindle pole formation and stability is dynein/dynactin mediated recruitment of structural proteins to the spindle pole (reviewed in (Zimmerman and Doxsey, 2000). Pericentrin, a 220 kDa coiled coil protein, plays an integral role in centrosomal stability by acting as a molecular scaffold and interacting with numerous proteins and protein complexes, including dynein (Zimmerman and Doxsey, 2000). Although centrosomal localization of pericentrin is microtubule independent (Gillingham and Munro, 2000), based on the observations that nocodazole disruption fails to abolish pericentrin centrosomal localization, recruitment of pericentrin to centrosomes requires an association with the dynein motor complex (Young et al., 2000) (Zimmerman and Doxsey, 2000). Nuclear Mitotic Apparatus protein (NuMA), a highly coiled coil 240 kDa

protein, is also concentrated at spindle poles, where it crosslinks microtubule minus ends, through an association with the dynein/dynactin complex (Gaglio et al., 1996). Recently, a direct microtubule interaction has been localized to the carboxy terminal tail domain of NuMA (Haren and Merdes, 2002). Thus, NuMA may function in microtubule sliding and spindle stability by directly binding with microtubules at the carboxy-terminus, complexing with the dynein/dynactin motor complex and anchoring one microtubule relative to another sliding microtubule (Gaglio et al., 1996).

The Transforming Acidic Coiled Coil (TACC) proteins, a family of proteins that concentrate to centrosomes through a conserved coiled coil carboxy-terminal domain called the TACC domain, also play a role in organizing centrosomal microtubules (Gergely et al., 2000a),(Gergely et al., 2000b; Lee et al., 2001). The TACC domain of drosophila-TACC, D-TACC, has been shown to interact with minispindles, msps, the drosophila homologue of human colonic and hepatic tumor overexpressed (TOGp) protein (Lee et al., 2001),(Cullen and Ohkura, 2001). The TOG family of proteins (TOGp, XMAP215, Msps) can bind directly to microtubules and promote their polymerization. In drosophila, Msps is transported to microtubule minus ends by the kinesin like protein Ncd and anchored to centrosomes by an association with D-TACC (Lee et al., 2001),(Cullen and Ohkura, 2001); centrosomal targeting of D-TACC is regulated by Aurora A kinase which, in turn, is dependent on TPX2-mediated targeting (Giet et al., 2002) (Kufer et al., 2002). Like RHAMM, TACC proteins have been intimately linked to carcinogenesis. TACC1 overexpression transforms mouse fibroblasts (Still et al., 1999a). A TACC2 isoform has been identified as the tumor suppressor

protein Azu-1 in breast carcinoma lines and TACC3 is upregulated in multiple cancer lines (Chen et al., 2000), (Still et al., 1999b). Moreover, TACC3 is essential for hematopoietic stem cell function and may play a primary role in the regulation of p53 function within hematopoietic cells (Piekorz et al., 2002).

This paper investigates the involvement of RHAMM at the mitotic spindle with emphasis on its localization in non-adherent cell lines derived from human lymphocytes. We demonstrate that RHAMM shares structural and functional similarity with proteins that are essential for the maintenance of the mitotic spindle. RHAMM localizes to the centrosome during interphase and to the spindle poles during mitosis. Consistent with sequence similarity to the Klp2 family, we demonstrate that RHAMM interacts with the dynein complex in vivo. The centrosomal targeting domain of RHAMM localizes to the previously characterized hyaluronan binding domain (Yang et al., 1994); we show this motif is phylogenetically related to the TACC and Klp2 centrosomal targeting motifs. We find that overexpression of GFP-RHAMM leads to mitotic delays and apoptosis. We also find that disruption of RHAMM mitotic function, through microinjection of purified anti-RHAMM antibodies, affects spindle integrity and results in the formation of tripolar and tetrapolar spindles. We have shown that in addition to its other functions, RHAMM is a centrosomal protein that interacts with the dynein microtubule motor complex, functions in the maintenance of spindle integrity, and is chromosomally located proximal to the putative *FGFR4-TACC4* gene cluster on chromosome 5qter.

Materials and Methods

Plasmids and antibodies

The RHAMM^{FL}, RHAMM$^{-exon\ 4}$, RHAMM$^{-exon13}$ were all amplified with the 5' XhoI-RHAMM and 3' KpnI-RHAMM^{FL} primers using Platinum High Fidelity Taq (Gibco/BRL) under standard conditions as recommended by the manufacturer. PCR products were cloned into pCR2.1-TOPO (Invitrogen). The RHAMM^{679}, RHAMM^{623}, RHAMM^{525} deletion constructs were all amplified from the pCR2.1-TOPO-RHAMM^{FL} vector, after sequencing, with 5' XhoI-RHAMM and the respective deletion primer. These products were cloned into pCR2.1-TOPO. The respective RHAMM constructs were then cloned into pEGFP-C1 (Clonetech) using XhoI and KpnI. All GFP-RHAMM constructs were prepared for transfection using the Qiagen EndoFree Maxi Kit (Qiagen). The GFP-tubulin construct was purchased from Clonetech.

Primer Sequences:

5' XhoI-RHAMM cG**Ctcgag**At*ATG*TCCTTTCCTAAG

3' KpnI-RHAMM^{FL} cc**gGTacc**CTTCCATGATTCTTG

3' KpnI-RHAMM^{679} TGGTGTTT**GgTACC**TAGAAC*TTa*ATTCAAT

3' KpnI-RHAMM^{623} CAATAA**ggTAcC**ATA*TtA*ATCTCTTATTTTATT

3' KpnI-RHAMM^{525} GAAACTGT**GgTacC**TTTAAT*TTa*TGTTTCCTTTAG

5' XhoI-RHAMM^{500} C**ctcgag**atGCAACTGAGAGCTC

5' XhoI-RHAMM^{624} AA**ctcGAG**ATTCATATGCTAAATT

3' KpnI-RHAMM^{stop} G**ggtaCc**GT*tta*CTTCCATGATTCTTG

Primer sequences are shown 5'-3', lower case letters denote mispriming from de novo mRNA, bold sequences denote restriction endonuclease recognition sites, and italics denote start and stop codons.

Antibodies used: α tubulin (clone B-5-1-2), γ tubulin (clone GTU-88), dynein (clone 70.1) from Sigma, pericentrin from BabCo, and the mouse monoclonal NuMA antibodies were identified in a monoclonal antibody screen for mitotic chromosome scaffold proteins (Compton et al., 1991). The polyclonal RHAMM antibody CM1 was produced by Washington Biotechnology, Inc to the following carboxy-terminal peptide sequence: G^{681}IKHFDPSKAFHHESK^{696}. The polyclonal serum was affinity purified over a peptide loaded NHS-activated Sepharose 4B column (Amersham Pharmacia), washed, eluted with glycine pH 2.5, neutralized and quantified by OD^{280}. Fractions were pooled and concentrated with Ultrafree-MC (Millipore Corp, Bedford MA) to >10mg/ml. The specificity of this serum was tested by immunoblot, immunoprecipitation and immunofluorescent analysis (see Fig. 5). A second anti-RHAMM serum was as described (Assmann et al., 1999); this antiserum is a pan-specific anti-RHAMM sera raised against a bacterially expressed GST-RHAMM fusion protein (RHAMM exons 10-13, $aa^{307-498}$)(Assmann et al., 1999). The anti-TOGp serum was as described (Dionne et al., 2000). Secondary antibodies were from Molecular Probes.

Cell Culture, transient transfection, nocodazole treatment and immunofluorescence

Cells from RPMI 8226, a human lymphoblastic cell line derived from the peripheral blood of a multiple myeloma patient, and Raji, a human lymphoblastic cell line derived from a Burkitts lymphoma patient, were grown in suspension in RPMI medium supplemented with 10% fetal bovine serum (Gibco/BRL), at 37°C in 5% CO_2. HeLa cells, a human adherent epithelial cell line derived from a patient with cervical adenocarcinoma, were grown in DMEM medium supplemented with 10% fetal bovine serum (Gibco/BRL), at 37°C in 5% CO_2.Cells were passaged 24 hours prior to transfection. Suspension cells were transfected by electroporation (270mV, 960uF, 47-53ms) and stable GFP-α-tubulin transfectants were selected for in 600ug/ml G418. HeLa cells were transfected with Lipofectamine 2000 (GibcoBRL) following manufacturers protocols. For nocodazole experiments, HeLa cells were incubated for 90 minutes in 25uM nocodazole (Sigma) prior to immunofluorescence. Suspension cells and HeLa were fixed and permeabilized in cold MeOH at defined time points post transfection. Cells were washed with PBS-0.5% Triton X-100 (Sigma) prior to immunofluorescence. Primary and secondary antibodies were diluted in PBS-0.1% TWEEN (Sigma)+ skim milk powder (blocking buffer) and all antibody incubations were for 30 min at room temperature. For double staining experiments, antibodies were added sequentially. Cells were washed 3x in PBS-0.5% TWEEN before and after incubations. Cells were mounted in 90% glycerol/PBS + DAPI and images were acquired using a Zeiss confocal LSM 510 or multiphoton microscope. Images were processed using MetaMorph Software (Universal Imaging Corp.) and Photoshop 5.02 software (Adobe Systems Inc.).

Immunoprecipitations

HeLa cells were transfected using Lipofectamine 2000 (GibcoBRL) and the manufacturer's protocol. Following transfection, cells were incubated for 12-16 hours, in the presence of OPTIMEM (GibcoBRL), while untransfected cells were incubated in fresh DMEM-10%FBS. Following incubation, cells were released from plates with 1x trypsin, washed 3x with PBS and lysed at $5x10^6$-10^7 cells/ml in 1% CHAPs plus 10 μg/mL leupeptin, 10 μg/mL antipain and 1 mM phenylmethylsulfonyl fluoride (all from Sigma). For some experiments, cells were washed and lysed in situ with lysis buffer. All immunoprecipitation procedures were performed at 4^OC. Lysates were precleared with Protein A-Sepharose beads (Pharmacia) with rotation for 30 min. Precleared lysates were incubated with antibodies (3μl/150ml lysate) for 2 hrs at 4^0C with rotation, then with protein A beads (40ul 1:1 slurry in CHAPS +) for 1 hr at 4^0C with rotation. Beads were collected with centrifugation and washed 4x with CHAPS+ buffer. Immunoprecipitated proteins were eluted with boiling SDS buffer and analyzed by a 5% stacking/8% separating SDS-PAGE. 25 μl of precleared lysates and post-immunoprecipitation fractions were analysed to determine efficiency and relative quantity of the immunoprecipitations.

Microinjection

HeLa cells were plated onto coverslips and synchronized at the G1/S boundary by double thymidine block (2.5 mM thymidine). Cells were injected 1 hour after release from thymidine block. Microinjection was performed with a semi-automatic microinjector (Eppendorf, model 5412). For each coverslip, 200-300 cells were injected

with each antibody mix over the course of approximately 30 minutes. Affinity purified antibodies were kept in calcium and magnesium free PBS and were filtered through a 0.22 μm Millipore microfiltration cup before microinjection. Cells were released from the G1/S block by washing with PBS and replaced with fresh media before microinjection. Cells were fixed with 3.5% paraformaldehyde approximately 12 hours after release from the G1/S boundary. Cells were permeabilized with 0.2% Triton X-100 in KB (10 mM Tris pH7.5, 0.15 M NaCl, 0.1% BSA) for 5 minutes and washed with KB before antibody incubation. To minimize loss of loosely attached mitotic cells, the coverslips were centrifuged at 200 g for 2 minutes in a clinical centrifuge (GPKR; Beckman). The injected antibodies were detected by Cy5 conjugated anti-rabbit secondary antibodies (Jackson ImmunoResearch Laboratories).

Results

RHAMM localizes to centrosomes, spindle poles and midzone microtubules. The carboxy-terminal structure of RHAMM is similar to the Klp2 family.

The subcellular localization of RHAMM to interphase microtubules and the mitotic spindle has been demonstrated in adherent lines (Assmann et al., 1999). Because RHAMM over-expression and function also characterizes human lymphocytes and B lymphoid malignancies (Masellis-Smith et al., 1996),(Crainie et al., 1999),(Gares et al., 1998), we investigated RHAMM localization in non-adherent, suspension cell lines derived from lymphocyte malignancies (RPMI 8226 and Raji). The subcellular localization of endogenous RHAMM was investigated by indirect immunofluorescence using two polyclonal antisera. The first, termed IHABP, was previously characterized as a pan-specific anti-RHAMM antiserum (Assmann et al., 1999) while the second, termed CM1, is characterized below (Figure 1-5A). The adherent line HeLa was used to confirm RHAMM localization in cells derived from solid tumors (not shown).

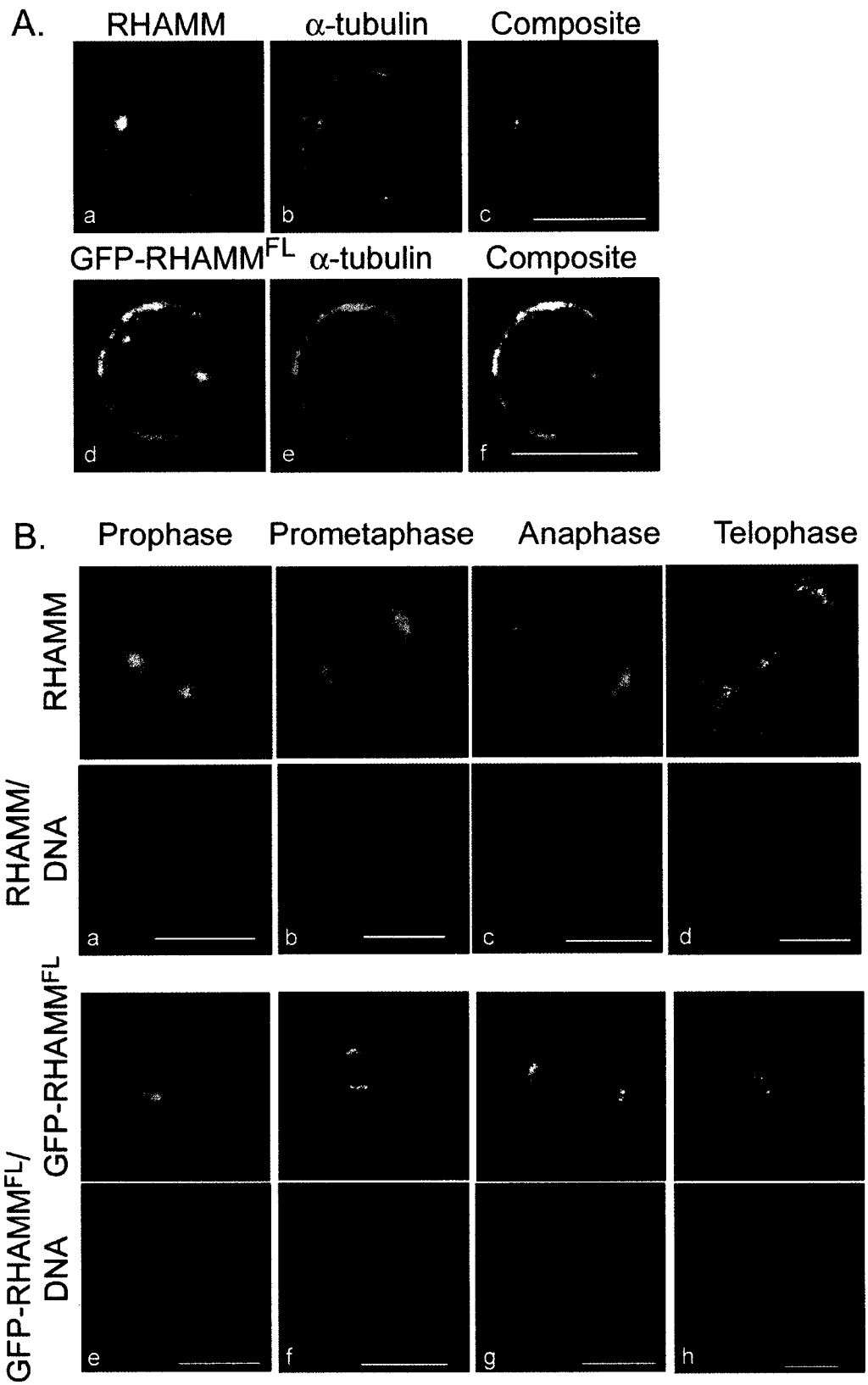

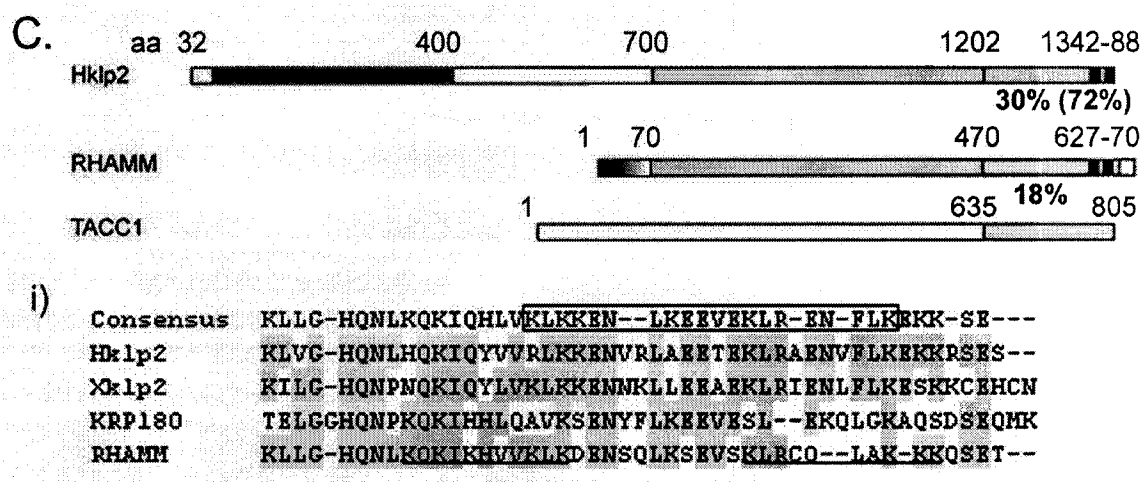

Figure 1-1: Structural analysis and localization of RHAMM in suspension cell lines.

(A) Interphase localization of RHAMM (left column) by indirect immunofluorescence (a-c) and GFP-RHAMM^{FL} fusion proteins (d-f) and colocalization with α-tubulin (middle column) is shown. Exponentially growing RPMI 8226 cells were transiently transfected with GFP-RHAMM^{FL} (d-f) or methanol treated and sequentially stained with antibodies against RHAMM and α-tubulin. In the composite image c, RHAMM is red and microtubules are green; in composite image d, GFP-RHAMM^{FL} is green while microtubules are red (B) Mitotic localization of RHAMM by indirect immunofluorescence (a-d) and GFP-RHAMM^{FL} fusion proteins (e-h) is shown. Exponentially growing RPMI 8226 cells were transiently transfected with GFP-RHAMM^{FL} (d-f) or methanol treated and sequentially stained with antibodies against RHAMM and α-tubulin. DNA was visualized with DAPI. Cells in prophase, prometaphase, anaphase and telophase are shown. Scale bars are equivalent to 10 μm.(C). Schematic diagram of RHAMM predicted secondary structure and functional domains with members of the Klp2 and TACC protein families. The molecular motor domain of Hklp2 (aa 32-400) is identified in black, the amino-terminal microtubule binding domain of RHAMM (aa 1-70) is in gradient, predicted coiled coil structure of the proteins is in grey, the carboxy-terminal B(X)$_7$B domain of RHAMM (aa 627-70) and basic leucine zipper of Hklp2 (aa 1342-88) is shown in hatched black. Percent identity between the COOH-terminal 200 aa are shown; percent identity within the basic leucine zipper/HA binding domain is shown in parentheses. (i) RHAMM COOH-terminal sequence was aligned with Klp2 family members using the PepTool software program. Identical amino

acids are outlined in grey. The Klp2 consensus COOH-terminal leucine zipper is boxed. The HA-binding $B(X)_7B$ domains of RHAMM are underlined.

Examination of RHAMM localization within interphase, non-adherent cell lines revealed pronounced centrosomal localization in addition to microtubule association (Figure 1-1A). Although less pronounced in adherent HeLa cells, centrosomal localization was identified within interphase and prophase cells (not shown). We speculate that the more polymerized, filamentous microtubule arrays of adherent lines have prevented previous observation of RHAMM centrosomal localization. During prophase, in both adherent and suspension lines, RHAMM concentrated at the center of microtubule asters and associated with microtubules growing between the two asters (Figure 1-1B). During prometaphase and metaphase, RHAMM intensified at the spindle pole and extended along spindle microtubules during metaphase. Additionally, RHAMM localized to the spindle midzone during anaphase and telophase. During telophase, RHAMM redistributed from the centrosomes and concentrated to the spindle midzone (Figure 1-1B). To compare the localization of RHAMM in fixed and live cells and to control for possible fixation and permeabilization artifacts, the distribution of full-length RHAMM ($RHAMM^{FL}$)-GFP was examined in transiently transfected RPMI 8226, Raji and HeLa cells. Consistent with the localization of endogenous RHAMM in fixed samples, $RHAMM^{FL}$-GFP proteins localized to centrosomes, interphase microtubules, the mitotic spindle pole and midzone microtubules in suspension and in adherent cells. Although microtubules are suboptimally visualized in non-adherent cells, RHAMM

antibodies colocalized with microtubules in all interphase cells examined, including methanol fixed suspension cells (Figure 1-1A).

Previous analysis of RHAMM established the existence of three major structural domains: the amino-terminal head (aa1-69; pI 10.72), which interacts with microtubules, an extensive coil coiled stalk (aa70-680; pI 5.06) and a short carboxy-terminal tail (aa 681-724; pI 8.12)(Assmann et al., 1999). Sequence alignments and structural prediction reveals a relationship between RHAMM and the Klp2 protein family (Figure 1-1C). Structure prediction for RHAMM, like Xklp2, predicts extensive coiled-coil structure within the carboxy-terminal 600 amino acids (Figure 1-1C)(Assmann et al., 1999),(Boleti et al., 1996). Moreover, BLAST 2 sequence analysis (Tatusova and Madden, 1999) of RHAMM primary structure against the Klp2 family reveals significant homology (e^{-28} for Hklp2) including conservation of the carboxy-terminal leucine zipper, which exhibits 72% identity (Figure 1-1Ci); this domain is vital to Klp2 centrosomal localization and function through an indirect interaction with the dynein/dynactin complex (Wittmann et al., 1998). The coiled-coil terminus of RHAMM, however, bears little sequence identity to the centrosomal targeting TACC domain of TACC1. The carboxy-terminal leucine zipper of RHAMM (boxed in Figure 1-1Ci) overlaps the defined HA-binding domains (underlined in Figure 1-1Ci); this region is conserved amongst RHAMM proteins in human, mouse and rat (Lynn et al., 2001). RHAMM lacks the highly conserved amino-terminal kinesin motor domain but contains a microtubule binding domain in its place (aa 1-70, Figure 1-1C). Based on these similarities, we tested whether the conserved carboxy-terminal leucine zipper directed RHAMM to centrosomes and spindle poles.

The amino-terminus of RHAMM is required for interaction with interphase microtubules while the carboxy-terminal leucine zipper targets RHAMM to the centrosome

To define the domains in RHAMM responsible for centrosomal targeting, we constructed GFP fusion proteins that correspond to known RHAMM splice variants ($RHAMM^{-exon4}$ and $RHAMM^{-exon13}$) as well as RHAMM carboxy-terminal deletion mutants ($RHAMM^{1-525}$, $RHAMM^{1-623}$ and $RHAMM^{1-679}$) and carboxy-terminal fragments ($RHAMM^{625-725}$ and $RHAMM^{500-725}$) (Figure 1-2A).

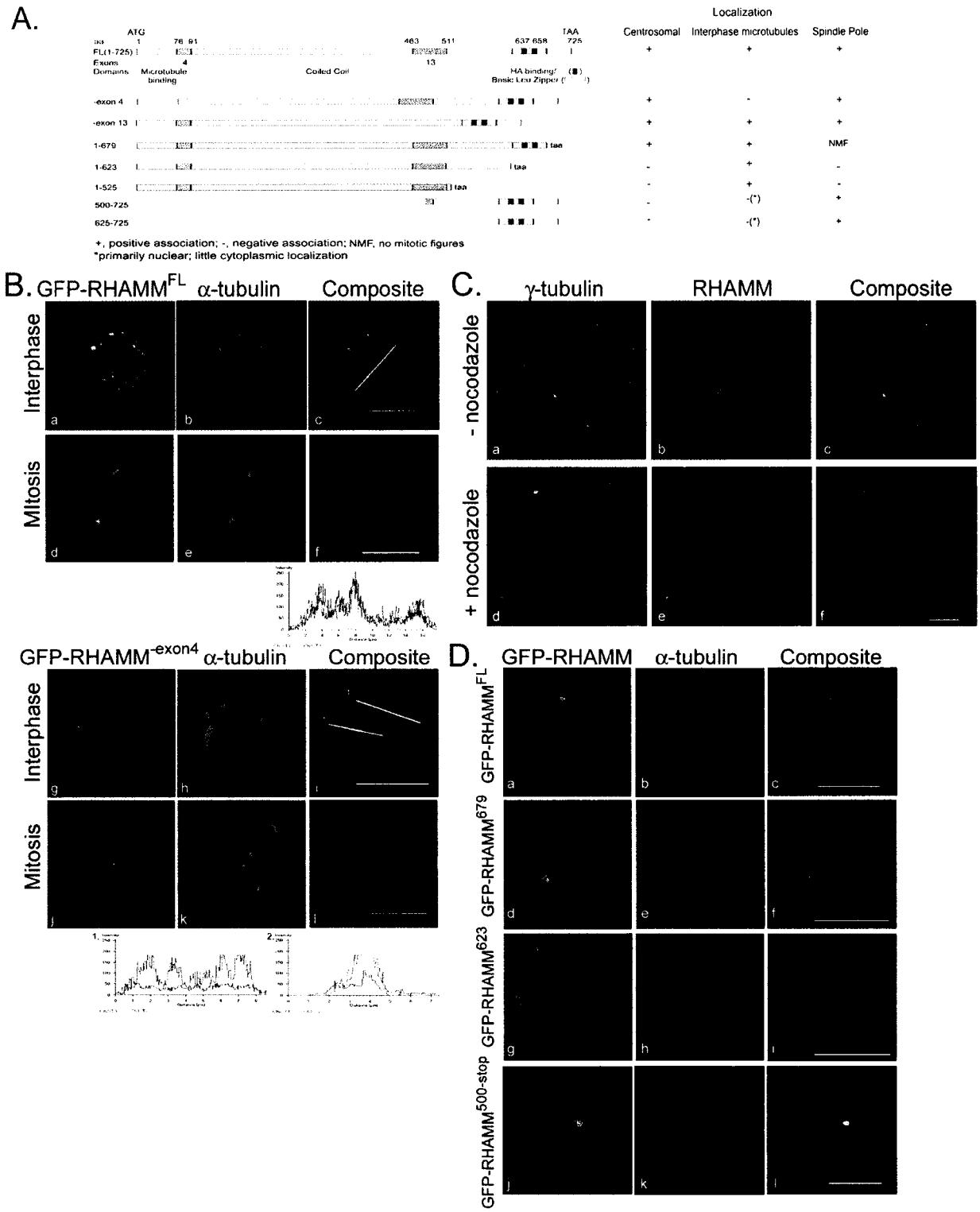

Figure 1-2 RHAMM interacts with microtubules at the amino terminus and is targeted to the centrosomes by the carboxy terminus

Figure 1-2: RHAMM interacts with microtubules at the amino terminus and is targeted to centrosomes by the carboxy-terminus. **A)** Cartoon diagram of $RHAMM^{FL}$ and the RHAMM splice variants along with the deletion mutants utilized in the following experiments. The table outlines results of centrosomal localization experiments. For GFP-$RHAMM^{679}$ variant, no mitotic figures (NMF) were observed for 5 transfection experiments **(B)** EGFP-C1 (not shown), EGFPC1-$RHAMM^{FL}$ (top box), EGFPC1-$RHAMM^{-exon13}$ (not shown) and EGFPC1-$RHAMM^{-exon4}$ (bottom box) were transfected into RPMI 8226 and stained for α-tubulin six to eight hours post transfection (middle lanes). α-tubulin stain allows identification of microtubule colocalization and microtubule organizing center (centrosome) localization. Cells were visualized in PBS/glycerol (a-f) or cytospun at 200 rpm and visualized (g-l). Line (inset in panel c and i) profile analysis of channel intensities was used to demonstrate colocalization, or lack thereof, between GFP-RHAMM isoforms and α-tubulin. Representative profiles are shown. Scale bars equivalent to 10 um. **(C)** HeLa cells were treated with, or without, nocodazole for 90 min, and sequentially stained for RHAMM, or pericentrin (not shown), and γ tubulin, a centrosomal marker. In the composite images, RHAMM is red, γ-tubulin is green and DNA is blue. DNA was visualized with DAPI. Scale bars equivalent to 10 um. **(D)** Deletion constructs were transfected into RPMI 8226 and cells were stained for γ tubulin six to eight hours post-transfection to indicate centrosomal localization. DAPI channel is included for the GFP-$RHAMM^{625\text{-}stop}$ variant to demonstrate prometaphase stage of transfected cell. Interphase cells transfected with GFP-$RHAMM^{500\text{-}stop}$ or GFP-$RHAMM^{625\text{-}stop}$ demonstrated nuclear accumulation but not centrosomal localization (not shown). Scale bars are equivalent to 10 um.

To investigate the centrosomal localization of RHAMM in non-adherent cells, GFP-RHAMM fusion constructs were transiently transfected into RPMI 8226 and Raji lines. Consistent with previous observations in HeLa cells (Assmann et al., 1999), RHAMM variants that contain exon 4 (i.e. $RHAMM^{FL}$ and $RHAMM^{-exon13}$) colocalized with interphase microtubules (Figure 1-2B). The degree of colocalization is illustrated by the intensity profile along the inset line within panel c (Figure 2B). Although the low

cytoplasm to nucleus ratio of the suspension cells makes microtubule colocalization experiments difficult, occasional cells with well-defined microtubule networks were observed. Within these cells, GFP-RHAMM variants, containing exon 4, demonstrated precise colocalization with microtubules (not shown). Loss of exon 4 (GFP-RHAMM^{-exon4}) disrupts interphase microtubule interactions as demonstrated by the lack of colocalization along the inset line 1 within panel i (Figure 1-2B). In fact, GFP-RHAMM^{-exon4} demonstrated diffuse, relatively invariant, cytoplasmic localization (line 1, Figure 1-2B). However, GFP-RHAMM^{-exon4} localized to centrosomes (see line 2 profile) and mitotic spindle poles (Figure 1-2B). Nocodazole inhibition of microtubule polymerization was used to determine whether polymerized microtubules were required for the association of RHAMM with centrosomes and the mitotic spindle pole. Pericentrin was used as a positive control as it is known to localize at the centrosome in a microtubule-independent manner (Gillingham and Munro, 2000). Centrosomal localization was analyzed by γ-tubulin staining and DAPI staining was used to determine the mitotic status of the cells. In the presence of polymerized microtubules (-nocodazole), RHAMM localizes at centrosomes and the mitotic spindle (Figure 1-2C). As demonstrated by the RHAMM staining within metaphase cells (Figure 1-2C, panel e), nocodazole treatment affected cellular architecture and disrupted metaphase mitotic spindles. Consistent with previous reports, pericentrin localization at centrosomes was microtubule-independent (not shown); in the absence of polymerized microtubules, RHAMM maintained an association with interphase centrosomes and the mitotic spindle pole (Figure 1-2C). It is important to note that microtubule-independent centrosomal localization is distinct from microtubule-independent centrosomal targeting. Although

RHAMM and other centrosomal proteins such as pericentrin do not require microtubules to remain localized at the centrosome, it is likely that RHAMM centrosomal targeting is facilitated through an interaction, either direct or indirect, with a minus-end directed microtubule molecular motor (see below).

The carboxy-terminal 300 aa coiled-coil domain of RHAMM shares identity with the basic leucine zipper (BZIP) of the Klp2 family (Figure 1-1C). To test the importance of the conserved leucine zipper in centrosomal targeting, deletion constructs of RHAMM, lacking the carboxy-terminal 200, 102 and 47 aa, were constructed (Figure 1-2A). Transient transfection of empty vector EGFPC1 was used as a negative control for centrosomal and spindle pole localization; both the centrosome and spindle pole showed slight amplification of transfected EGFP-C1 (not shown). Deletion of the carboxy-terminal 200 aa ($RHAMM^{525}$, not shown) or 102 aa ($RHAMM^{623}$, Fig. 2D), inhibited the centrosomal localization of the fusion proteins. However, RHAMM proteins that contained the leucine zipper, $RHAMM^{FL}$ (Figure 1-2D), $RHAMM^{-exon4}$ (Figure 1-2B), $RHAMM^{-exon13}$ (not shown) and $RHAMM^{679}$ (Figure 1-2D), localized to the centrosome. The BZIP motif was also essential for localization of RHAMM constructs to the mitotic spindle pole; after examination of 5 transfection experiments, we were unable to identify a mitotic figure within GFP-$RHAMM^{679}$ transfected cells. This observation was tested and quantitated in HeLa cells. Transient transfectants of GFP-$RHAMM^{679}$ and GFP-$RHAMM^{FL}$ were examined for mitotic stage at 12, 13, 14 and 20 hours post transfection and compared to neighbouring untransfected cells. GFP-$RHAMM^{679}$ transfection resulted in only prophase transfectants (n=47) while GFP-$RHAMM^{FL}$ transfection led to

accumulation of prometaphase and metaphase cells {58.6% (34/58) of transfected cells vs 26.2% (101/386) within the untransfected population; see also Figure 1-4}. Moreover, the majority of GFP-RHAMM^{679} transfectants demonstrated large aggregation of GFP fluorescence (not shown). Microtubule associations and centrosomal localization were maintained in transfectants with low levels of fluorescence. Interestingly, ^{704}TPLK^{707}, a consensus cdc2 phosphorylation site conserved in mouse and rat, falls within the deleted region of RHAMM^{679}. To test the sufficiency of the BZIP motif for centrosomal targeting, we constructed GFP-tagged, carboxy-terminal RHAMM fragments consisting of the terminal 100 and 225 aa, respectively. When transiently transfected into RPMI 8226, these constructs localized to the interphase nucleus and mitotic spindle pole. Although the carboxy terminus does not include a predicted (predictNLS analysis) simple or bipartite nuclear localization signal, characterized by a short stretch of basic aa or two interdependent positively charged clusters separated by a short linker region, it is highly basic (Cokol et al., 2000). Given their basic nature, the nuclear localization of the small carboxy-terminal fragments may be the result of transport, and not simple diffusion, into the nucleus. Both fragments also showed slight localization to the centrosome although not greater than GFP alone. Therefore, the carboxy-terminal basic leucine zipper of RHAMM, which overlaps the defined B(X)$_7$B HA binding domains and is homologous to the Klp2 family, is essential for centrosomal targeting and sufficient for spindle pole localization.

RHAMM interacts with the dynein motor complex in vivo

As the carboxy-terminal leucine zipper is conserved between RHAMM and the Klp2 family and this domain mediates the indirect interaction of Xklp2 and dynein (Wittmann et al., 1998), we investigated whether RHAMM interacts with the dynein motor complex in cells. We first determined the spatial relationship of endogenous RHAMM and dynein intermediate chain in HeLa cells. Double immunofluorescence by confocal microscopy demonstrated colocalization of dynein and RHAMM at the spindle pole within mitotic HeLa cells (Figure 1-3A). As a large fraction of intracellular RHAMM, and dynein, does not localize to the spindle pole, it is likely that only a subset of the total RHAMM protein interacts with the dynein/dynactin motor complex, and vice versa.

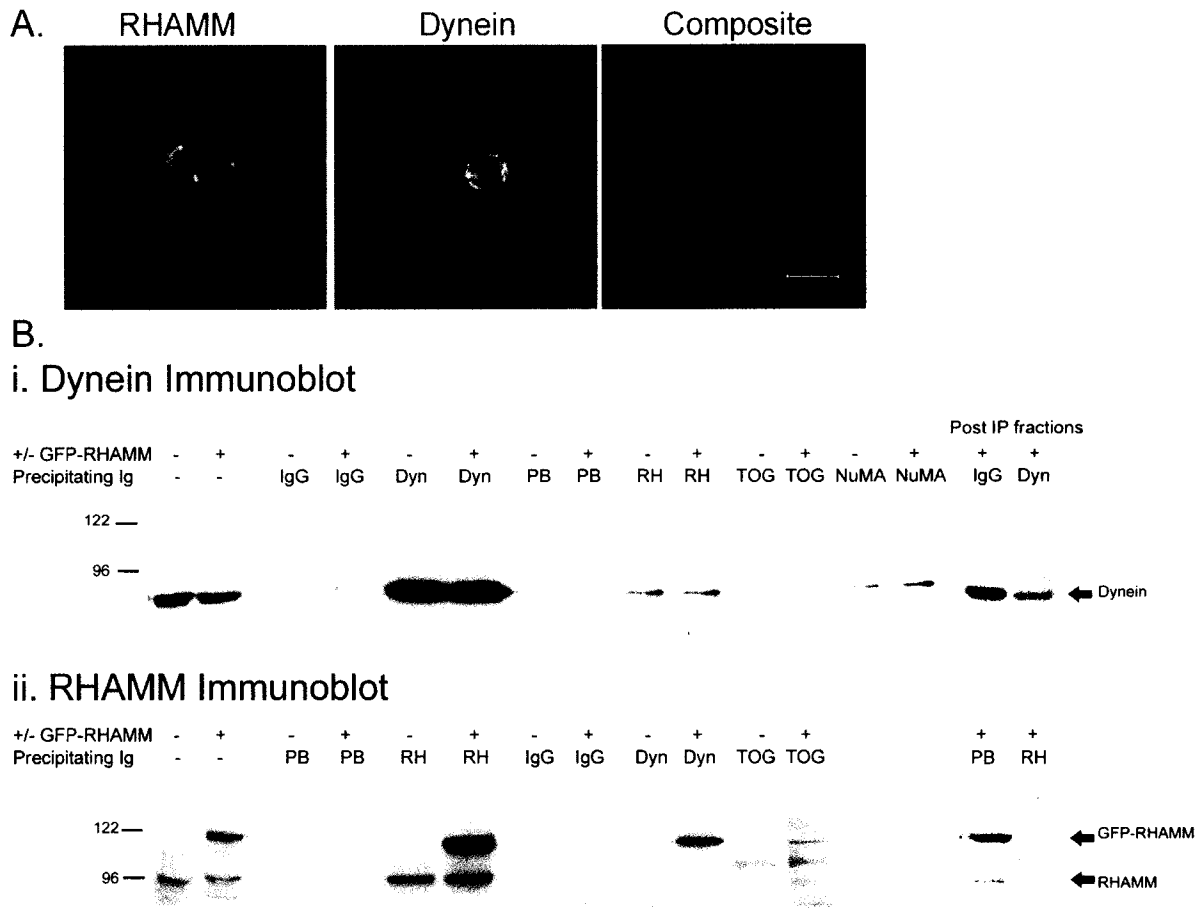

Figure 1-3: RHAMM interacts with the dynein motor complex (A) Endogenous RHAMM and dynein colocalize at the spindle pole in mitotic HeLa cells. HeLa cells were methanol treated and stained sequentially with antibodies against RHAMM (polyclonal) and dynein light intermediate chain (monoclonal); Scale bar equals 10 um. (B) HeLa lysates were prepared as described in Materials and Methods. Immunoblot analysis of RHAMM and dynein levels indicates equivalent amounts within transfected and untransfected lysates. An additional band at 120 kDa within the transfected populations represents the GFP-RHAMM^{FL} species. Immunoprecipitation experiments were separately performed on 150 µl precleared lysates using a polyclonal RHAMM antibody, the prebleed immune sera, a polyclonal TOGp antibody, a polyclonal NuMA antibody, a monoclonal dynein intermediate chain antibody (Sigma) or a IgG2a isotype control antibody (Southern Biotechnology Inc.) as described in Materials and Methods. 25µl (one-fifth of the immunoprecipitation volume) of precleared lysate and post-IP fractions were analysed to determine relative quantity and efficiency of the precipitations. The resulting immunprecipitates were

blotted with dynein intermediate chain monoclonal antibodies (i. Dynein immunoblot)) or a RHAMM polyclonal serum (ii. RHAMM immunoblot). The expected band size for dynein (dynein immunoblot) as well as endogenous RHAMM and GFP-RHAMM (RHAMM immunoblot) are shown with arrows. Transfected (+ GFP-RHAMM) and untransfected (- GFP-RHAMM) lysates are indicated above the blot as are the precipitating antibodies for the experiment. Post precipitation (IP) fractions for the transfected lysates are shown to indicate the relative efficiency of precipitation for IgG and dynein (dynein immunoblot) or prebleed and RHAMM (RHAMM immunoblot). For Dynein immunoblot, all lanes exposed for 30 seconds. For RHAMM immunoblot, lanes 2-6 were exposed for 15 secs while lanes 1,2,7-14 were exposed for 60 secs. Lane 1; untransfected (ut) lysates. 2; transfected (t) lysates. 3; ut lysate precipitated by prebleed (PB) antiserum. 4; t lysates precipitated with PB antiserum. 5; ut lysate precipitated by RHAMM (RH) antiserum. 6; t lysates precipitated with RH antiserum. 7; ut lysate precipitated by IgG isotype matched monoclonal antibody. 8; t lysates precipitated with IgG antibody. 9; ut lysate precipitated by monoclonal anti-dynein (Dyn) antibody. 10; t lysate precipitated by monoclonal anti-dynein (Dyn) antibody. 11; ut lysate precipitated by TOG antiserum. 12; t lysates precipitated with TOG antiserum; t lysates precipitated with anti-dynein antibody. 13; post-IP fractions following negative control precipitation (IgG or PB). 14; post-IP fractions demonstrating efficiency of positive control precipitation (Dyn or RHAMM).

To extend the confocal colocalization data, we investigated the ability of RHAMM antibodies to coimmunoprecipitate dynein intermediate chain from interphase and mitotic Xenopus extracts. A cell cycle-dependent NuMA-dynein-dynactin complex has been identified in immunoprecipitates using either anti-dynein or anti-NuMA antibody within the Xenopus system (Merdes et al., 1996),(Merdes et al., 2000). However, the NuMA-dynein-dynactin complex seems to be less stable in higher vertebrate cells with some, but not others, able to co-immunoprecipitate these protein complexes (Zeng, 2000). This raised the possibility that it may also be difficult to detect a RHAMM-dynein complex in HeLa cells. Thus, we analysed RHAMM-dynein

interactions in Xenopus extracts. Immunoprecipitation of mitotic and interphase Xenopus extracts with RHAMM antibodies revealed a major species at 95 kDa as well as minor bands around 150, 113 and 85 kDa (not shown). These sizes are consistent with those published for RHAMM species in various mammalian tissues (Assmann et al., 1999), (Hall et al., 1995). RHAMM antibodies coimmunoprecipitated dynein, with slight amplification within M phase extracts, but some dynein was found to interact with RHAMM during interphase (not shown). Interestingly, the monoclonal dynein intermediate chain antibody was unable to co-immunoprecipitate RHAMM protein, consistent with our observation that only a fraction of dynein was associated with RHAMM, and vice versa.

To confirm this association in mammalian cells, HeLa extracts were transiently transfected with GFP-RHAMM^{FL}. CHAPS soluble lysates from transfected, or untransfected, populations were separately immunoprecipitated with an anti-intermediate chain dynein monoclonal antibody, IgG2a control antibody, a polyclonal RHAMM antibody, a polyclonal TOGp antibody, a polyclonal NuMA antibody and a non-immune serum. As demonstrated in Figure 1-3C lanes 1 and 2, transfected and untransfected lysates contained comparable amounts of endogenous proteins with the transfected populations overexpressing a GFP-RHAMM species of approximately 120 kDa molecular weight (lane 2, RHAMM immunoblot). Recently, dynein has been coimmunoprecipitated from HeLa extracts with NuMA antiserum; for this reason, we included a NuMA immunoprecipitation as a positive control for association with dynein (Bhattacharya et al., 2002). Also, as the drosophila homolog of TOGp, msps, utilizes the

Ncd motor, and not the dynein complex, to localize to centrosomes (Cullen and Ohkura, 2001), TOGp immunoprecipitation of dynein served as a negative control. RHAMM antibodies coimmunoprecipitated dynein from transfected and untransfected lysates. Comparison of the amount of co-precipitated dynein with the western blot signal seen in the total lysates indicates that, under the conditions used here, only a fraction of dynein is recovered in a complex with RHAMM. Although the level of coprecipitated dynein was low, the amount was similar to that precipitated by NuMA antibodies. The specificity of the RHAMM-dynein interaction is demonstrated by the inability of TOGp antibodies, control IgG2a and non-immune serum to coimmunoprecipitate dynein. The reciprocal coimmunoprecipitation of RHAMM with dynein intermediate chain antibodies was achieved in transfected and untransfected HeLa lysates; again, comparison with the western blot signal indicates that only a fraction of endogenous RHAMM is precipitated by dynein. TOG antibodies also co-immunoprecipitated GFP-RHAMM^{FL} from transfected lysates; this result is consistent with live cell observation, within RPMI 8226, of accumulation of GFP-RHAMM^{FL} aggregates at the cell periphery and vectoral movement of GFP-RHAMM^{FL} towards the cell body (see Chapter 2, Figure 2-3B). Thus, the dynamic redistribution of GFP-RHAMM^{FL} in live suspension cells is consistent with minus-end directed motion, mediated by the dynein motor complex, and plus-end association, likely mediated through an interaction with TOG.

Overexpression of GFP-RHAMM fusions initiates a mitotic block in RPMI 8226 and HeLa cells

As GFP-RHAMM^{FL} does not generate stable transfectants within RPMI 8226 and HeLa cells, time-lapse confocal microscopy was used to follow the kinetics of mitosis within these transfectants. Transiently transfected GFP-RHAMM^{FL} cells arrested in mitosis (Figure 1-4Ai). These transfected cells failed to divide, mitotic spindles broke down and the cells underwent apoptosis (Figure 1-4i). In order to demonstrate that the visualization techniques were not causing the mitotic block and that the GFP tag was not influencing the kinetics of mitosis, tubulin-GFP fusions were stably transfected into 8226 cells and followed through mitosis. These cells demonstrated normal division (Figure 1-4Aii).

A. i)GFP-RHAMM^{FL} (8226)

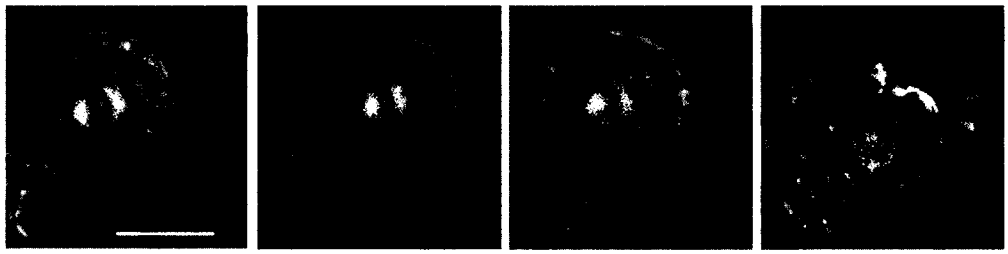

ii)GFP-tubulin (8226)

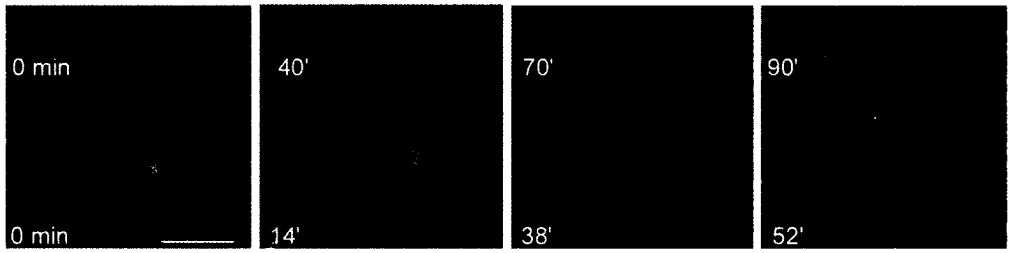

B. GFP-RHAMM^{FL} α-tubulin/DAPI Composite

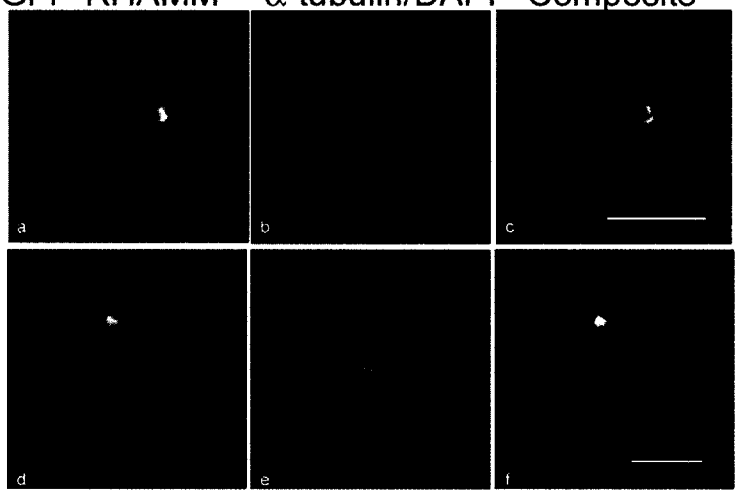

C.

Cells	Cells Examined (n)	Mitoses (n)	Mitotic Index	Metaphases* (n)	Metaphase/ Mitotic	M : A + C**	Apoptotic	Abnormal***
8226	3680	186	5.05	48	25.80%	1.1 : 1	0.30%	0
8226_EGFPC1	3952	201	5.09	54	26.90%	1.2 : 1	1.70%	0
8226_C1RHAMMFL	3436	136	3.96	77	56.62%	4.3 : 1	5.20%	3.90%
8226_C1RHAMMFL(>20hr post)	2142	100	4.67	68	68.00%	4.9 : 1	7.50%	6.60%

*Metaphases (M) defined by bipolar spindle or nuclear envelope breakdown
**ration of M to the sum of Anaphases (A) and Cytokinesis (C)
***defined by large GFP clusters
Cells examined 12, 16, 20 and 36 hours post transfection

Figure 1-4 GFP-RHAMM^{FL} overexpression inhibits mitotic progression in 8226 and HeLa (not shown).

Figure 1-4: GFP-RHAMM^{FL}overexpression inhibits mitotic progression in RPMI 8226 and HeLa (not shown). RPMI 8226 or HeLa cells were transfected with EGFPC1-RHAMM^{FL}, incubated at 37^{0}C for six hours and visualized in the presence or absence of Hoescht 33342 at 5ug/ml. i) Overexpression of EGFPC1-RHAMM^{FL} within RPMI 8226 and HeLa (not shown) during metaphase induced a block in chromosome alignment and spindle separation, leading to spindle breakdown and cell death. Transfected cells were incubated at 37^{0}C, 5% CO_2 and visualized every 5min for 10 hrs. (ii) Overexpression of EGFPC1-tubulin within RPMI 8226 did not affect progression through the cell cycle. Within this population, anaphase was completed (~40min) approximately 25 min following metaphase (14min). Scale bars equivalent to 10 μm **(B)** Overexpression of GFP-RHAMM^{FL} in RPMI 8226 led to the accumulation of mitotic cells in prometaphase (a-c) and metaphase (d-f) with unaligned chromosomes. Cells were transfected, methanol treated at defined timepoints and stained with monoclonal antibodies against α-tubulin. DNA was visualized with DAPI. Scale bars equivalent to 10μm **(C)** Graphical representation for time-line analysis of mitotic and apoptotic status of untransfected RPMI 8226, EGFP C1 (vector control) transfected RPMI 8226, and GFP-RHAMM^{FL} transfected RPMI 8226 at 12, 16, 20 and 36 hours post transfection. Transfected cells were sorted based on viability and fluorescence at 8-10 hours post transfection. Transfected cells were identified as interphase, prophase, prometaphase, metaphase, anaphase, cytokinesis and apoptotic based on the state and condensation of their DNA. Transfected cells were classified as abnormal if they contained large aggregates of GFP-RHAMM (data not shown); the microtubule staining of these cells seemed more diffuse and less organized than cells lacking these aggregates. However, DAPI staining did not indicate that these cells were apoptotic.

To quantitate the level of GFP-RHAMM^{FL} overexpression and its effect on mitosis, RPMI 8226 cells were transiently transfected with GFP-RHAMM^{FL} or EGFP-C1 vector and sorted 8 hours later. An aliquot of transfected cells was examined by immunoblot for overexpression at 16 hours post transfection (Figure 1-5A). 8226 transfected with EGFPC1 (Figure 1-5A, lane 1) expresses an endogenous RHAMM

species of approximately 90 kDa while the 8226 cells transiently transfected with GFP-RHAMM^{FL} (Figure 1-5A, lane 2) express endogenous RHAMM and a GFP-RHAMM protein at approximately 120 kDa. Band intensities, using digital imaging quantitation, indicated that the GFP-RHAMM intensity was approximately 5x that of the endogenous RHAMM. The level of overexpression in these sorted populations of transiently transfected RPMI 8226 cells is greater than that in the unsorted population of HeLa cells used in the immunoprecipitation experiments. This difference is due to the sorting of populations (i.e. many unsorted, lysed HeLa cells may not be expressing GFP-RHAMM) and likely gives a more definitive representation of the level of GFP-RHAMM, relative to endogenous RHAMM, within transfected cells. Transfected cells were fixed at 12, 16, 20 and 36 hours post transfection and stained with α tubulin, to identify the spindle, and with DAPI, to determine mitotic status. Untransfected RPMI 8226 and EGFPC1 (control vector) transfected RPMI 8226 served as controls. GFP-RHAMM^{FL} overexpression resulted in an increase in the frequency of prometaphase cells; approximately 70% of mitotic GFP-RHAMM^{FL} cells were prometaphase arrested 20 hours post transfection (Figure 1-4B and 1-4C). Interestingly, true metaphase alignment of chromosomes was not achieved in GFP-RHAMM^{FL} transfected cells. Likely due to the prometaphase arrest, few GFP-RHAMM^{FL} transfected cells were observed in anaphase or cytokinesis as demonstrated by the increasing metaphase: anaphase + cytokinesis ratio (Figure 1-4C). In combination with the prometaphase arrest, GFP-RHAMM^{FL} overexpression resulted in a dramatic increase in apoptotic cells as well as the presence of cells with large GFP-RHAMM^{FL} clusters (not shown). It is unclear if these large GFP-RHAMM^{FL} clusters precede apoptosis; these clusters did not colocalize with α-tubulin and were

phenotypically similar to those identified by overexpression of GFP-TACC domain fusions (Gergely et al., 2000a).

Inhibition of endogenous RHAMM results in abnormal mitotic figures

In order to further investigate the mitotic functions of RHAMM, a polyclonal peptide-specific antibody was created against the carboxy-terminal peptide sequence G^{682}-K^{697}, of RHAMM (Figure 1-5A). This sequence is outside the conserved basic leucine zipper motif to avoid inhibiting Hklp2 function. This serum was affinity purified and the specificity of the antibody was tested by immunoblotting endogenous RHAMM and GFP-$RHAMM^{FL}$, immunoprecipitating endogenous RHAMM from HeLa and 8226 and colocalization with GFP-$RHAMM^{FL}$ in HeLa and 8226 (Figure 1-5A).

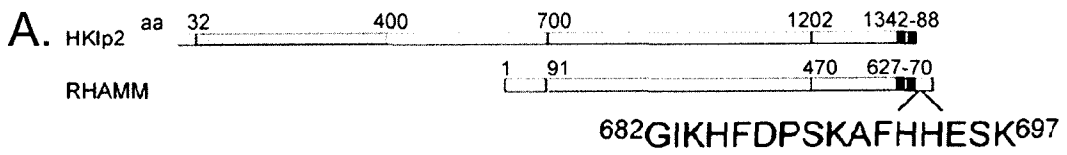

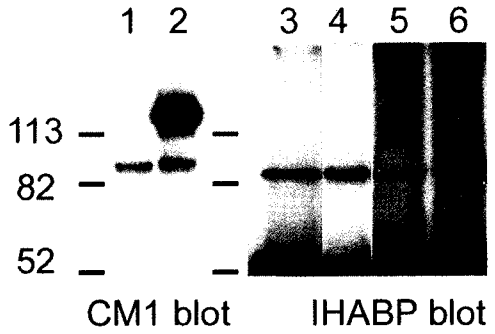

1. CM1 blot of 8226-EGFPC1
2. CM1 blot of 8226-GFPRHAMM^{FL}

3. IHABP IP of HeLa
4. IHABP IP of 8226
5. CM1 IP of HeLa
6. CM1 IP of 8226

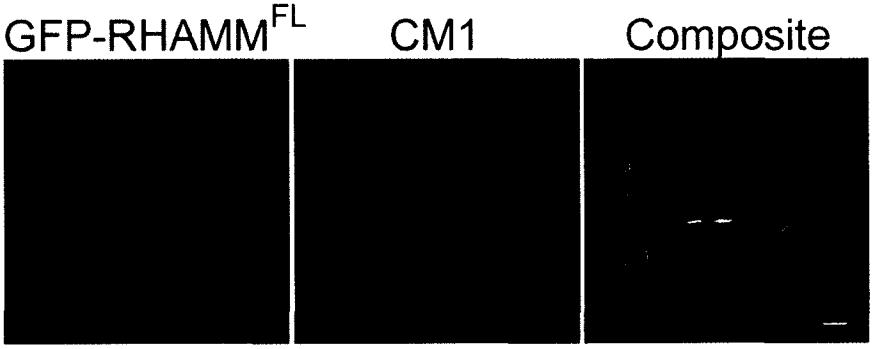

B.

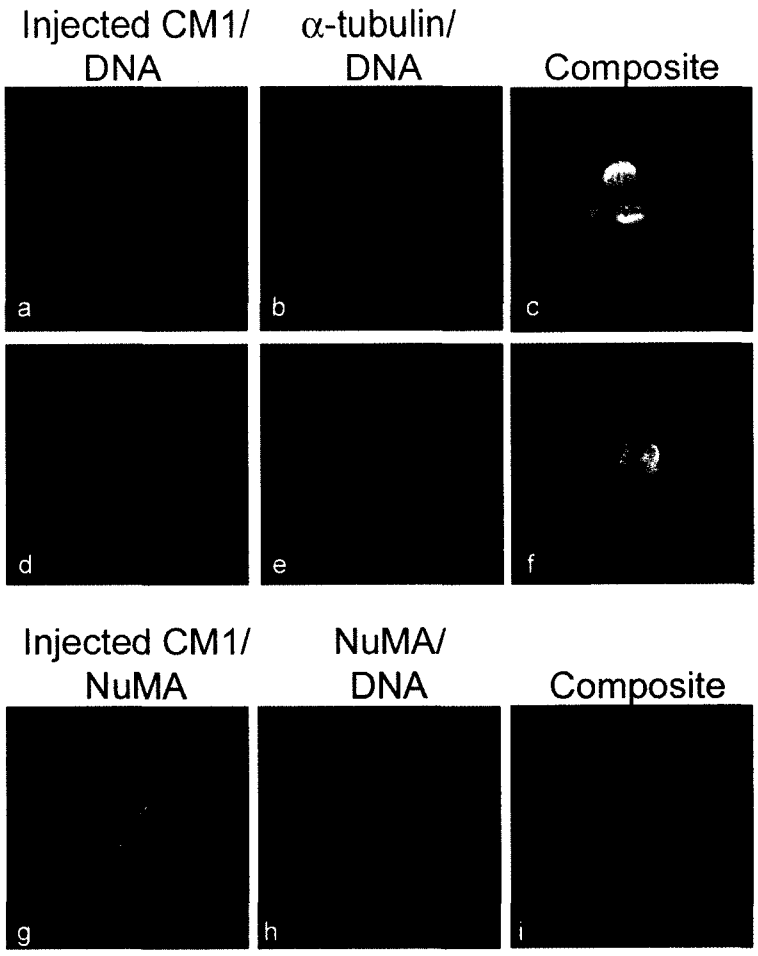

C.

Injected IgG	Cells Examined(n)	Bipolar (%)	Tripolar (%)	Tetrapolar (%)
-	325	92 +/- 4.7	5 +/- 2.5	3 +/- 3
non-immune	177	91 +/- 7.6	5 +/- 5	4 +/- 2.5
CM1	272	75 +/- 2.1	11 +/- 3.5	14 +/- 4.3

Figure 1-5 Microinjection of anti-RHAMM antibodies induce multipolar spindles

Figure 1-5: Microinjection of anti-RHAMM antibodies induces multipolar spindles.

(A) A representation of the location, relative to Hklp2, and sequence of the peptide from which a polyclonal anti-RHAMM serum (CM1) was derived. The specificity of the purified CM1 serum was determined by immunofluorescence, immunoblotting (lane 1 and 2), immunoprecipitation (lane 3-6) and reactivity with GFP-RHAMM^{FL} fusion proteins. Lane 1 and 2 demonstrates that CM1 specifically blots endogenous RHAMM and GFP-RHAMM in RPMI 8226 cells transfected with GFP-RHAMM (lane 2) or vector control (EGFP-C1, lane 1). Lanes 3-6 demonstrates that CM1 immunoprecipitates from HeLa and RPMI 8226 lysates an equivalent sized protein as the previously validated IHABP antibody. Scale bar equals 5um. (B) Hela cells were plated onto gridded coverslips and were synchronized at the G1/S boundary by a double thymidine block. Cells were injected 1–2 h after they were released from the G1/S boundary. Asymmetrical and symmetrical tripolar and tetrapolar spindles were observed. DAPI staining revealed that all spindles in these abnormal mitotic figures segregated DNA. Microinjected RHAMM Ab (first column) reveals that the injected antibody localizes to the spindle poles. NuMA staining (g-i) confirms that the abnormal spindle poles contain NuMA. (C) Graphical representation of microinjection results. Four separate experiments were performed and spindles were scored as bipolar, tripolar, tetrapolar and hexapolar spindles (not shown). The results are given as mean percentage and standard deviation of the mean for each spindle phenotype.

To determine whether spindle integrity was affected by disruption of RHAMM function, RHAMM peptide antibodies were microinjected into the cytoplasm of cells arrested at the G_1/S boundary. The microinjected cells were released from the G_1/S boundary and allowed to proceed to mitosis before fixation and analysis by immunofluorescence. In four separate experiments, microinjection of anti-RHAMM antibodies into HeLa cells led to the formation of tripolar and tetrapolar spindles within 11+/- 3.4 % and 14 +/- 4.3 % of injected cells, respectively (Figure 1-5B). Immunoblocking RHAMM function resulted in symmetrical and asymmetrical tripolar and tetrapolar spindles. Asymmetrical tetrapolar spindles (Figure 1-5B) were

phenotypically similar to those observed within NuMA-immunoblocked CFPAC-1 cells (Gordon et al., 2001); however, microinjection of RHAMM antibodies did not significantly affect spindle focussing. Thus, RHAMM does not appear to be essential for spindle focussing but rather for maintenance of spindle integrity. The fact that roughly three-quarters of injected cells have phenotypically normal spindles suggests that other proteins can compensate for loss of RHAMM function. With all abnormal spindles, the injected RHAMM antibodies and NuMA colocalized to the aberrant spindle poles (Figure 1-5B).

Chromosomal location and phylogenetic analysis of RHAMM primary sequence suggests membership in the TACC family.

The TACC protein family members are centrosomal proteins that associate with microtubules minus ends through a conserved coiled-coil carboxy-terminal TACC domain and are putative regulators of the mitotic apparatus. Despite the low sequence identity within the TACC domain (Figure 1-1C), RHAMM shares structural and functional similarity to the TACC family. A defining feature of the TACC proteins is an evolutionary conserved relationship with the fibroblast growth factor receptor (FGFR) gene family (Still et al., 1999b). *TACC* 1,2 and 3 genes map proximal to *FGFR*1, 2, and 3 genes on chromosomes 8p11, 10q26 and 4p16.3, respectively. Currently, no TACC gene has been identified proximal to the *FGFR*4 locus on chromosome 5q35.1-qter. *RHAMM* maps to a chromosomal region near to the *FGFR4* gene locus at 5q33.2-qter. Given the proximity of *RHAMM* to *FGFR4*, we utilized phylogenetic analysis to compare

the carboxy-terminal 240 aa of RHAMM to its current protein family members, the $B(X)_7B$ hyaladherins, the TACC family and the Klp2 family (Figure 1-6).

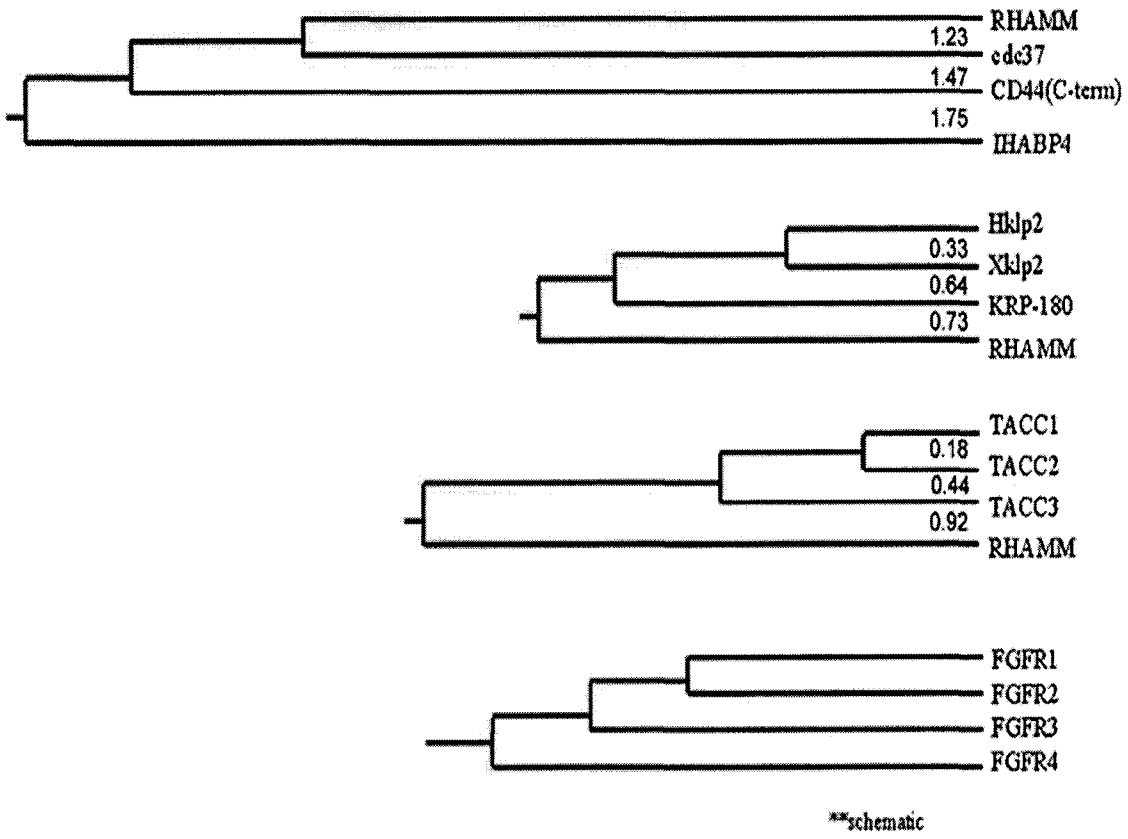

Figure 1-6: Phylogenetic relationships between members of the BX_7B, TACC, Klp2 and FGFR families. Phylogenetic relationships and distances were determined by the MEGA software package using UPGMA phylogenetic analysis. COOH-terminal sequnces were aligned with BLAST and PEPTOOL software, the alignments were entered and analysed by MEGA Software. (A) Relationship between the COOH-terminal 240 aa, which contains the BX_7B motif (s), of BX_7B family members. (B) Relationship between the COOH-terminal 240 aa, which contains the leucine zipper motif, of klp2 family members and RHAMM. (C) Relationship between the COOH-terminal 240 aa, which contains the TACC domain, of TACC family members and RHAMM. (D) Schematic relationship between FGFR family members as outlined in Still et al., 1999b.

Phylogenetic analysis was performed with the MEGA software program using carboxy-terminal sequences previously aligned by BLAST and PEPTOOL software (Kumar et al., 2000) (Tatusova and Madden, 1999) (Wishart et al., 1997). Phylogeny inference was performed using the Unweighted Pair Group Method with Arithmetic Mean (UPGMA) and Neighbour-Joining (not shown) distance methods and branch lengths are shown. Theoretically, the evolutionary distance separating two sequences can be defined as the number of mutational events per site underlying the evolutionary history separating these sequences (Brocchieri, 2001). We utilized the Poisson-correction method to approximate these distances.

BLAST analysis of the $B(X)_7B$ family members revealed no significant similarity in the $B(X)_7B$ containing domains. CD44, which binds HA with a classical extracellular link domain, contains an intracellular, carboxy-terminal $B(X)_7B$ domain and this motif was included in the phylogenetic analysis. As demonstrated by their pairwise evolutionary distances, the $B(X)_7B$ family members maintain little evolutionary convergence in their functional domains. The carboxy-terminus of RHAMM, currently defined as a $B(X)_7B$ domain, shares no significant sequence similarity, and a minimal evolutionary relationship, with other $B(X)_7B$ family members.

Comparison of the carboxy-terminus of RHAMM with the TACC family reveals that RHAMM diverged prior to the formation of the TACC3 and TACC1/2 ancestor. This is consistent with the divergence of FGFR4 in the phylogenetic tree of the FGFR family. The carboxy-terminus of RHAMM shares minimal identity (~20%) with TACC1.

Therefore, we included the PACT domain of human pericentrin in the phylogenetic analysis to control for the possibility that the RHAMM/TACC relationship is wholly due to RHAMM's coiled-coil structure. The PACT domain is an alternative conserved centrosomal targeting domain (Gillingham and Munro, 2000). Pericentrin occupied a separate branch that was 1.10 evolutionary distance units from TACC1 (not shown). Thus, the carboxy-terminus of RHAMM is more closely related to the TACC domain than is the PACT domain of human pericentrin.

BLAST analysis of the carboxy-terminal 240 aa of RHAMM reveals significant homology to the Klp2 family (e^{-13}). As there is currently only one human protein member of the Klp2 family (Hklp2), we compared the carboxy-terminal domain of human RHAMM and the sea urchin Klp2-related KRP-180 with those of Hklp2 and Xklp2 to estimate the evolutionary distance between these motifs. As shown in Figure 6, the evolutionary distance between RHAMM (0.73) and Hklp2/Xklp2 approximates that of KRP-180 (0.64). Therefore, the centrosomal targeting motif of RHAMM is more closely related to the Klp2 family than the TACC family. However, the fact that RHAMM lacks the highly conserved molecular motor domain precludes it from membership in the Klp2 family.

Discussion

In this study, we have identified an important functional association between RHAMM, the centrosome, and microtubule associated proteins. We find that: (1) RHAMM is a centrosomal protein that localizes to interphase microtubules, spindle poles, the anaphase midbody and the telophase midzone microtubules; (2) RHAMM contains a centrosome targeting, carboxy-terminal basic leucine zipper and, like Xklp2, interacts with the dynein motor complex; and (3) RHAMM participates in the maintenance of the mitotic spindle. Moreover, RHAMM is an 85 kDa, acidic coiled coil protein that is transforming when overexpressed (Hall et al., 1995), functionally related to other TACC family members and, like *TACC* 1-3, the *RHAMM* gene is located near the putative *FGFR4-TACC4* gene locus.

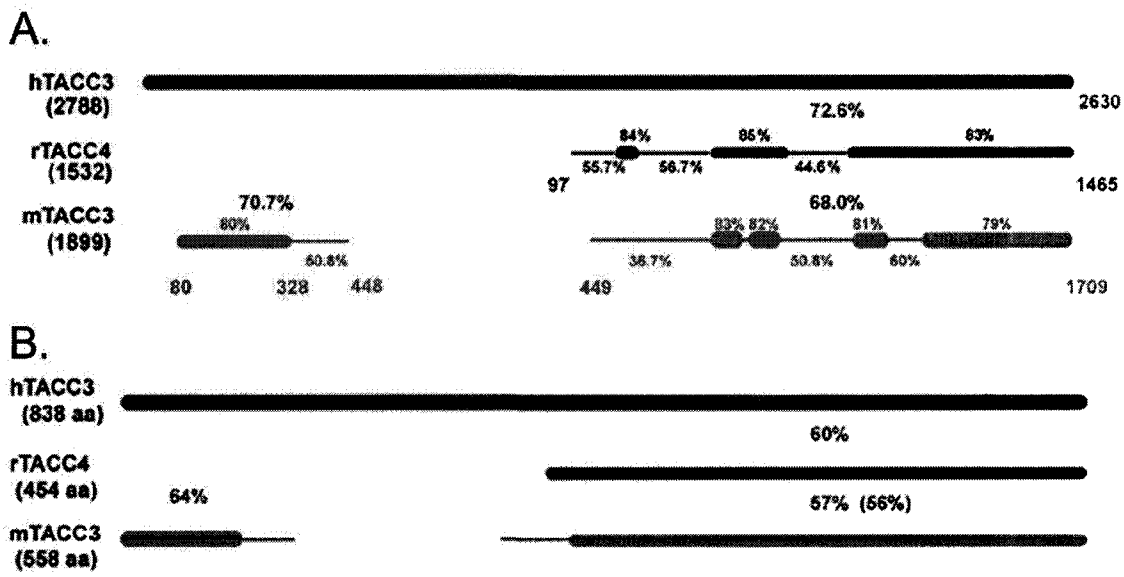

Figure 1-7 Sequence comparison at the cDNA and protein level suggests that rTACC4 is a TACC3 variant initiating at an alternative 5' start site

Figure 1-7: Sequence comparison at the cDNA and protein level suggests that rTACC4 is a TACC3 variant initiating at an alternative 5' start site. Schematic representation of BLAST 2 sequence (nucleotide) analysis of rabbit TACC4 (rTACC4; accession number AF372837) and murine TACC3 (mTACC3; accession number NM_011524) against human TACC3 (hTACC3; accession number NM_006342). The length of the sequences, in base pairs, are bracketed under the sequence name. rTACC4 and mTACC3 were compared to hTACC3 sequence. The overall identities between rTACC4, or mTACC3, and hTACC3 are shown in large font while the identities of smaller segments are shown in small font. The lower levels of identity (</= 60%) were insignificant from BLAST analysis and were obtained by PEPTOOL alignment of the sequences. B) Schematic representation of BLAST 2 sequence (protein) analysis of rabbit TACC4 (rTACC4; accession number AAK54244) and murine TACC3 (mTACC3; accession number XP_132002) against human TACC3 (hTACC3; accession number Q9Y6A5). The length of the sequences, in amino acids (aa), are bracketed under the sequence name. rTACC4 and mTACC3 were compared to hTACC3 sequence. The overall identities between rTACC4, or mTACC3, and hTACC3 are shown while the level of identity between mTACC3 and rTACC4 is bracketed.

To date, no human TACC4 protein has been identified. A TACC4 protein has been identified in rabbits (rTACC4) (accession number AAK54244, 454 aa) and shown to directly interact with AKAP350 (Steadman et al., 2002). However, BLAST analysis of the corresponding cDNA (AF372837) against the human genome localized this gene to chromosome 4p16.3 (up to e^{-29}) with exon boundaries that mirror TACC3. This gene product may be the result of a secondary start site in rTACC3 rather than a bone fide rTACC4; in fact, alignment of rTACC4 protein sequence (AAK54244) with a hTACC3 variant (Q9Y6A5) reveals higher identity (60%) than alignment of mTACC3 (XP_132002) with hTACC3 (57%) (Figure 1-7). Perhaps more convincingly,

examination of rTACC4, hTACC3 and mTACC3 cDNA demonstrates that regions of lowest identity between rTACC4 and hTACC3 are also less conserved in mTACC3 (Figure 1-7). Moreover, the tissue expression of rTACC4 is similar to that defined for mTACC3. MTACC3, but not mTACC2, is highly expressed in the testis, spleen, and lung and absent in the brain, liver, kidney and muscle (Piekorz et al., 2002); similarly, rTACC4 is highly expressed in the spleen and gut and absent in the brain and liver (Steadman et al., 2002). Interestingly, RHAMM, like TACC3 and rTACC4, is highly expressed in the testis, colon and stomach but absent in the brain, liver, heart, kidney and lung (Line et al., 2002).

Currently, RHAMM is characterized by its HA binding potential through the carboxy-terminal $B(X)_7B$ domains (Yang et al., 1993, 1994). RHAMM has two additional $B(X)_7B$ domains within its NH_2-terminal globular head ($K^{40}(X)_7K^{48}$ and $R^{67}(X)_7K^{75}$) which, like the carboxy-terminal domains, contain two internal basic residues.These domains have been identified as binding motifs for interphase and mitotic microtubules (Assmann et al., 1999). We have also shown that the Klp2 family contain putative $B(X)_7B$ HA binding domains that are virtually identical to those in RHAMM. For the Klp2 family, these domains are defined as a BZIP motif that allows for centrosomal localization through an indirect interaction with the dynein/dynactin motor complex. We suggest that in addition to their participation in HA binding (Yang et al., 1993), the carboxy-terminal $B(X)_7B$ domains of RHAMM are vital components of a consensus BZIP domain that targets this protein to the centrosome and allows for an interaction with the dynein/dynactin complex.

As an acidic (pI 5.64), extensively coil coiled centrosomal protein that maintains mitotic spindle integrity and is chromosomally located proximal to the *FGFR4* locus, RHAMM is a good candidate to be the fourth member of the TACC family. However, RHAMM does not contain the highly conserved, carboxy terminal, centrosomal targeting TACC domain. In fact, RHAMM utilizes a carboxy-terminal BZIP motif ($L\text{-}X_6\text{-}L\text{-}X_6\text{-}L\text{-}X_6$), preceded by lengthy coil coiled structure, to localize to centrosomes. Interestingly, many centrosomal targeting domains may be defined by coiled coil structure terminating in a BZIP motif. Examination of the alignments of two defined centrosomal targeting domains, the TACC and PACT domain protein, reveals carboxy-terminal conservation of leucine residues (not shown). Interestingly, Xenopus and Human NuMA, which also interact with the dynein motor complex, contain a stretch of conserved leucines, $L^{209}\text{-}X_9\text{-}L\text{-}X_3\text{-}L\text{-}X_9\text{-}L\text{-}X_3\text{-}L\text{-}X_6\text{-}L$ that precedes an extensive predicted coiled coil structure (not shown). Recent sequence analysis predicts that NuMA may interact with dynactin through a predicted CH domain (aa 110-210) interaction with Arp 1 (Novatchkova and Eisenhaber, 2002); interestingly, the conserved BZIP motif outlined above lies at the terminus of the predicted CH domain. Moreover, a direct interaction between EB1 and the dynactin subunit $p150^{glued}$ has recently been localized to the carboxy-terminus of EB1 which contains a BZIP motif (Askham et al., 2002). Thus, evolutionary pressures may have allowed for divergence amongst centrosomal targeting domains while dictating conservation of coiled-coil structure terminating, or initiating, in a BZIP motif. RHAMM is unique to the human TACC family in its ability to interact with the dynein motor complex. To date, no association has been demonstrated between TACC1,2 or 3 and the dynein motor complex although it has been suggested that D-TACC and Msps may be

maintained in the vicinity of the spindle poles by the activity of microtubule-motor complexes like NuMA/dynein/dynactin (Lee et al., 2001). The divergence of the carboxy-terminal coiled coil domain of RHAMM from the TACC domain may have enabled a RHAMM-dynein interaction allowing for RHAMM-specific mitotic functions. Thus, RHAMM may be a new member of the TACC family or there may be another, yet to be identified, TACC protein located at 5q35.1. Currently, we conclude that RHAMM is a TACC-like protein and may, in fact, be TACC4.

As RHAMM can interact with microtubules both directly and indirectly, through an interaction with dynein, RHAMM may function in the maintenance of mitotic spindles by crosslinking centrosomal microtubules. A similar function has been proposed for NuMA, although NuMA has also been shown to affect spindle focussing as well as integrity. As RHAMM (85 kDa) is much smaller than NuMA (240 kDa), RHAMM-dynein complexes may function proximal to the centrosome compared to NuMA-dynein complexes. Thus, in RHAMM immunoblocked cells, NuMA-dynein complexes may maintain spindle focussing but, in a quarter of injected cells, not spindle integrity. In fact, NuMA is not displaced from the RHAMM-immunoblocked abnormal spindle poles. Endogenous RHAMM function may assist in spindle integrity and microtubule focussing, along with the minus end directed KIN C motor HSET, in the absence of NuMA but be inadequate to maintain spindle focussing.

To date, it is unclear if the interaction between RHAMM and the dynein motor complex is direct or indirect; the structural similarity of the carboxy-terminus of

RHAMM to Xklp2 would suggest that RHAMM, like Xklp2, is targeted to microtubule minus ends through an association with TPX2. The localization of RHAMM, as determined by immunofluorescence and GFP-RHAMM^{FL}, mirrors that of TPX2 throughout mitosis (Gruss et al., 2002). GFP-hTPX2 overexpression, like GFP-RHAMM^{FL}, initiates a prometaphase block and inhibition of TPX2 function, through microinjection of anti-TPX2 antibodies, resulted in abnormal mitoses in 37.8% of injected cells (Gruss et al., 2002). Interestingly, TPX2 has been recently shown to be essential for the spindle targeting of Aurora A kinase (Kufer et al., 2002). Thus, it is possible that RHAMM, like Aurora A kinase and Klp2, is dependent on TPX2 for spindle pole localization.

This work outlines an essential role for RHAMM in the organization and integrity of a bipolar spindle. The role of RHAMM in mitotic stability may partially explain its relationship to cancer. Overexpression of RHAMM, and its variants, characterizes both hematological malignancies and solid tumors (Crainie et al., 1999; Wang et al., 1998); additionally, RHAMM has been identified by SEREX (serological identification of antigens by recombinant expression cloning) analysis to be a tumor associated antigen in colon cancer, AML and CML (Greiner et al., 2002; Line et al., 2002). Autoantibodies to centrosomal proteins, like pericentrin, are a hallmark of autoimmune disease, like scleroderma (Doxsey et al., 1994)(Gavanescu et al., 1999)(Rattner et al., 1998). Moreover, NuMA has been investigated as a biomarker for colorectal cancer (Briggman et al., 1999). It is possible that the tumor-specific anti-RHAMM autoantibodies may be indicative of overexpression of RHAMM, or tumor specific expression of RHAMM

variants. Such RHAMM disregulation could potentially affect centrosomal and spindle pole dynamics with consequent dramatic, and possibly oncogenic, effects on cell shape, motility and ploidy.

References

Askham, J.M., K.T. Vaughan, H.V. Goodson, and E.E. Morrison. (2002). Evidence That an Interaction between EB1 and p150(Glued) Is Required for the Formation and Maintenance of a Radial Microtubule Array Anchored at the Centrosome. Mol Biol Cell. *13*:3627-45.

Assmann, V., D. Jenkinson, J.F. Marshall, and I.R. Hart. (1999). The intracellular hyaluronan receptor RHAMM/IHABP interacts with microtubules and actin filaments. J Cell Sci. *112*:3943-54.

Bhattacharya, N., Z. Wang, C. Davitt, I.F. McKenzie, P.X. Xing, and N.S. Magnuson. (2002). Pim-1 associates with protein complexes necessary for mitosis. Chromosoma. *111*:80-95.

Bitangcol, J.C., A.S. Chau, E. Stadnick, M.J. Lohka, B. Dicken, and E.K. Shibuya. (1998). Activation of the p42 mitogen-activated protein kinase pathway inhibits Cdc2 activation and entry into M-phase in cycling Xenopus egg extracts. Mol Biol Cell. *9*:451-67.

Boleti, H., E. Karsenti, and I. Vernos. (1996). Xklp2, a novel Xenopus centrosomal kinesin-like protein required for centrosome separation during mitosis. Cell. *84*:49-59.

Briggman, J., R. Genduso, C. Camara, B. Healy, K. Shapiro, R. Roos, S. Merrifield, J. Lifter, Y.J. Wu, E. Elder, and M. Talamonti. (1999). NuMA: evaluation of a new biomarker for the detection of low stage colorectal cancer. Anticancer Res. *19*:2411-4.

Brocchieri, L. (2001). Phylogenetic inferences from molecular sequences: review and critique. Theoretical Population Biology. *59*:27-40.

Cheeseman, I.M., S. Anderson, M. Jwa, E.M. Green, J. Kang, J.R. Yates, C.S. Chan, D.G. Drubin, and G. Barnes. (2002). Phospho-regulation of kinetochore-microtubule attachments by the aurora kinase ipl1p. Cell. *111*:163-72.

Chen, H.M., K.L. Schmeichel, I.S. Mian, S. Lelievre, O.W. Petersen, and M.J. Bissell. (2000). AZU-1: a candidate breast tumor suppressor and biomarker for tumor progression. Mol Biol Cell. *11*:1357-67.

Cokol, M., R. Nair, and B. Rost. (2000). Finding nuclear localization signals. EMBO Rep. *1*:411-5.

Compton, D.A., T.J. Yen, and D.W. Cleveland. (1991). Identification of novel centromere/kinetochore-associated proteins using monoclonal antibodies generated against human mitotic chromosome scaffolds. J Cell Biol. *112*:1083-97.

Crainie, M., A.R. Belch, M.J. Mant, and L.M. Pilarski. (1999). Overexpression of the receptor for hyaluronan-mediated motility (RHAMM) characterizes the malignant clone in multiple myeloma: identification of three distinct RHAMM variants. Blood. *93*:1684-96.

Cullen, C.F., and H. Ohkura. (2001). Msps protein is localized to acentrosomal poles to ensure bipolarity of Drosophila meiotic spindles. Nat Cell Biol. *3*:637-42.

Dionne, M.A., A. Sanchez, and D.A. Compton. (2000). ch-TOGp is required for microtubule aster formation in a mammalian mitotic extract. J Biol Chem. *275*:12346-52.

Doxsey, S.J., P. Stein, L. Evans, P.D. Calarco, and M. Kirschner. (1994). Pericentrin, a highly conserved centrosome protein involved in microtubule organization. Cell. *76*:639-50.

Gaglio, T., A. Saredi, J.B. Bingham, M.J. Hasbani, S.R. Gill, T.A. Schroer, and D.A. Compton. (1996). Opposing motor activities are required for the organization of the mammalian mitotic spindle pole. J Cell Biol. *135*:399-414.

Gares, S.L., N. Giannakopoulos, D. MacNeil, R.J. Faull, and L.M. Pilarski. (1998). During human thymic development, beta 1 integrins regulate adhesion, motility, and the outcome of RHAMM/hyaluronan engagement. J Leukoc Biol. *64*:781-90.

Gavanescu, I., D. Vazquez-Abad, J. McCauley, J.L. Senecal, and S. Doxsey. (1999). Centrosome proteins: a major class of autoantigens in scleroderma. J Clin Immunol. *19*:166-71.

Gergely, F., C. Karlsson, I. Still, J. Cowell, J. Kilmartin, and J.W. Raff. (2000a). The TACC domain identifies a family of centrosomal proteins that can interact with microtubules. Proc Natl Acad Sci U S A. *97*:14352-7.

Gergely, F., D. Kidd, K. Jeffers, J.G. Wakefield, and J.W. Raff. (2000b). D-TACC: a novel centrosomal protein required for normal spindle function in the early Drosophila embryo. Embo J. *19*:241-52.

Giet, R., D. McLean, S. Descamps, M.J. Lee, J.W. Raff, C. Prigent, and D.M. Glover. (2002). Drosophila Aurora A kinase is required to localize D-TACC to centrosomes and to regulate astral microtubules. J Cell Biol. *156*:437-51.

Gillingham, A.K., and S. Munro. (2000). The PACT domain, a conserved centrosomal targeting motif in the coiled- coil proteins AKAP450 and pericentrin. EMBO Rep. *1*:524-9.

Gordon, M., L. Howard, and D. Compton. (2001). Chromosome Movement in Mitosis Requires Microtubule Anchorage at Spindle Poles. J Cell Biol. *152*:425-34.

Greiner, J., M. Ringhoffer, M. Taniguchi, A. Schmitt, D. Kirchner, G. Krahn, V. Heilmann, J. Gschwend, L. Bergmann, H. Dohner, and M. Schmitt. (2002). Receptor for hyaluronan acid-mediated motility (RHAMM) is a new immunogenic leukemia-associated antigen in acute and chronic myeloid leukemia. Exp Hematol. *30*:1029.

Gruss, O.J., R.E. Carazo-Salas, C.A. Schatz, G. Guarguaglini, J. Kast, M. Wilm, N. Le Bot, I. Vernos, E. Karsenti, and I.W. Mattaj. (2001). Ran induces spindle assembly by reversing the inhibitory effect of importin alpha on TPX2 activity. Cell. *104*:83-93.

Gruss, O.J., M. Wittmann, H. Yokoyama, R. Pepperkok, T. Kufer, H. Sillje, E. Karsenti, I.W. Mattaj, and I. Vernos. (2002). Chromosome-induced microtubule assembly mediated by TPX2 is required for spindle formation in HeLa cells. Nat Cell Biol. *4*:871-9.

Hall, C.L., B. Yang, X. Yang, S. Zhang, M. Turley, S. Samuel, L.A. Lange, C. Wang, G.D. Curpen, R.C. Savani, and et al. (1995). Overexpression of the hyaluronan receptor RHAMM is transforming and is also required for H-ras transformation. Cell. *82*:19-26.

Hardwick, C., K. Hoare, R. Owens, H.P. Hohn, M. Hook, D. Moore, V. Cripps, L. Austen, D.M. Nance, and E.A. Turley. (1992). Molecular cloning of a novel hyaluronan receptor that mediates tumor cell motility [published erratum appears in J Cell Biol 1992 Aug;118(3):753]. J Cell Biol. *117*:1343-50.

Haren, L., and A. Merdes. (2002). Direct binding of NuMA to tubulin is mediated by a novel sequence motif in the tail domain that bundles and stabilizes microtubules. J Cell Sci. *115*:1815-24.

Karsenti, E., and I. Vernos. (2001). The mitotic spindle: a self-made machine. Science. *294*:543-7.

Kirschner, M., and T. Mitchison. (1986). Beyond self-assembly: from microtubules to morphogenesis. Cell. *45*:329-42.

Kufer, T.A., H.H. Sillje, R. Korner, O.J. Gruss, P. Meraldi, and E.A. Nigg. (2002). Human TPX2 is required for targeting Aurora-A kinase to the spindle. J Cell Biol. *158*:617-23.

Lee, M.J., F. Gergely, K. Jeffers, S.Y. Peak-Chew, and J.W. Raff. (2001). Msps/XMAP215 interacts with the centrosomal protein D-TACC to regulate microtubule behaviour. Nat Cell Biol. *3*:643-9.

Line, A., Z. Slucka, A. Stengrevics, K. Silina, G. Li, and R.C. Rees. (2002). Characterisation of tumour-associated antigens in colon cancer. Cancer Immunol Immunother. *51*:574-82.

Lynn, B.D., X. Li, P.A. Cattini, E.A. Turley, and J.I. Nagy. (2001). Identification of sequence, protein isoforms, and distribution of the hyaluronan-binding protein RHAMM in adult and developing rat brain. J Comp Neurol. *439*:315-30.

Masellis-Smith, A., A.R. Belch, M.J. Mant, E.A. Turley, and L.M. Pilarski. (1996). Hyaluronan-dependent motility of B cells and leukemic plasma cells in blood, but not of bone marrow plasma cells, in multiple myeloma: alternate use of receptor for hyaluronan-mediated motility (RHAMM) and CD44. Blood. *87*:1891-9.

Merdes, A., R. Heald, K. Samejima, W.C. Earnshaw, and D.W. Cleveland. (2000). Formation of spindle poles by dynein/dynactin-dependent transport of NuMA. J Cell Biol. *149*:851-62.

Merdes, A., K. Ramyar, J.D. Vechio, and D.W. Cleveland. (1996). A complex of NuMA and cytoplasmic dynein is essential for mitotic spindle assembly. Cell. *87*:447-58.

Murray, A.W., and M.W. Kirschner. (1989). Cyclin synthesis drives the early embryonic cell cycle. Nature. *339*:275-80.

Nachury, M.V., T.J. Maresca, W.C. Salmon, C.M. Waterman-Storer, R. Heald, and K. Weis. (2001). Importin beta is a mitotic target of the small GTPase Ran in spindle assembly. Cell. *104*:95-106.

Novatchkova, M., and F. Eisenhaber. (2002). A CH domain-containing N terminus in NuMA? Protein Sci. *11*:2281-4.

Piekorz, R.P., A. Hoffmeyer, C.D. Duntsch, C. McKay, H. Nakajima, V. Sexl, L. Snyder, J. Rehg, and J.N. Ihle. (2002). The centrosomal protein TACC3 is essential for hematopoietic stem cell function and genetically interfaces with p53-regulated apoptosis. Embo J. *21*:653-64.

Pilarski, L.M., C.M. Maxwell, and S.L. Gares. (2001). RHAMM (CD168/IHABP). Protein Reviews on the Web. *2*:76-84.

Purohit, A., S.H. Tynan, R. Vallee, and S.J. Doxsey. (1999). Direct interaction of pericentrin with cytoplasmic dynein light intermediate chain contributes to mitotic spindle organization. J Cell Biol. *147*:481-92.

Rattner, J.B., G.J. Mack, and M.J. Fritzler. (1998). Autoantibodies to components of the mitotic apparatus. Mol Biol Rep. *25*:143-55.

Spicer A. .P, M. L. Roller, C. A. Camper, J. D. McPherson, J. J. Wasmuth, S. Hakim, C. Wang, E. A. Turley, J. A. McDonald. (1995) The human and mouse receptors for hyaluronan-mediated motility, RHAMM, genes (HMMR) map to human chromosome 5q33.2-qter and mouse chromosome 11. Genomics *30:*115-7

Steadman, B.T., P.H. Schmidt, R.A. Shanks, L.A. Lapierre, and J.R. Goldenring. (2002). Transforming acidic coiled-coil containing protein 4 interacts with centrosomal AKAP350 and the mitotic spindle apparatus. J Biol Chem. *15*:15.

Still, I.H., M. Hamilton, P. Vince, A. Wolfman, and J.K. Cowell. (1999a). Cloning of TACC1, an embryonically expressed, potentially transforming coiled coil containing gene, from the 8p11 breast cancer amplicon. Oncogene. *18*:4032-8.

Still, I.H., P. Vince, and J.K. Cowell. (1999b). The third member of the transforming acidic coiled coil-containing gene family, TACC3, maps in 4p16, close to translocation breakpoints in multiple myeloma, and is upregulated in various cancer cell lines. Genomics. *58*:165-70.

Tatusova, T.A., and T.L. Madden. (1999). BLAST 2 Sequences, a new tool for comparing protein and nucleotide sequences. FEMS Microbiol Lett. *174*:247-50.

Turley E. A. (1992). Hyaluronan and cell locomotion. Cancer Metastasis Rev 11:21-30.

Turley E. A., J. Torrance. (1985). Localization of hyaluronate and hyaluronate-binding protein on motile and non-motile fibroblasts. Exp Cell Res 1:17-28

Turley E. A., D. Moore, J. J Hayden. (1987). Characterization of hyaluronate binding proteins isolated from 3T3 and murine sarcoma virus transformed 3T3 cells. Biochemistry *26*:2997-3005

Turley E. A., L. Austen, K. Vandeligt, C. Clary. (1991). Hyaluronan and a cell-associated hyaluronan binding protein regulate the locomotion of ras-transformed cells. J Cell Biol *12*:1041-7.

Wang, C., A.D. Thor, D.H. Moore, 2nd, Y. Zhao, R. Kerschmann, R. Stern, P.H. Watson, and E.A. Turley. (1998). The overexpression of RHAMM, a hyaluronan-binding protein that regulates ras signaling, correlates with overexpression of mitogen- activated protein kinase and is a significant parameter in breast cancer progression. Clin Cancer Res. *4*:567-76.

Wiese, C., A. Wilde, M.S. Moore, S.A. Adam, A. Merdes, and Y. Zheng. (2001). Role of importin-beta in coupling Ran to downstream targets in microtubule assembly. Science. *291*:653-6.

Wishart, D.S., S. Fortin, D.R. Woloschuk, W. Wong, T. Rosborough, G. Van Domselaar, J. Schaeffer, and D. Szafron. (1997). A platform-independent graphical user interface for SEQSEE and XALIGN. Comput Appl Biosci. *13*:561-2.

Wittmann, T., H. Boleti, C. Antony, E. Karsenti, and I. Vernos. (1998). Localization of the kinesin-like protein Xklp2 to spindle poles requires a leucine zipper, a microtubule-associated protein, and dynein. J Cell Biol. *143*:673-85.

Yang B., L. Zhang , E. A. Turley. (1993). Identification of two hyaluronan-binding domains in the hyaluronan receptor RHAMM. J Biol Chem *268*:8617-23

Yang B., B. L. Yang, R. C. Savani, E. A. Turley (1994). Identification of a common hyaluronan binding motif in the hyaluronan binding proteins RHAMM, CD44 and link protein. EMBO J *13*:286-96

Young, A., J.B. Dictenberg, A. Purohit, R. Tuft, and S.J. Doxsey. (2000). Cytoplasmic dynein-mediated assembly of pericentrin and gamma tubulin onto centrosomes. Mol Biol Cell. *11*:2047-56.

Zeng, C. (2000). NuMA: a nuclear protein involved in mitotic centrosome function. Microsc Res Tech. *49*:467-77.

Zimmerman, W., and S.J. Doxsey. (2000). Construction of centrosomes and spindle poles by molecular motor-driven assembly of protein particles. Traffic. *1*:927-34.

Chapter 2: Receptor for hyaluronan mediated motility (RHAMM) overexpression: A potential mechanism contributing to extensive centrosomal abnormalities in multiple myeloma

This research was submitted to Cancer Research April 2004. MS# CAN-04-1416 by C.A. Maxwell, J.J. Keats, A.R. Belch, L.M. Pilarski, T. Reiman is currently under review.

Introduction

The receptor for hyaluronan mediated motility (RHAMM), first described by Turley(Turley, 1982), has cell surface and intracellular distribution, has been shown to bind HA(Yang *et al.*, 1993), erk kinase(Zhang *et al.*, 1998), microtubules(Assmann *et al.*, 1999) and the centrosome(Maxwell *et al.*, 2003). RHAMM participates in cell motility(Masellis-Smith *et al.*, 1996), signaling (Turley *et al.*, 2002) and oncogenic events(Hall *et al.*, 1995). RHAMM is also a microtubule associated protein that localizes to the centrosome and spindle pole(Maxwell *et al.*, 2003). RHAMM, like Nuclear protein of the mitotic apparatus (NuMA), may function in the maintenance of spindle integrity by cross-linking microtubules through direct microtubule interactions at one terminus and an interaction with the dynein motor complex (Assmann *et al.*, 1999) (Maxwell *et al.*, 2003). RHAMM bears striking structural similarity to human kinesin-like protein 2 (Hklp2) within it carboxy-terminus including conservation of a basic leucine zipper domain (Maxwell *et al.*, 2003); this motif is essential for the cell-cycle specific interaction between Hklp2 and the dynein motor complex, which is mediated through targeting protein for Xklp2 (TPX2)(Wittmann *et al.*, 1998). Thus, it is intriguing to hypothesize that RHAMM may interact with the dynein complex and TPX2 and function in spindle assembly and integrity.

By RT-PCR, RHAMM transcripts are detected in malignant cells from B lineage malignancies, but are weak or absent from normal B cells of healthy donors (Crainie *et al.*, 1999), (Greiner *et al.*, 2004). In multiple myeloma (MM), a malignancy of post-germinal center B-lineage cells characterized by extensive chromosomal instability,

elevated RHAMM expression is significantly correlated to increased disease related events and reduced survival (Maxwell et al., in press). Moreover, the prevalence of cytogenetic abnormalities was greater in high (n=97), compared to low (n=94), RHAMM expressors (41% vs 30%); specifically, hypodiploidy is more prevalent with elevated RHAMM expression (28.9% vs. 14.9%)(Maxwell *et al.*, in press). RHAMM expression is linked to progression and metastasis of a variety of epithelial tumors including endometrial, stomach and breast carcinomas (Rein *et al.*, 2003) (Li *et al.*, 2000) (Wang *et al.*, 1998). The association of RHAMM with centrosomes, cell division and mitotic integrity may explain the correlation observed between RHAMM expression and the progression of malignancies with extensive chromosomal instability (CIN).

Centrosomes, composed of two centrioles and an amorphous cloud of pericentriolar material (PCM), are the major microtubule organizing centers in the cell and play an essential role in mitotic spindle assembly (Kellogg *et al.*, 1994). Numerical and/or structural centrosome abnormalities have been reported in a wide range of malignant epithelial tumors including breast, colon, and pancreatic cancer with positive correlation to genetic instability and cancer progression (Lingle and Salisbury, 1999) (Pihan *et al.*, 1998) (Ghadimi *et al.*, 2000) (Sato *et al.*, 1999); to date, however, centrosomal disregulation has not been investigated within myeloma cells. Centrosomal abnormalities appear to occur early in tumorigenesis as they are identified in pre-invasive carcinomas of the uterine cervix, prostate and female breast (Pihan *et al.*, 2003). Structural (i.e. excess PCM), rather than numerical, centrosomal abnormalities are most

highly associated with abnormal mitoses within breast cancer epithelia (Lingle and Salisbury, 1999).

Formation of a bipolar spindle is essential to the proper segregation of replicated chromosomes and the maintenance of genetic stability within the two resulting daughter cells. In frog egg extracts, spindle assembly is induced in a Ran-GTP dependent manner (Carazo-Salas *et al.*, 1999) (Kalab *et al.*, 1999) (Ohba *et al.*, 1999) (Wilde and Zheng, 1999). Enrichment of active Ran proximal to chromosomes (Kalab *et al.*, 2002) (Moore *et al.*, 2002) promotes microtubule nucleation through downstream effector proteins such as TPX2, NuMA and Aurora A kinase (AurA) (Gruss *et al.*, 2001) (Nachury *et al.*, 2001) (Wiese *et al.*, 2001) (Tsai *et al.*, 2003). TPX2, for example, initiates spindle assembly by nucleating and bundling microtubules (Gruss *et al.*, 2001) (Schatz *et al.*, 2003) and by directly activating AurA in a microtubule dependent manner (Wiese *et al.*, 2001) (Tsai *et al.*, 2003) (Bayliss *et al.*, 2003). The importance of AurA, TPX2 and NuMA has been illustrated in mammalian systems as well (Gruss *et al.*, 2002; Andrews *et al.*, 2003) (Khodjakov *et al.*, 2003). Once spindles have been established, their integrity is dependent upon the balance of forces generated by microtubule-dependent motors (ex. Dynein/dynactin). Disruption of this balance, through overexpression or inhibition of structural participants, would be expected to disrupt spindle structure (Garrett *et al.*, 2002).

Because RHAMM is associated with the progression of multiple tumors and, within myeloma, elevated RHAMM is associated with cytogenetic abnormalities,

aggressive disease and patient survival, we investigated the effects of RHAMM overexpression on centrosomal and spindle structure. We demonstrate that RHAMM overexpression induces centrosomal structural abnormalities, similar to those identified in myeloma cells *ex vivo* and *in situ*, and abnormal spindle architecture. RHAMM interacts with the spindle assembly factors dynein/dynactin and TPX2, but not NuMA, and disregulation of RHAMM expression affects G_2/M transition and spindle integrity. Based upon the work presented here, we postulate that augmentation of RHAMM expression may adversely affect chromosomal segregation.

Materials and Methods

Cell Culture, transient transfection, immunofluorescence (IF) and RNA interference.

RPMI 8226, a myeloma cell line, Raji, a Burkitt's lymphoma cell line, and HeLa, a cervical adenocarcinoma line, were grown as recommended (ATCC). Cells were passaged 24 hours prior to transfection. Suspension cells were transfected by electroporation (270mV, 960uF, 47-53ms) while HeLa cells were transfected with Lipofectamine 2000 (Invitrogen) following the manufacturer's protocols. At defined time points post transfection, cells were fixed and permeabilized in cold MeOH and washed with PBS-0.5% Triton X-100 (Sigma) prior to IF. For double and triple staining experiments, antibodies were added sequentially. Cells were washed 3x in PBS-0.5% TWEEN before and after incubations. Cells were mounted in 90% glycerol/PBS + DAPI and images were acquired using a Zeiss confocal LSM 510 or multiphoton microscope. Images were processed using MetaMorph Software (Universal Imaging Corp., Downington, PA) and Photoshop 5.02 software (Adobe Systems Inc., Ottawa, Canada).

We carried out RNA interference as described (Elbashir *et al.*, 2001). siRNA targeting human TPX2 (NM_012112) and human RHAMM (NM_012484) were ordered pre-designed using the Cenix Bioscience algorithm from Ambion® (Austin, TX). TPX2 targeted sequence was 5'GGAGAUACACAAAACAUAGtt3' and RHAMM targeted sequence was 5'GGUGCUUAUGAUGUUAAAAtt3'; RHAMM sequence targets all $RHAMM^{FL}$, $RHAMM^{-ex4}$ and $RHAMM^{-ex13}$ isoforms. Control RNA, targeting Luciferase GL2, was ordered from Dharmacon, Inc (Lafayette, CO). Oligos were annealed and transfected with Lipofectamine 2000 (Invitrogen) as per manufacturer's suggested

protocols. Briefly, 1.5μl of 20mM siRNA complex was incubated with 50μl of OPTIMEM (Invitrogen) and 1μl Lipofectamine 2000 was incubated with 50μl of OPTIMEM. These solutions were mixed and incubated at room temperature for 20 min before being diluted to 2ml and added to cells. Cells were isolated for immunoblotting or immunofluorescence 24, 30 and 48 hours post transfection.

Antibodies and plasmids.

Staining utilized α tubulin (clone B-5-1-2) and γ tubulin (clone GTU-88) (Sigma, St. Louis MO), β actin (Sigma), pericentrin (Covance, Richmond CA) CD138-FITC (Serotec, Raleigh NC), CD38-PE (BD Biosciences Palo Alto, CA), and CD45-FITC (Beckman Coulter). The polyclonal RHAMM antibody was produced and characterized as described(Maxwell *et al.*, 2003). A second polyclonal RHAMM antiserum was kindly provided by V. Assmann (Assmann *et al.*, 1999). TPX2 antiserum was kindly provided by O. Gruss (Kufer *et al.*, 2002). The mouse monoclonal NuMA antibodies were identified in a monoclonal antibody screen for mitotic chromosome scaffold proteins (Compton *et al.*, 1991). CENP-F antiserum was kindly provided by G. Chan (Chan *et al.*, 1999). Secondary antibodies were from Molecular Probes. GFP-RHAMM^{FL} and pEGFP-C1 (Invitrogen, Carlsbad CA) plasmids were prepared as previously described (Maxwell *et al.*, 2003).

Image Analysis and three-dimensional volume rendering.

Following IF, confocal z-slices were imaged from core biopsies. For all analysis, confocal slices were imaged at defined zoom (40x objective, 8 zoom), speed and depth

(0.2μm) and were acquired using a Zeiss confocal LSM 510 or multiphoton microscope. In general, 3 confocal stacks, including at least 30 PCs, were collected. Centrosomes were identified by γ-tubulin immunofluorescence and regions of interests, containing individual centrosomes, were extracted using Zeiss 510 image analysis software. Centrosomal images were transferred to Imaris™ 3.2.2 software (Bitplane AG) for volumetric analysis. Centrosomes were manually counted for at least 80 $CD138^+$ PCs per patient; PCs with ≥3 centrosomes were considered abnormal. Abnormal centrosomal structure was assessed using previously published parameters (Pihan *et al.*, 1998).

Patients and Clinical Data.

Bone marrow (BM) biopsies from 41 MM patients, 8 monoclonal gammopathy of uncertain significance (MGUS, a "pre-malignant" condition that may precede development of myeloma) and 4 lymphoma patients with uninvolved BM were identified from the pathology records at the Cross Cancer Institute from 1997-2000. BM core samples from lymphoma patients were examined for malignant infiltration and uninfiltrated marrows were selected to provide control archived BM samples; thus, control plasma cells (PCs) were processed and archived analogously to archived MM cores. The results may *under*estimate the true extent of centrosomal abnormalities in MM if these uninvolved marrows include cryptic lymphoma cells. If cryptic involvement were present, this potentially minimizes the differences between control and MM samples, possibly biasing the results against the conclusions drawn here. Aspirates were BM from newly diagnosed MM patients (n=12), relapse myeloma (n=3) and non-infiltrated BM from lymphoma patients (n=2). All patients consented to the use of their

BM samples. Patient records were reviewed retrospectively to verify the diagnosis of MM based on standard criteria (Hussein, 1994).

Preparation and analysis of MM BM aspirates and core biopsies.

BM core biopsies were fixed, decalcified and paraffin embedded. Sections (4μm) were mounted on sialinized glass slides. For antigen retrieval, slides were placed in EDTA (1.0 mM, pH 8.0) pre-heated to 100° C and placed in a temperature-controlled microwave (TTMega) for 10 minutes. Biopsies were sequentially stained with γ tubulin (1:200), anti-mouse Alexa^{594}(1:200), mouse IgG for blocking, and CD138-FITC (1:20), and mounted with glycerol medium containing DAPI for DNA staining.

For fluorescence activated cell sorting (FACS) analysis of intracellular RHAMM, purified BMMC were fixed and permeabilized with Intraprep (Beckman Coulter, Mississauga CAN). Prior to fixation, cells were stained with 1:20 CD138-FITC followed by fixation, permeabilization, according to the manufacturer's suggested protocol, and sequential staining with anti-RHAMM polyclonal serum (CM1 at 1:200), or prebleed serum (1:200), followed by RPE- goat anti-rabbit Ig (Molecular Probes). Normalized RHAMM fluorescence was calculated as the geometric mean fluorescence of RHAMM, divided by that for prebleed, for CD138^{+} cells within the patient's population.

Quantitative RT-PCR.

BMMC were stained with anti-CD138 microbeads (Miltenyi Biotec, Auburn CA) as suggested by the manufacturer and single column isolations were performed on an

autoMACS Magnetic Cell Sorter (Miltenyi Biotec). Purity of the selected, CD138 positive plasma cells, was verified to be greater than 90% by cytospin and morphology examination. DAPI staining, following EtOH fixation, confirmed the cell cycle stage of cell lines analyzed by q-RT-PCR. RNA isolation, sample quality examination, and reverse transcription were as suggested by the manufacturer Applied Biosystems, Foster City CA). Each quantitative RT-PCR reaction was performed in a 50 ul volume consisting of 1x Universal PCR Master Mix No AmpErase® UNG (Applied Biosystems), 2 ul of the respective Taqman® Assays-on-Demand™ Gene Expression Products primer and probe mix for GAPDH (Hs99999905_m1) or RHAMM (Hs00234864_m1)(Applied Biosystems), and 5 ng of RNA converted to cDNA as template. Reactions were run on an ABI PRISM™ 7700 Sequence Detection System (Applied Biosystems). Quantitation using the Relative Standard Curve Method was performed using a 2 Log dilution range of Raji cDNA to generate a standard curve for each reaction. The expression level of each sample was normalized to the sample with the lowest level of RHAMM expression, which was set to an expression level of 1.

Synchronization, immunoprecipitations and quantitation

Raji (qRT-PCR) and HeLa (qRT-PCR and co-immunoprecipitation) cells were synchronized by double thymidine (2mM, 14-16 hours) and nocodazole (300ng.ml, 10-12 hours) block. Unsynchronized populations were released from plates with 1x trypsin. Both mitotic and unsynchronized populations were then washed 3x with PBS and lysed at $5x10^6$-10^7 cells/ml in 1% CHAPs plus 10 μg/mL leupeptin, 10 μg/mL antipain and 1 mM phenylmethylsulfonyl fluoride (all from Sigma). All immunoprecipitation procedures

were performed at 4^{O}C as previously described (Maxwell *et al.*, 2003). For quantitation of co-precipitated proteins, post IP lysates were collected and analyzed by SDS-PAGE. Protein quantitation utilized the Odyssey v1.1 Infrared imaging system (LI-COR) with detection of polyclonal sera using IRDye 800 conjugated anti-rabbit IgG (Rockland, Gilbertsville, PA)

Statistical Methods.

Data were analyzed using SAS version 8.2 for Windows (SAS Inc). Correlation between centrosomal parameters and continuous variables utilized Pearson's correlation coefficient. Two-group comparisons of centrosome parameters utilized Student's t-test. Statistical significance was set at a p-value of 0.05 using two-sided analysis.

Results

RHAMM overexpression affects centrosomal size and structure

RHAMM is a multifunctional protein that localizes to centrosomes and the mitotic spindle (Maxwell *et al.*, 2003). To examine the effect(s), if any, that elevated RHAMM expression has on centrosomal structure, RPMI 8226 cells were transiently transfected with EGFP-C1 empty vector or GFP-RHAMM^{FL} and centrosomal structure was examined 16-20 hours later. Centrosomal volumes were determined by three-dimensional rendering of fluorescent signals from indirect immunofluorescence with γ-tubulin, a defined centrosomal structural protein, or GFP-RHAMM^{FL}, a putative component of the PCM (Figure 2-1). Measurement of centrosomal volumes significantly correlated with structural and numerical centrosomal abnormalities (see below) and is a quantitative measurement that incorporates the two phenotypes.

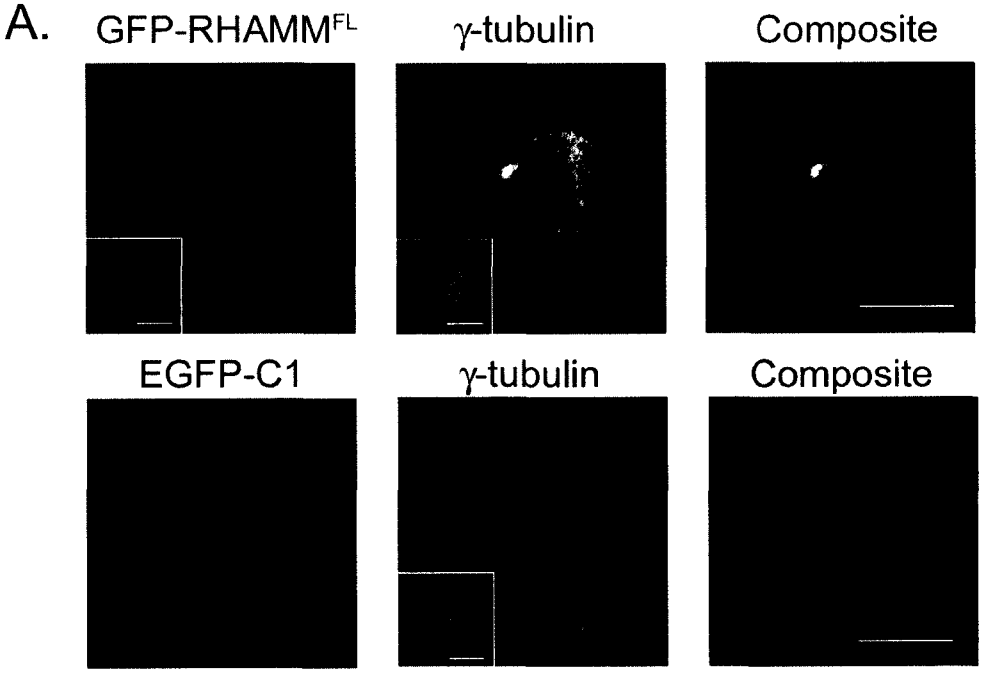

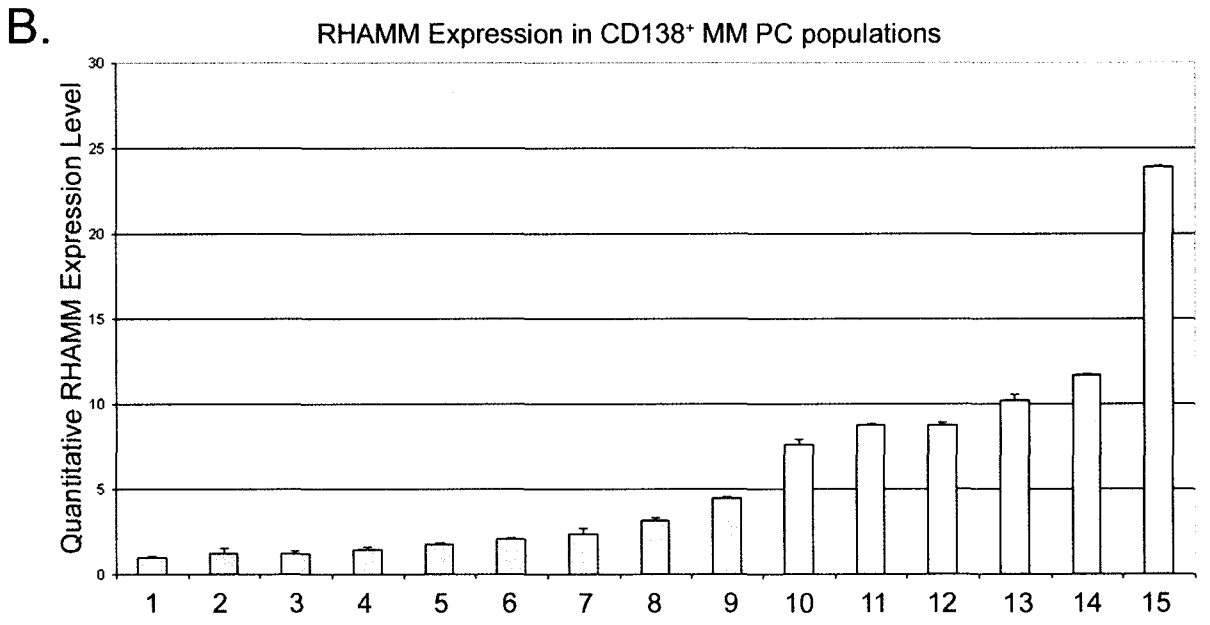

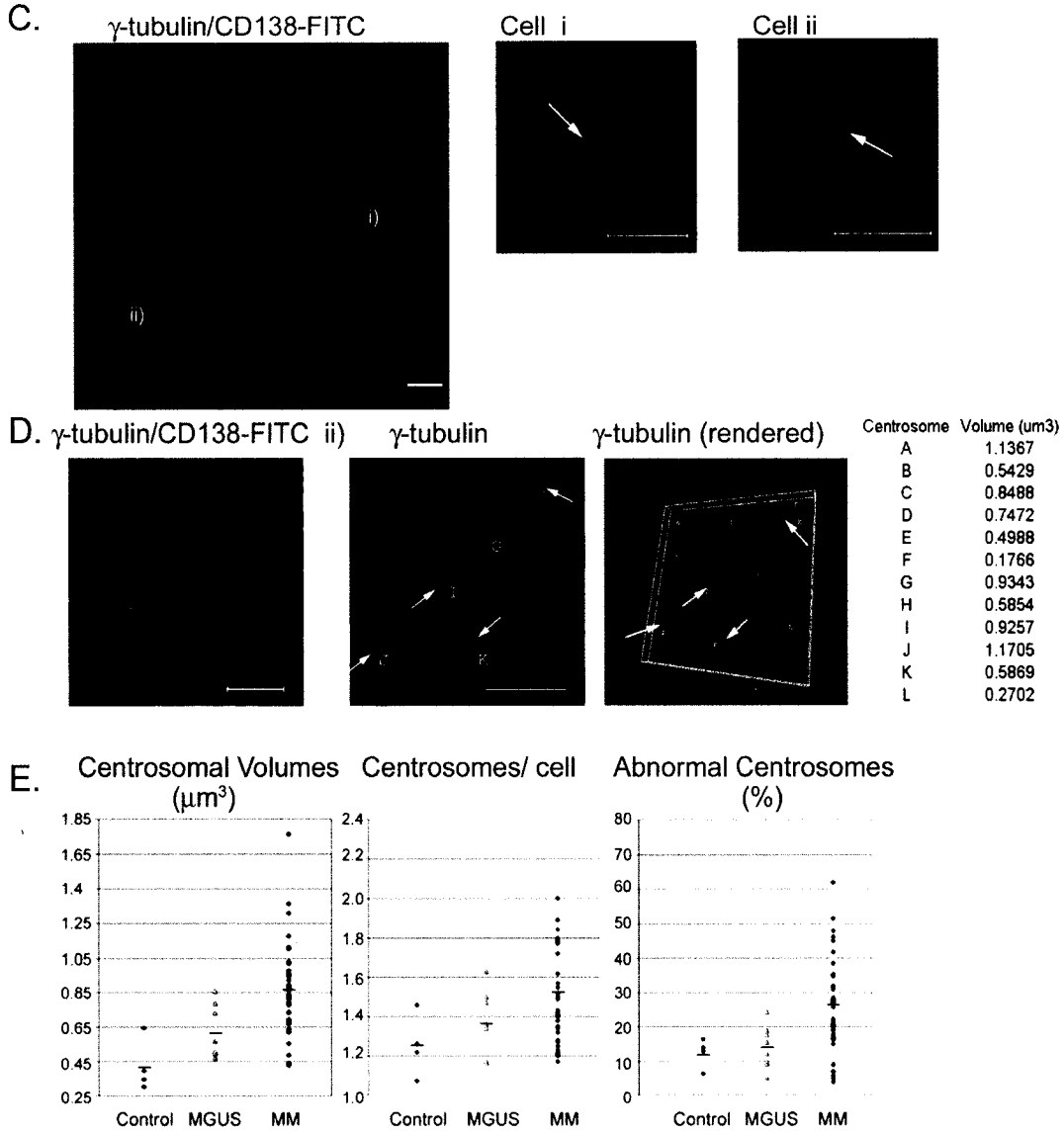

Figure 2-1: RHAMM overexpression, both exogenous and endogenous, induces extensive centrosomal defects. A) RPMI 8226 cells were transiently transfected with GFP-RHAMM^{FL}, or EGFP-C1, and stained with γ-tubulin. Confocal z-stacks were collected through individual cells and regions of interest, containing the γ-tubulin signal, were exported to Imaris^{TM} for three-dimensional rendering. Scale bars equal 10 μm. Inset boxes are 2.5 μm x 2.5 μm extracted regions around the centrosome. A median (of 2 pixels) filter was applied to extracted regions. Effective zoom is 4x original image. Scale bars equal 1 μm. B) RHAMM expression within purified MM CD138^{+} PCs was determined by

quantitative RT-PCR analysis. Relative RHAMM expression was normalized to the lowest patient expresser (Patient 1). C) Archived diagnostic MM BM cores were immunofluorescently labeled with CD138-FITC, to indicate plasma cells, and γ-tubulin. $CD138^+$ PC were scored for structural (cell i) and numeric (cell ii) centrosomal abnormalities. White arrows indicate abnormal centrosomes. Scale bar equals 10 μm. D) i) Archived diagnostic MM BM cores (ex. B97-62) were immunofluorescently labeled with CD138-FITC, to indicate PC, and γ-tubulin. Scale bar equals 50μm. Boxed area (red) shown in ii) Confocal slices were collected through the core sections. Individual centrosomes are labeled alphabetically and indicated with white arrows. Scale bar equals 10μm. The γ-tubulin channel was analyzed by Imaris™ software and the centrosomes were 3-dimensionally rendered. Volumes for represented centrosomes (white arrows) are C: 0.849 μm^3, F: 0.177 μm^3, I: 0.926 μm^3, J: 1.171 μm^3, K: 0.587 μm^3, L: 0.270 μm^3 for sample B97-62. E) Scatter plot graph for range in centrosomal volumes, centrosome/cell, and percent abnormal centrosome calculations for MM (n=42), MGUS (n=8) and control (n=4) PC. Mean values (see Table 4) are as indicated with bar lines.

RPMI 8226 transiently transfected with GFP-$RHAMM^{FL}$, under the control of a CMV promoter, express approximately 5 fold more exogenous RHAMM protein than endogenous levels by immunoblot analysis (Maxwell *et al.*, 2003), comparable to the overexpression levels observed in vivo (see below). γ-tubulin fluorescence within RPMI 8226 transfected with EGFP-C1 and RPMI 8226 cells that failed to express GFP-$RHAMM^{FL}$ was used as a negative control for PCM volume determination (Figure 2-1). The mean centrosomal volumes for negative control samples were 0.541 $^+/-$ 0.081 μm^3 and 0.532 $^+/-$ 0.123 μm^3, respectively (Table 2-1). Overexpression of GFP-$RHAMM^{FL}$ dramatically increased the PCM volume as determined by GFP-$RHAMM^{FL}$ fluorescence (1.039 $^+/-$ 0.262 μm^3) (Table 2-1). Interestingly, transient overexpression of GFP-$RHAMM^{FL}$ also resulted in larger γ-tubulin volumes (0.682 $^+/-$ 0.079 μm^3) suggesting

that RHAMM may not only localize to centrosomes but also recruit γ-tubulin to the centrosome (Table 2-1). Thus, overexpression of RHAMM affects both centrosomal size and structure.

Table 2-1: Disregulation of centrosomal volumes with GFP-RHAMM^{FL} overexpression. RPMI 8226 transient transfection

Transfection	Centrosomal Signal	Mean Centrosomal Volume (μm^3)	Fold overexpression GFP-RHAMM^{FL}
Non-transfected	γ-tubulin	0.532 ± 0.123	1.0
EGFP-C1	γ-tubulin	0.541 ± 0.081	1.0
GFP-RHAMM^{FL}	γ-tubulin	0.682 ± 0.079^{B}	5•
	GFP-RHAMM^{FL}	1.039 ± 0.262^{A}	5•

RPMI 8226 cells were transiently transfected with GFP-RHAMM^{FL} using electroporation. Following transfection, live cells were adhered to 1 mg/ml fibronectin, MeOH fixed and stained for γ-tubulin. At least ten measurements (i.e. confocal stacks and three-dimensional rendering) were acquired for GFP-RHAMM^{FL} and γ-tubulin signals within transfected and nontransfected cells.

[A] $p<0.05$ compared to EGFP-C1 and nontransfected values

[B] $p=0.22$ compared to nontransfected values

• Immunoblot analysis: Maxwell et al., (2003) MBOC **14**(6):2262-76(2003)

RHAMM expression varies within MM patient plasma cells

To examine the physiological relevance of these findings we utilized quantitative RT-PCR to investigate whether RHAMM expression varied dramatically within MM patients. RNA was obtained from MM patient (n=15) CD138^{+} PC for quantitative analysis; sufficient purified CD138^{+} PCs could not be obtained from control patients for qRT-PCR analysis. Previous experimentation demonstrated that RHAMM is undetectable, or weakly detectable, in the peripheral blood (PB) of control patients (Greiner *et al.*, 2003) (Crainie *et al.*, 1999) and RHAMM is undetectable in bulk populations of control BM and infrequently detected in single CD138^{+} normal PCs by

highly sensitive (sensitivity limit 10^{-18}g) RT-PCR and fragment analysis (Maxwell et al., in press). Within this cohort, RHAMM expression was normalized to the level of the lowest RHAMM expresser (Figure 2-1B). MM patients varied considerably in the absolute amount of RHAMM expression (Figure 2-1B).

Elevated RHAMM expression within myeloma patient plasma cells coincides with centrosomal abnormalities.

We hypothesized that elevated RHAMM expression may coincide with centrosomal abnormalities in myeloma. To investigate our hypothesis, centrosomal volumes were measured in CD138-FITC labeled MM PCs from MM patients for which quantitative RHAMM data was known (n=5). Centrosomal volumes were determined by three-dimensional rendering of fluorescent signals from indirect IF with γ-tubulin, a defined centrosomal structural protein. Within these patients, elevated RHAMM expression was accompanied by centrosomal amplification suggesting that RHAMM, in part, may contribute to centrosomal disregulation (Table 2-2). These results were confirmed at the protein level (flow cytometry analysis) by examining RHAMM expression in control patient (n=2) PCs versus MM patient (n=2) PC; on average, the MM patients examined contained elevated RHAMM expression (4.2 fold) accompanied by larger centrosomal volumes (0.98 $^{+}/_{-}$ 0.2 vs 0.40 $^{+}/_{-}$ 0.05).

Table 2-2: Disregulation of centrosomal volumes with RHAMM overexpression.

Ex Vivo Patient $CD138^+$ cells Analysis

Patient	Fold Overexpression (qRT-PCR)	Mean Centrosomal Volume (μm^3)
MM7	2.41	0.57± 0.11
MM5	1.74	0.60± 0.05
MM10	7.58	0.75 ± 0.14
MM12	8.80	0.95 ± 0.21
MM11	8.77	0.99 ± 0.13

BMMC were derived from BM aspirates. Patients are numbered as in Figure 1B. RNA was prepared as described for quantitative RT-PCR analysis. Fold overexpression was normalized to the lowest RHAMM expression within the MM patient cohort (Patient 1, Figure 1B). Prior to $CD138^+$ PC isolation, an aliquot of BMMC were cytospun, fixed and examined with indirect IF against centrosomal markers and CD138-FITC. One microscope slide was examined with at least ten measurements per patient.

Centrosomal abnormalities characterize myeloma cells.

As RHAMM expression is a prognostic factor in myeloma, RHAMM induces centrosomal abnormalities in vitro and elevated RHAMM expression is related to centrosomal abnormalities in vivo, we analyzed centrosome number, structure and volume in situ within $CD138^+$ PCs from archived BM core biopsies using multicolor immunofluorescence to determine if centrosomal abnormalities, if present, are also prognostic. BM cores were examined from MM patients (n=41), monoclonal gammopathy of undetermined significance (MGUS) (n=8) patients, and control patient (n=4) PCs. Myeloma patient characteristics are summarized in Supplemental Table 2-1. Experimenters were blinded to sample identity/diagnosis at the time of analysis and quantitation. Centrosomes in $CD138^+$ PCs were visually assessed for qualitative structural abnormalities (see Abnormal centrosomes, Table 2-3) as previously described (Pihan *et al.*, 1998). The number of centrosomes per cell was also visually determined. To simultaneously quantitate numerical and structural abnormalities, PC

centrosomal volumes were determined using image analysis of three-dimensional confocal stacks transversing $CD138^+$ cells (Figure 2-1).

N (%)		41
Age (yrs)		*median (range)* 67(44-85)
Sex		29 male, 17 female
		No. (%)
Stage	I	7 (17)
	II	5 (12)
	III	34 (83)
	B (sCr >2 mg/dL)	14 (34)
Clinical Isotype	IgG	22 (54)
	IgA	6 (14)
	light chain	11 (27)
	other/unspecified	2 (5)
Lytic bone disease		26 (63)
Calcium >12 mg/dL		5 (12)
Hgb < 8.5 g/dL		10 (24)
Elevated LDH		5 (12)
Urine protein > 4 g/day		9 (22)
Primary Therapy	Radiation only	4 (10)
	Chemotherapy	27 (66)
	Auto SCT	14 (34)
	Allo SCT	1 (2)
Patients deceased, No. (%)		22 (54)
Median overall survival, years		2.7
Survivor follow-up, years		*median (range)* 3(0-8)

Supplemental Table 2-1: Myeloma patient characteristics for examination of centrosomal abnormalities

	%abnormal cells	#centrosomes/cell	volume
%abnormal cells	1	0.28	0.13
#centrosomes/cell	-	1	0.27
volume	-	-	1

Supplemental Table 2-2: Correlations between centrosomal parameters in 41 MM patients. Pearson's r-squared values are shown. P<0.001 for all correlations.

PC from all MM samples analyzed demonstrated numerical, structural and volumetric abnormalities (Figure 2-1). Centrosome abnormalities, including the mean number of centrosomes/cell and the mean total centrosome volume, were highly correlated with one another in MM (Pearson's r^2 coefficient 0.27, $p<0.001$, Supplemental Table 2-2). Qualitative assessment of centrosomal abnormalities demonstrated a significant difference in the percentage of abnormal centrosomes within MM PCs and MGUS or control PCs ($p<0.001$). On average, MM PCs demonstrated a significantly greater number of centrosomes per cell than MGUS and control PCs ($p<0.05$). Finally, quantitative volumetric assessment of structural abnormalities revealed a highly significant difference between MM and MGUS or control PCs ($p<0.005$). MGUS PCs had centrosomal parameters intermediate to those of control PCs and MM PCs (Table 2-3); indeed, MGUS PCs had larger centrosomal volumes that approached a statistically significant difference when compared to those within control PCs ($p=0.08$). In this small sample, no statistically significant relationship was seen between any of the centrosome

measurements and survival, either from the date of diagnosis or from the date of the bone marrow biopsy.

Table 2-3: Centrosomal abnormalities characterize MM CD138$^+$ BM PC.

CD138$^+$ in situ PCs	Patients Examined (n)	Centrosomal Volume (mean, μm^3)	Centrosomal Volume (range, μm^3)	Centrosomes/ Cell (mean)	Centrosomes/ Cell (range)	Abnormal Centrosomes (Mean , %)	Abnormal Centrosomes (range, %)
MM	41	0.86± 0.04[A]	0.43-1.76	1.52± 0.03[B]	1.2-2.0	26.4±2.11[A]	4.0-62
MGUS	8	0.62± 0.05	0.47-0.86	1.37± 0.06	1.2-1.6	14.1±2.19	5- 24.4
Control	4	0.42± 0.08	0.30-0.65	1.25± 0.08	1.1-1.5	12.3±2.15	6.3-16.3

BM cores were fixed, decalcified, paraffin embedded and sectioned. Antigen retrieval preceded double immunofluorescence with CD138-FITC, to highlight PC, and γ-tubulin, to demarcate centrosomes. Centrosome/cell values and percent abnormal centrosomes were determined by qualitative assessment; experimenters were blinded to core diagnosis at the time of assessment and quantitation. Centrosomal volumes were determined by three-dimensional rendering of confocal z stacks.

[A] $p<0.005$ compared to control and MGUS values

[B] $p<0.05$ compared to control and MGUS values

RHAMM overexpression affects mitotic integrity.

While centrosomal abnormalities can occur through amplification of structural pericentrosomal material, a major pathway for centrosomal disregulation is the disruption of mitosis. We next analyzed whether RHAMM overexpression augmented mitotic integrity. For these experiments, transiently transfected HeLa cells were examined as they represent a standard in vitro system within which mitoses, and aberrant mitoses, can be analyzed and compared. Similar experiments were performed in RPMI 8226, a myeloma cell line. EGFP-C1 transfected and neighboring, non-transfected HeLa were used as negative controls for spindle abnormalities induced by GFP-RHAMM^{FL} overexpression. Similar to observations in RPMI 8226 (Maxwell *et al.*, 2003), GFP-

RHAMM^{FL} transfection results in a metaphase block with dramatically fewer transfected cells observed in prophase (3.92% vs. 12.1% and 9.8%) and telophase/cytokinesis (13.1% vs 33.5% and 29.1%) compared to EGFP-C1 and non-transfected controls (Table 2-4A). Despite the high transfection efficiency (60-70%), fewer GFP-RHAMM^{FL} transfected cells were mitotic (n=153) than non-transfected controls (n=306) suggesting a significant decrease in viable mitotic cells dependent on GFP-RHAMM^{FL} overexpression (Table 2-4A).

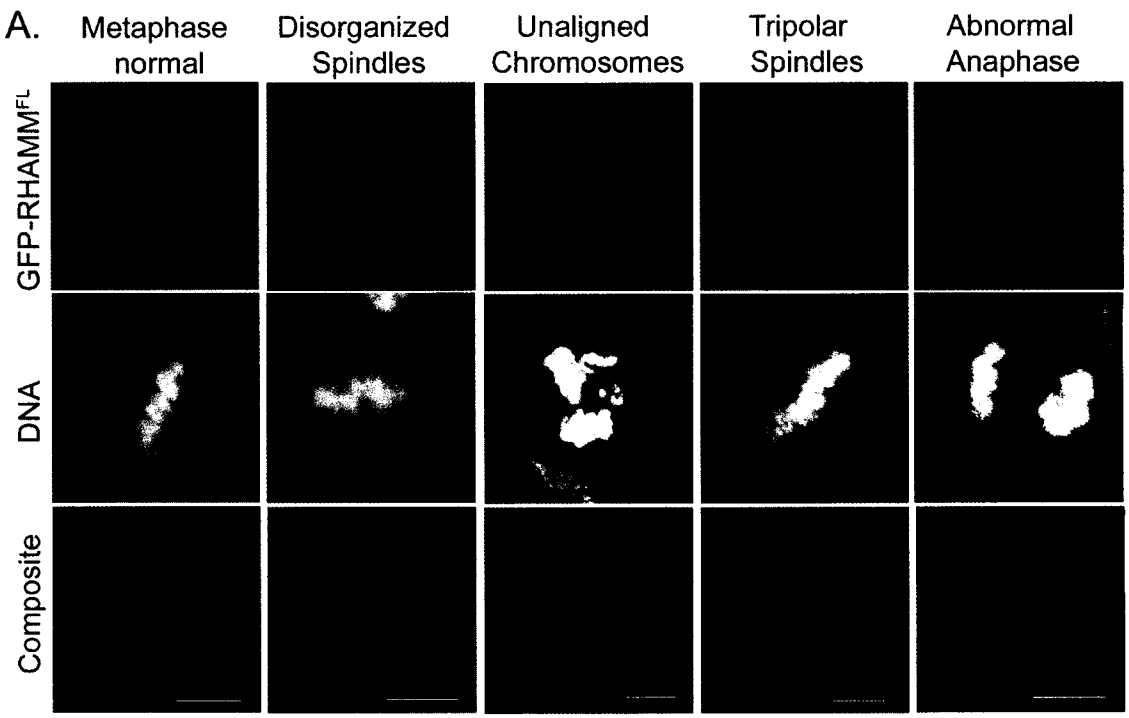

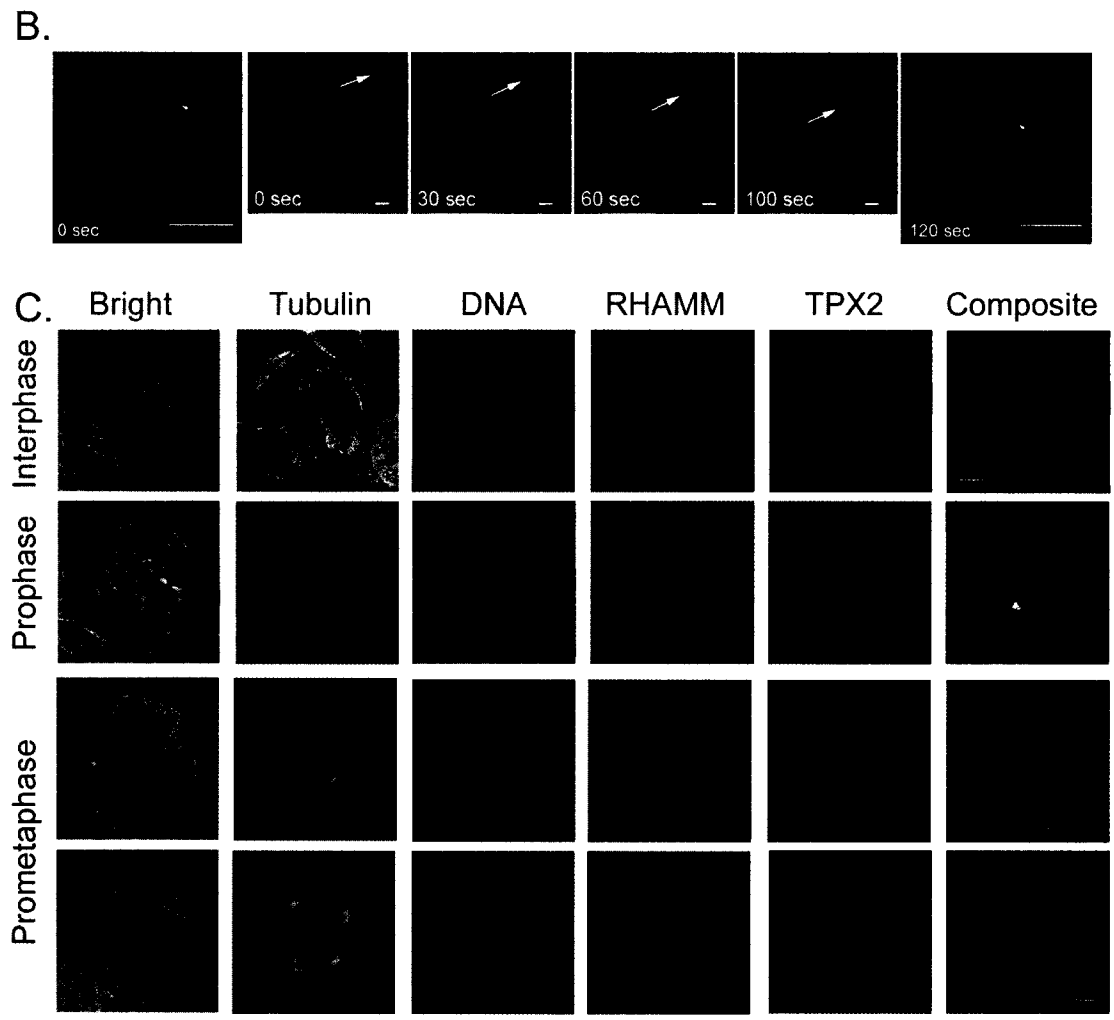

Figure 2-2: RHAMM overexpression affects mitosis, mitotic RHAMM interacts with the dynein motor complex in vivo and colocalizes with TPX2 A) HeLa cells were transiently transfected with GFP-RHAMM^{FL}, or EGFP-C1, and stained with α-tubulin (not shown). DNA was visualized with DAPI. Both transfected and non-transfected cells were scored within GFP-RHAMM^{FL} transfected populations. Cells were examined for normal DNA alignment and segregation as well as for symmetrical, organized bipolar spindles (GFP-RHAMM^{FL} and α-tubulin signals). Individual metaphase cells were scored as normal, disorganized spindles, unaligned chromosomes, monopolar, tripolar, tetrapolar or mulitpolar spindles. Cells scored as unaligned chromosomes had phenotypically normal spindles. Scale

bars equal 10 μm. B) HeLa, or RPMI 8226 (not shown), cells were transiently transfected with EGFPC1-RHAMM^{FL}. Live RPMI 8226 were plated on coverslips coated with 100μg/ml HA to facilitate imaging. Cells recovered for 8-12 hours post transfection at 37^{0}C, 5% CO_2 and were visualized at room temperature and 5% CO_2. 40 images were collected at 15 sec intervals (time= 10 min) and velocities were analyzed on MetaMorph software. Arrow (time=0 sec) indicates a GFP-RHAMM aggregate that is relatively positionally stable. Line (time=0sec) indicates MetaMorph-determined, minus end directed path of GFP-RHAMM aggregate. Mean velocities of minus-end movement was 2.34 +/- 0.39 (HeLa), or 1.48 +/- 0.28 (8226, not shown), μm/min. C) RHAMM and TPX2 colocalize throughout mitosis. HeLa were transiently transfected with GFP-RHAMM^{FL} as described. RHAMM localization was indicated by GFP-RHAMM^{FL}, TPX2 and α-tubulin localization was determined by indirect immunofluorescence with polyclonal TPX2 antiserum and a monoclonal anti-α-tubulin antibody followed by goat anti-mouse Alexa-546 and goat anti-rabbit Alexa 633. DAPI staining indicates DNA. White arrows in prophase panel indicates extra centrosomal aggregates. Bottom prometaphase panel demonstrates RHAMM and TPX2 colocalization within abnormal (multipolar) mitotic cells. Scale bars equal 10 μm.

Table 2-4A: Overexpression of GFP-RHAMM^{FL} induces metaphase block.

	Percentage of Mitotic Cells					
	N	Prophase	Prometaphase	Metaphase	Anaphase	Telophase/ Cytokinesis
EGFP-C1	182	12.1	9.3	38.5	6.6	33.5
GFP-RHAMM^{FL} (non-transfected)	306	9.8	6.9	42.8	8.2	29.1
GFP-RHAMM^{FL}	153	**3.92**	15	**65.4**	5.2	**13.1**

HeLa cells were grown on coverslips and transiently transfected with Lipofectamine 2000 according to manufacturers suggested protocol. Three coverslips were examined for EGFP-C1 and GFP-RHAMM^{FL} transfections. Transfections resulted in 60-70% transfectants; both transfected (60-70%) and non-transfected (30-40%) populations were analyzed on GFP-RHAMM^{FL} transfected slips. Coverslips were fixed and permeabilized in cold MeOH 20 hours post transfection and immunofluorescently labeled for α-tubulin, to detect microtubules, and DAPI, to detect DNA. DNA condensation, alignment and segregation, bipolar spindle formation and midzone microtubules were utilized to differentiate mitotic stages.

Table 2-4B: Overexpression of GFP-RHAMM^{FL} induces extensive mitotic defects.

	Percent Abnormal Mitotic Cells (cells examined)					
	Prophase	Prometaphase	Metaphase	Mono/ Multipolar[A]	Anaphase	Telophase/ Cytokinesis
EGFP-C1	0 (22)	5.9 (17)	17.1 (70)	8.6	16.7 (12)	3.3 (61)
GFP-RHAMM^{FL} (non-transfected)	0(30)	0 (21)	10.7 (131)	6.9	0 (25)	3.4 (89)
GFP-RHAMM^{FL}	**16.7** (6)	**21.7** (23)	**63.0** (100)	**25**	**37.5** (8)	**20** (20)

HeLa cells were grown on coverslips and transiently transfected with Lipofectamine 2000 according to the manufacturers suggested protocol. Three coverslips were examined for EGFP-C1 and GFP-RHAMM^{FL} transfections. Transfections resulted in 60-70% transfectants; both transfected (60-70%) and non-transfected (30-40%) populations were analyzed on GFP-RHAMM^{FL} transfected slips. Coverslips were fixed and permeabilized in cold MeOH 20 hours post transfection and immunofluorescently labeled for α-tubulin, to detect microtubules, and DAPI, to detect DNA. DNA condensation, alignment and segregation, bipolar spindle formation and midzone microtubules were utilized to differentiate mitotic stages. Binucleated prophase, aberrant/disorganized bipolar spindles, mono/tri/tetra/multipolar spindles, tri/multipolar anaphase segregation, lagging anaphase chromosomes, telophase chromosomal bridges, tripolar telophase/cytokinesis daughter cells were scored as abnormal. Number of transfected cells examined are indicated in brackets.

[A] percentage of metaphase cells that were scored abnormal. Metaphase cells examined are bracketed in metaphase column.

To further investigate the effects of RHAMM overexpression on the disregulation of mitosis, the number of abnormal mitotic cells, at various stages, was quantitated. To differentiate between normal and abnormal mitotic cells, DNA condensation, alignment and segregation was analyzed with DAPI while microtubule organization and the number of spindle poles were analyzed with α-tubulin, indirectly labeled with anti-mouse Alexa^{594}, and GFP-RHAMM^{FL} fluorescence. The criteria for abnormal metaphase and anaphase was similar to that reported for Aurora A inhibited S2 cells (Giet *et al.*, 2002). GFP-RHAMM^{FL} overexpression induced multiple abnormalities at various stages with the most frequent being disorganized/long metaphase spindle fibers (28/100) and mono/tri/tetra/multipolar metaphase spindles (25/100) (Figure 2-2); the frequency of

disorganized spindle phenotypes was 0/131 (0%) and 1/70 (1.4%) while mono/multipolar spindles occurred in 9/131 (6.9%) and 6/70 (8.6%) cells within non-transfected and EGFP-C1 transfected control populations, respectively (Table 2-4B). Similar aberrant metaphase spindles are identified in RPMI 8226 transfectants (not shown). In RPMI 8226 transfectants, however, frequent spindle poles appear shorter than non-transfected controls (not shown). As mentioned previously, few (n=28) mitotic, GFP-RHAMM^{FL} overexpressing HeLa and RPMI 8226 (Maxwell *et al.*, 2003) cells were observed post metaphase (Table 2-4B). Interestingly, 7/28 (25%) transfected HeLa cells demonstrated lagging chromosomes, multipolar segregation or chromosome bridges (Table 2-4B). These phenotypes were present in 3/114 (2.6%) and 4/73 (5.5%) of non-transfected and EGFP-C1 transfected controls.

RHAMM functionally interacts with the dynein motor complex and colocalizes with TPX2 in mitosis

Previous investigation of RHAMM function revealed that a subset of RHAMM colocalized, and coprecipitated, dynein, and vice versa (Maxwell *et al.*, 2003). To extend upon these findings, we investigated the dynamics of GFP-RHAMM^{FL} in transiently transfected live HeLa, and RPMI 8226 cells, at room temperature (22-25°C). In addition to the mitotic spindle association, we observed aggregates of GFP-RHAMM^{FL} that would occasionally load to the spindle pole with vectoral movement (Figure 2-2B). We observed poleward movement of RHAMM^{FL}-GFP aggregates with velocities ranging from 0.62-3.80 μm/min (HeLa) and 1.25- 1.81 (8226) μm/min and an average velocity of 2.34 +/-

0.39 (HeLa, n=7) and 1.48 +/- 0.28 (8226, n=5) μm/min (Figure 2-2B). The observed RHAMM^{FL}-GFP velocities are similar to those observed for minus-end directed movement of NuMA-GFP by cytoplasmic dynein (1.0 +/- 0.3 to 2.6 +/- 1.0 μm/min)(Merdes *et al.*, 2000). These observations, in combination with our previous co-precipitation data (Maxwell *et al.*, 2003), demonstrates that RHAMM associates with the dynein motor complex to localize to the spindle pole within live cells.

Experiments with deletion constructs of GFP-RHAMM revealed that the protein's COOH-terminus is responsible for spindle pole localization (Maxwell *et al.*, 2003). Structural and sequence analysis revealed that this motif bears significant homology to the COOH-terminal, microtubule minus end targeting domain of Xklp2 (Maxwell *et al.*, 2003) (Wittmann *et al.*, 1998). Xklp2 targeting requires the dynein/dynactin motor complex and TPX2 (Wittmann *et al.*, 1998); thus we investigated whether RHAMM colocalizes with TPX2 during mitosis. During interphase, GFP-RHAMM^{FL} colocalizes with microtubules and centrosomes while TPX2 is nuclear (Figure 2-2C). At prophase, however, both RHAMM and TPX2 redistribute to the separating centrosomes (Figure 2-2C). At prometaphase, and throughout metaphase, both proteins localize to the poles, and along the arms, of phenotypically normal, as well as multipolar, mitotic spindles (Figure 2-2C). Both proteins localize to the spindle midzone during anaphase and concentrate at the midzone during telophase (not shown).

GFP-RHAMM^{FL} localizes at centrosomes and proximal to kinetochores during prometaphase

To further investigate the prometaphase localization of GFP-RHAMM^{FL}, RPMI 8226 were examined in early and late prophase, as determined by centrosomal separation. Centrosomes (single arrows, Supplemental Figure 2-1A) were identified by γ-tubulin staining and confocal z-stacks were acquired through the mitotic cell body. Consistent with observations in HeLa, GFP-RHAMM^{FL} localized to the centrosomes as well as to discrete aggregates throughout the replicated chromosomes (Supplemental Figure 2-1A). To identify these aggregates as kinetochores, prometaphase cells were stained with the kinetochore marker BUBR1. Early in prometaphase, GFP-RHAMM^{FL} localizes proximal to kinetochore sites with (single arrow) and without (double arrow) attached microtubules (Supplemental Figure 2-1B).

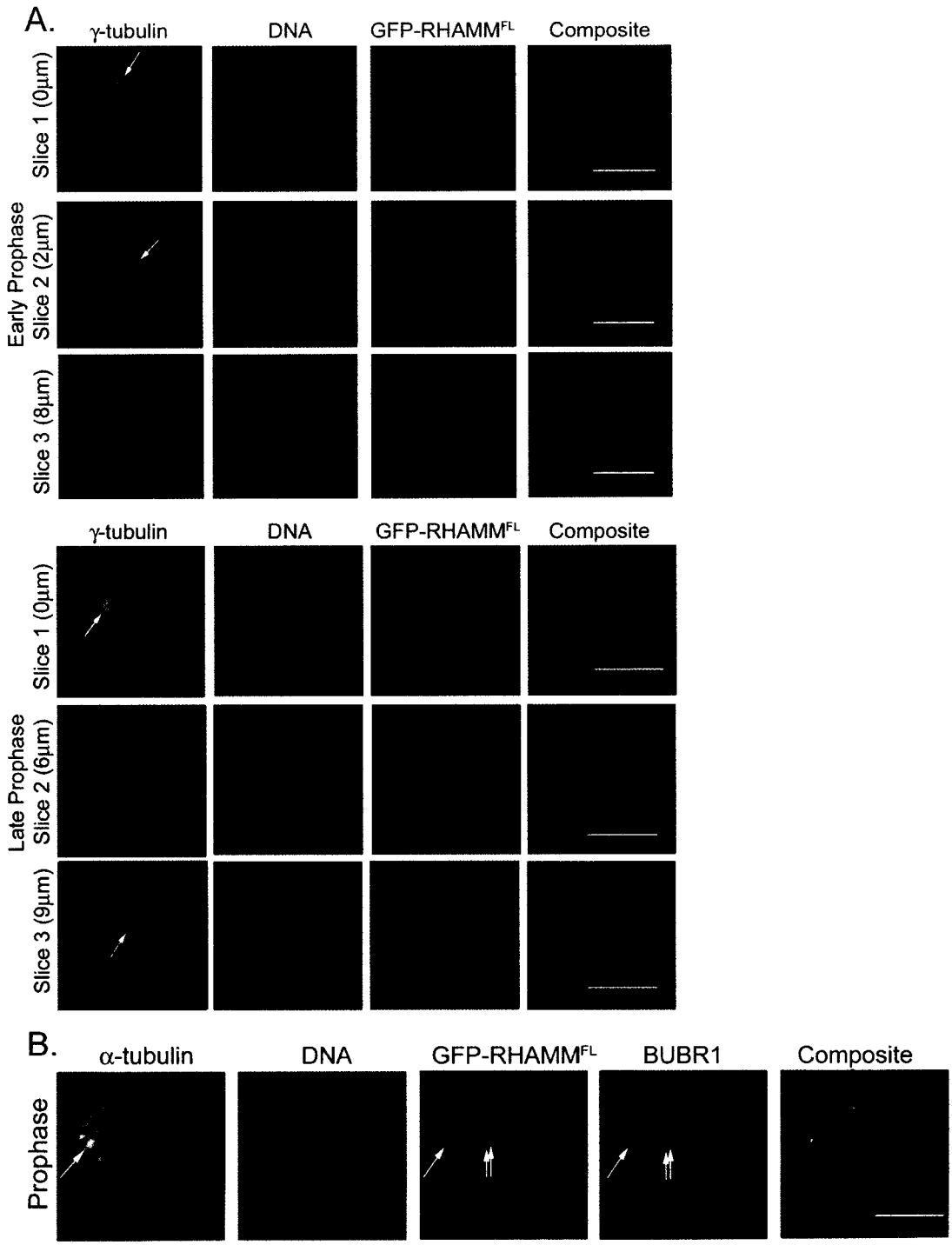

Supplemental Figure 2-1: RHAMM localizes to sites of microtubule nucleation during prophase

Supplemental Figure 2-1: RHAMM localizes to sites of microtubule nucleation during prophase A) RPMI 8226 cells were transiently transfected with GFP-RHAMM^{FL} and examined for centrosomal localization at prophase. Early and late prophase were determined based upon degree of separation of replicated centrosomes (as indicated by γ-tubulin stain). Arrows indicate centrosomes. Confocal slices were acquired throughout the mitotic cell body. Extra-centrosomal aggregates, which are phenotypically similar to kinetochore localization, are present throughout the condensed DNA. Scale bars equal 10 μm. B) RHAMM localizes proximal to kinetochores with and without attached microtubules. Polyclonal anti-BUBR1 antiserum and monoclonal anti-α-tubulin antibodies, detected by goat anti-mouse Alexa-546 and goat anti-rabbit Alexa 633, confirm the kinetochore localization of GFP-RHAMM^{FL} in HeLa. Single arrow indicates kinetochores with attached microtubules while double arrows indicate kinetochores without detectable α-tubulin immunofluorescence. Scale bar equals 10μm.

RHAMM co-immunoprecipitates a significant fraction of TPX2, and vice versa, in a cell cycle dependent manner

To investigate a putative RHAMM-TPX2 association, HeLa cells were synchronized through double thymidine and nocodazole block to provide mitotic extracts. Mitotic and unsynchronized extracts were separately immunoprecipitated with prebleed serum and sera targeting RHAMM, TPX2 and NuMA. NuMA/dynein complexes play an integral role in spindle assembly and focussing (Khodjakov *et al.*, 2003) (Merdes *et al.*, 2000) and thus NuMA served as an excellent control for the specificity of a putative RHAMM-TPX2 interaction. Lysis of equivalent numbers of cells from mitotic (M) and unsynchronized (US) populations resulted in amplification of both RHAMM and TPX2 levels in the mitotic extracts (Figure 2-3A). These results are consistent with a previous report (Gruss *et al.*, 2002) demonstrating cell cycle regulation of TPX2 levels within

HeLa cells and suggest that RHAMM, like TPX2, is up-regulated during mitosis (see Figure 2-3D,E). The high efficiency of immunoprecipitation was confirmed by examination of post-IP lysates with 70-100% of mitotic TPX2 and RHAMM being precipitated (Figure 2-3A). During mitosis, RHAMM antibodies co-precipitated a significant amount of TPX2, and vice versa. This reciprocal co-precipitation was not obtained within unsynchronized lysates. To quantitate the level of co-precipitation, infrared detection of protein was utilized to determine the levels of RHAMM, and TPX2, remaining in the post-IP lysates (Figure 2-3B). The fraction remaining is directly affected by the efficiency of precipitation. Infrared detection, unlike ECL detection, results in linear detection of IRDye 800-labeled antibodies, as opposed to detection of enzymatic amplifications resulting from HRP-labeled antibodies; as a consequence of different detection methodologies, the levels of RHAMM, and to a lesser extent TPX2, within analyzed mitotic lysates appear greater with ECL™, as compared to Odyssey™, detection. Neither prebleed nor NuMA precipitation resulted in a significant loss of RHAMM or TPX2 protein levels in the post IP fractions. For this reason, the concentrations of the bands resulting from PB and NuMA precipitations, the negative control experiments, were averaged to give an expected post-precipitation fraction. Thus, the fraction remaining was determined by dividing the band concentration of each lane by the expected post-precipitation fraction. Immunoprecipitation with RHAMM antibodies resulted in a depletion of 36% and 100% of the cellular TPX2 and RHAMM in mitotic lysates, respectively. Within mitotic lysates, TPX2 precipitation resulted in a 70% and 56% loss of TPX2 and RHAMM, respectively (Figure 2-3B). These results demonstrate

that a significant population of RHAMM is associated with TPX2 within HeLa mitotic cells and vice versa.

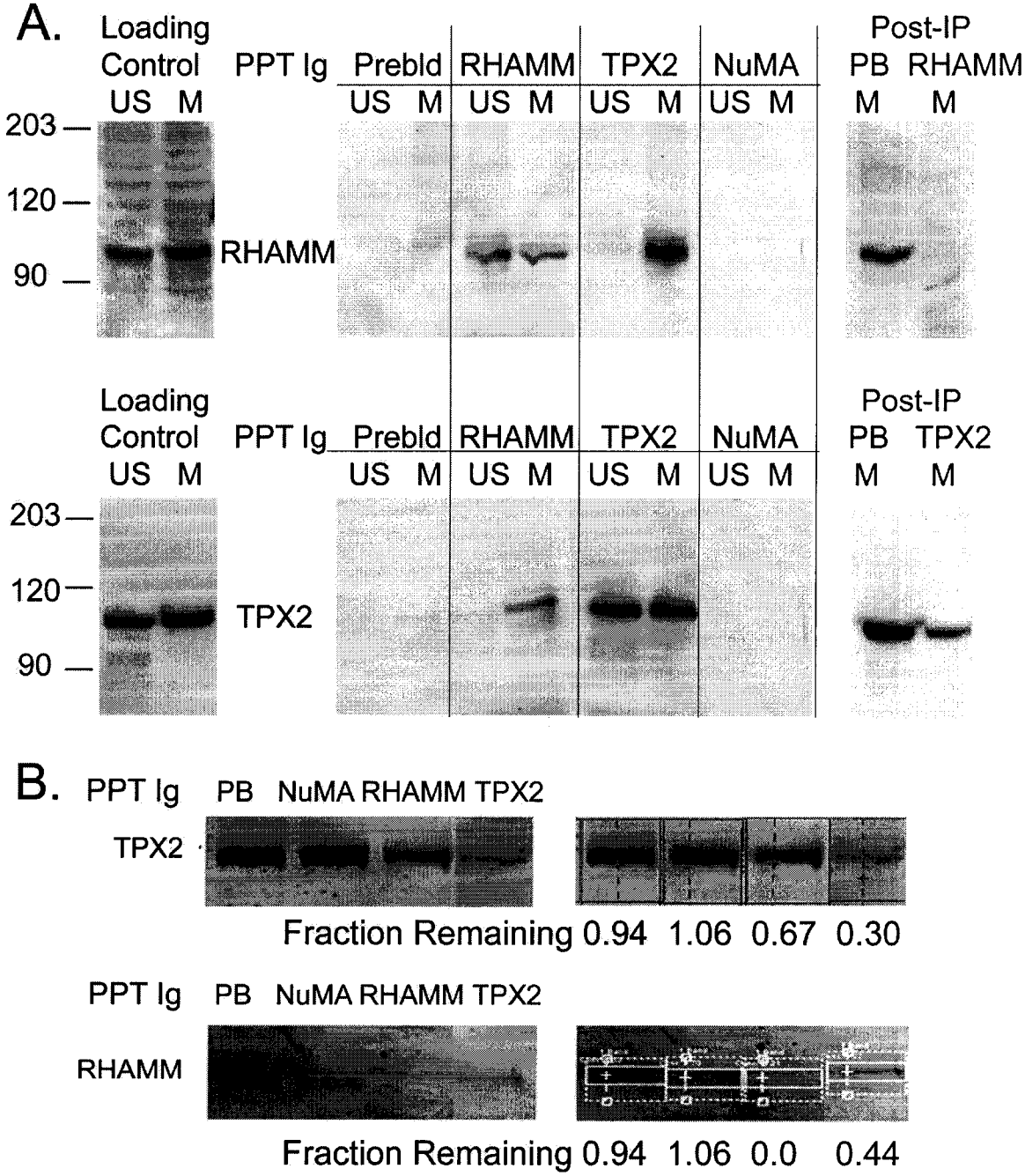

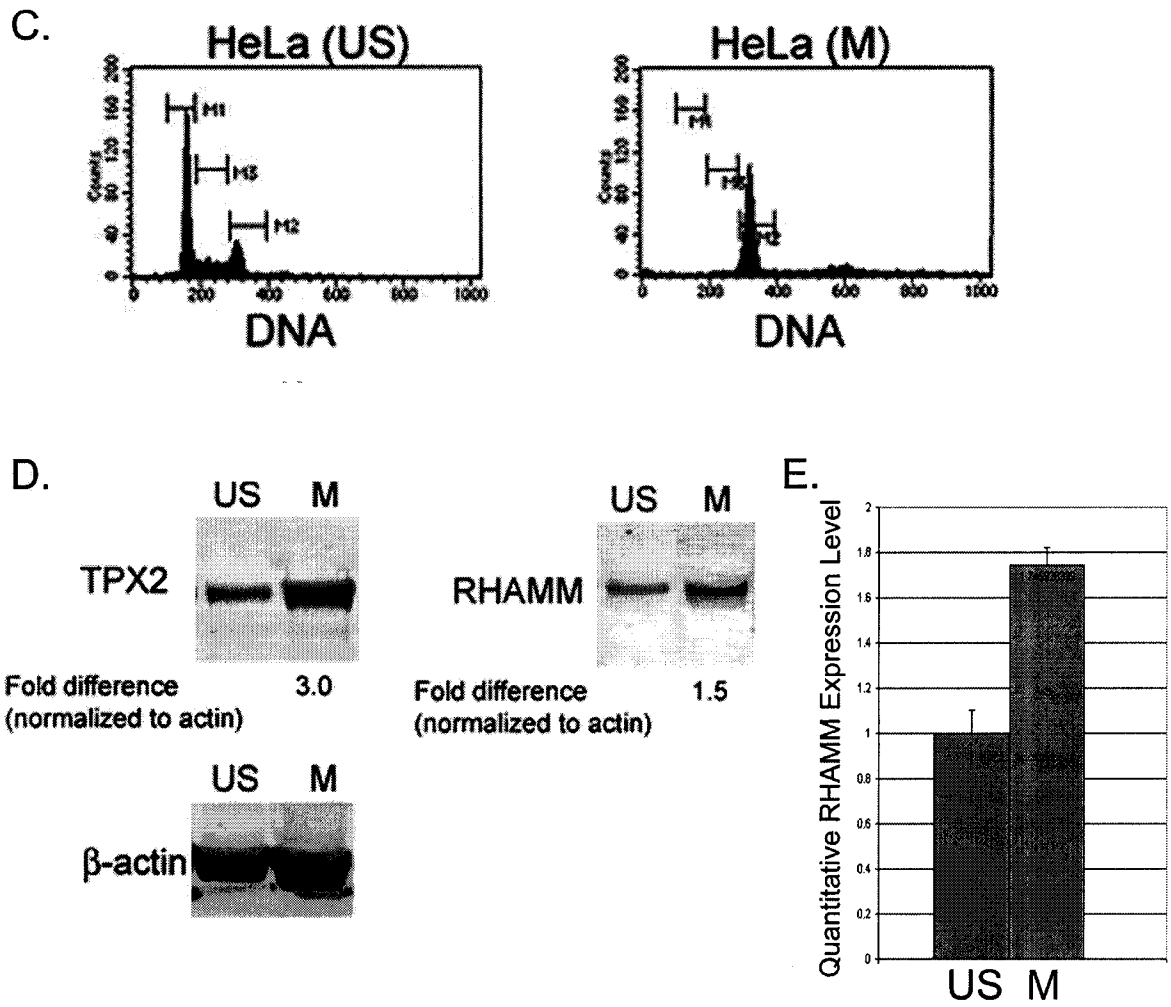

Figure 2-3: RHAMM antibodies co-immunoprecipitate TPX2 in a cell cycle dependent manner. A) HeLa lysates were prepared as described in Materials and Methods. Immunoblot analysis of RHAMM and TPX2 levels indicates equivalent amplification of RHAMM and TPX2 in mitotic (M), as compared to unsynchronized (US), lysates. IP experiments were separately performed on 150 µl precleared lysates using a polyclonal RHAMM antibody, the prebleed (PB) immune sera, a polyclonal TPX2 antibody, and a monoclonal NuMA antibody as described. 25µl (one-fifth of the IP volume) of precleared lysate (Loading control) and post-IP fractions were analysed to determine relative quantity and efficiency of the precipitations. The resulting IP were blotted with a RHAMM polyclonal serum or a TPX2 polyclonal serum. Blots showing RHAMM and TPX2 detection of Prebleed and RHAMM precipitation lanes were performed in repetitive experiments. Detection of protein bands utilized

ECL™ detection (Amersham biosciences). B) Post-IP fractions for the mitotic lysates are shown to indicate the relative amounts of RHAMM or TPX2 co-precipitated by various antisera. Quantitative detection utilized the Odyssey v1.1 Infrared imaging system (LI-COR) with detection of polyclonal sera using IRDye 800 conjugated anti-rabbit IgG (1:20000) to determine protein band concentrations. Quantitation of protein bands with the Odyssey™ systems subtracts background fluorescence intensity around the region of interest (in this case, the boxed regions outlining the protein bands). The top row shows the bands without concentration determination while the bottom row indicates the raw concentration measurements. The concentrations of the PB and NuMA bands were averaged to give a mean total fraction. Thus, the fraction remaining was determined by dividing the band concentration of each lane by the mean total fraction. C) HeLa and Raji (not shown) cells were synchronized by double thymidine block followed by nocodazole treatment. Mitotic HeLa cells were shaken off the plate and examined for DNA, message and protein content. Flow cytometry profile of DAPI stained HeLa populations confirms >90% synchronization. G_0/G_1 populations are defined by M1 marker, S populations by M3 marker and G_2/M populations by M2 markers. D) Unsynchronized (US) and mitotic (M) HeLa, and Raji (not shown), populations were lysed in CHAPS and the soluble fraction was analysed by quantitative immunoblot analysis. Quantitative detection utilized the Odyssey v1.1 Infrared imaging system (LI-COR) with detection of polyclonal sera using IRDye 800 conjugated anti-rabbit IgG. Note that detection of RHAMM antiserum utilized 1:5000 dilution while TPX2 detection utilized 1:20000. β-actin intensities were determined and utilized as a quantitative control for lane loading; M phase lysates consistently contained more protein per cell volume lysed. E) Unsynchronized (US) and mitotic (M) HeLa, and Raji (not shown), populations were reverse transcribed as per manufacturer's (Applied Biosystems) recommendation for quantitative RT-PCR analysis. RHAMM expression in mitotic populations were normalized to the unsynchronized populations.

RHAMM, like TPX2, is regulated during the cell cycle

As mentioned, TPX2 is subject to cell-cycle regulation (Gruss *et al.*, 2002). As RHAMM interacts with a significant proportion of TPX2 during mitosis, we investigated whether RHAMM was also cell cycle regulated. HeLa, and Raji (not shown), lines were

synchronized during G_2/M with a double thymidine/nocodazole block. The efficiency of these treatments were confirmed by flow cytometry analysis of DAPI staining within the synchronized populations (Figure 2-3C). Cell lysates were prepared through equivalent CHAPS lysis of HeLa ($5x10^6$/ml), and Raji ($20x10^6$/ml), synchronized populations. Quantitative immunoblot analysis was performed by normalizing the RHAMM, or TPX2, level to the corresponding β-actin levels. Qualitative, and quantitative, analysis reveals that RHAMM protein levels, like TPX2, are cell-cycle regulated (Figure 2-3D). The level of RHAMM protein in G_2/M populations is 1.5-2.0 times greater than in unsynchronized Raji and HeLa lysates. Quantitative RT-PCR revealed a 1.43-1.75 times amplification of RHAMM message in G_2/M Raji and HeLa populations (Figure 2-3E).

Inhibition of RHAMM function results in aberrant mitoses that approximate TPX2 inhibition

As significant amounts of RHAMM and TPX2 interact during mitosis, we hypothesized that RNA inhibition of RHAMM may induce similar phenotypes to that of TPX2 inhibition. RNA inhibition resulted in sustained loss of greater than 95% of cellular RHAMM and TPX2 protein 24 hours, through 48 hours, post transfection (Figure 2-4A). Cells were lysed and examined by immunoblot 24 and 48 hours post transfection and compared to control-treated cells (GL2, Dharmacon). Treatments were examined in triplicate. Inhibited and control cells were then fixed at defined timepoints and examined for mitotic index, using the marker CENP-F and α-tubulin. CENP-F expression, and localization, varies during the cell cycle demonstrating increasing nuclear staining during G_2 and accumulation on kinetochores early in G_2/M transition (Liao *et al.*, 1995). Mitotic

index was scored for an average of 493 cells per treatment at 30 and 48 hours post transfection.

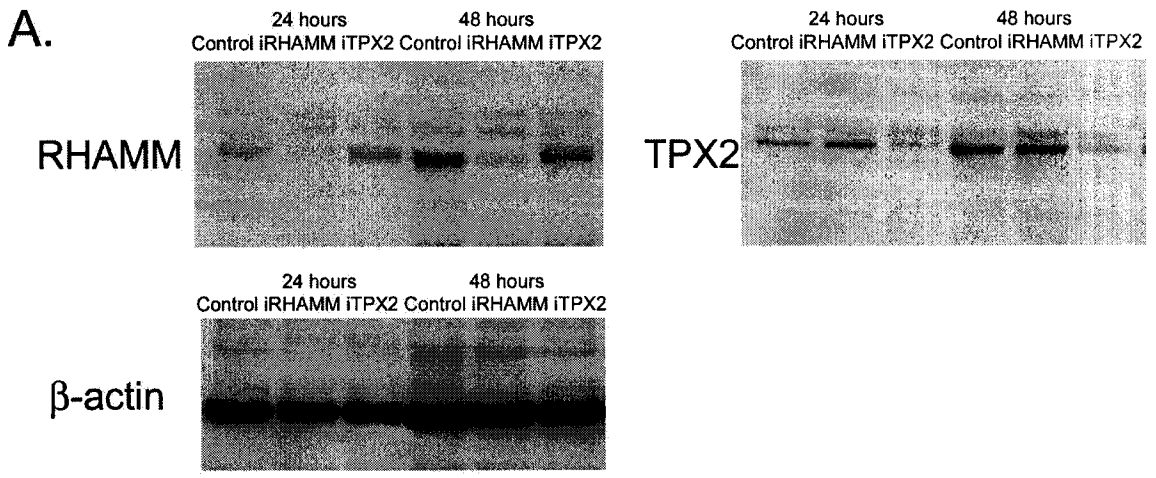

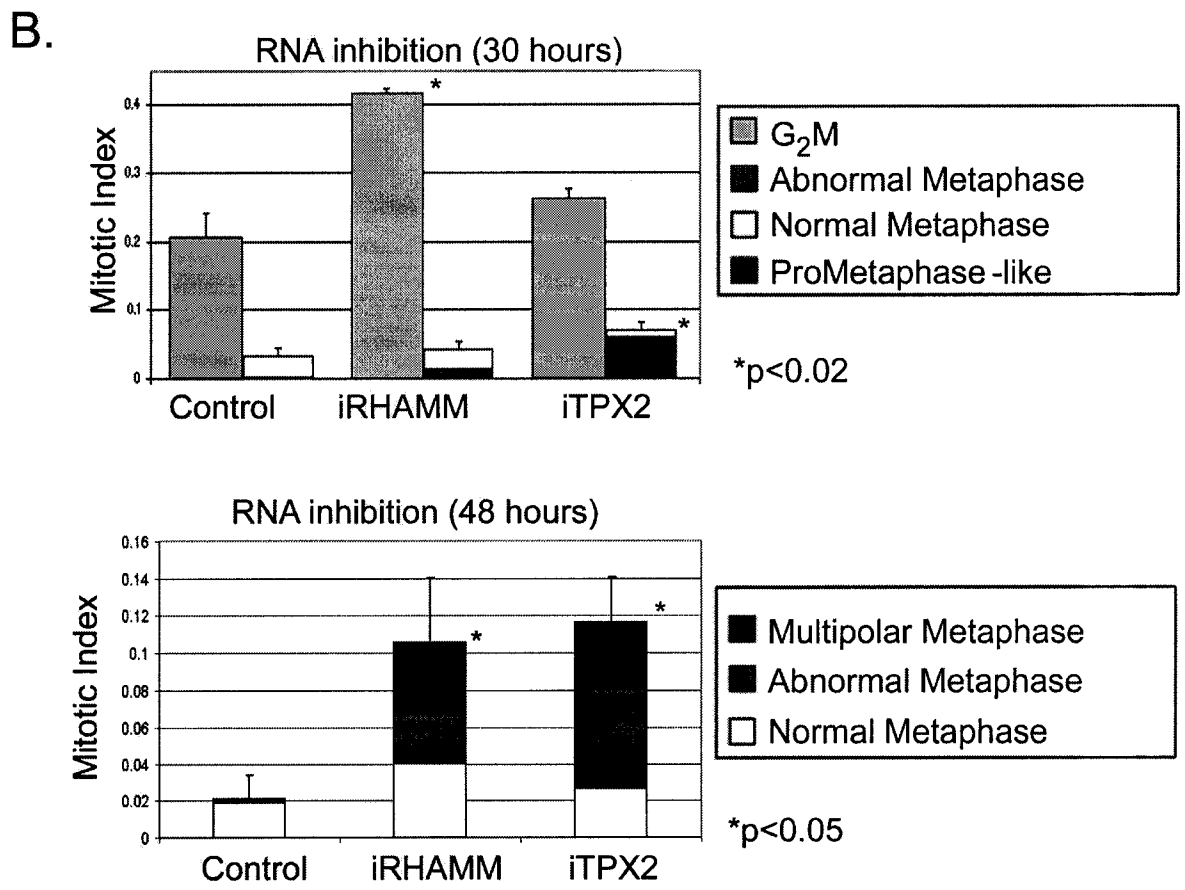

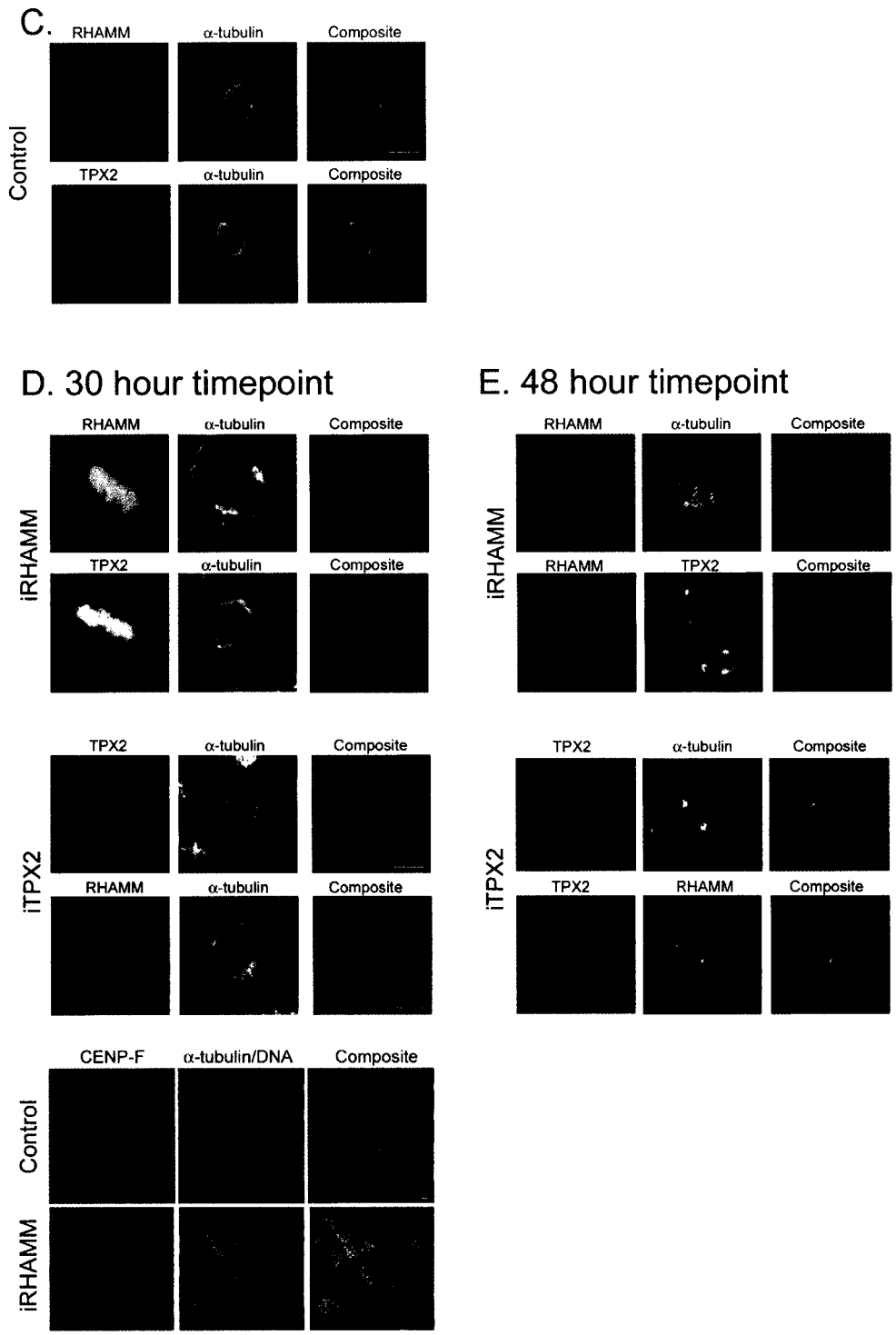

Figure 2-4: RNA inhibition of RHAMM and TPX2 reveal a common role in the maintenance of mitotic integrity. We carried out RNA interference as described (Elbashir *et al.*,

2001). A) Cells were treated with test, or control, duplexed RNA/Lipofectamine 2000 mixes overnight in OPTIMEM (GibcoBRL). At 24 and 48 hours, CHAPS soluble fractions were analysed by immunoblot. Immunoblotting confirmed greater than 95% inhibition of RHAMM and TPX2 24 and 48 hours post transfection. Blots were detected with ECL (shown) and LICOR detection. Equivalent loading was confirmed with β-actin B) Coverslips were recovered at appropriate timepoints following transfection. Cells were stained with CENP-F, α-tubulin and DAPI to quantitate mitotic index. At the 30 hour timepoint, inhibited cells were scored for stage, mitotic spindle structure and chromosome condensation/alignment. Error bars represent the standard deviation of mitotic index calculations (approx. 500 cells per treatment scored). For analysis of mitotic defects, RNA inhibition was confirmed in individual cells by staining for the appropriate target protein. Individual inhibited cells were assessed for DNA alignment and spindle structure to determine mitotic stage. TPX2 inhibition resulted in a significant increase in mitotic index ($p=0.017$) while RHAMM inhibition resulted in a significant increase in G_2 cells ($p=0.007$) when compared, by a student t-test, to control inhibited cells at the 30 hour timepoint. At the 48 hour timepoint, both RHAMM and TPX2 inhibition resulted in significant increases in metaphase cells ($p<0.05$) and in multipolar architecture ($p<0.03$). All graphical data is shown as percentage of all cells examined. C) Control RNA inhibition did not affect normal localization or intensity of RHAMM and TPX2 staining at all mitotic stages. Scale bars equal 10 μm. D) At the 30 hour timepoint, RHAMM inhibition induced phenotypically normal spindles with a proportion of metaphase cells (28.2%) exhibiting chromosome missegregation defects as demonstrated by DAPI (shown in white to facilitate viewing). TPX2 intensity and localization was not affected by RHAMM inhibition. At the 30 hour timepoint, TPX2 inhibition induced an increase in mitotic cells with prometaphase-like phenotypes (separated microtubule asters, condensed chromosomes but little microtubule connections between the two asters). RHAMM localization to microtubule asters was reduced within TPX2-inhibited cells. Nuclear CENP-F intensity and localization initiates and increases throughout G_2, loading onto prekinetochore at G_2/M transition. Control inhibition resulted in a G_2 index of approximately 20.5% while RHAMM inhibition resulted in a significantly increased G_2 index (41.6%, $p<0.01$). Scale bars equal 10 μm. E) At the 48 hour timepoint, RHAMM inhibition resulted in a significant increase in metaphase cells. A large proportion of these metaphase cells

(27.1%) contained mutlipolar spindle architecture. TPX2 localization to multipolar spindles was not affected by RHAMM inhibition. At the 48 hour timepoint, TPX2 inhibition also resulted in a significant increase in metaphase cells. Like RHAMM inhibition, these metaphase cells frequently (27.0%) displayed a multipolar phenotype. RHAMM localization to poles was dependent upon TPX2. Scale bars equal 10 μm.

At 30 hours, inhibition of TPX2 resulted in an increased mitotic index (7.0% vs 3.3%, $p<0.02$) and the suppression of spindle formation (Figure 2-4C). As described by Gruss et al. 2002, prometaphase-like phenotypes, characterized by chromosome condensation, aster separation and decreased microtubule polymerization, were observed in 82.1% of TPX2 inhibited mitotic cells (Figure 2-4D). Within these cells, RHAMM fluorescence was not significantly localized to the separated microtubule asters suggesting a role for TPX2 in the spindle pole targeting of RHAMM (Figure 4D). Very few mitotic cells (2.4%) were observed post-metaphase which strongly supports the hypothesis that TPX2 is important in the initiation of spindle assembly (Figure 2-4D). However, as TPX2 inhibited cells clearly proceed through mitosis, albeit at later timepoints and with significantly aberrant spindles (see Figure 2-4E), we conclude that it is not essential for mitotic assembly. We confirm previous work(Garrett *et al.*, 2002) and report that, at later timepoints, TPX2 inhibition induces a mitotic block with approximately 30.9% of TPX2-inhibited metaphase cells containing multipolar spindle phenotypes. Within this population of cells, we detected reduced amounts of TPX2 at the spindle poles. In the presence of reduced TPX2, RHAMM localized to the poles (Figure 2-4E). However, a proportion of TPX2-inhibited cells lacked polymerized spindles similar to that described above; within this population RHAMM was not localized to microtubule asters.

At 30 hours, RHAMM inhibition resulted in a significant increase in G_2 cells (41.6% vs 20.5%, $p<0.01$), characterized by CENP-F positive nucleii (Figure 2-4B,D). Although bipolar spindles formed by the 30 hour timepoint, approximately one-third of the metaphase cells had chromosomal missegregation defects (see Figure 2-4D). The increased G_2 population suggests that RHAMM inhibition results in a G_2/M stall prior to the initiation of prophase. At the 48 hour timepoint, RHAMM inhibition resulted in an accumulation of mitotic cells in metaphase (See Figure 2-4B,E). A large proportion of these metaphase cells (36.8%) contained multipolar architecture, confirming our previous microinjection observations (Maxwell *et al.*, 2003). RHAMM inhibition also resulted in a population of mitotic cells, designated abnormal metaphase, with small spindles or no spindles (similar to that described for TPX2 inhibition). Within the RHAMM-inhibited multipolar populations, TPX2 localized to the mitotic spindle poles (Figure 4E). At the 48 hour timepoint, both RHAMM and TPX2 inhibition resulted in dramatic increases in apoptotic cells and few G_1/S cells, demarcated by CENP-F negative nucleii (not shown). These results support a role for RHAMM and TPX2 in the maintenance of mitotic integrity, consistent with the conclusions drawn previously for TPX2 (Garrett *et al.*, 2002). Temporal examination of RHAMM and TPX2 inhibition reveal that these proteins perform distinct roles early in mitotic assembly; inhibition of RHAMM delays mitosis at the G_2/M boundary while TPX2-inhibition delays spindle assembly after nuclear envelope breakdown. These differences in early mitotic function are to be expected between proteins that localize to the centrosome and nucleus during interphase. However, the functions of these proteins converge during metaphase. In the absence of

RHAMM (or TPX2), mitotic spindles stall and fragment during metaphase; this phenomenon implicates both RHAMM and TPX2 as structural components of the spindle that cross-link microtubules and maintain spindle integrity as various microtubule –dependent motors exert force on spindle microtubules.

Discussion

In myeloma, chromosomal instability and elevated RHAMM expression characterize aggressive malignant cells; we hypothesized that elevated RHAMM expression may affect centrosomal and mitotic integrity with consequences on chromosomal segregation. This hypothesis is strengthened by ex vivo analysis of myeloma patients. Elevated RHAMM expression coincides with centrosomal abnormalities and cytogenetic abnormalities (CA) (Maxwell et al., in press.). 41% of MM patients with elevated RHAMM expression contained CA while 30% of low expressers contained CA; within the elevated RHAMM population 70% of CA were hypodiploid phenotype versus 50% of low expressers ($p=0.095$) (Maxwell et al, in press). Here, we report that exogenous GFP-RHAMM^{FL}, like endogenous RHAMM (Maxwell *et al.*, 2003), localizes to centrosomes, increasing their size and the amount of γ-tubulin present. These results model the aberrant centrosomal phenotypes observed within MM PC ex vivo; centrosomal abnormalities characterize MM PCs but fail to be prognostic. We further report that overexpression of GFP-RHAMM^{FL} has dramatic consequences on mitotic division. Nearly two-thirds of metaphase cells overexpressing GFP-RHAMM^{FL} have aberrant spindle phenotypes or misaligned chromosomes. Indeed, one quarter of these cells have monopolar or multipolar metaphase spindles. While the data suggests that the majority of these aberrant metaphase cells do not progress through subsequent mitotic phases (due to the low frequency of anaphase and telophase/cytokinesis transfected cells), one quarter of those that do progress demonstrate chromosome missegregation defects (i.e. lagging chromosomes, chromosome bridges) and may proceed through aberrant divisions.

Live cell GFP-RHAMM dynamics, coimmunoprecipitation and RNA inhibition experiments were utilized to investigate the mechanism(s) responsible for RHAMM-induced mitotic abnormalities. Live cell imaging revealed poleward movement of RHAMM aggregates in a manner and velocity consistent with dynein mediated movement; these observations confirm previous coprecipitation data and suggest that RHAMM targets spindle poles through an interaction with the dynein motor complex. We hypothesized that RHAMM, like Hklp2, may interact with TPX2, the protein that facilitates the klp2-dynein interaction and plays important roles in spindle assembly and integrity (Wittmann *et al.*, 2000) (Gruss *et al.*, 2002) (Garrett *et al.*, 2002). RHAMM colocalizes with TPX2 throughout mitosis and coprecipitates a significant amount of cellular TPX2 in a cell cycle dependent manner. Like TPX2, RHAMM protein and message is upregulated during mitosis. RNA inhibition experiments demonstrate that at early timepoints TPX2 plays an important, but non-essential, role in spindle assembly while RHAMM functions in the progression through G_2. Interestingly, addition of a soluble RHAMM variant, lacking the NH_2-terminal microtubule binding domain, also disregulates G_2/M progression (Mohapatra *et al.*, 1996) while overexpression of a RHAMM COOH-deletion variant inhibits mitotic progression (Maxwell *et al.*, 2003). After spindle assembly, RHAMM and TPX2 converge to play essential roles in maintaining spindle integrity.

During metaphase, chromosomal alignment and segregation is dependent on the generation of forces by microtubule based motor proteins and microtubule crosslinking

proteins, like RHAMM. Our results demonstrate that TPX2 function is important to RHAMM spindle pole localization. This data is consistent with a model in which TPX2 facilitates an interaction between RHAMM and the dynein motor complex. This ternary RHAMM-TPX2-dynein complex is essential to the maintenance of spindle integrity. Depletion of either TPX2 or RHAMM results in an imbalance of motor forces and subsequent spindle fragmentation. Conversely, overexpression of RHAMM results in an opposite imbalance of force cumulating in disorganized or multipolar spindles and an inability to appropriately align and segregate DNA. Similarly, TPX2 overexpression in Xenopus extracts results in unbalanced monopolar spindles (Wittmann *et al.*, 2000). While multipolar phenotypes are likely catastrophic, disorganized or fragmented spindles may induce more subtle losses of genetic material (see Figure 2-4D), or impede mitotic progression, and potentially result in hypodiploid progeny. The progression of such defects through mitosis is likely dependent on simultaneous disruption of the p53-dependent cell cycle checkpoint (Meraldi *et al.*, 2002) (Raff, 2002) (Figure 2-5). A direct link between RHAMM overexpression, oncogenesis and apoptosis may be mediated through TPX2 and Aurora A kinase (AurA).

Like RHAMM, AurA localizes to interphase centrosomes, duplicating prophase centrosomes and the mitotic spindle pole (Maxwell *et al.*, 2003) (Katayama *et al.*, 2004); AurA localization and function at spindle poles is also dependent on the action of TPX2 (Eyers *et al.*, 2003) (Kufer *et al.*, 2003). Multiple studies have demonstrated that TPX2 is responsible for the activation of AurA at the mitotic spindle (Bayliss *et al.*, 2003) (Eyers *et al.*, 2003) (Kufer *et al.*, 2002) (Kufer *et al.*, 2003). Here, we describe a cell cycle

dependent interaction between significant mitotic fractions of RHAMM and TPX2 suggesting that RHAMM may affect TPX2-mediated AurA activation. AurA is an essential determinant of G_2/M progression (Hirota *et al.*, 2003) that regulates, and is regulated by, the activities of p53 (Chen *et al.*, 2002; Gigoux *et al.*, 2002; Katayama *et al.*, 2004), ras-GAP (Gigoux *et al.*, 2002), BRCA1 (Ouchi *et al.*, 2004) and apoptotic pathways (Anand *et al.*, 2003). Overexpression of RHAMM, through an interaction/sequesteration of TPX2, may disrupt these pathways and induce/permit aberrant, or abortive, mitoses with consequent centrosome amplification and chromosomal instability; alternatively, overexpression of RHAMM may disrupt spindle forces leading to spindle fragmentation and chromosomal segregation defects. It is most likely that within MM, overexpression of RHAMM acts in concert with other genetic events to disregulate centrosomal structure, and/or replication, and modify mitotic chromosomal segregation and genetic stability.

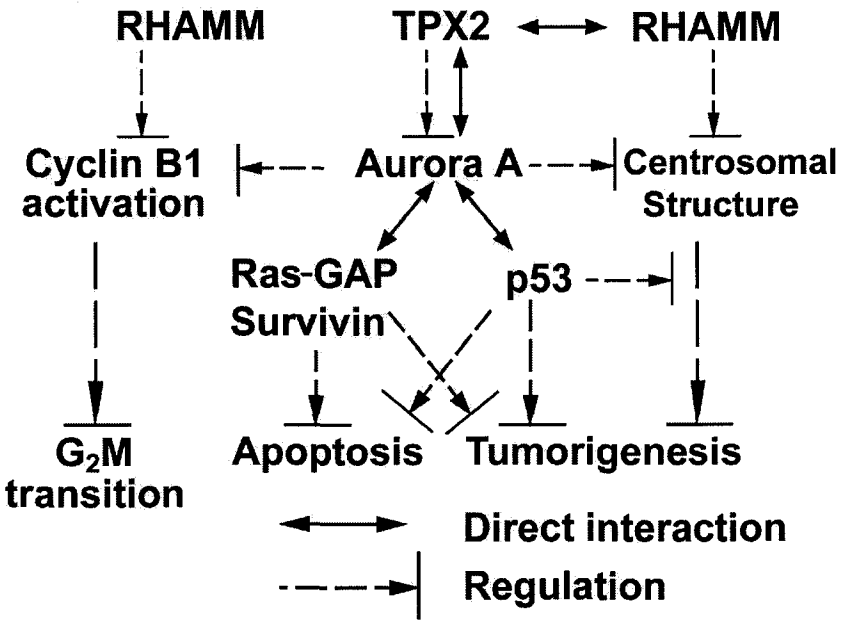

Figure 2-5: Model for the effects of RHAMM on centrosomal structure and tumorigenesis. As a centrosomal protein, overexpression of RHAMM may directly affect centrosomal size and structure. Consistent with previous reports, inhibition of RHAMM function impairs mitotic progression. During mitosis, RHAMM-TPX2-dynein form a ternary complex that functions in the maintenance of mitotic spindle integrity by crosslinking spindle microtubules. Overexpression of RHAMM may initiate an imbalance in spindle forces leading to disorganized spindles phenotypes and chromosomal missegregation. Alternatively, RHAMM directly interacts with a large cellular fraction of TPX2 which may alter the ability of TPX2 to regulate, and activate, Aurora A kinase with consequent downstream affects on multiple pathways including spindle assembly, ras, p53, apoptosis and oncogenesis. RHAMM has reported to affect Cyclin B1 activation (Mohapatra *et al.*, 1996); inhibition of this function may impair G_2/M progression.

References

Anand, S., Penrhyn-Lowe, S., and Venkitaraman, A.R. (2003). AURORA-A amplification overrides the mitotic spindle assembly checkpoint, inducing resistance to Taxol. Cancer Cell *3*, 51-62.

Andrews, P.D., Knatko, E., Moore, W.J., and Swedlow, J.R. (2003). Mitotic mechanics: the auroras come into view. Curr Opin Cell Biol *15*, 672-683.

Assmann, V., Jenkinson, D., Marshall, J.F., and Hart, I.R. (1999). The intracellular hyaluronan receptor RHAMM/IHABP interacts with microtubules and actin filaments. J Cell Sci *112 (Pt 22)*, 3943-3954.

Bayliss, R., Sardon, T., Vernos, I., and Conti, E. (2003). Structural basis of Aurora-A activation by TPX2 at the mitotic spindle. Mol Cell *12*, 851-862.

Carazo-Salas, R.E., Guarguaglini, G., Gruss, O.J., Segref, A., Karsenti, E., and Mattaj, I.W. (1999). Generation of GTP-bound Ran by RCC1 is required for chromatin-induced mitotic spindle formation. Nature *400*, 178-181.

Chan, G.K., Jablonski, S.A., Sudakin, V., Hittle, J.C., and Yen, T.J. (1999). Human BUBR1 is a mitotic checkpoint kinase that monitors CENP-E functions at kinetochores and binds the cyclosome/APC. J Cell Biol *146*, 941-954.

Chen, S.S., Chang, P.C., Cheng, Y.W., Tang, F.M., and Lin, Y.S. (2002). Suppression of the STK15 oncogenic activity requires a transactivation-independent p53 function. Embo J *21*, 4491-4499.

Compton, D.A., Yen, T.J., and Cleveland, D.W. (1991). Identification of novel centromere/kinetochore-associated proteins using monoclonal antibodies generated against human mitotic chromosome scaffolds. J Cell Biol *112*, 1083-1097.

Crainie, M., Belch, A.R., Mant, M.J., and Pilarski, L.M. (1999). Overexpression of the receptor for hyaluronan-mediated motility (RHAMM) characterizes the malignant clone in multiple myeloma: identification of three distinct RHAMM variants. Blood *93*, 1684-1696.

Elbashir, S.M., Harborth, J., Lendeckel, W., Yalcin, A., Weber, K., and Tuschl, T. (2001). Duplexes of 21-nucleotide RNAs mediate RNA interference in cultured mammalian cells. Nature *411*, 494-498.

Eyers, P.A., Erikson, E., Chen, L.G., and Maller, J.L. (2003). A novel mechanism for activation of the protein kinase Aurora A. Curr Biol *13*, 691-697.

Garrett, S., Auer, K., Compton, D.A., and Kapoor, T.M. (2002). hTPX2 is required for normal spindle morphology and centrosome integrity during vertebrate cell division. Curr Biol *12*, 2055-2059.

Ghadimi, B.M., Sackett, D.L., Difilippantonio, M.J., Schrock, E., Neumann, T., Jauho, A., Auer, G., and Ried, T. (2000). Centrosome amplification and instability occurs exclusively in aneuploid, but not in diploid colorectal cancer cell lines, and correlates with numerical chromosomal aberrations. Genes Chromosomes Cancer *27*, 183-190.

Giet, R., McLean, D., Descamps, S., Lee, M.J., Raff, J.W., Prigent, C., and Glover, D.M. (2002). Drosophila Aurora A kinase is required to localize D-TACC to centrosomes and to regulate astral microtubules. J Cell Biol *156*, 437-451.

Gigoux, V., L'Hoste, S., Raynaud, F., Camonis, J., and Garbay, C. (2002). Identification of Aurora kinases as RasGAP Src homology 3 domain-binding proteins. J Biol Chem *277*, 23742-23746.

Greiner, J., Ringhoffer, M., Taniguchi, M., Hauser, T., Schmitt, A., Dohner, H., and Schmitt, M. (2003). Characterization of several leukemia-associated antigens inducing humoral immune responses in acute and chronic myeloid leukemia. Int J Cancer *106*, 224-231.

Greiner, J., Ringhoffer, M., Taniguchi, M., Li, L., Schmitt, A., Shiku, H., Dohner, H., and Schmitt, M. (2004). mRNA expression of leukemia-associated antigens in patients with acute myeloid leukemia for the development of specific immunotherapies. Int J Cancer *108*, 704-711.

Gruss, O.J., Carazo-Salas, R.E., Schatz, C.A., Guarguaglini, G., Kast, J., Wilm, M., Le Bot, N., Vernos, I., Karsenti, E., and Mattaj, I.W. (2001). Ran induces spindle assembly by reversing the inhibitory effect of importin alpha on TPX2 activity. Cell *104*, 83-93.

Gruss, O.J., Wittmann, M., Yokoyama, H., Pepperkok, R., Kufer, T., Sillje, H., Karsenti, E., Mattaj, I.W., and Vernos, I. (2002). Chromosome-induced microtubule assembly mediated by TPX2 is required for spindle formation in HeLa cells. Nat Cell Biol *4*, 871-879.

Hall, C.L., Yang, B., Yang, X., Zhang, S., Turley, M., Samuel, S., Lange, L.A., Wang, C., Curpen, G.D., Savani, R.C., and et al. (1995). Overexpression of the hyaluronan receptor RHAMM is transforming and is also required for H-ras transformation. Cell *82*, 19-26.

Hirota, T., Kunitoku, N., Sasayama, T., Marumoto, T., Zhang, D., Nitta, M., Hatakeyama, K., and Saya, H. (2003). Aurora-A and an interacting activator, the LIM protein Ajuba, are required for mitotic commitment in human cells. Cell *114*, 585-598.

Hussein, M. (1994). Multiple myeloma: an overview of diagnosis and management. Cleve Clin J Med *61*, 285-298.

Kalab, P., Pu, R.T., and Dasso, M. (1999). The ran GTPase regulates mitotic spindle assembly. Curr Biol *9*, 481-484.

Kalab, P., Weis, K., and Heald, R. (2002). Visualization of a Ran-GTP gradient in interphase and mitotic Xenopus egg extracts. Science *295*, 2452-2456.

Katayama, H., Sasai, K., Kawai, H., Yuan, Z.M., Bondaruk, J., Suzuki, F., Fujii, S., Arlinghaus, R.B., Czerniak, B.A., and Sen, S. (2004). Phosphorylation by aurora kinase A induces Mdm2-mediated destabilization and inhibition of p53. Nat Genet *36*, 55-62.

Kellogg, D.R., Moritz, M., and Alberts, B.M. (1994). The centrosome and cellular organization. Annu Rev Biochem *63*, 639-674.

Khodjakov, A., Copenagle, L., Gordon, M.B., Compton, D.A., and Kapoor, T.M. (2003). Minus-end capture of preformed kinetochore fibers contributes to spindle morphogenesis. J Cell Biol *160*, 671-683.

Kufer, T.A., Nigg, E.A., and Sillje, H.H. (2003). Regulation of Aurora-A kinase on the mitotic spindle. Chromosoma *112*, 159-163.

Kufer, T.A., Sillje, H.H., Korner, R., Gruss, O.J., Meraldi, P., and Nigg, E.A. (2002). Human TPX2 is required for targeting Aurora-A kinase to the spindle. J Cell Biol *158*, 617-623.

Li, H., Guo, L., Li, J.W., Liu, N., Qi, R., and Liu, J. (2000). Expression of hyaluronan receptors CD44 and RHAMM in stomach cancers: relevance with tumor progression. Int J Oncol *17*, 927-932.

Liao, H., Winkfein, R.J., Mack, G., Rattner, J.B., and Yen, T.J. (1995). CENP-F is a protein of the nuclear matrix that assembles onto kinetochores at late G2 and is rapidly degraded after mitosis. J Cell Biol *130*, 507-518.

Lingle, W.L., and Salisbury, J.L. (1999). Altered centrosome structure is associated with abnormal mitoses in human breast tumors. Am J Pathol *155*, 1941-1951.

Masellis-Smith, A., Belch, A.R., Mant, M.J., Turley, E.A., and Pilarski, L.M. (1996). Hyaluronan-dependent motility of B cells and leukemic plasma cells in blood, but not of bone marrow plasma cells, in multiple myeloma: alternate use of receptor for hyaluronan-mediated motility (RHAMM) and CD44. Blood *87*, 1891-1899.

Maxwell, C.A., Keats, J.J., Crainie, M., Sun, X., Yen, T., Shibuya, E., Hendzel, M., Chan, G., and Pilarski, L.M. (2003). RHAMM is a centrosomal protein that interacts with dynein and maintains spindle pole stability. Mol Biol Cell *14*, 2262-2276.

Meraldi, P., Honda, R., and Nigg, E.A. (2002). Aurora-A overexpression reveals tetraploidization as a major route to centrosome amplification in p53-/- cells. Embo J *21*, 483-492.

Merdes, A., Heald, R., Samejima, K., Earnshaw, W.C., and Cleveland, D.W. (2000). Formation of spindle poles by dynein/dynactin-dependent transport of NuMA. J Cell Biol *149*, 851-862.

Mohapatra, S., Yang, X., Wright, J.A., Turley, E.A., and Greenberg, A.H. (1996). Soluble hyaluronan receptor RHAMM induces mitotic arrest by suppressing Cdc2 and cyclin B1 expression. J Exp Med *183*, 1663-1668.

Moore, W., Zhang, C., and Clarke, P.R. (2002). Targeting of RCC1 to chromosomes is required for proper mitotic spindle assembly in human cells. Curr Biol *12*, 1442-1447.

Nachury, M.V., Maresca, T.J., Salmon, W.C., Waterman-Storer, C.M., Heald, R., and Weis, K. (2001). Importin beta is a mitotic target of the small GTPase Ran in spindle assembly. Cell *104*, 95-106.

Ohba, T., Nakamura, M., Nishitani, H., and Nishimoto, T. (1999). Self-organization of microtubule asters induced in Xenopus egg extracts by GTP-bound Ran. Science *284*, 1356-1358.

Ouchi, M., Fujiuchi, N., Sasai, K., Katayama, H., Minamimori, Y.A., Ongusaha, P.P., Deng, C., Sen, S., Lee, S.W., and Ouchi, T. (2004). BRCA1 phosphorylation by Aurora-A in the regulation of G2 to M transition. J Biol Chem.

Pihan, G.A., Purohit, A., Wallace, J., Knecht, H., Woda, B., Quesenberry, P., and Doxsey, S.J. (1998). Centrosome defects and genetic instability in malignant tumors. Cancer Res *58*, 3974-3985.

Pihan, G.A., Wallace, J., Zhou, Y., and Doxsey, S.J. (2003). Centrosome abnormalities and chromosome instability occur together in pre-invasive carcinomas. Cancer Res *63*, 1398-1404.

Raff, J.W. (2002). Centrosomes and cancer: lessons from a TACC. Trends Cell Biol *12*, 222-225.

Rein, D.T., Roehrig, K., Schondorf, T., Lazar, A., Fleisch, M., Niederacher, D., Bender, H.G., and Dall, P. (2003). Expression of the hyaluronan receptor RHAMM in endometrial carcinomas suggests a role in tumour progression and metastasis. J Cancer Res Clin Oncol *129*, 161-164.

Sato, N., Mizumoto, K., Nakamura, M., Nakamura, K., Kusumoto, M., Niiyama, H., Ogawa, T., and Tanaka, M. (1999). Centrosome abnormalities in pancreatic ductal carcinoma. Clin Cancer Res *5*, 963-970.

Schatz, C.A., Santarella, R., Hoenger, A., Karsenti, E., Mattaj, I.W., Gruss, O.J., and Carazo-Salas, R.E. (2003). Importin alpha-regulated nucleation of microtubules by TPX2. Embo J *22*, 2060-2070.

Tsai, M.Y., Wiese, C., Cao, K., Martin, O., Donovan, P., Ruderman, J., Prigent, C., and Zheng, Y. (2003). A Ran signalling pathway mediated by the mitotic kinase Aurora A in spindle assembly. Nat Cell Biol *5*, 242-248.

Turley, E.A. (1982). Purification of a hyaluronate-binding protein fraction that modifies cell social behavior. Biochem Biophys Res Commun *108*, 1016-1024.

Turley, E.A., Noble, P.W., and Bourguignon, L.Y. (2002). Signaling properties of hyaluronan receptors. J Biol Chem *277*, 4589-4592.

Wang, C., Thor, A.D., Moore, D.H., 2nd, Zhao, Y., Kerschmann, R., Stern, R., Watson, P.H., and Turley, E.A. (1998). The overexpression of RHAMM, a hyaluronan-binding protein that regulates ras signaling, correlates with overexpression of mitogen-activated protein kinase and is a significant parameter in breast cancer progression. Clin Cancer Res *4*, 567-576.

Wiese, C., Wilde, A., Moore, M.S., Adam, S.A., Merdes, A., and Zheng, Y. (2001). Role of importin-beta in coupling Ran to downstream targets in microtubule assembly. Science *291*, 653-656.

Wilde, A., and Zheng, Y. (1999). Stimulation of microtubule aster formation and spindle assembly by the small GTPase Ran. Science *284*, 1359-1362.

Wittmann, T., Boleti, H., Antony, C., Karsenti, E., and Vernos, I. (1998). Localization of the kinesin-like protein Xklp2 to spindle poles requires a leucine zipper, a microtubule-associated protein, and dynein. J Cell Biol *143*, 673-685.

Wittmann, T., Wilm, M., Karsenti, E., and Vernos, I. (2000). TPX2, A novel xenopus MAP involved in spindle pole organization. J Cell Biol *149*, 1405-1418.

Yang, B., Zhang, L., and Turley, E.A. (1993). Identification of two hyaluronan-binding domains in the hyaluronan receptor RHAMM. J Biol Chem *268*, 8617-8623.

Zhang, S., Chang, M.C., Zylka, D., Turley, S., Harrison, R., and Turley, E.A. (1998). The hyaluronan receptor RHAMM regulates extracellular-regulated kinase. J Biol Chem *273*, 11342-11348.

Chapter 3: RHAMM expression and isoform balance predicts aggressive disease and poor survival in multiple myeloma

This research was originally published in *BLOOD.* C.A. Maxwell, E. Rasmussen, F. Zhan, J. J. Keats, S. Adamia, E. Strachan, M. Crainie, R. Walker, A.R. Belch, L.M. Pilarski, B. Barlogie, J. Shaughnessy Jr., T. Reiman. RHAMM expression and isoform balance predicts aggressive disease and poor survival in multiple myeloma. BLOOD. 2004; August 15, 2004; 104 (4) © by the American Society of Hematology.

Introduction

Multiple myeloma (MM) is a B-cell neoplasm characterized by accumulation of clonal plasma cells (PC) in the bone marrow, secretion of a monoclonal protein (M-protein), and osteolytic lesions accompanied by bone pain and anemia (Grogan *et al.*, 2001). MM is further characterized by chromosomal instability (CIN) and a defining VDJ rearrangement of the immunoglobulin heavy chain (IgH) gene locus, termed clonotypic (Kuehl and Bergsagel, 2002) (Szczepek *et al.*, 1997). Recurrent genetic translocations into switch recombination regions of the IgH locus occur in up to 75% of myelomas (Avet-Loiseau *et al.*, 2002) (Fonseca *et al.*, 2004); one of the most common of these is t(4;14)(p16.3;q32) (Avet-Loiseau *et al.*, 2002) (Keats *et al.*, 2003). MM PC contain extensive chromosomal abnormalities, both numerical and structural (Fonseca *et al.*, 2004). The presence of specific genetic lesions are prognostic (Grogan *et al.*, 2001) (Avet-Loiseau *et al.*, 2002) (Keats *et al.*, 2003).

An additional ubiquitous feature MM is the expression of the Receptor for Hyaluronan Mediated Motility (RHAMM) (Crainie *et al.*, 1999). RHAMM was cloned in 1992 and described as a hyaluronan binding protein (Yang *et al.*, 1993) (Hardwick *et al.*, 1992). A variant of RHAMM, that is predominantly cytoplasmic and involved in multiple signaling pathways (Hall *et al.*, 1996) (Zhang *et al.*, 1998), is transforming and essential for *ras* transformation (Hall *et al.*, 1995). Human $RHAMM^{FL}$ was cloned in 1996 as a predicted 85-95 kDa protein encoded by 18 exons (Wang *et al.*, 1996). $RHAMM^{FL}$ has been described as an actin and microtubule associated protein that

localizes to the centrosome and mitotic spindle pole and is essential for mitotic stability (Assmann *et al.*, 1999; Maxwell *et al.*, 2003). The NH_2-terminus of RHAMM directly interacts with microtubules, via exon 4, while the COOH-terminus targets the centrosome, presumably through an indirect interaction with dynein (Assmann *et al.*, 1999; Maxwell *et al.*, 2003). Loss of exon 4 inhibits the ability of RHAMM to interact with interphase microtubules (Assmann *et al.*, 1999); disruption of the COOH-terminus, by microinjection of polyclonal antiserum, affects mitotic integrity and induces tripolar and tetrapolar spindles (Maxwell *et al.*, 2003).

While RHAMM is ubiquitously expressed in murine tissues (with elevated expression in testes, thymus and spleen) (Fieber *et al.*, 1999), consistent detection of RHAMM expression within normal human tissues appears to be limited to the testis (Line *et al.*, 2002) (Greiner *et al.*, 2002). Reports of RHAMM expression have identified the testis, spleen, colon, and stomach (Line *et al.*, 2002), the testis, placenta and thymus (Greiner *et al.*, 2002)and the testis, placenta, lung, and pancreas (Greiner *et al.*, 2004) as RHAMM positive tissues (in decreasing orders, respectively). RHAMM expression is rare in normal peripheral blood (Greiner *et al.*, 2002) (Line *et al.*, 2002) (Crainie *et al.*, 1999) and purified $CD19^+$ (Crainie *et al.*, 1999) or $CD34^+$ PBMC (Greiner *et al.*, 2004). RHAMM expression influences tumor progression and metastasis in melanoma, pancreatic, breast and endometrial carcinomas (Abetamann *et al.*, 1996; Wang *et al.*, 1998; Ahrens *et al.*, 2001; Rein *et al.*, 2003) and RHAMM is detected as a tumor associated antigen in AML, CML (Greiner *et al.*, 2002) and colon cancer (Line *et al.*, 2002). A splice variant of exon 4, $RHAMM^{-exon4}$ ($RHAMM^{-48}$), was first described in

myeloma patients and subsequently identified in diverse tumours and cancer cell lines (Assmann *et al.*, 1999; Crainie *et al.*, 1999; Line *et al.*, 2002). RHAMM^{-exon4} is also found in normal tissues, and the relative ratio of these two isoforms differs between paired cancerous and adjacent normal tissue in colon cancer patients (Line *et al.*, 2002). While RHAMM^{FL} and RHAMM^{-exon4} expression are associated with malignancy, until now it has been unclear whether RHAMM isoforms are expressed concurrently in the same cell and what, if any, is the clinical significance of their expression.

In this study we report MM PC gene expression array data showing that elevated RHAMM mRNA levels correlate with the presence of osteolytic bone lesions, and that high RHAMM expression negatively correlates with event-free and overall survival. We identify a partial correlation in MM PC between elevated RHAMM expression and increased splicing of RHAMM^{-exon4}. In cell lines, while absolute RHAMM expression increases through mitosis, exon 4 splicing remains consistently low. We further demonstrate that individual myeloma plasma cells rarely express both isoforms concurrently, and that patients differ in their RHAMM isoform expression profiles. RHAMM isoform ratios in the blood vary within individual patients through the course of disease, decreasing post treatment and increasing with disease relapse. High RHAMM^{-exon4}/RHAMM^{FL} ratios in the bone marrow at the time of diagnosis correlate with poor survival, independent of standard prognostic factors.

Materials and Methods

Patients and Clinical Data

In Alberta, Canada, total RNA extracts from BM biopsies of 101 newly diagnosed MM patients were used to assess the prognostic impact of RHAMM exon 4 splicing. Sorted BM PC from an additional 22 patients were used to examine RHAMM expression and splicing at the single-cell level (n=8) and absolute RHAMM expression at the population level (n=14). Peripheral blood cellular RNA samples from 5 $t(4;14)^+$ MM patients were obtained at various time points in the course of disease, as described previously (Keats *et al.*, 2003), and were used to examine temporal changes in RHAMM expression patterns.

In Arkansas, USA, samples for microarray experiments included purified PC from a separate cohort of 210 newly diagnosed cases of MM. Isolation from mononuclear cell fraction was performed and purity was confirmed as previously described (Zhan *et al.*, 2002). Skeletal roentgenogram surveys (n=199) and skeletal MRI (n=193) were performed on the Arkansas cases to sub-classify patients as having no focal bone lesions, at least one focal lesion, and three or more focal lesions. Arkansas patients were treated with Total Therapy II (Barlogie *et al.*, 1999; Shaughnessy *et al.*, 2003) and were followed for event-free and overall survival.

Total RNA isolation, cDNA synthesis, preparation of labeled cRNA, hybridization to microarrays, and analysis of GeneChip data (Arkansas patients)

Total RNA was isolated from PC using the RNeasy Mini kits (QIAGEN, Valencia, CA). Detailed protocols for cDNA synthesis, cRNA preparation, hybridization to the U95Av2 microarray (Affymetrix Inc., Santa Clara, CA) and analysis of raw data have been described (Zhan *et al.*, 2002). All microarray data used in the analyses were derived from Affymetrix 5.0 software. GeneChip 5.0 output files provide signal that represents the difference between the intensities of the sequence-specific perfect match probe set and mismatch probe set, or as a detection of present, marginal, or absent as determined by the GeneChip 5.0 algorithm. Gene arrays were scaled to a target intensity of 1,500 and then analyzed independently. All signal calls were transformed by the log base 2 and each sample was normalized to give a mean of 0 and variance of 1. The oligonucleotide probes target the carboxy terminal sequences of RHAMM mRNA and therefore detect both $RHAMM^{-exon4}$ and $RHAMM^{FL}$ without distinguishing the two variants. High and low RHAMM gene expression is defined as expression above and below the median.

RNA extraction, cDNA synthesis and RT-PCR (Alberta patients)

Patient bone marrow mononuclear cells (BMMC) and peripheral blood mononuclear cells (PBMC) were purified on Ficoll-Hypaque Plus (Amersham Pharmacia Biotech, Uppsala, Sweden) density gradients. For single cell analysis, BMMC were

stained with CD138 or CD38 to mark PC. Individual PC, or 1000 cells/well, were sorted into PCR tubes using a direct lysis protocol, followed by single cell RT-PCR as previously described (Szczepek *et al.*, 1998). For aggregate populations (PBMC, BMMC or sorted PC), cells were suspended in TRIzol Reagent (Invitrogen, Carlsbad, CA) at 2-10 $\times 10^6$ cells/mL and total RNA was extracted according to the manufacturer's instructions. Poly-A-tailed RNA was reverse transcribed for 1 hour at 42°C followed by enzyme inactivation at 99°C for 3 minutes from 1 μg total RNA with 500 μM dT15, 500 μM each dNTP, 10 mM dithiothreitol (DTT), 50 mM Tris (tris[hydroxymethyl]aminomethane)-HCl, 75 mM KCl, 3 mM $MgCl_2$, and 200 U Superscript RNase H Reverse Transcriptase (Invitrogen) in a 20-μL reaction.

All RT-PCRs contained 20 mM Tris-HCl, 50 mM KCl, 2.0 mM $MgCl_2$, 200 μM each dNTP, 1.0 U Platinum Taq DNA polymerase (Invitrogen), and 0.2 μM each PCR primer. Reactions were carried out in 25-μL reactions using 4% of the cDNA as template. Reactions consisted of an initial 5-minute denaturation at 94°C, followed by 30 cycles of amplification at an annealing temperature of 64°C and 30 second extensions at 72°C. RHAMM primers were as follows:

5' primer: TGACAAAGATACTACCTTGCCTGCT

3' primer: CAGCATTTAGCCTTGCTTCCATC

The primers were designed to flank exon 4, so that two RT-PCR products of different sizes could be detected in a single reaction, representing full-length RHAMM and the splice variant lacking exon 4. A 6-FAM fluoresceinated label was added to the 3'

primer for detection using fragment capillary electrophoresis (FCE) (ABI3100, Applied Biosystems, Foster City, CA). RT-PCR products were visualized by ethidium bromide (EtBr) staining on 2% agarose (Invitrogen) gels or by capillary electrophoresis as described (Pilarski *et al.*, 2002; Adamia *et al.*, 2003). Single cell RT-PCR products were precipitated prior to capillary electrophoresis, to increase sensitivity of detection. Sequencing of clonotypic VDJ was performed as described (Szczepek *et al.*, 1998).

The relative amount of exon 4 splicing in a given sample was estimated by calculating the ratio of fluorescence intensity of the $RHAMM^{-exon4}$ and $RHAMM^{FL}$ products following RT-PCR and FCE (i.e. the $RHAMM^{-exon4}/RHAMM^{FL}$ ratio, hereafter "RHAMM ratio"). Each sample was analyzed in triplicate. Fluorescence intensity was analyzed using GeneScan ® software (Applied Biosystems).

Quantitative RT-PCR (Alberta).

BMMC were stained with anti-CD138 microbeads (Miltenyi Biotec, Auburn CA) as suggested by the manufacturer and single column isolations were performed on an autoMACS Magnetic Cell Sorter (Miltenyi Biotec). Purity of the selected, CD138 positive PC, was verified to be greater than 90% by cytospin and morphology examination. RNA isolation, sample quality examination, and reverse transcription were as suggested by the manufacturer Applied Biosystems, Foster City CA). Each quantitative RT-PCR reaction was performed in a 50 ul volume consisting of 1x Universal PCR Master Mix No AmpErase® UNG (Applied Biosystems), 2 ul of the respective Taqman® Assays-on-Demand™ Gene Expression Products primer and probe

mix for GAPDH (Hs99999905_m1) or RHAMM (Hs00234864_m1)(Applied Biosystems), and 5 ng of RNA converted to cDNA as template. Reactions were run on an ABI PRISM™ 7700 Sequence Detection System (Applied Biosystems). Quantitation using the Relative Standard Curve Method was performed using a 2 Log dilution range of Raji cDNA to generate a standard curve for each reaction.

Cell Culture, transient transfection, and plasmids

Cells from RPMI 8226, a human lymphoblastic cell line derived from the peripheral blood of a multiple myeloma patient, and HeLa cells, a human adherent epithelial cell line derived from a patient with cervical adenocarcinoma, were cultured as recommended. Cells were passaged 24 hours prior to transfection. Suspension cells were transfected by electroporation (270mV, 960uF, 47-53ms) while HeLa cells were transfected with Lipofectamine 2000 (Invitrogen) following the manufacturer's protocols. GFP-RHAMM^{FL}, GFP-RHAMM$^{-exon\ 4}$ and pEGFP-C1 (Clonetech) plasmids were prepared as described (Maxwell *et al.*, 2003).

Fluorescence Recovery After Photobleaching

A laser-scanning confocal microscope (Zeiss LSM 510) with a 15-mA argon laser was used to perform all photobleaching experiments using a 40 1.3 N.A. objective. We performed FRAP experiments as described previously (Lever *et al.*, 2000). Briefly, defined regions of interest (ROI) within cells (i.e. spindle pole, centrosome, cytoplasm) were exposed to 100% laser intensity for 10–20 iterations. Imaging was performed at 1-4 % laser intensity. The interval between scans was set so that between 25 and 40 image

scans were collected per experiment. Recovery was considered complete when the intensity of the bleached ROI stabilized. For quantitative analysis, fluorescence intensity was measured at each time point for (1) the photobleached region, (2) the entire cell volume and (3) the extracellular background intensity using Zeiss LSM software. Background was subtracted from each data point. Fluorescence loss occurs during bleaching and the repeated image acquisition. The fluorescence in each ROI was therefore corrected at each time point for whole-cell fluorescence (i.e. if the whole-cell fluorescence at time t_x was 85% of time t_0 (postbleach) then the fluorescence at t_x was corrected (divided) by 0.85). The mobile population (percent recovery) was determined by dividing the normalized photobleached region at maximal recovery (the mean normalized fluorescence of the last five scans) by the corrected fluorescence intensity of the photobleached region before photobleaching. Because of the contribution of electronic noise in the detector system, some measured recoveries were greater than 100%.

Synchronization, Immunoprecipitations and quantitation (Alberta)

HeLa and Raji cells were synchronized by double thymidine block. Briefly, cells were plated at sub-confluency and incubated with, or without, 2mM thymidine for 14-16 hours. Cells were washed, released from thymidine block and incubated in fresh media for 8 hours. Cells were washed and the synchronized populations were incubated with 2mM thymidine for 14-16 hours. Cells were released into fresh media for 3-4 hours and synchronized populations were incubated in 300ng/ml nocodazole (Sigma) for 10-12 hours, washed with PBS and released by shake-off. Unsynchronized HeLa populations

were released from plates with 1x trypsin. Both mitotic and unsynchronized populations were then washed 3x with PBS and lysed at $5x10^6$-10^7 cells/ml in 1% CHAPs plus 10 μg/mL leupeptin, 10 μg/mL antipain and 1 mM phenylmethylsulfonyl fluoride (all from Sigma). Protein quantitation utilized the Odyssey v1.1 Infrared imaging system (LI-COR) with detection of polyclonal sera using IRDye 800 conjugated anti-rabbit IgG (Rockland, Gilbertsville, PA).

Statistical Methods

Statistical analyses were performed with the software packages SPSS (SPSS, Chicago, IL) and SAS v8 for Windows (SAS Inc., Cary, NC). Differences in proportions were compared using Fisher's Exact Test. Between-group comparisons of continuous variables were with Student's t-test, or the Wilcoxon rank sum test. Linear relationships were determined by Pearson's or Spearman's correlation coefficient. Survival curves were plotted using the Kaplan-Meier method. Comparison of survival distributions was with the log rank test. Logistic regression was used to assess the independent associations of RHAMM and DKK1 with osteolytic lesions. Cox proportional hazards analysis was used to assess the independent prognostic significance of the RHAMM ratio. Statistical significance was set at a level of $p < 0.05$ using 2-sided analysis.

Results

Increased RHAMM expression levels correlate with bone lesions, but not with DKK1 expression (Arkansas patients)

The characteristics of the 210 Arkansas patients are outlined in Table 3-1, for the total population as well as for the two subgroups of patients defined based on the median level of RHAMM expression. Patients expressing RHAMM at levels below the median are classified as "low" RHAMM expressers; patients above the median are classified as "high" RHAMM expressers. Among the conventional measures of disease severity listed in Table 1, only LDH is correlated with RHAMM at a p-value of 0.05 or less.

Preliminary microarray experiments had identified RHAMM as one of the genes most highly correlated with the presence of bone lesions in myeloma (Zhan *et al.*, 2002), prompting us to investigate further the association between RHAMM and bone lesions. The proportion of patients with 1+ MRI-detected focal bone lesions was significantly higher in the "high" than in the "low" RHAMM expressers (Table 3-1). The association between bone lesions and RHAMM expression was also found to be significant when using the less sensitive technique of skeletal x-rays as the basis for assessment of bone disease, or when comparing only those patients with multiple bone lesions to the group lacking bone lesions (Table 3-1).

Factor	Overall	Low Expression	High Expression	P-value
Age>=65	28/210 (13%)	14/105 (13%)	14/105 (13%)	1.000
White	186/210 89%)	93/105 (89%)	93/105 (89%)	1.000
Female	84/210 (40%)	48/105 (46%)	36/105 (34%)	0.091
Kappa	124/196 (63%)	60/98 (61%)	64/98 (65%)	0.553
Lambda	72/196 (37%)	38/98 (39%)	34/98 (35%)	0.553
IgA Isotype	48/195 (25%)	25/102 (25%)	23/93 (25%)	0.971
B2M>=4 mg/L	77/210 (37%)	40/105 (38%)	37/105 (35%)	0.667
Creatinine>=2.0 mg/dL	21/210 (10%)	8/105 (8%)	13/105 (12%)	0.250
LDH>=190 UI/L	67/210 (32%)	23/105 (22%)	44/105 (42%)	0.002*
Albumin<3.5 g/dL	31/210 (15%)	12/105 (11%)	19/105 (18%)	0.173
HGB<10 g/dL	57/210 (27%)	32/105 (30%)	25/105 (24%)	0.277
PCLI>=1.0%	28/184 (15%)	11/91 (12%)	17/93 (18%)	0.242
BMPC>=33%	107/169 (63%)	56/90 (62%)	51/79 (65%)	0.753
Cytogenetics abnormalities	68/191 (36%)	28/94 (30%)	40/97 (41%)	0.098
--CA13 or hypodiploid	42/68 (62%)	14/28 (50%)	28/40 (70%)	0.095
--Other CA	26/68 (38%)	14/28 (50%)	12/40 (30%)	0.095
FISH13 20%	88/168 (52%)	42/89 (47%)	46/79 (58%)	0.153
FISH13 80%	46/168 (27%)	23/89 (26%)	23/79 (29%)	0.635
1+ MRI focal bone lesions	151/193 (78%)	65/93 (70%)	86/100 (86%)	0.007*

Factor	Overall	Low Expression	High Expression	P-value
3+ MRI focal bone lesions	120/193 (62%)	45/93 (48%)	75/100 (75%)	<.001*
1+ X-ray focal bone lesions	122/199 (61%)	52/97 (54%)	70/102 (69%)	0.030*
3+ X-ray focal bone lesions	80/199 (40%)	27/97 (28%)	53/102 (52%)	<.001*

Table 3-1. Clinical characteristics of 210 myeloma patients from the Arkansas cohort, stratified by RHAMM expression below or above the median level for the cohort (dubbed "low" or "high" expression). RHAMM expression was determined from oligonucleotide microarray experiments on sorted MM PC. P-values refer to statistical comparisons between low and high RHAMM expressers; p-values <0.05 are labeled with an asterisk (*).

A recent publication by the Arkansas group has demonstrated a significant correlation between expression of the DKK1 gene and the presence of osteolytic lesions (Tian *et al.*, 2003). We examined the correlation between RHAMM and DKK1 expression in the microarray experiments. Remarkably, there was no statistically significant correlation between the expression of RHAMM and DKK1 (Spearman's r=0.077, p=0.26). Logistic regression modeling of MRI-detectable bone lesions revealed that RHAMM and DKK1 are both independently and significantly associated with the presence of lytic bone disease (Odds Ratio (OR) for bone lesions in 2-variable regression model: for DKK1, OR = 1.37 (95% CI, 1.18-1.60), p<0.0001; for RHAMM, OR = 1.72 (95% CI, 1.14-2.59), p<0.001).

RHAMM expression correlates with poor disease-free and overall survival (Arkansas patients)

Figures 3-1a and 3-1b show overall and event-free survival for 210 Arkansas patients stratified by high versus low RHAMM expression (median cutoff) as assessed by microarray. High RHAMM expression is significantly associated with poor outcome. The 2-year overall survival estimate for patients with high RHAMM expression is 76% and with low RHAMM is 88% (p=0.04). The 2-year event-free survival in high RHAMM expressers is 76%, versus 88% in the low RHAMM expressers (p=0.05).

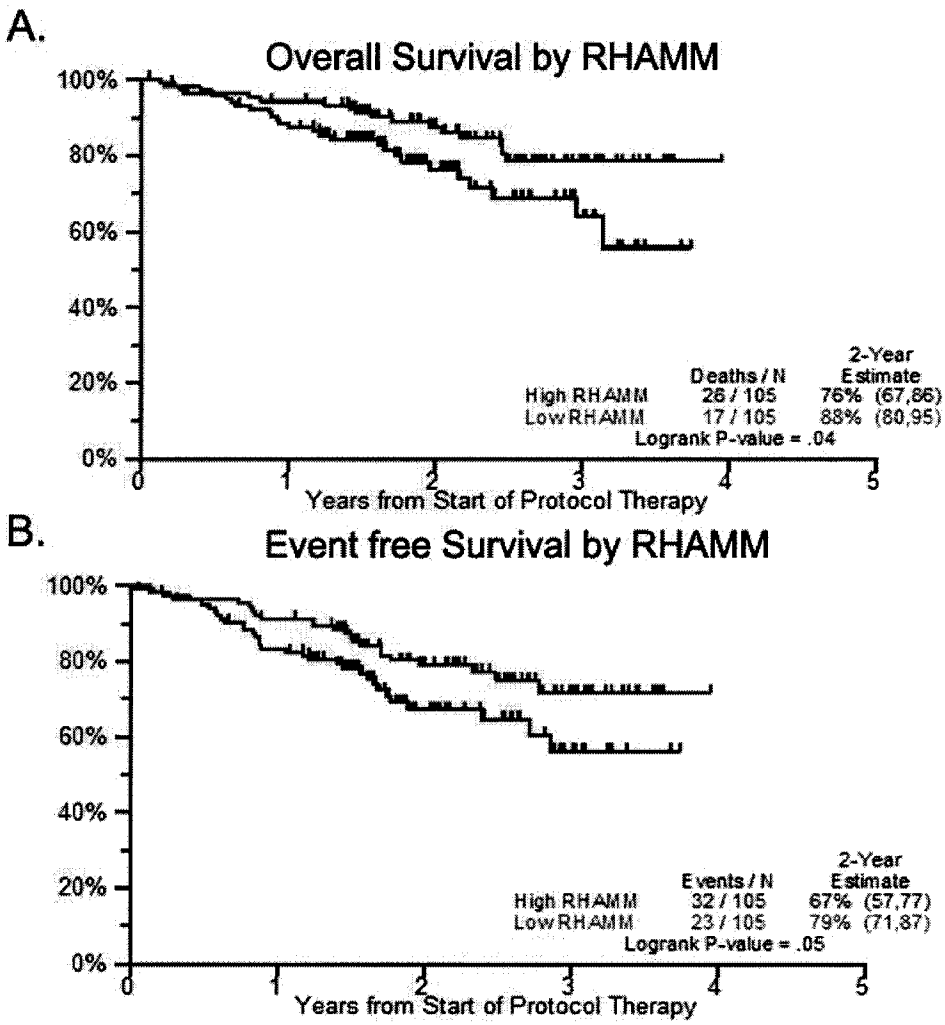

Figure 3-1: RHAMM expression predicts event-free and overall survival. Figures 1a and 1b show Kaplan-Meier overall and event-free survival distributions for 210 Arkansas patients stratified by high versus low expression of RHAMM (median cutoff) according to Affymetrix U95Av2 microarray experiments. High RHAMM expression is significantly and negatively associated with both event-free and overall survival.

RHAMM isoforms are rarely co-expressed in individual MM plasma cells.

Previous examination of RHAMM expression within myeloma revealed the presence of splice variants; $RHAMM^{-exon4}$ was qualitatively detected at a level approximating $RHAMM^{FL}$ while detection of $RHAMM^{-exon13}$ transcripts required more sensitive methodologies(Crainie *et al.*, 1999). Within colon cancer patients, the ratio of $RHAMM^{-exon4}/RHAMM^{FL}$ increases qualitatively in tumor, compared to autologous normal, tissue(Line *et al.*, 2002). Moreover, in AML, CML and renal cell carcinoma patients, $RHAMM^{FL}$ expression was accompanied with $RHAMM^{-exon4}$ expression while $RHAMM^{-exon13}$ was undetectable (Greiner *et al.*, 2002). We thus investigated the differential expression of $RHAMM^{-exon4}$ and $RHAMM^{FL}$ within single MM PC.

To investigate the differential expression of $RHAMM^{-exon4}$ and $RHAMM^{FL}$, we utilized RT-PCR, with fluoresceinated RHAMM primers, and FCE to detect RHAMM isoform transcripts at the single cell level (Figure 3-2A). Optimal PCR conditions were determined to provide reproducible RHAMM ratios from purified PC, PBMC and BM samples (Figure 3-2B). FCE was approximately 5000x more sensitive than agarose detection, detecting PCR products resulting from amplification of attogram (10^{-18}g) levels of template. Moreover, FCE could discriminate the $RHAMM^{-exon4}$ and/or $RHAMM^{FL}$ products resulting from amplification of attogram amounts of template while agarose detection required 100 femtograms of template for such discrimination. Sequencing of randomly selected RT-PCR products confirmed the identity of the two fragments as $RHAMM^{FL}$ and $RHAMM^{-exon4}$. Consistent with previous reports (Line *et al.*, 2002) the RHAMM clones (n=12), sequenced from three patients, all exhibited an additional triplet

(AAG), as compared to the sequence reported by Assmann et al., 1998, at the 5' end of exon 4.

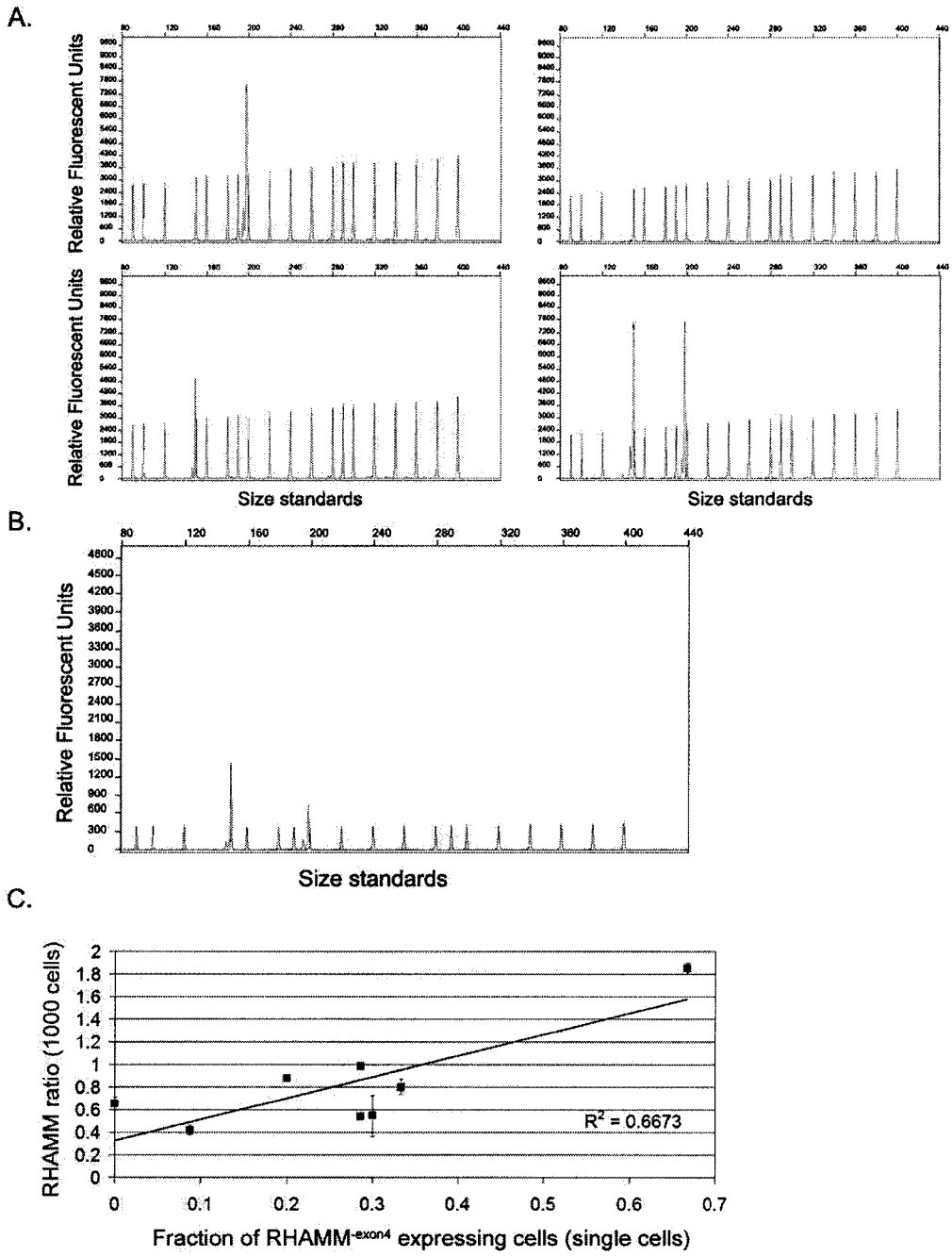

Figure 3-2 Single cell analysis of RHAMM isoform expression patterns in MM plasma cells.

Figure 3-2: Single cell analysis of RHAMM isoform expression patterns in MM plasma cells. A. Electropherogram analysis of sorted, single, clonotypic MM (Patient 2) plasma cell (PC) expressing (clockwise from top left) $RHAMM^{FL}$ alone, neither $RHAMM^{FL}$ nor $RHAMM^{-exon4}$, both $RHAMM^{FL}$ and $RHAMM^{-exon4}$ and $RHAMM^{-exon4}$ alone. All samples were RT-PCR positive, by ethidium bromide detection, for β_2–microglobulin and clonotypic message. RT-PCR products were EtOH precipitated prior to GeneScan® analysis. To maximize the sensitivity of the single cell assay, large amounts of RT-PCR product were analyzed, as seen by the large product peaks. B. Electropherogram analysis of RHAMM-specific RT-PCR amplification of cDNA from 1000 sorted MM (Patient 2) plasma cells. For ratio determination, product peaks were kept below 3500 relative fluorescent units (RFU) and size standards were within the manufacturer's suggested levels (i.e 150-600 RFU). C. Plot of RHAMM ratio (1000 cells) versus the fraction of $RHAMM^{-exon4}$ single cells. A Pearson's r^2 correlation coefficient of 0.667 indicates a significant linear relationship ($p<0.02$) between the two parameters.

CD38+ or CD138+ BM PC from eight Alberta MM patients, for whom patient-specific clonotypic IgH primers had been derived, were sorted into PCR tubes at 1 or 1000 cells per well and frozen until analyzed. For each patient, 24, or 48, single cell RT-PCR reactions were performed depending on available samples (mean 31.5 cells). For each single cell sample, cDNA was produced and divided to detect $ß_2$-microglobulin (to control for RNA integrity), clonotypic VDJ (to identify clonal PC) and RHAMM. Table 3-2 illustrates the findings for single PC cDNA preparations from these eight patients that were positive for clonal transcripts (mean 26.8 cells per patient). Interestingly, $RHAMM^{FL}$ and $RHAMM^{-exon4}$ transcripts are rarely detected within the same clonal MM PC (mean 6.1% of PC, range 0-17.4 %). Rather, a population of PC within individual myeloma patients predominantly expresses $RHAMM^{FL}$, or $RHAMM^{-exon4}$, or neither transcript (Figure 3-2A). Single and 1000 PC samples were isolated from three control

patients and evaluated for RHAMM expression. Interestingly, in control samples RHAMM-expressing PC predominantly express both isoforms. A greater fraction of single PC (63% vs. 43%) lack detectable RHAMM transcripts in the control populations examined; due to low expression levels we were unable to determine RHAMM ratios within purified 1000 PC control samples. We expanded our analysis to include total RNA from unpurified BM of additional control patient (n=4) samples. Again, expression levels were too low to determine RHAMM ratios from these samples. These results strongly suggest that within populations of control PC the absolute levels of RHAMM transcripts, although detectable by extremely sensitive FCE at the single cell level, are so insignificant as to be undetectable at the bulk cell population level.

MM patient	$RHAMM^{-exon4}/RHAMM^{FL}$ Ratio (+/- S.E.) in 1000 PC	Clonal Cells Examined	$RHAMM^{FL}$ Expression	$RHAMM^{-exon4}$ Expression	Both	Absent (%)
1	0.404 +/- 0.01	24	20	2	1	1 (4.2)
2	0.548 +/- 0.18	35	11	6	3	15 (42.9)
3	0.565 +/- 0.13	24	4	2	1	17 (70.8)
4	0.655 +/- 0.06	17	8	0	0	9 (52.9)
5	0.802 +/- 0.07	15	4	2	0	9 (60.0)
6	0.875 +/- 0.001	46	21	6	3	16 (34.8)
7	0.987 +/- 0.02	29	4	2	1	22 (75.9)
8	1.799 +/- 0.01	24	3	14	4	3 (12.5)
Mean (MM)		26.8	9.4 (35.0)	4.3 (15.9)	**1.6 (6.1)**	11.5 (43.0)

Control Patients	$RHAMM^{exon4}/RHAMM^{FL}$ Ratio (+/- S.E.) in 1000 PC	Plasma Cells Examined	$RHAMM^{FL}$ Expression (%)	$RHAMM^{-exon4}$ Expression (%)	Both (%)	Absent (%)
(n=3)	UD	92	8 (8.7)	8 (8.7)	**18 (19.6)**	58 (63.0)

$CD138^+$ or $CD38^+$ PC derived from BM aspirates, were sorted into PCR tubes containing lysis buffer at 1 cell/tube or 1000 cells/tube and stored at $-80^{O}C$. RT-PCR was performed as outlined in Methods using RHAMM-specific primers that flank exon 4. Only cDNA samples that were positive for both beta-2-microgobulin (MM and control) and clonal message (MM) are tabulated. Single cell RT-PCR products were precipitated prior to GeneScan® analysis. RHAMM specific RT-PCR amplification of 1000 cell/well samples resulted in two product peaks representing $RHAMM^{-exon4}$ product (150 bp) and $RHAMM^{FL}$ product (200 bp). The area under each peak was calculated by GeneScan® Analysis software and exported to Microsoft® Excel to determine the ratio of $RHAMM^{-exon4}/RHAMM^{FL}$ peak intensities. UD= unable to determine. RHAMM ratios were unobtainable from 1000 PC/well (n=3 patients examined) and bulk BM(n=4 patients examined) populations from 7 control patient populations.

Table 3-2: Comparable patterns of RHAMM isoform expression by PC in individual and aggregate PC.

RHAMM ratios measured in populations of MM PC reflects the distribution of RHAMM isoforms seen in individual clonal cells.

RHAMM ratios were determined for 1000 sorted PC from the same 8 patients who were examined at the single PC level. As expected from previous data (Crainie *et al.*, 1999; Line *et al.*, 2002), RT-PCR of aggregate populations of PC using exon 4 spanning primers resulted in two fluoresceinated peaks (198 and 150 bp) representing both isoforms (Figure 3-2B). To determine the RHAMM ratios for individual patients, RT-PCR was performed, in triplicate, and the area under the peak for the 150 bp fragment ($RHAMM^{-exon4}$) was divided by the area under the peak for the 198 bp fragment ($RHAMM^{FL}$). Three of four patients whose individual PC predominantly expressed $RHAMM^{FL}$ (patients 1, 2 and 4) had RHAMM ratios lower than 0.7, while the patient whose individual PCs predominantly expressed $RHAMM^{-exon4}$ (patient 8) had a dramatically higher RHAMM ratio in the 1000-cell samples (1.8 ± 0.01). Two patients whose individual PC tended not to express detectable RHAMM (patients 5,7), as well as one $RHAMM^{FL}$ expresser (patient 6), had moderate RHAMM isoform ratios in 1000-cell samples ranging from 0.8-1.0. Thus, there is a strong relationship between the single cell results and the 1000-cell results in these patients. Regression analysis revealed a significant linear relationship ($p<0.02$) between single PC isoform expression and 1000 PC RHAMM ratio (Figure 3-2C). From these results we conclude that the RHAMM ratio in aggregate populations of cells, detected semi-quantitatively by RT-PCR, provides a valid indicator of the RHAMM isoform expression profile at the single cell level.

Elevated RHAMM expression, in MM patient PCs, correlates modestly with a relative increase in RHAMM^{exon4} expression

We investigated whether elevated RHAMM expression was associated with preferential expression of one isoform (high or low RHAMM ratio). RNA was isolated from purified CD138^{+} PCs from fourteen MM patients, quantitative RT-PCR was performed as described and ratios were determined. RHAMM expression was normalized to the lowest RHAMM expresser and plotted against the corresponding RHAMM ratio for individual patients. As shown in Figure 3-3, the patients clustered into three groups based upon their RHAMM ratios; three patients exhibited ratios <0.9, six patients exhibited ratios 0.9>N<1.2, and five patients exhibited ratios >1.2. Three of four of the lowest RHAMM expressers were clustered in the <0.9 group while four of six of the highest RHAMM expressers were clustered in the >1.2 group. While these two parameters demonstrated a statistically significant linear relationship, the degree of correlation was modest (r^2= 0.337, $p<0.03$), and one patient exhibited an elevated RHAMM ratio (1.33) in the absence of elevated absolute RHAMM expression (1.2 fold). The partial correlation of RHAMM expression and splicing results suggest that RHAMM expression and splicing are two phenomena that are linked but are also, in part, independently regulated.

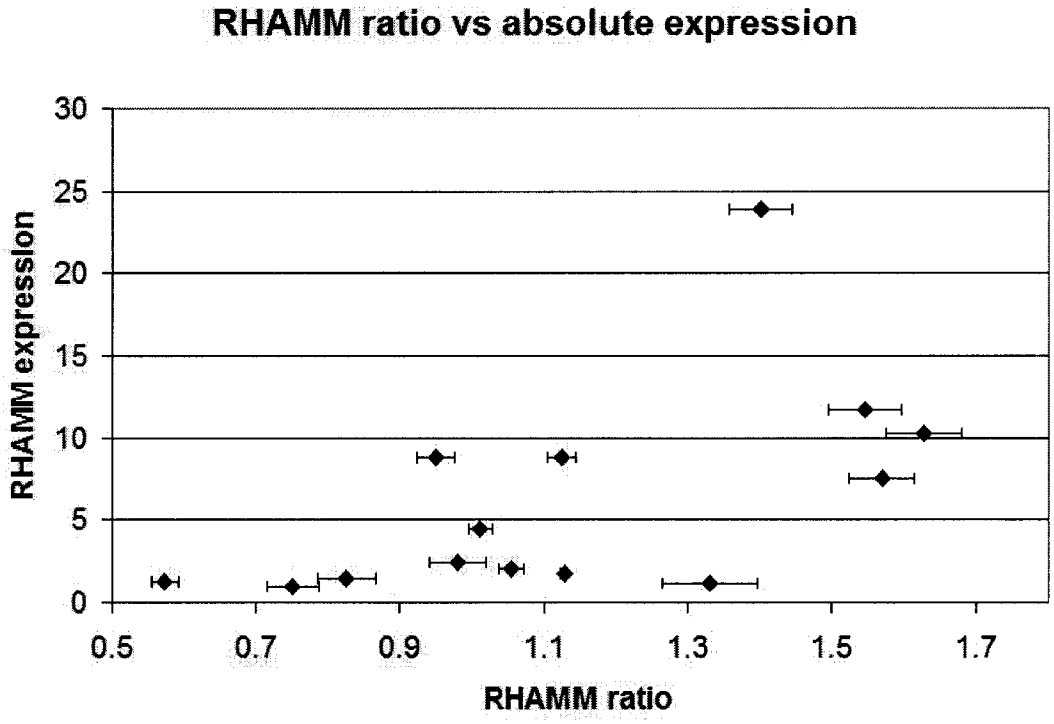

Figure 3-3. Plot of absolute RHAMM expression versus RHAMM ratios for fourteen MM patients. **Elevated expression of RHAMM is significantly related to an increase in RHAMM^{-exon4} expression within MM patients. RHAMM expression within purified MM CD138^{+} PCs was determined by quantitative RT-PCR analysis. Relative RHAMM expression was normalized to the lowest patient expresser. RHAMM ratio (+/- Standard Error) was determined as described. Statistical comparison utilized the Pearson correlation coefficient.**

RHAMM expression, but not exon 4 deletion, is upregulated during mitosis

Previous experimentation demonstrated that RHAMM expression is upregulated during mitosis in adherent (HeLa) and suspension (Raji) cell lines (Maxwell et al., submitted). We investigated whether RHAMM ratios were also altered during mitosis.

Interestingly, while both RHAMM message and protein levels were elevated during mitosis, the RHAMM ratio did not change significantly (Table 3-3). Within both mitotic and unsynchronized populations of cycling cell lines, the level of $RHAMM^{FL}$ was much greater than $RHAMM^{-exon4}$. This fits with our previous work suggesting that RHAMM may function in the crosslinking and stabilization of the mitotic spindle, through microtubule contacts at its NH_2- and COOH-termini (Maxwell *et al.*, 2003); as $RHAMM^{-exon4}$ is inhibited in its NH_2-terminal interphase microtubule interactions and may not associate/stabilize spindle poles as efficiently as $RHAMM^{FL}$, amplified expression of this variant during mitosis may have debilitating effects on spindle integrity. Thus, while increases in RHAMM expression levels could reflect in part the mitotic rate in MM PC, increases in RHAMM exon 4 splicing are not expected to be associated with an increased mitotic rate.

	Quantitative RT-PCR*	Quantitative Immunoblot*	RHAMM ratio
HeLa (unsynchronized)	1.0	1.0	0.48 +/- 0.06
HeLa (mitotic)	1.74 +/- 0.08	1.62	0.56 +/- 0.04
Raji (unsynchronized)	1.0	1.0	0.61 +/- 0.05
Raji (mitotic)	1.43 +/- 0.08	1.51	0.57 +/- 0.03

HeLa and Raji cells were synchronized by double thymidine and nocodazole block. Quantitative RT-PCR was performed as described. Quantitative immunoblot analysis was performed on CHAPS+ soluble lysates using infrared detection and Odyssey imaging as described. Band quantitation was normalized to B-actin levels. RHAMM ratios were determined as described.
* data included in Maxwell et al., submitted.

Table 3-3: Relationship between absolute RHAMM expression, at the message and protein level, and RHAMM isoform ratio in mitotic and unsynchronized cell lines.

RHAMM isoforms differ in exchange with the mitotic spindle in cell lines

During mitosis, RHAMM likely functions by crosslinking microtubules through a direct NH_2-terminal interaction and an indirect COOH-terminal interaction (Maxwell *et al.*, 2003). We have demonstrated that inhibition of RHAMM function, through injection of polyclonal serum targeting the COOH-terminus, dramatically affects mitotic integrity (Maxwell *et al.*, 2003). As loss of exon 4 affects interphase microtubule interactions (Assmann *et al.*, 1999)(Maxwell *et al.*, 2003), we speculated that $RHAMM^{-exon4}$ may be inhibited in the ability to associate with the mitotic spindle. Thus, we investigated the *in vivo* affinity of $GFP\text{-}RHAMM^{FL}$ and $GFP\text{-}RHAMM^{-exon4}$ for sub-cellular structures, including the centrosome, cytoplasm and spindle pole, with fluorescence recovery after photobleaching (FRAP) experiments (Supplemental Figure 3-1). FRAP analysis allows quantitative assessment of the recovery of fluorescent molecules into a laser bleached

region. The mobile population, that is the population that recovers fluorescent intensity, is a direct measure of the fluoresceinated molecules that diffuse into/out of, or are not immobilized within, the bleached region. Therefore, the greater the mobile fraction, the lower the affinity of the fluoresceinated molecule for the region of interest. GFP alone is diffusely distributed throughout the cell (not shown) and demonstrates rapid ($t_{1/2} < 0.5$ sec) and complete recovery (mobile fraction 1.04 $^{+}$/- 0.08) following photobleaching (Supplemental Table 3-1).

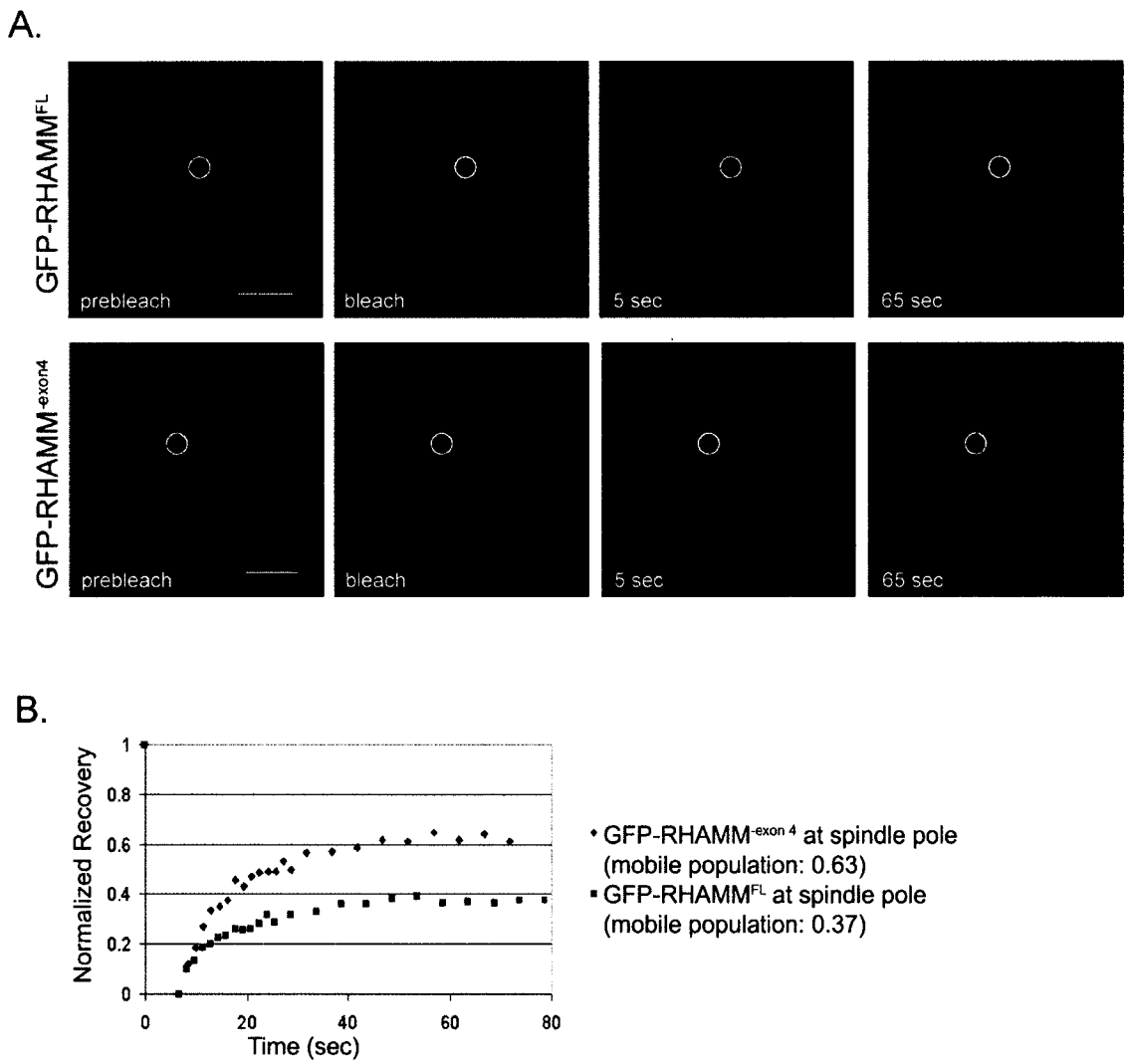

Supplemental Figure 3-1: Fluorescence recovery after photobleaching (FRAP) demonstrates that RHAMM isoforms differ in mobilities at the mitotic spindle but not at the MTOC or within the cytoplasm. A. FRAP analysis of GFP-RHAMM^{FL} and GFP-RHAMM$^{-exon\ 4}$ at the mitotic spindle within HeLa. Cells were plated on coverslips, transiently transfected with GFP alone, GFP-RHAMM^{FL}, or GFP-RHAMM^{-exon4} using Lipofectamine 2000 and live cells were analyzed on a Zeiss 510 confocal or multiphoton microscope 20 hours later. Contrast of images adjusted to correct for photobleaching due to imaging. Scale bars equal 10 μm. B. Normalized recovery at the spindle pole for representative HeLa cells transfected with GFP-RHAMM^{FL} and GFP-RHAMM^{-exon4}. Mobile populations were determined within Microsoft® Excel after correcting for whole cell fluorescent loss due to

initial bleach and progressive bleaching during scans. In addition to differences in FRAP results, the morphology of the spindle also appears consistently different between the two transfectants, with a more widened spindle appearance in the RHAMM^{FL} transfected cells compared to the RHAMM^{-exon4} transfected cells.

Supplemental Table 3-1: Fluorescence Recovery After Photobleaching analysis of the relative mobility of GFP alone and GFP fusion constructs of RHAMM isoforms at specific sub-cellular locations.

Mobile Fraction ($^{+}$/- Standard Error)

GFP-Fusion	Cell line	Cytoplasm	Interphase MTOC	Mitotic Spindle
EGFP-C1	8226	1.04 $^{+}$/- 0.08	-	-
GFP-RHAMM^{FL}	8226	0.71 $^{+}$/- 0.04 ^{A}	0.52 $^{+}$/- 0.09 ^{B}	-
GFP-RHAMM^{-exon4}	8226	0.77 $^{+}$/- 0.03 ^{A}	0.52 $^{+}$/- 0.05 ^{B}	-
GFP-RHAMM^{FL}	HeLa	-	-	0.37 $^{+}$/- 0.03
GFP-RHAMM^{-exon4}	HeLa	-	-	0.63 $^{+}$/- 0.06
P (RHAMM^{FL} vs. RHAMM^{-exon4})		0.18	0.96	0.002

RPMI 8226 cells were transiently transfected with EGFP-C1, GFP-RHAMM^{-exon4}, or GFP-RHAMM^{FL} using electroporation. Following transfection, live cells were adhered to 1 mg/ml fibronectin on coverslips and visualized with a Zeiss 510 confocal or multiphoton microscope. HeLa cells were grown on coverslips and transiently transfected with Lipofectamine 2000 according to the manufacturer's suggested protocol. All photorecovery experiments were performed with identical parameters (i.e. scan speed, zoom, scale, bleach iterations, ROI size etc.); only the amount of recovery scans and the time between them varied.

^{A} p=0.03 compared to EGFP-C1 motility (cytoplasm)

^{B} p=0.0013 compared to EGFP-C1 motility (cytoplasm)

The mobility of GFP-RHAMM isoforms within interphase cells was examined in RPMI 8226. Mean values are given for normalized mobile fractions obtained from nine measurements at the centrosome (MTOC) for each isoform and at least 18 measurements within the cytoplasm for each isoform (Supplemental Table 3-1). The mobility of both isoforms differed significantly from GFP alone ($p<0.03$, data not shown) at all sub-

cellular sites, indicating that neither variant is freely diffusable. Both isoforms showed a higher affinity for the MTOC than for the cytoplasm; these differences were at or near statistical significance ($p=0.081$ for GFP-RHAMM^{FL}, $p=0.001$ for GFP-RHAMM^{-exon4}). Although the mobile fraction at the interphase centrosome is similar for the two isoforms (Supplemental Table 3-1), the rate of exchange is twice as high for RHAMM^{-exon4} ($t_{1/2}$= 3.37^{+}/- 0.54 sec) as for RHAMM^{FL} ($t_{1/2}$= 7.36^{+}/- 2.35 sec).

The mitotic mobility of GFP-RHAMM isoforms was analyzed in the adherent line HeLa due to the increased vibrational movement and low transfection efficiency of mitotic RPMI 8226. Mean values are given for normalized mobile fractions obtained from 15 measurements at the spindle pole for each isoform (Supplemental Table 3-1). Typical time course experiments are shown in Supplemental Figure 3-1A for FRAP analysis at the spindle pole and within the mitotic cytoplasm. Normalized recovery curves for two separate FRAP experiments examining GFP-RHAMM^{-exon4} and GFP-RHAMM^{FL} recovery with transiently transfected HeLa cells are also shown (Supplemental Figure 3-1B). These data indicate a significant difference ($p=0.002$) between GFP-RHAMM^{-exon4} and GFP-RHAMM^{FL} recovery at the spindle pole. The affinity of GFP-RHAMM^{-exon4} for the spindle pole approximates, or is slightly less than, that for the interphase MTOC. From *in vivo* FRAP analysis we conclude that GFP-RHAMM^{-exon4} has a decreased affinity for mitotic spindle poles.

RHAMM ratios in the peripheral blood reflect disease burden over time

Our lab has previously published the temporal examination of FGFR3 expression within t(4;14) positive myeloma patients (Keats *et al.*, 2003). t(4;14) positive patients can be identified by RT-PCR amplification of IgH-MMSET fusion transcripts (Chesi *et al.*, 1998). This provides an extremely specific, sensitive assay for the detection of the myeloma cells. To investigate whether the expression of $RHAMM^{-exon4}$ relative to $RHAMM^{FL}$ changes over the disease course, PBMC samples from sequential clinic visits were examined for five MM patients. The use of PBMC allows examination of multiple timepoints throughout the course of disease but necessitates detection and differentiation between samples with, or without, transformed cells. PBMC samples from patients, previously identified as $t(4;14)^{+}$, with sequenced clonotypic transcripts were examined. The advantage of using blood samples from these particular patients is that three RT-PCR reactions can detect malignant clones within the blood: amplification of clonal transcript (CDR2/CDR3), Iμ1-MMSET and JH-MMSET hybrid transcripts. The sensitivity of the single-stage Iμ1-MMSET, and the single stage JH-MMSET, assay is 2% positive cells (Keats *et al.*, 2003). Thus, for all IgH-$MMSET^{+}$ blood samples, at least 2% of the total PBMC population is malignant. The integrity of each cDNA sample (n=88) was confirmed with β_2-microglobulin. Only the t(4;14) status of the patient was known to the experimenter; the analysis was blind for all other parameters. For each patient, the RHAMM ratio was plotted against time and compared to a standard clinical measure of BM PC burden, the serum M protein level (g/L). RHAMM ratios from samples that were positive for clonotypic transcript and for at least one t(4;14) RT-PCR reaction, as well as the immediate neighboring negative samples, are plotted and trendlines, generated with

Microsoft Excel software, are given. Figure 4 illustrates results typical of the patients examined. For samples in which t(4;14) message was detected, an increase in the relative $RHAMM^{-exon4}$ message was associated with increasing serum M-protein levels. For samples lacking detectable IgH-MMSET transcript (not shown), the RHAMM ratio fluctuated from ~0.6-0.9. As shown in Figure 3-4, the fluctuations of the RHAMM ratio closely approximate that of the M protein prior to transplant and following relapse. In four out of five patients examined, clinical relapse coincided with a dramatic increase in RHAMM ratios. These observations illustrate a significant association between $RHAMM^{-exon4}$ mRNA expression in PBMC and tumor burden.

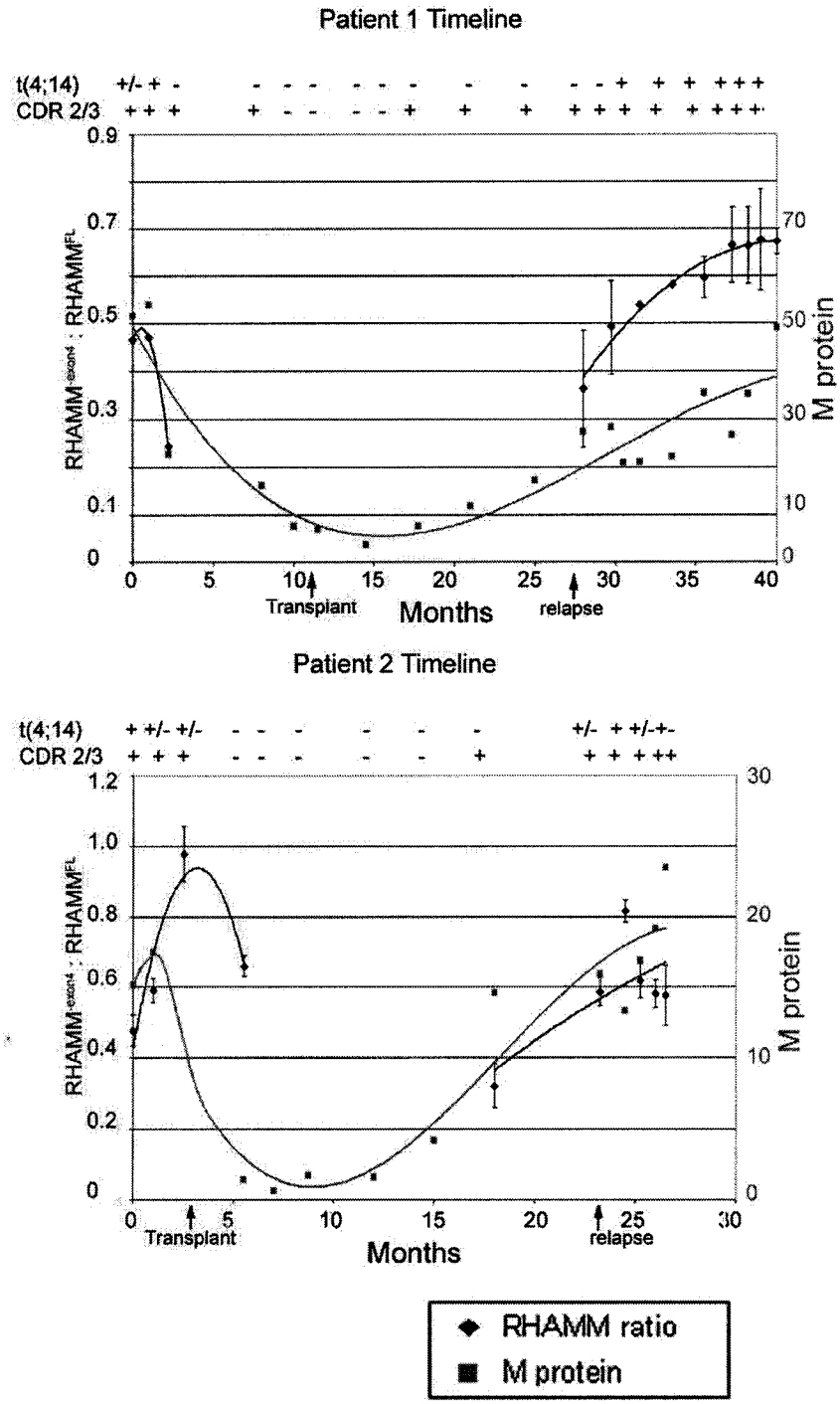

Figure 3-4: Timeline analysis of $RHAMM^{-exon4}/RHAMM^{FL}$ ratios within $t(4;14)^{+}$ MM patient blood samples.

Figure 3-4. Timeline analysis of RHAMM^{-exon4}/RHAMM^{FL} ratios within t(4;14)$^{+}$ MM patient blood samples. PBMC samples were acquired and archived between 1998 and 2002 as described previously[5]. Detection of t(4;14) fusion transcript utilized two RT-PCR reactions targeting JH/MMSET and Iμ/MMSET respectively[5]. Samples are classified as MMSET negative (-), MMSET positive for both reactions (+), or MMSET positive for one reaction ($^{+}$/-). Samples are also classified as containing clonotypic CDR2/3 message (+) or lacking clonotypic CDR2/3 message (-). Only samples that were MMSET positive in at least one reaction are shown along with the immediately neighboring MMSET negative samples. Polynomial trendlines for RHAMM^{-exon4}/RHAMM^{FL} ratios (Excel) are indicated for samples with detectable t(4;14) message. Serum M-protein levels at the time of each PBMC sample are also indicated. Arrows indicate time of transplant and disease relapse.

High RHAMM ratios in the diagnostic bone marrow correlate with poor survival in MM

We investigated the prognostic significance of relative RHAMM^{-exon4} expression in diagnostic bone marrow samples. The RHAMM ratio was measured in total RNA extracts from the bone marrow of 101 MM patients from Alberta, Canada. The fact that RHAMM ratios in control BM were too low to determine RHAMM ratios indicates that the RHAMM ratio in total BM from MM patients is largely contributed by the malignant cells, justifying the use of the available total BM samples for this experiment. These patients are a subset of a previously described cohort (Keats *et al.*, 2003). The characteristics of the 101 Alberta patients are listed in Table 3-4.

Factor	Prevalence
Age>=65	63/101 (63%)
Female	35/101 (35%)
Kappa	58/95 (61%)
Lambda	34/95 (36%)
IgA Isotype	19/97 (20%)
B2M>=4 mg/L	41/74 (55%)
Creatinine>=2.0 mg/dL	19/100 (19%)
LDH elevated	13/75 (26%)
Albumin<3.5 g/dL	44/98 (45%)
Hypercalcemia	7/97 (7%)
HGB<10 g/dL	40/100 (40%)
BMPC>=33%	54/98 (55%)
1+ X-ray focal esions	72/101 (71%)
3+ X-ray focal esions	59/101 (58%)
High-dose chemotherapy	30/101 (30%)

Table 3-4: Characteristics of 101 Alberta patients for whom RHAMM ratio determination was assessed in bone marrow samples taken at the time of diagnosis. RHAMM ratios did not significantly correlate with any of the parameters listed.

There was no statistically significant correlation between the RHAMM ratio and any baseline characteristic examined (age, sex, clinical isotype, M-protein level, creatinine, calcium, LDH, or ß-2 microglobulin). Although patients in this portion of the study were treated heterogeneously, there was no association between RHAMM ratio and the type of therapy received. There was no correlation between the RHAMM ratio and the

presence of X-ray detectable lytic bone lesions; these patients did not undergo MRI scanning. In spite of the correlation between disease burden and the RHAMM ratio seen in our studies of circulating cells, there was no correlation between the BM RHAMM ratio and the level of BM plasmacytosis. Of the 101 patients, 18 had RHAMM ratios less than 0.8. Twenty patients within the cohort had ratios greater than 1.20. Thus, patients were classified as $RHAMM^{FL}$ expressers (n=18, R<0.80), $RHAMM^{-exon4}$ expressers (n=20, R>1.20) and intermediate expressers (n=63, 0.80>R<1.20), analogous to what was seen in the sorted PC experiments. These three groups exhibited significantly differing overall survival (OS) distributions (Figure 3-5), with increasingly poorer outcomes associated with increasingly higher RHAMM ratios (p=0.003).

In a single-variable Cox model, an increasing RHAMM ratio significantly correlated with poor survival (HR=2.18, 95% CI, 1.11-4.26, p=0.024). The RHAMM ratio was an independent predictor of survival when included in a multivariable Cox regression model with albumin and ß2M as covariates (HR=3.34, 95% CI 1.14-9.79, p=0.028). Albumin and ß2M are the factors used in the SWOG model (Jacobson *et al.*, 2003), a currently accepted standard prognostication method in MM; thus, the RHAMM ratio adds independent information to standard prognostic factors.

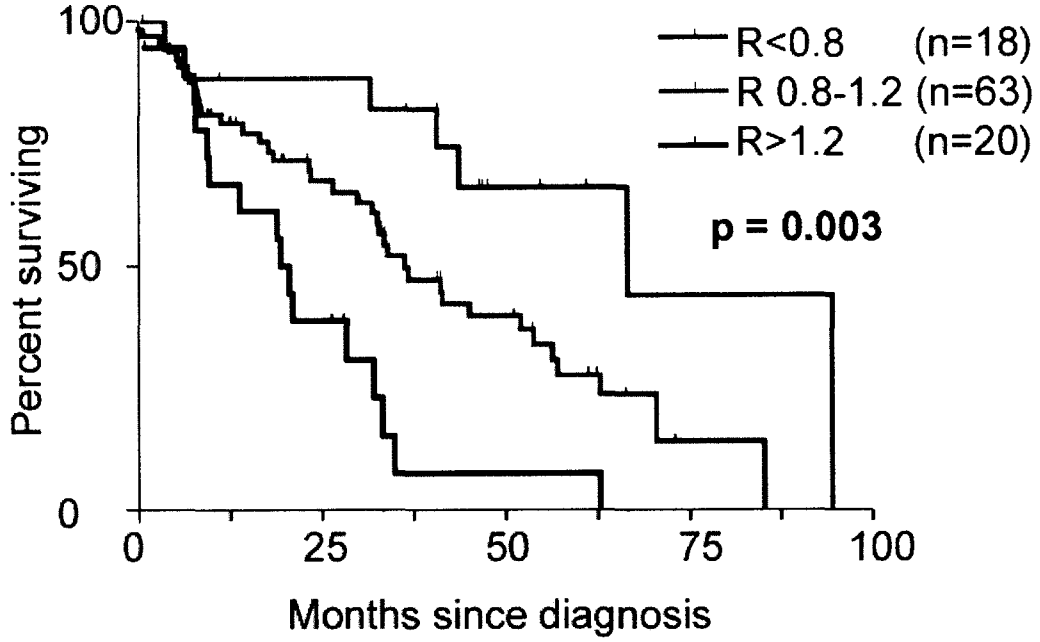

	R < 0.80	0.80 > R < 1.20	R > 1.20
Median Survival (months)	66	32	20

Figure 3-5: RHAMM isoform balance in BM samples are prognostic in multiple myeloma. Kaplan-Meier survival curves for myeloma patients with RHAMM ratios of <0.8 (red), 0.8-1.2 (green), and >1.2 (blue) in the bone marrow at diagnosis. Survival is increasingly poor with increasing RHAMM ratio (p=0.003 by the log rank test). RHAMM ratios were determined using RT-PCR and capillary fragment analysis.

Discussion

The clinical impact of $RHAMM^{-exon4}$ was evaluated in 101 newly diagnosed MM patients by correlating the $RHAMM^{-exon4}/RHAMM^{FL}$ ratio in the diagnostic BM sample to survival. A high RHAMM ratio strongly correlates with poor survival, and provides information on prognosis that is independent of standard factors such as beta-2-microglobulin and albumin. In five t(4;14)+ MM patients, we performed time course analysis of blood samples; we found that in samples containing malignant cells, as assessed with both t(4;14) and clonotypic mRNA assays, the RHAMM ratio decreased post autologous transplant and increased at the time of relapse. While the RHAMM ratio in circulating malignant cells correlates with tumour burden, a high RHAMM ratio in the BM does not appear to be simply a measure of disease burden, since it does not correlate with the degree of marrow plasmacytosis, nor with LDH or beta-2-microglobulin levels.

Also interesting is the finding that, in eight patients, $RHAMM^{-exon4}$ and $RHAMM^{FL}$ are rarely co-expressed within individual malignant MM PC, despite the fact that both isoforms are present in all patients examined. RHAMM exon 4 splicing appears to be largely an "all or none" phenomenon in individual plasma cells. There is clearly heterogeneity of RHAMM splicing among MM malignant cells from individual patients suggesting the presence of aggressive myeloma subclones, characterized by preferential $RHAMM^{-exon4}$ expression, which may mediate disease progression.

RHAMM expression levels, irrespective of exon 4 splicing, correlate with the presence of bone disease in microarray studies, as well as event-free and survival.

Osteolytic lesions in myeloma presumably result from a disruption of the bone deposition/resorption balance towards resorption. DKK1 is an inhibitor of osteoblast differentiation which is secreted by myeloma cells in patients with lytic bone disease (Tian *et al.*, 2003). However, the impact of RHAMM expression in MM cells on this balance of bone growth and bone loss is unclear. Given the lack of correlation between RHAMM and DKK1 expression, and given the lack of any currently known biological link between the two genes, the mechanism underlying the association between RHAMM and osteolytic lesions is in all probability quite distinct from that for DKK1. The simplest explanation for the association between RHAMM levels and disease severity would be that RHAMM expression is intimately linked to myeloma proliferation; elevated RHAMM expression may be analogous to an elevated bromodeoxyuridine plasma cell labeling index (PCLI), a measure of proliferative activity that is an important prognostic factor in newly diagnosed MM (Steensma *et al.*, 2001). However, actively cycling cell lines predominantly express $RHAMM^{FL}$ as indicated by their reduced RHAMM ratios. Further, within MM patients, elevated RHAMM expression did not correlate with a high PCLI (Table 1). A parallel hypothesis is that altered RHAMM expression may dramatically affect chromosomal segregation and chromosomal instability (CIN) within the malignant clone, analogous to the mitotic errors seen previously in our RHAMM immunoblocking experiments (Maxwell *et al.*, 2003). We have previously postulated that RHAMM mitotic function depends upon microtubule crosslinking resulting from microtubule interactions at the NH_2- and COOH- termini (Maxwell *et al.*, 2003). Antibody targeting of the COOH-terminus of RHAMM disrupts spindle integrity leading to fragmentation and multipolar spindle architecture (Maxwell *et al.*, 2003). Elevated

expression of RHAMM^{-exon4}, a variant incapable of interacting with interphase microtubules (Maxwell *et al.*, 2003) (Assmann *et al.*, 1999), may have similar deleterious effects on spindle integrity. Increasing CIN within the malignant clone may have substantial effects on gene expression profiles in malignant 'sub-clones' with dramatic consequential effects on the bone marrow microenvironment.

Both RHAMM isoforms exchange with the centrosome during interphase. Interestingly, while the mobile fractions in interphase RPMI 8226 are comparable (at 0.52 for both isoforms), the exchange rate for RHAMM^{-exon4} is twice as rapid as RHAMM^{FL}. Thus, the inhibited microtubule binding capability of RHAMM^{-exon4} may increase its exchange rate by disrupting its ability to maintain centrosomal localization. The very low mobile fraction for GFP-RHAMM^{FL} during mitosis strongly suggests that it functions as a structural protein of the mitotic apparatus. In striking contrast, GFP-RHAMM^{-exon4} is quite mobile at the mitotic spindle pole, strongly suggesting that it, unlike RHAMM^{FL}, does not structurally support the spindle pole. Analogies to our data can be found in previous FRAP experiments done with other centrosome/spindle pole proteins; the structural proteins NuMA and gamma-tubulin have slower recovery rates and lower mobilities (Stenoien *et al.*, 2003)(Khodjakov and Rieder, 1999), whereas other non-structural centrosome proteins such as Aurora A kinase have rapid exchange rates (Stenoien *et al.*, 2003). Given that RHAMM^{FL} and RHAMM^{-exon4} are rarely co-expressed in MM plasma cells, expression of RHAMM^{-exon4} alone may detrimentally affect spindle integrity in a manner analogous to RHAMM inhibition. These data, in combination with previous functional evidence for the RHAMM isoforms (Maxwell *et al.*, 2003)(Assman

et al., 1999), suggest that differences in isoform function at the centrosome/mitotic spindle may explain at least part of the link between isoform balance and survival in MM patients.

The association of RHAMM expression and isoform balance with disease relapse and survival is intriguing, particularly the clinical impact of clonal expansion by individual MM plasma cells preferentially expressing RHAMM^{-exon4}. Standard markers of poor prognosis may not have any direct bearing on disease pathogenesis, but are simply markers of tumor burden and/or poor physiological functioning (e.g. serum beta-2-microglobulin and albumin levels) (Jacobson *et al.*, 2003). At present, standard prognostic factors in MM are not particularly useful for determining the best treatment for each patient. Newer, molecular prognostic factors, such as RHAMM, t(4;14) (Keats *et al.*, 2003) and other IgH translocations (Moreau *et al.*, 2002; Fonseca *et al.*, 2003), are exciting not just for their prognostic value but because their associations with survival are also linked to a biologically plausible reasoning behind the observed association. It is hoped that such molecular epidemiological studies as this one will be more clinically useful than older studies of prognosis by helping us to understand the biology of myeloma, and more particularly by identifying novel targets for therapy.

In summary, we speculate that abnormal RHAMM^{-exon4} splice variant expression in MM promotes mitotic abnormalities, genetic instability and possibly spread of disease, providing mechanistic insight into the adverse clinical impact of RHAMM^{-exon4} on survival. We show that co-expression of both isoforms is rare in individual MM plasma

cells and, at the cell population level, elevated expression of $RHAMM^{-exon4}$ relative to $RHAMM^{FL}$ coincides with disease relapse and is prognostic of poor outcome when assessed at the time of diagnosis. The association of RHAMM expression with lytic bone disease, disease-related events and survival in microarray experiments provides further evidence of the importance of this gene in myeloma. Further study of the role of RHAMM in myeloma pathogenesis is warranted. There may be value in the development of therapeutic strategies to target RHAMM, with the goal of slowing myeloma disease progression.

References

Abetamann, V., Kern, H.F., and Elsasser, H.P. (1996). Differential expression of the hyaluronan receptors CD44 and RHAMM in human pancreatic cancer cells. Clin Cancer Res *2*, 1607-1618.

Adamia, S., Crainie, M., Kriangkum, J., Mant, M.J., Belch, A.R., and Pilarski, L.M. (2003). Abnormal expression of hyaluronan synthases in patients with Waldenstrom's macroglobulimenia. Semin Oncol *30*, 165-168.

Ahrens, T., Assmann, V., Fieber, C., Termeer, C., Herrlich, P., Hofmann, M., and Simon, J.C. (2001). CD44 is the principal mediator of hyaluronic-acid-induced melanoma cell proliferation. J Invest Dermatol *116*, 93-101.

Assmann, V., Jenkinson, D., Marshall, J.F., and Hart, I.R. (1999). The intracellular hyaluronan receptor RHAMM/IHABP interacts with microtubules and actin filaments. J Cell Sci *112 (Pt 22)*, 3943-3954.

Avet-Loiseau, H., Facon, T., Grosbois, B., Magrangeas, F., Rapp, M.J., Harousseau, J.L., Minvielle, S., and Bataille, R. (2002). Oncogenesis of multiple myeloma: 14q32 and 13q chromosomal abnormalities are not randomly distributed, but correlate with natural history, immunological features, and clinical presentation. Blood *99*, 2185-2191.

Barlogie, B., Jagannath, S., Desikan, K.R., Mattox, S., Vesole, D., Siegel, D., Tricot, G., Munshi, N., Fassas, A., Singhal, S., Mehta, J., Anaissie, E., Dhodapkar, D., Naucke, S., Cromer, J., Sawyer, J., Epstein, J., Spoon, D., Ayers, D., Cheson, B., and Crowley, J. (1999). Total therapy with tandem transplants for newly diagnosed multiple myeloma. Blood *93*, 55-65.

Chesi, M., Nardini, E., Lim, R.S., Smith, K.D., Kuehl, W.M., and Bergsagel, P.L. (1998). The t(4;14) translocation in myeloma dysregulates both FGFR3 and a novel gene, MMSET, resulting in IgH/MMSET hybrid transcripts. Blood *92*, 3025-3034.

Crainie, M., Belch, A.R., Mant, M.J., and Pilarski, L.M. (1999). Overexpression of the receptor for hyaluronan-mediated motility (RHAMM) characterizes the malignant clone in multiple myeloma: identification of three distinct RHAMM variants. Blood *93*, 1684-1696.

Fieber, C., Plug, R., Sleeman, J., Dall, P., Ponta, H., and Hofmann, M. (1999). Characterisation of the murine gene encoding the intracellular hyaluronan receptor IHABP (RHAMM). Gene *226*, 41-50.

Fonseca, R., Barlogie, B., Bataille, R., Bastard, C., Bergsagel, P.L., Chesi, M., Davies, F.E., Drach, J., Greipp, P.R., Kirsch, I.R., Kuehl, W.M., Hernandez, J.M., Minvielle, S., Pilarski, L.M., Shaughnessy, J.D., Jr., Stewart, A.K., and Avet-Loiseau, H. (2004). Genetics and cytogenetics of multiple myeloma: a workshop report. Cancer Res *64*, 1546-1558.

Fonseca, R., Blood, E., Rue, M., Harrington, D., Oken, M.M., Kyle, R.A., Dewald, G.W., Van Ness, B., Van Wier, S.A., Henderson, K.J., Bailey, R.J., and Greipp, P.R. (2003). Clinical and biologic implications of recurrent genomic aberrations in myeloma. Blood *101*, 4569-4575.

Greiner, J., Ringhoffer, M., Taniguchi, M., Li, L., Schmitt, A., Shiku, H., Dohner, H., and Schmitt, M. (2004). mRNA expression of leukemia-associated antigens in patients with acute myeloid leukemia for the development of specific immunotherapies. Int J Cancer *108*, 704-711.

Greiner, J., Ringhoffer, M., Taniguchi, M., Schmitt, A., Kirchner, D., Krahn, G., Heilmann, V., Gschwend, J., Bergmann, L., Dohner, H., and Schmitt, M. (2002). Receptor for hyaluronan acid-mediated motility (RHAMM) is a new immunogenic leukemia-associated antigen in acute and chronic myeloid leukemia. Exp Hematol *30*, 1029-1035.

Grogan, T.M., Muller-Hermelink, H.K., Van Camp, B., Harris, N.L., and , and Kyle, R.A. (2001). Plasma cell neoplasms. In: Pathology and genetics of tumors of hematopoietic and lymphoid tissues., eds. E.S. Jaffe, N.L. Harris, H. Stein, and , and J.W. Vardiman, World Health Organization Classification of Tumours: IARC Press.

Hall, C.L., Lange, L.A., Prober, D.A., Zhang, S., and Turley, E.A. (1996). pp60(c-src) is required for cell locomotion regulated by the hyaluronanreceptor RHAMM. Oncogene *13*, 2213-2224.

Hall, C.L., Yang, B., Yang, X., Zhang, S., Turley, M., Samuel, S., Lange, L.A., Wang, C., Curpen, G.D., Savani, R.C., and et al. (1995). Overexpression of the hyaluronan receptor RHAMM is transforming and is also required for H-ras transformation. Cell *82*, 19-26.

Hardwick, C., Hoare, K., Owens, R., Hohn, H.P., Hook, M., Moore, D., Cripps, V., Austen, L., Nance, D.M., and Turley, E.A. (1992). Molecular cloning of a novel hyaluronan receptor that mediates tumor cell motility. J Cell Biol *117*, 1343-1350.

Jacobson, J.L., Hussein, M.A., Barlogie, B., Durie, B.G., and Crowley, J.J. (2003). A new staging system for multiple myeloma patients based on the Southwest Oncology Group (SWOG) experience. Br J Haematol *122*, 441-450.

Keats, J.J., Reiman, T., Maxwell, C.A., Taylor, B.J., Larratt, L.M., Mant, M.J., Belch, A.R., and Pilarski, L.M. (2003). In multiple myeloma, t(4;14)(p16;q32) is an adverse prognostic factor irrespective of FGFR3 expression. Blood *101*, 1520-1529.

Khodjakov A, Rieder CL. The sudden recruitment of gamma-tubulin to the centrosome at the onset of mitosis and its dynamic exchange throughout the cell cycle, do not require microtubules. J Cell Biol. 1999;146:585-596.

Kuehl, W.M., and Bergsagel, P.L. (2002). Multiple myeloma: evolving genetic events and host interactions. Nat Rev Cancer *2*, 175-187.

Lever MA, Th'ng JP, Sun X, Hendzel MJ. Rapid exchange of histone H1.1 on chromatin in living human cells. Nature. 2000;408:873-876.

Line, A., Slucka, Z., Stengrevics, A., Silina, K., Li, G., and Rees, R.C. (2002). Characterisation of tumour-associated antigens in colon cancer. Cancer Immunol Immunother *51*, 574-582.

Maxwell, C.A., Keats, J.J., Crainie, M., Sun, X., Yen, T., Shibuya, E., Hendzel, M., Chan, G., and Pilarski, L.M. (2003). RHAMM is a centrosomal protein that interacts with dynein and maintains spindle pole stability. Mol Biol Cell *14*, 2262-2276.

Moreau, P., Facon, T., Leleu, X., Morineau, N., Huyghe, P., Harousseau, J.L., Bataille, R., and Avet-Loiseau, H. (2002). Recurrent 14q32 translocations determine the prognosis of multiple myeloma, especially in patients receiving intensive chemotherapy. Blood *100*, 1579-1583.

Pilarski, L.M., Seeberger, K., Coupland, R.W., Eshpeter, A., Keats, J.J., Taylor, B.J., and Belch, A.R. (2002). Leukemic B cells clonally identical to myeloma plasma cells are myelomagenic in NOD/SCID mice. Exp Hematol *30*, 221-228.

Rein, D.T., Roehrig, K., Schondorf, T., Lazar, A., Fleisch, M., Niederacher, D., Bender, H.G., and Dall, P. (2003). Expression of the hyaluronan receptor RHAMM in endometrial carcinomas suggests a role in tumour progression and metastasis. J Cancer Res Clin Oncol *129*, 161-164.

Shaughnessy, J., Jr., Tian, E., Sawyer, J., McCoy, J., Tricot, G., Jacobson, J., Anaissie, E., Zangari, M., Fassas, A., Muwalla, F., Morris, C., and Barlogie, B. (2003). Prognostic impact of cytogenetic and interphase fluorescence in situ hybridization-defined chromosome 13 deletion in multiple myeloma: early results of total therapy II. Br J Haematol *120*, 44-52.

Steensma, D.P., Gertz, M.A., Greipp, P.R., Kyle, R.A., Lacy, M.Q., Lust, J.A., Offord, J.R., Plevak, M.F., Therneau, T.M., and Witzig, T.E. (2001). A high bone marrow plasma cell labeling index in stable plateau-phase multiple myeloma is a marker for early disease progression and death. Blood *97*, 2522-2523.

Stenoien DL, Sen S, Mancini MA, Brinkley BR. Dynamic association of a tumor amplified kinase, Aurora-A, with the centrosome and mitotic spindle. Cell Motil Cytoskeleton. 2003;55:134-146.

Szczepek, A.J., Bergsagel, P.L., Axelsson, L., Brown, C.B., Belch, A.R., and Pilarski, L.M. (1997). CD34+ cells in the blood of patients with multiple myeloma express CD19 and IgH mRNA and have patient-specific IgH VDJ gene rearrangements. Blood *89*, 1824-1833.

Szczepek, A.J., Seeberger, K., Wizniak, J., Mant, M.J., Belch, A.R., and Pilarski, L.M. (1998). A high frequency of circulating B cells share clonotypic Ig heavy-chain VDJ rearrangements with autologous bone marrow plasma cells in multiple myeloma, as measured by single-cell and in situ reverse transcriptase-polymerase chain reaction. Blood *92*, 2844-2855.

Tian, E., Zhan, F., Walker, R., Rasmussen, E., Ma, Y., Barlogie, B., and Shaughnessy, J.D., Jr. (2003). The role of the Wnt-signaling antagonist DKK1 in the development of osteolytic lesions in multiple myeloma. N Engl J Med *349*, 2483-2494.

Wang, C., Entwistle, J., Hou, G., Li, Q., and Turley, E.A. (1996). The characterization of a human RHAMM cDNA: conservation of the hyaluronan-binding domains. Gene *174*, 299-306.

Wang, C., Thor, A.D., Moore, D.H., 2nd, Zhao, Y., Kerschmann, R., Stern, R., Watson, P.H., and Turley, E.A. (1998). The overexpression of RHAMM, a hyaluronan-binding protein that regulates ras signaling, correlates with overexpression of mitogen-activated protein kinase and is a significant parameter in breast cancer progression. Clin Cancer Res *4*, 567-576.

Yang, B., Zhang, L., and Turley, E.A. (1993). Identification of two hyaluronan-binding domains in the hyaluronan receptor RHAMM. J Biol Chem *268*, 8617-8623.

Zhan, F., Hardin, J., Kordsmeier, B., Bumm, K., Zheng, M., Tian, E., Sanderson, R., Yang, Y., Wilson, C., Zangari, M., Anaissie, E., Morris, C., Muwalla, F., van Rhee, F., Fassas, A., Crowley, J., Tricot, G., Barlogie, B., and Shaughnessy, J., Jr. (2002). Global gene expression profiling of multiple myeloma, monoclonal gammopathy of undetermined significance, and normal bone marrow plasma cells. Blood *99*, 1745-1757.

Zhang, S., Chang, M.C., Zylka, D., Turley, S., Harrison, R., and Turley, E.A. (1998). The hyaluronan receptor RHAMM regulates extracellular-regulated kinase. J Biol Chem *273*, 11342-11348.

Final Chapter: Discussion

D.1: RHAMM: potential structure and function relationships

The receptor for hyaluronan mediated motility (RHAMM) was initially cloned in 1992 and has since been characterized as a 58-125 K protein that is secreted and localizes to extracellular and intracellular compartments. RHAMM has been termed an itinerant receptor, potentially GPI-anchored, that interacts with HA at the cell surface and functions in intracellular signaling through interactions with ERK, MEK, and src and localizes to mitochondria, microtubules, actin and the nucleus. The complex roles of extracellular hyaluronan, and its receptors CD44 and RHAMM, in tumorigenesis has recently been reviewed by Toole (Toole, 2004). While the primary structure of RHAMM argues against a direct membrane association for this receptor (see below), the literature highlights a number of observations, including its initial cloning as a member of the hyaluronan receptor complex, which are consistent with RHAMM functioning as a receptor, or co-receptor, for hyaluronan (Hardwick et al., 1992)(Masselis-Smith et al., 1996)(Hall et al., 1994). Moreover the evidence is mounting for the accumulation of intracellular hyaluronan, at various subcellular localizations, during cellular processes like mitosis and inflammation (Hascall et al., 2004). During mitosis, HAS2 and RHAMM expression is amplified (Cho et al., 2001)(Chapter 2) and extracellular hyaluronan accumulates; it appears that uptake and translocation of extracellular HA leads to accumulation of intracellular pools (Hascall et al., 2004). The accumulation may be CD44 dependent but may also require extracellular RHAMM-HA interactions as

demonstrated for intracellular HA accumulation within the nucleus of motile cells (Collis et al., 1998). Thus, the possibility exists for inter-compartmental cross-talk involving RHAMM-HA interactions outside and within the cell during processes such as motility and mitosis; the effect(s) of this putative cross-talk on signaling pathways and cytoskeletal dynamics are currently undefined and may shed considerable insight into the oncogenic mechanism(s) of RHAMM. Although RHAMM has other documented functions, the focus of this thesis is the investigation of the role this protein plays at the centrosome within mitosis and myeloma. As such, this final chapter will discuss these centrosome specific functions in the context of the protein's structure, tissue distribution and previous experimental findings. Given the heterogenous nature of this protein's diverse functions, it is important to take a step back and inquire what the protein's primary and predicted secondary structure infers of RHAMM's putative functions.

D.1.1: RHAMM and predicted motifs

Motif searches of RHAMM primary sequence, utilizing the PROSITE database (Bairoch *et al.*, 1997), revealed potential N-glycosylation sites (4), potential N-Myristylation sites (3), a putative amidation site and several putative phosphorylation sites (including consensus sites for Protein Kinase C (7), Casein kinase II (CK2)(12), tyrosine kinase (1) and CAMP/cGMP dependent protein kinase (2)) (see Figure D.1). N-glycosylation is a very common modification and the consensus sequence utilized by the PROSITE database, N-X- $^{T}/_{S}$, is abundant in proteins and only glycosylated ~2/3 of the time (Ben-Dor *et al.*, 2004). A survey of SWISS-PROT by Ben-Dor *et al.*, 2004 further characterized N-glycosylation sites and established sequences that tend to be glycosylated

or non-glycosylated. Utilizing these rules, only one site, $N^{478}XSL$, is favored for N-glycosylation; the presence of an asp residue upstream of $N^{134}XTL$ and a prohibitive lysine residue within $N^{589}KTK$ suggests that these sites may remain nonglycosylated while $N^{568}TTA$ contains neither glycosylated nor non-glycosylated favored sequences (Ben-Dor *et al.*, 2004). While glycosylation of RHAMM is still speculative it is interesting that the favored glycosylation site lies in exon 13, an alternative splice variant of yet undetermined function. Unfortunately, the consensus myristylation sequence utilized by PROSITE has been shown to be an inconsistent predictor (Boisson and Meinnel, 2003) (Maurer-Stroh *et al.*, 2002) and the location of the sites within the interior, and not at the NH_2-terminus, of RHAMM (G^{100}, G^{159} and G^{709}) strongly implies that RHAMM is not N-terminally myristylated; likewise, the position of the consensus amidation site, $E^{559}GRK$, within the interior of the protein strongly implies that RHAMM does not undergo post-translational COOH-terminal amidation. RHAMM contains multiple putative phosphorylation (PO_4) sites; while a COOH-terminal site may be the target of AurA (see below), these sites have not been investigated for PO_4 potential. It is interesting to note that $RHAMM^{-exon13}$ loses 3 potential CK2 sites (of 12) while $RHAMM^{-exon4}$ loses a putative protein kinase C site. CK2 is a vital regulator of G_2/M transition regulating the activation of cdc25B, through phosphorylation (Theis-Febvre *et al.*, 2003). Additionally, PROSITE prediction indicated the presence of two leucine zipper motifs at L^{130} and L^{276} however no transmembrane domains, signal peptides or nuclear localization signals were identified.

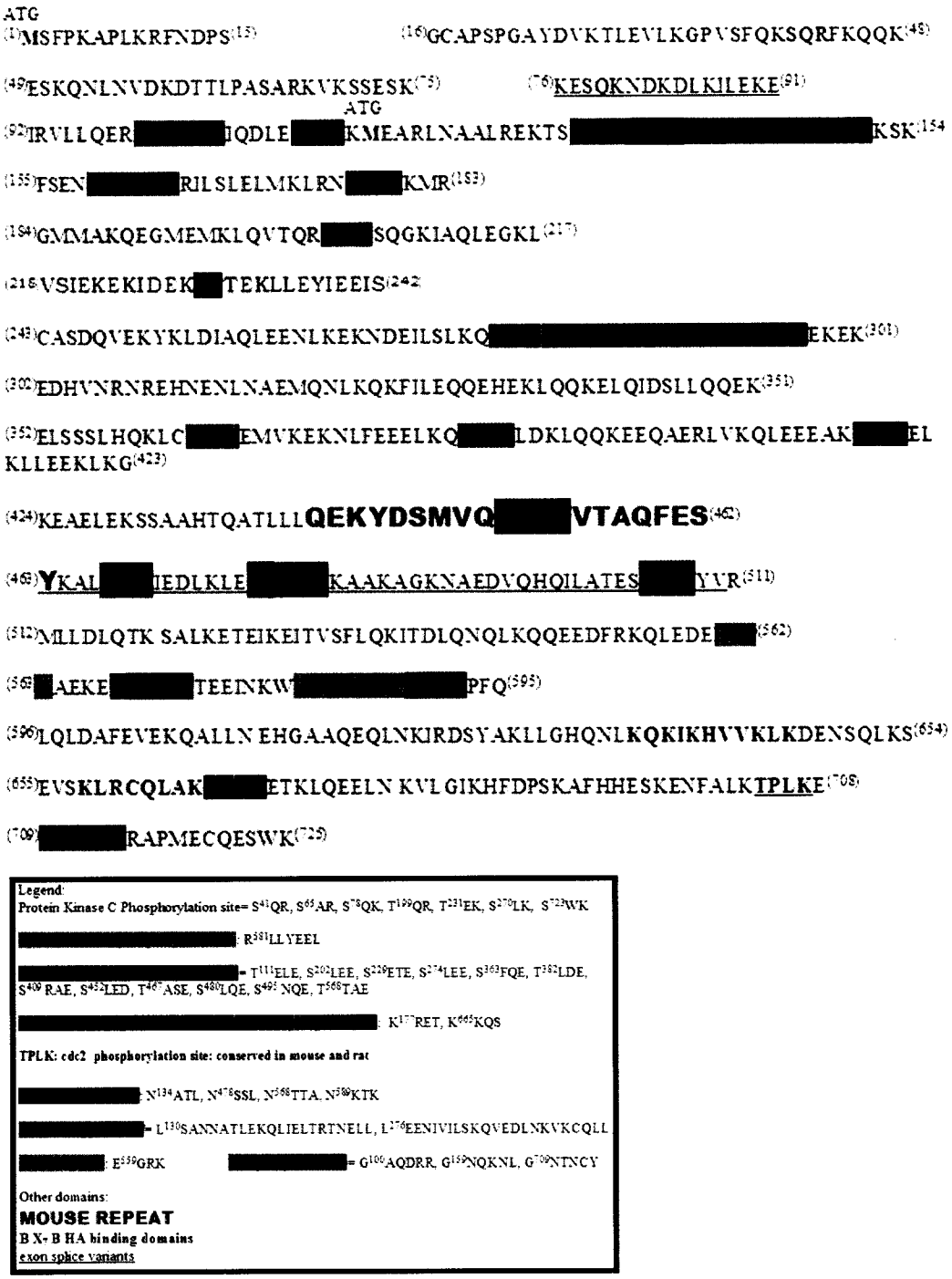

Figure D.1: Prosite ® prediction for consensus sequences in RHAMM primary sequence.

D.1.2: RHAMM and extracellular secretion

Multiple studies have implicated RHAMM in extracellular processes; the majority of these studies utilize mAbs, raised against the 58 K constituent of the HARC, to specifically block HA dependent motility. A requirement for 'classical' cell surface expression or extracellular secretion is entrance into secretory organelles such as the endoplasmic reticulum (ER) and golgi apparatus; a handful of proteins and polypeptides do undergo what is coined 'non-classical secretion'(reviewed in (Prudovsky *et al.*, 2003) (Nickel, 2003)). Most RHAMM literature highlights the absence of a defined signal sequence but examination of the hydophophobicity profile of RHAMM reveals an absolute deficit of hydrophobic stretches (Figure D.2). Indeed when one compares the hydrophobicity profile of RHAMM with that of another defined transmembrane HA surface receptor, CD44, and a defined glycosylphosphatidylinositol-(GPI)-anchored receptor, glypican 1, it is evident that RHAMM not only lacks the NH_2-terminal hydrophobic signal sequence and an internal hydrophobic transmembrane stretch but that RHAMM is an entirely hydrophilic protein (Figure D.2).

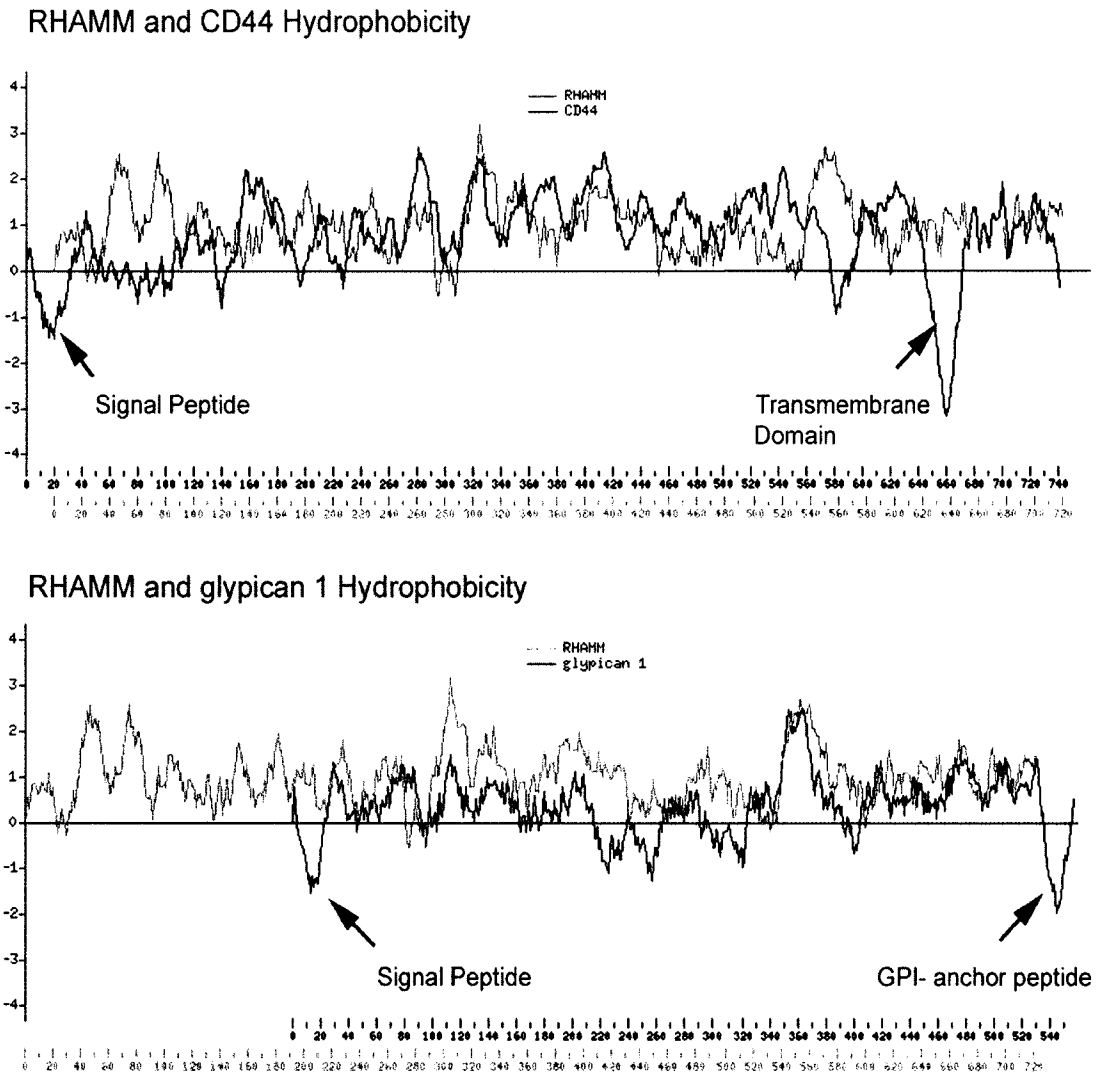

Figure D.2: Hydrophobicity profiles for RHAMM and prototypic transmembrane (CD44) and gpi-anchored (glypican) proteins

A current hypothesis speculates that RHAMM may be a GPI-anchored receptor which localizes to caveolae in migrating cells (Zaman and Savani, 2003). GPI-anchored proteins represent about 0.5% of eukaryotic proteins and result from the action of a GPI transamidase within the ER (Mayor and Riezman, 2004). The GPI-anchor attachment site is defined as a stretch of three aa with small side chains followed by a hydrophobic

spacer region and a COOH-terminal, hydrophobic signal sequence (Mayor and Riezman, 2004). Importantly, RHAMM lacks the hydrophobic NH_2-terminal signal sequence and the COOH-terminal GPI-anchor sequence necessary for insertion within the ER, cleavage and addition of a GPI-anchor. Moreover, should a GPI-anchor be added to the COOH-terminus of RHAMM, a process that requires cleavage of a 15-40 aa hydrophobic stretch, the position of the anchor would nearly overlap the defined HA-binding domains. Thus, the primary structure of RHAMM strongly argues against it functioning as a GPI-anchored cell surface receptor.

Proponents of RHAMM's extracellular functions highlight that other defined extracellular proteins (i.e. bFGF, epimorphin, HIV Tat protein, the homeobox protein engrailed, and the heat shock protein gp96) lack signal peptides (Turley *et al.*, 2002). Of the listed proteins, only epimorphin is a defined surface receptor while the others are secreted proteins or polypeptides. Interestingly, while all lack defined signal sequences (Turley *et al.*, 2002), epimorphin contains significant hydrophobicity (~20 aa) at its COOH-terminus while gp96 and bFGF contain a hydrophobic stretch (~20 aa) at their NH_2 terminus suggesting that insertion and translocation of these proteins into the ER and subsequent transit through secretory pathways may be possible. As mentioned, multiple non-classical secretion pathways have been elucidated. Secretion of FGF1 (150 aa), IL-Iα (271 aa), and IL-Iβ (269 aa) appears to be stress-induced through a Cu^{2+}-dependent 'molten globule' (reviewed in (Prudovsky *et al.*, 2003)) while HIV Tat , a small (14K, 86-101 aa) multi-functional, cationic polypeptide (Brigati *et al.*, 2003) that is released

from HIV-infected cells (Ensoli *et al.*, 1993), has been shown to utilize a protein transduction domain to directly traverse membranes (reviewed in (Nickel, 2003)). Other viral proteins (i.e. Herpes simplex virus VP22 and foamy virus Bet) are also exported by non-conventional means (Nickel, 2003). Given the much larger size of RHAMM, it is unlikely to share the non-conventional pathways enjoyed by much smaller polypeptides; the secretion of Engrailed, however, may shed some light into a potential mechanism for RHAMM secretion.

Engrailed (EN) is a member of the homeobox containg protein family, termed homeoproteins. Homeoproteins are a class of transcription factors that are defined by a 60 aa long DNA binding domain. Chicken EN2 predominantly localizes to the nucleus, as expected for a transcription factor, but is excreted in an unconvential manner (Joliet *et al.*, 1998). The homeodomain, located at the COOH-terminus of the protein, is necessary for this regulated secretion (Joliot *et al.*, 1998) as is Casein-kinase 2 (CK2) protein kinase (Maizel *et al.*, 2002). Maizel *et al.*, 2002 demonstrated that a serine-rich domain (SRD) in the NH_2 terminus of EN2 (S^{146}GAELSVSSDSDSSQAG^{169}) is phosphorylated by CK2, and this phosphorylation inhibits the secretion of EN2. It was also shown that the position of the SRD within the protein dramatically affects the PO_4 status and intercellular transfer/secretion (Maizel *et al.*, 2002). Interestingly, RHAMM also contains a SRD within its NH_2-terminus (S^{65}ARKVKSSESKKESQ^{79}) and multiple CK2 phosphorylation sites. Even more provocative is that the SRD contains the alternatively spliced exon 4 (aa 76-91); if RHAMM is targeted by CK2, and if RHAMM is secreted in

a manner analogous to that documented for EN2, loss of exon 4 may inhibit CK2 dependent phosphorylation resulting in an isoform that is more readily secreted.

D.1.3: RHAMM and coiled coil proteins

Alignment software, such as BLAST (Altschul *et al.*, 1997), allows for the identification of primary structure similarities between a defined sequence and sequences contained within a database. Examination of the extremely proline rich NH_2-terminus of RHAMM revealed no significant homology with sequences other than RHAMM variants. However, BLAST alignment of the complete sequence of RHAMM with the NCBI non-redundant database revealed significant homology (up to e^{-08}) with a number of coiled coil proteins (including myosin heavy chain, CENP-E and Xklp2). Interestingly, the alignments between these proteins and RHAMM all occurred throughout the middle ~600 aa of RHAMM sequence with the exception of Xklp2 which demonstrated significant additional homology with the COOH terminal B X_7 B domains in RHAMM. Provocatively, alignment of the COOH-terminal 650 aa of HKlp2 sequence (excluding the NH_2 terminal motor domain) revealed significant homology (e^{-30}) with RHAMM sequence; BLAST2 sequence comparison of the HKlp2 defined basic leucine zipper (BZIP) motif with the RHAMM defined HA-binding domain revealed 55% identity and 75% homology. Manual alignment of the sequences for *Xenopus* KLP2, human KLP2 and the sea urchin homologue KRP180 with RHAMM sequences revealed that >72% of residues within the B X_7 B HA-binding domain of RHAMM are conserved in at least one variant of the Klp2 BZIP motif (see Chapter 1). The extensive coiled coil nature of the

COOH terminus of RHAMM, in combination with the conservation of the BZIP motif in human, mouse and rat RHAMM (Lynn *et al.*, 2001a) suggested that, like the KLP2 family, RHAMM may target microtubule minus ends and localize to centrosomes and the spindle pole.

Both COILS (Lupas *et al.*, 1991) and PAIRCOIL (Berger *et al.*, 1995) software as well as analysis by Assmann *et al.*,1999 predict extensive coiled-coil structure through the 'stalk' region of RHAMM (aa 80-670). These assessments are supported by the significant BLAST alignment of RHAMM sequence with other coiled coil proteins. The α-helical coiled coil is a protein oligomerisation motif consisting of two or more α-helices that supercoil around one another. Coiled-coil proteins can be classified into two general categories. Leucine zippers are short coiled-coil domains that form homo- and hetero-dimers. Longer coiled-coil domains, as found in members of the intermediate filament family and RHAMM, form central rod configurations and have high polymerisation potential. In general, intermediate filament proteins function in the structural organisation of cells, as molecular scaffolds and also as cytoskeletal motors. As mentioned in the introduction, core centrosomal proteins, as well as spindle pole proteins, are characterized by extensive coiled coil structure (Salisbury, 2003) (Blagden and Glover, 2003).

Thus, analysis of RHAMM primary and secondary structure suggests that RHAMM is not secreted/surface expressed by classical means, RHAMM, therefore, is unlikely to be GPI-anchored but RHAMM may be secreted in an, as yet, poorly elucidated non-classical manner. The $RHAMM^{-exon4}$ variant is altered within a potential NH_2-terminal SRD, which in EN2 directs non-classical secretion, and this alteration may promote secretion. RHAMM shares considerable homology to various intermediate filament like coiled coil proteins, the secondary structure of RHamm is consistent with that seen in molecular scaffolding proteins and RHAMM shares intimate homology with the KLP2 protein family throughout the non-motor domains.

D.1.3b: RHAMM and coiled coil proteins: The TACC family

Chapter 1 investigates the structure, localization and function of RHAMM and demonstrates similarities between RHAMM and two distinct families of centrosomal proteins: the Transforming acidic coiled coil (TACC) and kinesin-like protein 2 (Klp2) families. Chapter 1 describes RHAMM as a ~90 kD, extensively coiled coil protein that is targeted to the centrosome through a basic leucine zipper (BZIP) motif within its COOH-terminus. Moreover, RHAMM participates in the maintenance of mitotic spindle integrity and interacts with the dynein motor complex. These functional data in combination with the chromosomal location of the *RHAMM* gene (5q33.2-qter) led to the hypothesis that RHAMM may be related to the TACC protein family. The TACC proteins, a family of proteins that bind to microtubules and concentrate to centrosomes through a conserved coiled coil carboxy-terminal domain called the TACC domain, also play a conserved role

in organizing centrosomal microtubules(Gergely *et al.*,2002)(Lee *et al.*, 2001). A defining feature of the TACC proteins, in addition to the TACC domain, is an evolutionary relationship with the fibroblast growth factor receptor gene family (Still *et al.*,1999). *TACC1-3* genes map proximal to *FGFR1-3* genes on chromosomes 8p11, 10q26 and 4p16.3, respectively. Chapter 1 investigates the phylogenetic relationship between RHAMM COOH-terminal sequence and the TACC family to decipher whether RHAMM may represent a distant member of the TACC family, specifically TACC4. In constructing an argument for RHAMM as a potential member of the TACC family, Chapter 1 postulated that rabbit TACC4, identified by Steadman *et al.*, 2002, may in fact be a TACC3 orthologue. Although RHAMM shares functional similarities, and a minimal phylogenetic relationship, with the centrosomal targeting domain of the TACC family, Chapter 1 highlighted the controversial nature of assigning RHAMM to the TACC family due to its lacking a true TACC domain; Chapter 1 concluded that "RHAMM is a TACC-like protein and may, in fact, be TACC4". A detailed examination of TACC family structural evolution has recently been published online to address these controversies (Still *et al.*, 2004).

As demonstrated in Chapter 1, Still *et al.*, 2004 provide additional evidence that the identified rabbit TACC4 represents a partial rabbit TACC3 cDNA with potentially artifactual sequence due to the 5' RACE methodology. Still *et al.*, 2004 outline an argument that the chordate genome has undergone 2 duplication events occuring roughly 700 million years ago; if the ancestral *TACC* gene was duplicated during both events, one

would expect to find four *TACC* genes. Analysis of the chromosomal regions containing *FGFR* genes revealed conservation of chromosomal segments between human, mouse and *D. melanogaster* suggesting that the ancestral chromosomal segment, containing *TACC* and *FGFR* genes, was duplicated twice (Still *et al.*, 2004). The first duplication resulted in human chromosome 4p16/5q32-qter potentially leading to FGFR/TACC genes at these loci (Still *et al.*, 2004). Analysis of human chromosome 5q32-qter and 4p16.3 demonstrates significant paralogous gene clusters (see Fig. 2 Still *et al.*, 2004); interestingly, a cluster of genes, containing the RHAMM gene (*HMMR),* maps precisely to location of a putative *TACC4* (Still *et al.*, 2004). Still *et al.*, 2004, however, were unable to locate a *TACC4* gene and speculated that *HMMR*, as well as other members of the gene cluster outlined by *GPX3* and *NKX2E*, were inserted at the site of *TACC4*. Still *et al.*, 2004 also analysed *RHAMM* and *TACC* primary sequence and, in agreement with Chapter 1, demonstrated that *RHAMM* does not contain a TACC domain and is phylogenetically more closely related to the Klp2 family. Still *et* al., 2004 further demonstrate, by phylogenetic analysis, that RHAMM forms a family of coiled coil proteins distinct from the TACC family. Still *et al.*, 2004 conclude that the second round of chromosomal duplication of the FGFR/TACC ancestor either did not include *TACC4*, and only *TACC4,* or the *TACC4* gene was lost very early in vertebrate evolution.

It is interesting to note, however, that the analysis of Still *et al.*, 2004 definitively locates *HMMR* precisely at the location of a putative *TACC4* (i.e. on hs chromosome 5q32-qter between *PDE6A/SLC26A2* and *FGFR4/NSD1*). It is also important to note that

Still *et al.*, 2004 conclusively argue that a potential hs*TACC4* should most closely resemble hsTACC3 in structure and function. Chapter 1 highlights similar centrosomal localization and a participatory role in the maintenance of mitotic integrity for RHAMM and TACC3. Moreover, the structure of TACC3 and RHAMM proteins can be divided into three sections: a NH_2 terminal region (~100-150 aa), a highly variable coiled coil central region and a centrosomal targeting COOH-terminal region (Still *et al.*, 2004)(Assmann *et al.*, 1999). Murine RHAMM contains an internal repeat (5 x 21 aa) as does murine TACC3 (7 x 24 aa) within the central stalk (Hardwick *et al.*, 1992)(Still *et al.*, 2004). All TACC proteins interact with the TOG family of centrosomal proteins and Aurora kinases (with TACC3 binding AurA)(Still *et al.*, 2004); our lab has demonstrated a RHAMM-TOG mitotic interaction (our unpublished observations, Chapter 1) and has suggested a role in AurA biology (Chapter 2). TACC proteins localize in the interphase nucleus, as do RHAMM variants (Gergeley *et al.*, 2000)(Sadek *et al.*, 2003)(Assmann *et al.*, 1999), and both have been implicated in the post-transcriptional regulation of cell cycle determinants (i.e. Cyclin B1 and cdc2)(Mohapatra *et al.*, 1996)(Groisman *et al.*, 2002)(Cao and Richter, 2002). Therefore, while the lack of a COOH-terminal TACC domain precludes the assignment of TACC4 to RHAMM, the *HMMR* gene is located at the predicted site for *TACC4,* RHAMM and TACC3 share multiple similarities including predicted secondary structure and, in the case of rodent species, primary structure repeats, subcellular localization, protein interaction partners, and participation in parallel functional pathways. Therefore, it is likely that insight into RHAMM biology may be provided by the TACC family and vice versa (see Section D.4).

D.2: RHAMM, microtubules, centrosomes, spindle poles: Looking back on the past

Chapters 1 and 2 of this thesis introduce and support the hypothesis that RHAMM is a centrosomal MAP which plays an essential role in maintaining mitotic spindle integrity. These chapters demonstrate the following: a) endogenous and exogenous RHAMM localize to these subcellular locations in adherent and suspension cells, b) this localization is dependent upon the COOH-terminus of the protein, c) RHAMM interacts with dynein and TPX2 but not NuMA, d) RHAMM, like TPX2, is cell cycle regulated, e) overexpression of GFP-RHAMM impairs mitotic progression and affects spindle integrity, and f) inhibition of RHAMM function, through microinjection of polyclonal antiserum or RNA inhibition, retards G_2/M transition and disrupts spindle integrity. The following section will evaluate this hypothesis in the context of experimental evidence provided by others.

As mentioned in Section D.1.3, the primary structure and predicted secondary structure of RHAMM strongly suggests that it may function as a molecular scaffold at centrosomes and spindle poles. The intermediate filament like structure is shared by multiple centrosomal and spindle pole proteins, including NuMA, TACC, and pericentrin proteins. Two additional features of RHAMM, each described by Assmann *et* al., 1999 and independently confirmed by others (Maxwell *et al.*, 2003) (Lynn *et al.*, 2001b), are the ability of exon 4 to interact with interphase microtubules and a calmodulin binding domain encoded by exon 16/17 ($aa^{575-598}$).

D.2.1a: RHAMM, microtubules, centrosomes, spindle poles: signal transduction

Assmann *et al.*, 1999 described the NH_2-terminal 69 aa (pI 10.72) as a basic 'head' domain responsible for an interaction between RHAMM and microtubules *in vitro*. *In vivo* microtubule binding is dependent on the retention of exon 4 (Maxwell *et al.*, 2003) (Assmann *et al.*, 1999). The ability of RHAMM to associate with microtubules likely explains its ability to associate with multiple signaling molecules (see *I.1.1)*. The role of microtubules within signal transduction has been exhaustively detailed; of particular interest to this thesis, disruption of microtubule dynamics, without addition of growth factors, will induce the rapid assembly of focal adhesions and FAK phosphorylation (Bershadsky *et al.*, 1996). The binding of ERK requires the basic leucine zipper/HA binding domains in the COOH terminus of RHAMM (Turley and Harrison, 1999). It is possible then that the COOH-terminus of RHAMM may be responsible for targeting RHAMM to a site at which it may interact with ERK (i.e. the centrosome). MAPK localizes to the centrosome during mitosis (Verlhac *et al.*, 1993) and RNA inhibition of ERK1 or MEK1, like RHAMM, results in a G_2 arrest (Liu *et al.*, 2004). Early work with MAPK/ERK revealed that ERK not only regulated microtubule dynamics, through the phosphorylation of MAPs (Hoshi *et al.*, 1992), but that a significant cellular proportion of ERK (~one-third) is associated with the microtubule cytoskeleton and this proportion increases to approximately one half upon mitogen stimulation in murine fibroblasts (Reszka *et al.*, 1995). Interestingly, c-src demonstrates two main distributions within murine fibroblasts: one that appears to be associated with the cell surface and one that coincides with centrosomes with additional patchy

distributions that are dependent on microtubules but not Golgi and rough ER (David-Pfeuty and Nouvian-Dooghe, 1990). Thus, previous demonstrations of the association of RHAMM with signaling factors that are important to mitosis and motility, localize to microtubules and centrosomes and are responsive to microtubule dynamics are entirely consistent with the current hypothesis that RHAMM is a centrosomal protein that functions in mitotic entry and spindle assembly and integrity. Indeed given the current hypothesis, one would predict that modulation of RHAMM expression levels, or expression of RHAMM variants lacking NH_2-terminal sequence (i.e. RHAMM1v4, RHAMM1, RHAMM2), may directly affect microtubule dynamics with consequent, indirect effects on intracellular signaling (see (Hall *et al.*, 1994) (Hall *et al.*, 1995) (Zhang *et al.*, 1998) etc.), cytoskeletal rearrangement (Hall *et al.*, 1994), motility (see (Turley *et al.*, 1993); (Kornovski *et al.*, 1994); (Turley *et al.*, 1994); (Savani *et al.*, 1995) etc.), division (see (Mohapatra *et al.*, 1996)) and, potentially, transformation (see (Hall *et al.*, 1995)).

D.2.1b: RHAMM, microtubules, centrosomes, spindle poles: Calmodulin

Calcium plays an essential role in multiple signaling pathways, centrosome maturation and mitotic, and meiotic, division. As mentioned in the introduction, and expanded upon below, RHAMM functions in the regulation of cdc2 (cdk1) (Mohapatra *et al.*, 1996). The focuses of this thesis has been the role of RHAMM in the mechanical processes of spindle assembly, integrity and disassembly and, thus, has not discussed the control of cell cycle progression. To further highlight the potential significance of a

calmodulin-binding domain within RHAMM, this section will briefly discuss the role of Ca^{2+} in cell cycle control, with a particular focus on oocyte meiosis. Meiosis is essentially mitosis that is designed to produce haploid gametes from the diploid precursors (Whitaker, 1996). Following chromosomal recombination, meiosis consists of two cycles of chromosome separation without intervening DNA synthesis; during the first cycle chromosome pairs are separated with haploid gametes being produced during the second meiotic divisions (Whitaker, 1996). Oocytes arrest twice during meiosis: the first arrest occurs at G_2/M, following recombination, just before the first meiotic division and the second arrest occurs during meiotic metaphase II (Whitaker, 1996)). Within oocytes, cell cycle control proteins were identified by transferring cytoplasm from a mitotic arrested oocyte into a quiescent oocyte and driving the quiescent oocyte into mitosis; this technique identified maturation promoting factor (MPF) (Maller, 1985). MPF was further characterized as two components, cell division control protein 2(cdc2) (now cyclin dependent kinase (cdk) 1) (Lee and Nurse, 1987) and cyclin B (Evans *et al.*, 1983) (Whitaker, 1996). Calcium signaling is responsible for breaking the second meiotic arrest, and in most species the first arrest as well (Whitaker, 1996). Calmodulin (CaM) is a calcium modulated protein that senses calcium levels and relays signals to calcium sensitive proteins and channels. Fertilization sets off a calcium transient which activates CaM, activating CaM kinase II leading to the destruction of cyclin, through ubiquitin mediated degradation, and the release of meiotic arrest (Whitaker, 1996). In mammalian oocytes, repeated calcium pulses may be essential for normal development (Whitaker, 1996). Calcium/calmodulin signaling are intimately associated with mitotic cell cycle as well (Santella, 1998). CaM-kinase II participates in G_2/M transition by activating cdc25C

in HeLa cells (Patel *et al.*, 1999) and participates in nuclear envelope breakdown in some systems (Santella, 1998). Transient Ca^{2+} increases occur (a) in late G_1 prior to initiation of S phase; (b) in G_2 before entry into M phase; (c) during mitosis between metaphase and anaphase, and (d), during cytokinesis (Santella, 1998). Interestingly, RHAMM function is potentially vital during the latter three stages.

As mentioned in the introduction (Section *I.2.2*), calcium/calmodulin play important roles in centrosomal replication and maturation. Centrosomes contain a pair of centrioles and pericentriolar material (PCM), which is the major microtubule-nucleating component consisting of a matrix-like protein structure and hundreds of γ-tubulin ring complexes (γTuRC). γTuRCs are composed of Tub4p complexes, which are tethered at the spindle pole via a calmodulin binding protein, Spc110 (Knop and Schiebel, 1997). Kendrin and AKAP450, also calmodulin binding proteins, bind to GCP2, an additional component of human γTuRC (Takahashi *et al.*, 2002), while centrin, a ubiquitous protein of the centrosome, is also responsive to Ca^{2+} (Salisbury, 2004). Thus, it is interesting to speculate that human centrosomal replication and maturation is regulated by calmodulin and calmodulin binding proteins, a hypothesis that has been supported by human (Takahashi *et al.*, 2002) yeast ((Kilmartin and Goh, 1996),(Stirling *et al.*, 1996), (Sundberg *et al.*, 1996)) and *Xenopus* (Matsumoto and Maller, 2002) studies. Thus, the presence of a calmodulin binding domain in RHAMM is consistent with a putative role for the protein in centrosomal maturation.

The past observations that RHAMM interacts with actin, microtubules, mitochondria and calmodulin (Assmann *et al.*, 1999) (Lynn *et al.*, 2001b), led the authors to speculate that RHAMM may represent a cytoskeletal accessory protein capable of participating in calmodulin signaling to the cytoskeleton. These hypotheses are consistent with the current hypothesis. However, qRT-PCR analysis reveals that RHAMM message increases 3.32 $^{+}/_{-}$ 0.08 and 2.52 $^{+}/_{-}$ 0.08 fold in G_2/M versus S lysates of HeLa and Raji. This data demonstrates a cell-cycle specific upregulation of RHAMM consistent with an important role for the protein during periods of centrosomal replication/maturation and division. RHAMM expression in normal tissue is greatly elevated within the testis of all species examined (see below) suggesting a role in meiotic and/or mitotic division. Moreover, overexpression of exogenous RHAMM leads to an increase in the γ-tubulin centrosomal volume. While one may argue that the increased centrosomal volume, as measured by GFP-RHAMM fluorescence, is an artifact of GFP-RHAMM overexpression, an increase in the amount of γ-tubulin at the centrosome argues for a role for RHAMM in γ-tubulin nucleation. Thus, the hypothesis that RHAMM is a centrosomal/spindle pole protein is consistent with its coiled coil structure, signal transduction effects, as well as its calmodulin and microtubule binding potential.

D.2.2a: RHAMM, transformation and cell cycle

As mentioned in the introduction (See Section *I.1.1*), two seminal papers were published in the mid-1990s regarding the participation of RHAMM in ras-transformation

and G_2/M progression. The former paper, Hall *et al.*, 1995, demonstrated the effects of RHAMM both upstream and downstream of ras activation. The latter publication demonstrated that soluble RHAMM induced arrest of cells at the G_2/M transition. This section will discuss these two findings in the context of the current hypothesis.

The major findings by Hall *et al.*, 1995 were that overexpression of RHAMM1v4 (recall RHAMM1v4 is analogous to human $RHAMM^{FL}$ exons 6-18 with repetition of exon 12) induced transformation of murine fibroblasts in a manner similar to ras-transformation, overexpression of a dominant negative variant of RHAMM (altered in the B $(X)_7$ B, recently identified BZIP, domain) reverted ras-transormed fibroblasts impairing their ability to form tumors *in vivo*, and antisense RHAMM conferred resistance to mutant H-ras transformation. The authors concluded that overexpression of RHAMM, a GPI-anchored cell surface receptor, led to HA dependent activation of FAK signaling and ras activation with consequences on cell motility and transformation (Hall *et al.*, 1995). This section will utilize the findings of Chapter 1 and 2 to propose an alternate explanation for the observations published by Hall *et al.*, 1995. Interestingly, six months after the publication of the findings of Hall *et al.*, 1995, another seminal paper was published in *Cell* that may illuminate an alternate explanation for the effect of RHAMM on ras transformation. Boleti *et al.*, 1996 cloned a centrosomal plus-ended molecular motor, named Xklp2, which functioned in mitotic spindle assembly in *Xenopus* extracts. Xklp2 was a large (1387 aa, ~160 kD) extensively coiled coil (~900 aa) protein characterized by an NH_2-terminal molecular motor domain and a COOH-terminal basic leucine zipper (Boleti *et al.*, 1996). To elucidate the function of this protein on *Xenopus* spindle

assembly, the authors microinjected the COOH-terminal tail (~250 aa) of the protein postulating that, given the coiled coil nature, this polypeptide would associate with the endogenous protein and act as a dominant negative inhibitor of function (Boleti *et al.*, 1996). The presence of this polypeptide, as well as the addition of anti-Xklp2 antibodies, led to a 46-80% reduction in bipolar spindle assembly with a predominance of monopolar or asymmetric spindles (Boleti *et al.*, 1996). Anti-Xklp2 antibodies also significantly disrupted spindle integrity (Boleti *et al.*, 1996). As mentioned in Chapter 1, the COOH-terminus of RHAMM bears significant homology to the analogous domain of Xklp2. While RHAMM lacks a NH_2-terminal motor domain, it does contain a NH_2 microtubule association domain and loss of exon 4, an important facilitator of interphase microtubule binding, dramatically affects the mobility of this isoform at the spindle (see Chapter 3). Given the homology at the COOH-terminus and the extensive coiled coil nature of both proteins, it is likely that RHAMM, like XKlp2, homodimerizes and introduction of a RHAMM variant lacking NH_2-terminal microtubule binding capacity (i.e. RHAMM1v4) may inhibit function analogous to microinjection of RHAMM antibodies (see Chapter 1) or RNA inhibition (See Chapter 2). Given these observations, it is reasonable to speculate that overexpression of the RHAMM1v4 variant may have affected clonal genetic stability which, after the 3 week G418 selection, led to selection of aggressive clones with transformed phenotypes. The dominant effect of RHAMM overexpression, and variant overexpression (See (Mohapatra *et al.*, 1996)), is a mitotic block; thus, introduction of a mutated dominant negative RHAMM variant (with modified basic residues of HA binding domain but conserved leucine residues of the BZIP domain) would be expected to inhibit the replication potential of ras-transformed cells. In this

way, overexpression of RHAMM, and the truncated RHAMM1v4 variant, may induce experimental results that are consistent with a conclusion that RHAMM functions both upstream and downstream of ras activation. As mentioned above, the observed effects of RHAMM1v4 overexpression on FAK phosphorylation and motility may be associated with a putative regulation of microtubule, or cytoskeletal, dynamics.

D.2.2b: Soluble RHAMM and G_2/M

Additional insight into the effect of RHAMM1v4 overexpression on ras-transformed fibroblasts was provided by Mohapatra *et al.*, 1996. The authors noted that incubation of ras-transformed cells with soluble GST-RHAMM1v4 led to the accumulation of cells in G_2/M with suppression of cdc2 and cyclin B (Mohapatra *et al.*, 1996). The described effects required incubation periods greater than 48 hours (Mohapatra *et al.*, 1996). After 48 hours, incubation with soluble RHAMM1v4 was associated with an increased degradation rate of cdc2 and resulted in reduced tumorigenicity and metastasis (Mohapatra *et al.*, 1996). These observations led to the hypothesis that soluble RHAMM interfered with extracellular RHAMM:HA signaling; RHAMM signaling, thus, targets cdc2 and cyclin B1 synthesis and controls entry into mitosis (Mohapatra *et al.*, 1996).

Should RHAMM be subject to non-classical secretion, it would likely be subject to internalization; for example, engrailed-2 is subject to intercellular transfer based upon nonconventional secretion and non-endocytic internalization (Maizel *et al.*, 2002). Even

if a regulated process for RHAMM internalization does not exist, the incubation of 10 μg/ml fusion protein for 48 hours would likely result in a degree of intracellular accumulation. The lack of noticeable response at 5, 10 and 24 hours incubation time suggests that the observed effects may not be due to dominant suppression of extracellular signaling, which should be immediate; this timeframe and the resulting effects, however, are consistent with the passive, or active, internalization of RHAMM1v4 fusion proteins leading to RHAMM inhibition, analogous to antibody microinjection or RNA inhibition, resulting in cell cycle arrest at G_2/M or metaphase, possibly with abberant spindle phenotypes and unaligned chromosomes. The authors also noted degradation of cyclin B1 by the 48 hour timepoint. While the precise timing of cyclin B1 degradation may depend upon the cell model used, cyclin B is degraded prior to the onset of anaphase in mammalian systems (Chang *et al.*, 2003). Within HeLa cells, cyclin B1 protein levels begin to decrease at early metaphase and 94.2% of cyclin B1 has been destroyed prior to the onset of anaphase (Chang *et al.*, 2003). Thus, cyclin B1 degradation, resulting from soluble RHAMM1v4, is consistent with the establishment of a metaphase block through the internalization of RHAMM1v4 protein. The authors state that the level of cdc2 (aka cdk1) remains constant throughout the cell cycle (Mohapatra *et al.*, 1996); the manuscript provides convincing evidence for the RHAMM1v4 dependent stimulation of cdc2 degradation (Mohapatra *et al.*, 1996). As mentioned in Chapter 1, RHAMM contains a consensus cdc2 phosphorylation site ^{704}TPLK^{707} within the COOH-terminus which is maintained in mouse, rat and human (as well as in RHAMM1v4). Overexpression of a RHAMM variant that lacks this site, RHAMM^{679}, results in failure to progress through G_2/M. This observation suggests a functionally important interaction

between RHAMM and cdc2. Chapter 2 demonstrates a significant interaction between mitotic pools of RHAMM and TPX2 and suggests that this interaction may affect Aurora A (AurA) kinase activation. Interestingly, AurA kinase is intimately linked to cdc2. RNA inhibition of AurA, like RNA inhibition of RHAMM (Chapter 2), significantly impaired progression through G_2 (Hirota *et al.*, 2003). The mechanism for this impaired progression is through the AurA mediated recruitment and activation of Cyclin B1/cdc2 complexes at G_2 centrosomes (Hirota *et al.*, 2003). Indeed, cdc2-cyclin B complexes, themselves activated by active AurA, are responsible in part for activation of AurA (Marumoto *et al.*, 2002) (Maton *et al.*, 2003). This reciprocal regulation is suggestive of feedback mechanisms; thus, if RHAMM affects AurA, either through TPX2 or another mechanism, the downregulation of cdc2 message noted by Mohapatra *et al.*, 1996, through increased cdc2 breakdown, may be a feedback response to the presence of excess COOH terminal RHAMM protein or a response to the inactivation of native RHAMM through RHAMM1v4:native RHAMM heterodimerization. Mechanism aside, the message degradation of cdc2 is provocative, and unique (by this author's literature review), and may further demonstrate an intimate associtation between RHAMM and AurA.

D.2.3: RHAMM, tissue distribution and SEREX

Evolution is an inherently efficient process; thus, one would postulate that a protein's function, which is dictated by its structure, would dictate its expression. Given the intimate association between centrosome replication/maturation and cell division, one

would expect that proteins involved in centrosomal replication/maturation would be more highly expressed in proliferative tissues. We have demonstrated that RHAMM is indeed upregulated ~3 fold from S through G_2/M but these experiments utilized transformed cell lines. Evident within meiosis/mitosis, the centrosome plays an essential role in microtubule organization and the establishment of cellular polarity. Indeed, the centrosome, along with APC, is essential to the establishment of asymetrical cell division during cell differentiation (Yamashita *et al.*, 2003). In drosophila testis, maintenance of stem cell identity, or initiation of differentiation, is determined by asymmetrical division (Yamashita et al., 2003). These two cell fates are determined by centrosome position relative to the stem cell niche (Yamashita et al., 2003). Centrosome position is dependent upon centrosomal components (i.e. centrosomin) and signaling intermediates (i.e. APC, DE-cadherin, armadillo) at the interface between the stem cell and its niche (Yamashita et al., 2003). Should RHAMM play an essential role in centrosome and spindle integrity, one would expect elevated RHAMM expression within normal tissues that are characterized by proliferation and differentiation and lower, or absent, expression in non-proliferative, differentiated tissues.

RT-PCR examination of RHAMM expression in murine tissues revealed ubiquitous expression in all examined tissues (including pancreas, heart, lungs, liver, kidney, brain, stomach, colon and salivary gland) with significantly elevated expression in the thymus spleen and testes. Consistent detection of RHAMM expression within normal human tissues appears to be limited to the testis (Line *et al.*, 2002) (Greiner *et al.*,

2002) (Greiner *et al.*, 2004) with various reports of elevated expression in the placenta, thymus, and spleen and lower expression in colon, stomach, lung and pancreas. Thus, RHAMM expression within human tissues is consistent with a role for the protein in proliferation and differentiation.

Tumors express an altered range of gene products when compared to autologous normal tissue. SEREX (serological identification of antigens by recombinant expression cloning) is a novel strategy for the identification of these aberrant tumor antigens (reviewed in (Sahin *et al.*, 1997)). Interestingly, RHAMM has been identified as a SEREX antigen in colon (Line *et al.*, 2002), AML, CML, melanoma, renal cell carcinoma, breast cancer and ovarian carcinoma (Greiner *et al.*, 2002).

The initiation of a tumor-specific immune response depends upon the release of antigens from tumor cells (i.e. secretion, shedding or necrosis), followed by their uptake and presentation by antigen-presenting cells and the generation of an anti-tumor humoral response within the patient. The basic approach of SEREX is to screen a cDNA library, constructed from fresh tumor tissue or cell lines, expressed recombinantly in *E. coli* (note: this expression system will mask glycosylated epitopes and epitopes that are inappropriately folded within bacteria) and transferred to nitrocellulose, with patient serum (Sahin *et al.*, 1997). High-titer IgG antibodies are detected, by ELISA, and the targeted cDNA is cloned and sequenced (Sahin *et al.*, 1997). This methodology has

identified a wide range of antigens that can be classified into seven categories: 1. 'shared' tumor antigens that are expressed in a variety of tumors but restricted to testis expression in normal tissues; 2. differentiation antigens that are lineage-specific gene products that are expressed in tumors but also expressed in normal cells of the same origin; 3. mutated gene products. These antigens are rarely detected with mutated p53 being an exception; 4. overexpressed gene products that override immunological tolerance; 5. splice variants; 6. cancer-related autoantigens that are expressed at similar levels in tumor and autologous normal tissues but elicit antibody responses only in cancer patients; 7. cancer-independent autoantigens that are antigens that ellicit antibody responses in cancer and autoimmune diseases (an example is pericentriolar material-1, PCM-1, which is an autoantigen in scleroderma and a SEREX identified antigen)(Sahin *et al.*, 1997).

When considering SEREX identification of RHAMM, one must analyze its potential membership in each of the preceding categories with the exception of differentiation antigen (RHAMM may be involved in differentiation but RHAMM does not demonstrate lineage-specific expression in normal or tumor tissues). RHAMM does not meet the definition of a cancer-related autoantigen as it is clearly overexpressed in a variety of cancers (see Chapter 2 and 3) (Wang *et al.*, 1998) (Line *et al.*, 2002) (Li *et al.*, 2000) (Crainie *et al.*, 1999). However, additional research will be necessary to exclude RHAMM from the cancer-independent autoantigen group. Many centrosomal/spindle pole proteins have been identified as autoantigens (Balczon and West, 1991) (Mack *et al.*, 1998) (Gavanescu *et al.*, 1999); indeed, centrosomal proteins appear to be major targets

of autoantibodies in systemic sclerosis (Gavanescu *et al.*, 1999). Some groups (Line *et al.*, 2002), but not others (Greiner *et al.*, 2002), have reported RHAMM reactive antibodies in the sera of healthy donors (3/35 tested vs. 0/20 tested). This discrepancy may be due to the presence of autoimmune RHAMM-reactive antibodies within patients of one 'healthy' group but not the other. Greiner *et al.*, 2002, however, reported that an additional 7 patients, with autoimmune diseases (of unspecified origin), contained RHAMM negative serological results. Thus, a more detailed and extensive study of healthy individuals will be needed to examine the presence of RHAMM positive sera within healthy and autoimmune patient populations.

Cancer/testis (CT) antigens are promising therapeutic targets as they are immunogenic in cancer patients and exhibit highly tissue-restricted expression (reviewed in (Scanlan *et al.*, 2004)). As mentioned, RHAMM is expressed in various human tissues which would apparently exclude it from the CT antigen family. However, RT-PCR screening has demonstrated that only 19/43 identified CT antigens are truly tissue restricted (Scanlan *et al.*, 2004); indeed, 10/43 demonstrated expression in >3 additional tissues (with common expression in placenta and pancreas), 9/43 demonstrated expression in 3-6 additional tissues and 5/43 were ubiquitously expressed (Scanlan *et al.*, 2004). Like RHAMM, however, testis expression was significantly greater than non-gametogenic tissues (Scanlan *et al.*, 2004). Indeed, Guinn *et* al., 2004 recently presented an abstract (AACR 2004) that identified RHAMM as one of 45 AML antigens presented in a testes cDNA library derived from 5 normal donors (Guinn *et al.*, 2004). As is often

the case in science, a label (like CT antigen) does not provide additional insight into protein function. However, if RHAMM is indeed a CT antigen, this does raise novel questions. For example, what are the underlying mechanisms controlling elevated RHAMM expression in the testis and restricting RHAMM expression in non-gametogenic tissues and are these mechanisms utilized by tumors? DNA methylation and histone acetylation influence CT gene expression (De Smet *et al.*, 1997) (Weiser *et al.*, 2001) and random hypomethylation in cancer has been implicated as a triggering event for CT expression (Scanlan *et al.*, 2004). Is RHAMM also targeted by these epigenetic regulation events?

Identification of NY-CO-13, a mutated version of p53, is one of the rare observations of antigenic mutated gene products in cancer (in this specific instance colon cancer) (reviewed in (Scanlan *et al.*, 2004)). Like NY-CO-13, RHAMM is an immunogenic antigen in colon cancer (Line *et al.*, 2002) and is mutated in a subset of colorectal cancers (microsatellite instable (MSI-H)) (Duval *et al.*, 2001). *RHAMM* was identified as a target gene likely to be mutated during MSI-H tumoral progression (Duval *et al.*, 2001). MSI-H tumors represent about 10-15% of colorectal, gastric and endometrial cancers but are much less frequent in other sites (Boland *et al.*, 1998). The SEREX detection of RHAMM in colon cancer may be due to the detection of mutated products. However, Line *et al.*, 2002 highlighted overexpression of total cellular RHAMM, or a splice variant, as potential mechanisms.

As described in Chapters 2 and 3, RHAMM overexpression characterizes aggressive myeloma plasma cells and predicts for poor patient survival; RHAMM is differentially expressed up to ~25 fold within myeloma patients. While it is unknown whether myeloma patients, especially those with elevated RHAMM expression, contain RHAMM-reactive antibodies, a subset of patients with other tumors do. For example, sera from ~67% of patients with breast cancer elicit serological response to RHAMM (Greiner *et al.*, 2002) and RHAMM overexpression is a significant parameter in breast cancer progression (Wang *et al.*, 1998). In colon cancer, RHAMM was overexpressed 2.2-7.5 fold (semi-quantitative RT-PCR) in cancer compared to adjacent non-cancerous tissue in 6/15 patients examined (Line *et al.*, 2002); interestingly 5/24 colon cancer patients exhibited RHAMM-positive serological response (Line *et al.*, 2002). Line *et al.*, 2002 also described a qualitative increase in $RHAMM^{-exon4}$ message in tumor tissue. Thus, the observed RHAMM-reactive serological response in colon cancer may be due to absolute RHAMM expression or elevated $RHAMM^{-exon4}$ expression; it may be interesting to test MM patients for RHAMM reactive antibodies and determine if a serological response correlated with absolute RHAMM expression or $RHAMM^{FL}/RHAMM^{-exon4}$ ratios.

D.3: RHAMM, microtubules, centrosomes, spindle poles: Looking to the future

The previous sections demonstrate that the primary structure, predicted secondary structure, defined functional domains, tissue distribution and past publication results for RHAMM support its role as a centrosomal protein which participates in spindle assembly

and mitotic integrity. In *Xenopus, XMAP150,* a homolog of human RHAMM, has been cloned and characterized. XMAP150 is a centrosomal MAP that localizes to spindle poles in a dynein dependent manner and appears to recruit TPX2 (Groen *et al.*, 2002); it is postulated that XMAP150 may regulate the sequestration of TPX2 by importins (Groen *et al.*, 2003). These results complement the findings of Chapter 1 and 2 and introduce exciting research avenues for future investigation of RHAMM function.

The discussion section of Chapter 1 investigates the RHAMM dependent maintenance of mitotic spindle integrity and suggests that this activity may be assisted by TPX2. Chapter 2 expands upon this hypothesis and demonstrates that RHAMM does indeed interact with a significant cellular proportion of TPX2 during mitosis. Moreover, inhibition of RHAMM function delays G_2/M progression suggesting that RHAMM may be involved in this process as well. The following sections will expand upon potential mitotic functions for RHAMM.

D.3.1: RHAMM and mitosis: a role in G_2/M transition

The significant mitotic association of RHAMM and TPX2, in mammalian and *Xenopus* systems (Groen *et al.*, 2003), in combination with the demonstration that RHAMM is functional in G_2/M transition, with both RNA inhibition (Chapter 2) and soluble RHAMM (Mohapatra *et al.*, 1996), is provocative and suggestive of a functional interaction between RHAMM and AurA kinase. Other provocative correlations exist between RHAMM and AurA including: 1. similar cell cycle dependent intracellular

localization; 2. similar cell cycle dependent elevated expression (Hirota *et al.*, 2003); 3. overexpression of both induces centrosomal abnormalities and genetic instability (Zhou *et al.*, 1998); 4. RNA inhibition of both affects G_2/M transition (Hirota *et al.*, 2003); 5. FRAP analysis demonstrates similar mobilities on mitotic centrosomes (Stenoien *et al.*, 2003); and 6. RHAMM contains a putative AurA kinase phosphorylation site within it COOH-terminus; loss of this site inhibits mitotic progression. Given these observations, a cell cycle dependent interaction between RHAMM and AurA is likely, and may involve cell-cycle dependent phosphorylation of the COOH-terminus of RHAMM, and should be investigated.

AurA undergoes both spatial and temporal activation through G_2/M (Hirota *et al.*, 2003); AurA protein levels are dynamic, elevated in late G_2, as are the protein's intracellular localization and phosphorylation state (Hirota *et al.*, 2003). Initially, AurA localizes to G_2 centrosomes and becomes activated, through phosphorylation, during late G_2 (Hirota et al., 2003). Activated AurA strongly localizes to the nucleus coincident with chromation condensation, later redistributing back to centrosomes, and spindle poles, following nuclear envelope breakdown (Hirota *et al.*, 2003). This dynamic cell-cycle dependent redistribution may help explain why variants of RHAMM ($RHAMM^{-exon4}$ and $RHAMM^{-exon4/exon13}$) have been identified within the nucleus (Assmann *et al.*, 1999). Like RHAMM (Mohapatra *et al.*, 1996), AurA is involved in the activation of cyclin B1-Cdk1(cdc2) at G_2 centrosomes, a process that is essential for centrosome maturation (Hirota *et al.*, 2003). RHAMM inhibition, like AurA inhibition and RHAMM

overexpression (Chapter 2), may also affect centrosomal maturation. AurA autophosphorylation during G_2 was dependent upon an interaction with a novel mitotic regulator termed Ajuba (Hirota *et al.*, 2003). Ajuba may stabilize active AurA or induce an activating conformational change, as demonstrated for TPX2-AurA interactions (Bayliss *et al.*, 2003). It would be interesting to investigate whether RHAMM interacts with Ajuba, as it does with TPX2, to function as a regulator of the regulators of AurA activation. Once activated, AurA interacts with and phosphorylates p53 (Katayama *et al.*, 2004). AurA mediated phosphorylation of p53 Ser315 facilitated degradation of p53 through Mdm 2 dependent ubiquitination (Katayama *et al.*, 2004). Overexpression, and inhibition, of AurA affected cisplatin-induced p53-dependent apoptosis (with overexpression of AurA confering resistance to apoptosis) (Katayama *et al.*, 2004). AurA also interacts with and phosphorylates BRCA1 at centrosomes, a process that may regulate mitotic entry (Ouchi *et al.*, 2004). Insight into a putative association, or regulatory relationship (through associations with TPX2 or Ajuba), between RHAMM and AurA would likely shed considerable insight into the relationship between RHAMM and carcinogenesis with particular emphasis on tumors characterized by extensive CIN (i.e. breast/epithelial and MM).

D.3.2: RHAMM and spindle integrity

In some systems spindle assembly is dependent upon a centrosome-directed pathway (Mitchison *et al.*, 1986) while other systems utilize a chromosome-directed pathway (Karsenti and Vernos, 2001); it appears that both systems are important for

mammalian spindle assembly (Mitchison *et al.*, 1986) (Khodjakov *et al.*, 2000) (Gruss *et al.*, 2002) (Khodjakov *et al.*, 2003). RHAMM:TPX2:dynein complexes are involved in the maintenance of spindle integrity however the role that RHAMM plays in spindle assembly requires further elucidation. A number of observations presented within this thesis may help illuminate the role of RHAMM in chromosome-directed spindle assembly. Overexpression of GFP-RHAMM reveals punctuate chromosomal localization that is proximal to kinetochores and consistent with a role in chromosome directed assembly; however, RNA inhibition of RHAMM, unlike that of TPX2 (Gruss *et al.*, 2002)(Chapter 2), does not result in separated microtubule asters lacking chromosome contacting microtubules. These results indicate that RHAMM may not be involved in microtubule nucleation at chromosome kinetochores. Microinjection of anti-RHAMM antibodies, unlike that for anti-NuMA antibodies (Gordon *et al.*, 2001), does not result in unfocussed spindles but rather multipolar spindles (Chapter 1). These results suggest that RHAMM, unlike NuMA, may not be the principle mechanism for focusing of chromosome directed microtubules into a bipolar spindle. However, the localization of RHAMM proximal to kinetochores, and a mitotic interaction with dynein, is consistent with a role for RHAMM in this process. Endogenous NuMA and HSET, due to their larger sizes, may be sufficient for spindle focusing while RHAMM:TPX2:dynein complexes play a supportive role.

RHAMM and NuMA share similar secondary structure, with RHAMM being much smaller (240 K vs. 95 K), can both directly contact microtubules (Assmann *et al.*, 1999) (Maxwell *et al.*, 2003) (Haren and Merdes, 2002) and interact with the dynein

complex (Maxwell *et al.*, 2003) (Merdes *et al.*, 1996) (Gaglio *et al.*, 1996), and may both support spindle focusing by coupling with the dynein motor complex to bind and recruit chromosome microtubules into a bipolar spindle as seen with NuMA (Khodjakov *et al.*, 2003). Analysis of monastrol treated cells (initiating a monopolar spindle by inhibiting the mitotic kinesin Eg5) may illuminate a role for RHAMM:dynein complexes in minus-end capture and focusing of mammalian kinetochore fibers. It is currently clear, however, that a role for RHAMM in spindle assembly may be important but not essential (Chakravarty *et al.*, 2004).

D.3.3: RHAMM and cytokinesis

There are a number of experimental observations that suggest RHAMM may be important during spindle disassembly and cytokinesis. First, RHAMM localizes to the central spindle and daughter cell centrosomes during cytokinesis. Second, RHAMM regulates cdc2 (cdk1) post-transcriptionally (Mohapatra *et al.*, 1996); a prevailing theory for mitosis is that cyclin dependent kinases regulate the activity of microtubule stabilizing, and destabilizing, proteins through phosphorylation events (Ookata *et al.*, 1995) (Desai and Mitchison, 1997). Degradation of cyclin B inactivates cdc2 (cdk 1) and leads to dephosphorylation of spindle assembly factors and mitotic disassembly (Desai and Mitchison, 1997). The Mitotic Exit Network (MEN), in *S. cerevisiae*, is the best described process for the inactivation of cdc2 (Simanis, 2003). Third, RHAMM interacts with spindle assembly factors (TOG and TPX2) that are spindle disassembly targets (Cao *et al.*, 2003).

The MEN monitors spindle position in anaphase; once metaphase-anaphase transition has been initiated, by the sequential ubiquitin-dependent degradation of numerous proteins cumulating in cleavage of cohesins, complete inactivation of mitotic CDK activity is essential for normal exit from mitosis (reviewed in (Simanis, 2003)). The MEN, a signal transduction pathway that targets spindle pole proteins, results in the activation (dephosphorylation) of Cdc14 phosphatase, and its release from the nucleolus, and a subsequent dephosphorylation wave that inactivates cyclin B-cdk1 and leads to actin ring formation and cytokinesis (Simanis, 2003). Recent examination in *Xenopus* egg extracts has highlighted an additional pathway, separate from cyclin B degradation, which is necessary for the regulation of microtubule structures during mitotic exit. This alternate pathway utilizes a member of the AAA-ATPase family, cdc48/p97, to disassociate spindle assembly factors from microtubules (Cao *et al.*, 2003) (Cheeseman and Desai, 2004). In combination with adaptor proteins (Ufd1-Npl4), Cdc48/p97, known to unfold proteins and dissociate multimolecular complexes, interacts with spindle assembly factors (i.e. TPX2, TOG and a polo-like kinase1) post-metaphase (Cao *et al.*, 2003). This protein complex is required for mitotic exit, even after cyclin B degradation, and results in the ubiquitin dependent degradation of some proteins but not of TPX2 or TOG; these proteins are apparently released from microtubules, in a cdc48 dependent manner, without degradation (Cao *et al.*, 2003) (Cheeseman and Desai, 2004).

RHAMM influences mitotic spindle integrity, can affect microtubule/γ-tubulin nucleation, interacts with significant amounts of mitotic TPX2 and localizes to spindle

pole bodies and the central spindle in mammalian (Maxwell *et al.*, 2003)(Chapter 2) and *Xenopus* (Groen *et al.*, 2002) (Groen *et al.*, 2003) systems. Taken together, these data suggest that RHAMM may be involved in the process of spindle disassembly during cytokinesis. The difficulty with investigating the mechanisms of spindle disassembly, which remain rather enigmatic compared to those of spindle assembly, is that inhibition of function, or overexpression, experiments for proteins involved in spindle disassembly often lead to pre-disassembly (pre-cytokinesis) mitotic arrest. For example, TPX2 RNA inhibition arrests prometaphase (Gruss *et al.*, 2002)/metaphase (Garrett *et al.*, 2002)(Chapter 2) while classical MEN mutants arrest with extended spindles and separated chromosomes (Simanis, 2003). Likewise, Chapters 1 and 2 describe a metaphase arrest for RHAMM overexpression and inhibition of function experiments. However, initial RNA inhibition experiments targeting RHAMM utilized constructs synthesized by Dharmacon, Inc (Boulder, CO) that were designed according to rules outlined by Elbashir *et al.*, 2001. The RHAMM constructs targeted exon 4 (aatgataaagatttgaagatatt) or exon 6 (aatgaactactaaaatctaagtt) while the TPX2 construct was as described (Gruss *et al.*, 2002). Immunoblot analysis revealed little inhibition of RHAMM, or TPX2 (positive control), protein expression levels at 24 or 48 hours (not shown); however, cell cycle analysis of RHAMM, TPX2 and GL2 (negative control) inhibition revealed differential cell cycle populations (see Figure D.3). With these constructs TPX2 inhibition resulted in a metaphase arrest without aberrant spindle phenotypes while RHAMM inhibition resulted in a cytokinesis block. While immunoblot analysis suggested that inhibition failed, or was incomplete, immunofluorescence analysis of RHAMM inhibited cytokinesis cells demonstrated repressed RHAMM expression

within these cells (Figure D.3). These results, while initially unexpected, may demonstrate that partial inhibition of RHAMM allows for G_2/M progression, segregation of chromosomes and transition through the spindle checkpoint but impairment of, and accumulation at, cytokinesis. A detailed investigation of RHAMM involvement in cytokinesis may provide further insight into this protein's biology and its participation in oncogenesis.

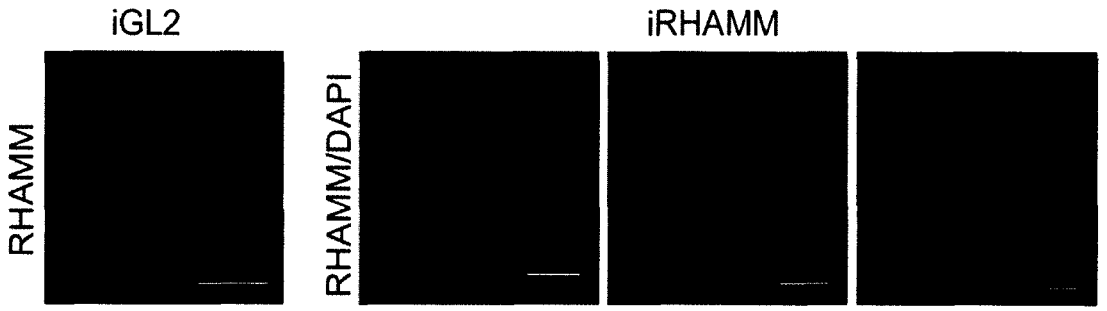

	iGL2 (n=228)	iRHAMM (n=220)	iTPX2 (n=295)
Prophase	15.3	16.4	10.5
Prometaphase	24.1	20.5	21.7
Metaphase	24.6	16.8	**46.5**
Anaphase	4	4.5	7.5
Cytokinesis	22	**41.8**	10.5

Figure D.3: RNA inhibition results demonstrating an increase in mitotic cells in cytokinesis dependent upon RHAMM, and not GL2 or TPX2, inhibition. Table shows percentage of cells within defined cell cycle stage. n is the numberof cell examined for each treatment.

D.4 A role for RHAMM, and other centrosomal proteins, in myelomagenesis

Multiple myeloma is a malignancy of post-germinal center B-lineage cells that are characterized by extensive chromosomal instability, a unique rearrangement of the immunoglobulin heavy chain (IgH) gene locus, termed clonotypic, and recurrent, genetic translocations of defined partner chromosomes into regions of the IgH locus. Similar to tumors of epithelial origins, myeloma clonotypic cells demonstrate extensive structural and numerical chromosomal anomalies in addition to recurrent primary and secondary IgH translocations (Ho *et al.*, 2002) (Sawyer *et al.*, 1995) (Smadja *et al.*, 1998) (Avet-Loiseau *et al.*, 2001) (Fonseca *et al.*, 2003a). Myeloma lacks a defining IgH translocation further differentiating it from other hematological malignancies, like mantle cell lymphoma in which all malignant cells contain a characteristic t(11;14)(q13;q32). Rather, myeloma is characterized by recurrent IgH translocations, the most frequent being t(11;14)(q13;q32), t(4;14)(p16.3;q32) and t(14;16)(q32;q23), that disregulate cell cycle progression by targeting oncogenes, including Cyclin D1, FGFR3, WHSC1/MMSET/NSD2 and c-maf (Bergsagel and Kuehl, 2001) (Kuehl and Bergsagel, 2002). It is postulated that these recurrent IgH translocations may be progression, or initiating, events that dramatically affect, or induce, chromosomal instability (CIN) and disease progression (Kuehl and Bergsagel, 2002). Currently, however, the mechanisms responsible for linking IgH translocations with chromosomal instability are unclear. This section will attempt to model IgH translocation-mediated CIN through examination of the effects of RHAMM on centrosomal and mitotic spindle integrity.

The majority of myeloma patients (55-70% of intramedullary MM) demonstrate recurrent translocations of specific genetic loci; the frequency of individual translocations is 5- 15% of the MM patient population (Avet-Loiseau *et al.*, 1998). These translocations are often unbalanced resulting in loss of derivative chromosomes and altering oncogene expression patterns (Keats *et* al., 2003)(Santra *et* al., 2003). The heterogeneity of partner chromosomal loci combined with the frequent loss of derivative chromosomes suggests that a common disregulated myelomagenesis pathway, based upon overexpression of defined gene products translocated proximal to the IgH locus, may not exist. There is strong evidence, however, that MM patients may be classified based upon the karyotype of the malignant plasma cells (Fonseca *et al.*, 2004) (Smadja *et al.*, 1998) with hypodiploidy, or non-hyperdiploidy, being a major prognostic factor (Smadja *et al.*, 2001). Provocatively, recurrent IgH translocations, despite their heterogeneous nature, strongly associate with non-hyperdiploid MM (Fonseca *et al.*, 2003b); indeed, 88% of tested patients with hypodiploidy (16 of 18) and 90% of tested patients with tetraploidy (9 of 10) had an IgH translocation (Fonseca *et al.*, 2003b). These data suggest that IgH translocation positive MM may have a common disregulated pathway which induces chromosomal instability with a strong predisposition for hypodiploid or tetraploid progeny. For this to be the case, however, one would expect that the disregulated target genes would need to be oncogenic, or induce genetic instability, when overexpressed or underexpressed, due to the frequent occurrence of unbalanced translocations (Keats *et al.*, 2003) (Santra *et al.*, 2003) (Fonseca *et al.*, 2003a), and the target genetic loci (4p16.3,

11q13, 16q23 and minor sites 6p21, 20q11) be intimately linked to a common pathway regulating genetic stability.

Cyclin D family members (D1 and D3) have been implicated as targets of recurrent t(11;14) and t(6;14) translocations, respectively (Chesi *et al.*, 1996) (Shaughnessy *et al.*, 2001). Overexpression of these gene products, due to their proximity to the IgH enhancer, may elongate DNA replication, induce centrosomal amplification and increase CIN. A similar pathway has been demonstrated for K cyclin (Verschuren *et al.*, 2002). FGFR3 is implicated as the defined target gene of t(4;14) however it is unclear whether wild-type FGFR3 is oncogenic or overexpressed in t(4;14) patients (Intini *et al.*, 2001) (Karoui *et al.*, 2001) with some $t(4;14)^{+}$ patients failing to express detectable FGFR3 (Keats *et al.*, 2003) (Santra *et al.*, 2003). C-maf is implicated as the target oncogene in $t(14;16)^{+}$ MM (Chesi *et al.*, 1998) (Hurt *et al.*, 2004) with maf-B potentially targeted in $t(6;14)^{+}$ MM (Hanamura *et al.*, 2001) (Hideshima *et al.*, 2004). C-maf transactivates the cyclin D2 promoter and enhances myeloma proliferation (Hurt *et al.*, 2004); these results have prompted the hypothesis that MM is characterized by cyclin D disregulation leading to plasma cell proliferation and chromosomal instability (Bergsagel and Kuehl, 2001) (Hideshima *et al.*, 2004). However, overexpression of cyclin D1 does not initiate chromosomal instability (Spruck *et al.*, 1999), MM plasma cells are poorly proliferative, and MM patients with elevated levels of Cyclin D1 expression demonstrate improved survival (Fonseca *et al.*, 2003a) (Soverini *et al.*, 2003). Moreover, gene expression analysis of 190 primary tumors of 14 different histological types highlights striking differences between the biochemical activities of cyclin D1 and cyclin

D3, genes previously thought to perform similar if not identical functions (Lamb *et* al., 2003). These discrepancies led us to postulate that additional disregulation was occurring at sites of IgH translocations and speculate that centrosomal/spindle pole proteins may be involved.

Centrosomes, the major microtubule organizing center in the cell, are composed of two centrioles and an amorphous cloud of pericentriolar material (PCM) (Kellogg *et al.*, 1994). Centrosomal structure undergoes maturation during cell cycle phases through recruitment of centrosomal proteins, such as γ-tubulin and pericentrin, that increase the microtubule nucleation potential (Kellogg *et al.*, 1994) (Schnackenberg *et al.*, 1998) (Dictenberg *et al.*, 1998). Numerical and/or structural centrosome abnormalities have been reported in a wide range of malignant epithelial tumors, including breast, colon, and pancreatic cancer (Lingle and Salisbury, 1999) (Pihan *et al.*, 1998) (Ghadimi *et al.*, 2000) (Sato *et al.*, 1999), as well as AML (Neben et al., 2003) and MM (Chapter 2); structural (i.e. excess PCM), rather than numerical, centrosomal abnormalities are most highly associated with abnormal mitoses (Lingle and Salisbury, 1999). Centrosomal abnormalities appear to occur early in tumorigenesis as they are identified in pre-invasive carcinomas of the uterine cervix, prostate and female breast (Pihan *et al.*, 2003). Several investigations have demonstrated positive correlation between centrosomal amplification, genetic instability and cancer progression (Pihan *et al.*, 1998) (Lingle *et al.*, 2002). In fact, altered centrosomal structure is associated with abnormal mitoses in breast tumors while overexpression of a key centrosomal structural protein, pericentrin, induces centrosomal defects, alters DNA content and enhances cell growth in soft agar (Lingle

and Salisbury, 1999) (Pihan *et al.*, 2001) (Pihan *et al.*, 2003). Overexpression of other centrosomal proteins, such as TACC and aurora, also induce tumor like features (Gergely *et al.*, 2000) (Meraldi *et al.*, 2002) (Zhou *et al.*, 1998); these features are likely dependent on disruption of the p53-dependent cell cycle checkpoint (Meraldi *et al.*, 2002) (Raff, 2002). In fact, multiple investigations have demonstrated centrosomal amplification resulting from loss of the p53 pathway (Fukasawa *et al.*, 1996) (Carroll *et al.*, 1999). Disruption of the p53 pathway may rescue cells that have undergone aborted division or affect centrosomal replication, which occurs concurrent with DNA replication (Nigg, 2002). Moreover, elongation or disruption of DNA synthesis, as achieved through overexpression of K cyclin, a cyclin D homolog, may cooperate with p53 loss to induce centrosomal amplification, CIN and oncogenesis (Verschuren *et al.*, 2002). Thus, it is attractive to speculate that disregulation of centrosomal proteins, in combination with cell cycle alterations, induce and/or escalate chromosomal instability and cancer progression.

Given the strong positive correlation between centrosomal abnormalities and CIN in a variety of human tumors (Nigg, 2002), it is not surprising that myeloma exhibits centrosomal abnormalities (see Chapter 2). Chapters 2 and 3 highlight a number of interesting additional correlations: 1. patients with elevated RHAMM expression, by qRT-PCR analysis, also contain elevated centrosomal volumes (Chapter 2); 2. patients with elevated RHAMM expression, by gene expression profiling (GEP) analysis, contain elevated levels of genetic instability characterized by hypodiploidy (Chapter 3); 3. the observed frequency of supernumerary centrosomes (mean percentage 21.3 $^{+}$/- 2.91) described herein (Chapter 2) approximates the published frequency of abnormal mitoses

(9.6/33.5, 28.5%) previously characterized by chromosomal analysis of 81 MM patients (Smadja *et al.*, 1998); and 4. MM patients demonstrate differential degrees of centrosomal abnormalities; while no correlation existed between elevated centrosomal abnormalities and patient survival within this small cohort, centrosomal abnormalities approximated levels of chromosomal instability (i.e. low in normal patients, moderate in MGUS patients and higher in MM patients). These ex vivo correlations suggest a relationship between RHAMM expression, centrosomal abnormalities and CIN.

To support a causal relationship between RHAMM expression, centrosomal abnormalities and mitotic integrity, we demonstrated that *in vitro* overexpression, and inhibition of function, of RHAMM affected centrosomal structure, similar to those observed within *ex vivo* MM plasma cells, and chromosomal segregation, inducing G_2/M arrest and multipolar spindle phenotypes (Chapters 1 and 2). Mulitpolar spindle architecture can result in hypodiploidy or tetraploidization, following G_2/M arrest and spindle defects (Chen *et al.*, 2003) (Dekker *et al.*, 2003) (Meraldi *et al.*, 2002). Thus, RHAMM overexpression (and inhibition) can induce centrosomal disregulation, retard G_2/M progression and induce spindle defects with resulting hypodiploid or tetraploid progeny. These results perfectly model IgH translocation-positive MM with chromosomal instability, emphasizing non-hyperdiploid karyotypes, resulting, in spite of impaired cell cycle progression, from overexpression (due to a strong IgH promoter) or underexpression (due to an unbalanced translocation), of a putative target gene product. RHAMM, however, does not map to a recurrent site of IgH translocation; interestingly

however, gene products that are intimately related to RHAMM function do map to IgH translocation partner loci.

At the 2001 annual ASH meeting, we noted that other centrosomal/spindle assembly gene products (i.e. TACC3, NuMA, dynein light intermediate chain 2B) map proximal to recurrent IgH loci (see Figure D-4) (Maxwell *et al.*, 2001); additionally, the motor HSET and pim-1, centrosomal gene products at 6p21.3, and aurora A (20q13.2-13.3) and TPX2 (20q11.2) map to minor IgH sites and are located proximal to postulated MM oncogenes (cyclin D3 and maf-B, respectively). These gene products are intimately associated (often in direct physical contact with regulatory roles) and, like RHAMM, essential for mitotic integrity, transformation and p53 function (Hall *et al.*, 1995) (Maxwell *et al.*, 2003) (Eyers and Maller, 2004) (Meraldi *et al.*, 2004) (Katayama *et al.*, 2004) (Gordon *et al.*, 2001) (Tsai *et al.*, 2003) (Piekorz *et al.*, 2002) (Bhattacharya *et al.*, 2002) (Roh *et al.*, 2003).

While *TACC3* maps 49K telomeric to *FGFR3*, *NuMA* and *DNCL2B* map 2.0 and 0.9 Mb telomeric to *CyclinD1* and *MAF* at 11q13 and 16q23, respectively (Figure D-4). Molecular analysis of 11q13 and 16q23 breakpoints demonstrates translocation specific overexpression of cyclinD1 and MAF despite distances of greater than 300K and 700K from the IgH enhancer (Ronchetti *et al.*, 1999) (Chesi *et al.*, 1998). In fact, some cell lines (U266 and 8226) overexpress *cyclinD1* and *MAF* despite breakpoints telomeric to their genetic loci (Ronchetti *et al.*, 1999) (Chesi *et al.*, 1998). Given the proximity of these gene products to translocation sites, we speculated that slight disruption of these

centrosomal/spindle pole gene products, concurrent with amplification of defined translocation oncogenes (i.e. Cyclin D family members), may affect centrosomal structure, spindle integrity, cell cycle progression and CIN. At ASH 2001, our characterization of extensive centrosomal abnormalities in MM was the first demonstration of these abnormalities in hematological malignancies (Maxwell *et al.*, 2001); Neben *et al.*, 2003 later showed similar centrosomal aberrations within AML patients and postulated, as we had previously in MM, that these abnormalities were related to acquisition of karyotypic abnormalities (Neben *et al.*, 2003). Neben *et al.*, 2004 expanded upon their previous AML observations and demonstrated that, similar to our postulate in MM, centrosomal abnormalities correlated with increased expression of centrosomal/spindle pole proteins (i.e. NuMA1, pericentrin, dynein and γ-tubulin) (Neben *et al.*, 2004). Proteomic analysis of leukemic blasts demonstrated elevated expression of NuMA (Ota *et al.*, 2003) which, like RHAMM in MM, was related to complex karyotype anomalies (Ota *et al.*, 2003). Conditional overexpression of NuMA in mouse myeloid 32D cells resulted in aneuploidy, G_2/M arrest and apoptosis (Ota *et al.*, 2003). Thus, slight augmentation of centrosomal/spindle pole proteins (i.e. RHAMM, NuMA, dynein) can disrupt centrosomal and genetic integrity within hematological malignancies.

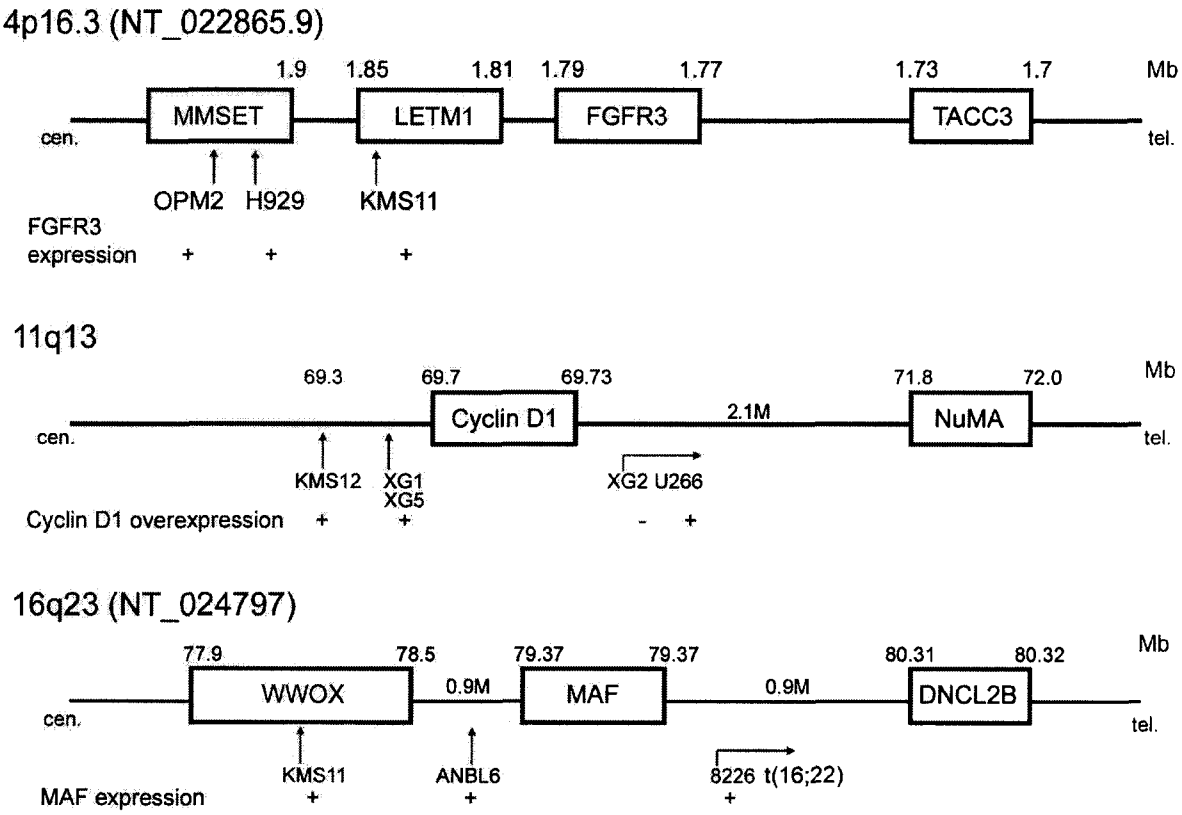

Figure D.4 Centrosomal/ spindle pole proteins map proximal to recurrent IgH translocation sites in multiple myeloma. Breakpoint sites are shown for myeloma cell lines containing defined IgH partner chromosomes. Expression of currently defined oncogene is denoted by + . Chromosomal location, in Mb from NCBI Map viewer, are given for gene products proximal to breakpoints.

While research in the AML field supports a role for centrosomal proteins in oncogenesis, little is known about the role, if any, of these proteins in myeloma. Three of four tested $t(4;14)^{+}$ myeloma cell lines show slight amplification of TACC3 by qRT-PCR (Keats and Pilarski, unpublished observations). However, MM patients do not demonstrate overexpression of TACC3 message at a level that approximates that for FGFR3 or MMSET, and its variants (Keats and Pilarski, unpublished observation). The

nature of these gene products are such that one would not expect dramatic differential overexpression; indeed, loss of expression of these gene products may be as dysfunctional as overexpression. DNCL2B, for example is consistently downregulated in hepatocellular carcinoma (Jiang *et al.*, 2001) and loss of function experiments with RHAMM, TPX2, Aurora A, NuMA, HSET and TACC proteins show dramatic disregulation of chromosomal segregation and mitotic progression (Chapter 1 and 2) (Garrett *et al.*, 2002) (Gruss *et al.*, 2002) (Gordon *et al.*, 2001) (Gergely *et al.*, 2000). Cell cycle regulated expression of these gene products adds to the complexity of the issue as these postulated targets are upregulated during proliferation (Gruss *et al.*, 2002) (Tanaka *et al.*, 2002) (Taimen *et al.*, 2000) (Aitola *et al.*, 2003); thus for a disease like MM, where proliferation is associated with aggressive disease and poor outcome (Zhan *et al.*, 2002), an aggressive translocation-negative MM patient, with elevated proliferation, may express significantly more TACC3 than a less-proliferative $t(4;14)^{+}$ positive patient. Thus, correlating TACC3, or NuMA, expression with t(4;14), or t(11;14), in a heterogeneous patient population may be impractical. Examination of translocation positive cell lines, within homogeneous cell cycle populations, may be the only method to determine if these postulated targets are indeed disregulated by IgH translocations. Alternatively, examination of MM patient cohorts with low proliferation indices (i.e. MM 1-3 but not MM4 as defined by Zhan et al., 2002) for correlation between TACC3, or NuMA, expression with FGFR3, or Cyclin D1, expression may provide insight into the role, if any, of centrosomal spindle assembly factors in myelomagenesis. This analysis takes on a greater significance as gene products that are important prognostic indicators for aggressive MM, by gene expression analysis, are intimately related to G_2/M progression

and spindle assembly (J. Shaughnessy, personal communication). We speculate that recurrent IgH translocations within MM result in the disruption of both cell cycle (cyclin D family) and centrosomal/spindle assembly (NuMA, TACC3, dynein, TPX2, Aurora A) systems, which lead to delayed, and dysfunctional, cell divisions. Deregulated expression of these centrosomal proteins may perturb anti-apoptotic pathways (i.e. p53-regulated and BRCA1 associated) by affecting aurora-A kinase activity (Katayama *et al.*, 2004) (Eyers and Maller, 2004) (Ouchi *et al.*, 2004) (Tsai *et al.*, 2003) (Conte *et al.*, 2003). Cumulatively, elongation of DNA synthesis (Cyclin D family) and disregulation of mitosis (spindle assembly family), with concurrent augmentation of p53 and apoptotic pathways, may be the mechanism through which IgH translocations induce karyotypic instability, with emphasis on hypodiploid and tetraploid progeny, and disease progression in a poorly proliferative cancer.

Conclusions:

The underlying hypothesis of this thesis was that expression of RHAMM, and its isoforms, is functionally related to the generation of aggressive myeloma clones. Previous investigations within the lab had demonstrated differential mobilities of malignant clonal B lineage MM cells as well as the overexpression of RHAMM, and the splice variants $RHAMM^{-exon4}$ and $RHAMM^{-exon13}$, within clonal MM cells (Masellis-Smith *et al.*, 1996) (Crainie *et al.*, 1999). $RHAMM^{-exon13}$ was identified as a relatively minor transcript within myeloma (Crainie *et al.*, 1999), and is absent in colon cancer (Line *et al.*, 2002), while $RHAMM^{-exon4}$ is present at approximately equivalent levels as $RHAMM^{FL}$ in tumor tissues (Crainie *et al.*, 1999) (Line *et al.*, 2002). Here we demonstrate a novel interphase centrosomal localization for RHAMM that is dependent on the COOH terminus BZIP/HA binding domain. During mitosis, we demonstrate that RHAMM complexes with the spindle assembly factors TPX2 and dynein, but not NuMA, and functions in the maintenance of spindle integrity. Loss of function experiments (i.e. antibody microtinjection and RNAi) demonstrate that RHAMM functions in spindle integrity, but possibly not assembly, and G_2/M transition. These observations are consistent with previous experimentation by Mohapatra *et al.*, 1996 and we speculate that RHAMM may regulate the regulator of Aurora A kinase (i.e. TPX2). RHAMM overexpression also disrupts spindle integrity and affects centrosomal structure. The *in vitro* effects of RHAMM overexpression on centrosomal structure model *ex vivo* observations within MM plasma cells. Patients with elevated RHAMM expression, as determined by qRT-PCR, also demonstrate elevated centrosomal volumes. While centrosomal volumes do not appear to be prognostically significantly, within the small cohort examined, RHAMM

expression, as determined by gene expression profiling (GEP) anaylsis, is significantly related to disease outcome and provocatively related to the degree of chromosomal instability. Thus, we demonstrate that RHAMM is vital to mitotic integrity, *in vitro* disruption of RHAMM expression, through inhibition of function or overexpression, augments centrosomal structure and is detrimental to proper chromosomal segregation, and elevated RHAMM expression, as determined by qRT-PCR and GEP analysis, within *ex vivo* MM plasma cells is related to centrosomal abnormalities, elevated chromosomal instability, aggressive MM disease and adverse outcome. These data point to a pivotal role for RHAMM in myelomagenesis.

We further investigated a putative correlation between RHAMM isoform expression and disease outcome. Due to the differential ability of $RHAMM^{FL}$ and $RHAMM^{-exon4}$ to interact with interphase microtubules (Assmann *et al.*, 1999) (Maxwell *et al.*, 2003), we speculated that $RHAMM^{-exon4}$ may be impaired in its ability to crosslink, and stabilize, antiparallel mitotic microtubules with detrimental effects, analogous to loss of function experiments, on mitotic integrity. With FRAP analysis, we demonstrate significantly different mitotic mobilities for $RHAMM^{FL}$ and $RHAMM^{-exon4}$ that are consistent with our hypothesis. *Ex vivo* analysis further demonstrates that $RHAMM^{-exon4}$ expression falls with remission and rises with relapse and, thus, may characterize the malignant MM clone. Indeed, elevated $RHAMM^{-exon4}$ expression, at diagnosis, is a significant independent prognostic indicator within MM. These data further illustrate the significance of RHAMM expression, and isoform balance, in myelomagenesis and suggests that the maintenance/disruption of mitotic stability may be a contributing factor

to this process; however, differential interphase effects of these isoforms, including but not restricted to regulation of cytoskeletal networks, extracellular secretion, and intracellular signaling events, may significantly contribute to this process as well.

In support of a seminal role for RHAMM and other centrosomal proteins in myelomagenesis, we demonstrate a potential relationship between IgH translocations and centrosomal disregulation (whether through the disruption of known centrosomal regulators, and defined MM oncogenes, like the cyclin D1 family or through the concurrent disregulation of additional potentially oncogenic determinants of MM, like TACC3, NuMA, and AurA). Many of these postulated MM determinants have been investigated in AML and found to be significantly related to chromosomal instability (Neben *et al.*, 2004) (Ota *et al.*, 2003); the significance of these gene products is unknown within MM however related gene products, intimately associated with spindle assembly, are very significant prognostic determinants of MM (personal communication J. Shaughnessey, Jr.).

Overall, this thesis outlines a novel biological function, and mechanism of action, for RHAMM that is consistent with previous data, primary and predicted secondary structure, tissue distribution, and recent, unpublished examination of the *Xenopus RHAMM* homologue (Groen *et al.*, 2002) (Groen *et al.*, 2003). Moreover, this thesis outlines a significant correlation between RHAMM expression and myelomagenesis and, while investigating the mechanism of action of RHAMM, highlights a process (i.e. centrosomal structure and chromosomal stability) that is universally desregulated in MM.

This thesis provides insight into the biology of a protein and a mechanism of disease while highlighting potentially novel therapeutic targets (i.e. RHAMM, TPX2, AurA, TACC3) that may be important in multiple chromosomally unstable malignancies, including MM.

References:

Aitola, M., Sadek, C.M., Gustafsson, J.A., and Pelto-Huikko, M. (2003). Aint/Tacc3 is highly expressed in proliferating mouse tissues during development, spermatogenesis, and oogenesis. J Histochem Cytochem *51*, 455-469.

Altschul, S.F., Madden, T.L., Schaffer, A.A., Zhang, J., Zhang, Z., Miller, W., and Lipman, D.J. (1997). Gapped BLAST and PSI-BLAST: a new generation of protein database search programs. Nucleic Acids Res *25*, 3389-3402.

Assmann, V., Jenkinson, D., Marshall, J.F., and Hart, I.R. (1999). The intracellular hyaluronan receptor RHAMM/IHABP interacts with microtubules and actin filaments. J Cell Sci *112 (Pt 22)*, 3943-3954.

Avet-Loiseau, H., Daviet, A., Brigaudeau, C., Callet-Bauchu, E., Terre, C., Lafage-Pochitaloff, M., Desangles, F., Ramond, S., Talmant, P., and Bataille, R. (2001). Cytogenetic, interphase, and multicolor fluorescence in situ hybridization analyses in primary plasma cell leukemia: a study of 40 patients at diagnosis, on behalf of the Intergroupe Francophone du Myelome and the Groupe Francais de Cytogenetique Hematologique. Blood *97*, 822-825.

Avet-Loiseau, H., Li, J.Y., Facon, T., Brigaudeau, C., Morineau, N., Maloisel, F., Rapp, M.J., Talmant, P., Trimoreau, F., Jaccard, A., Harousseau, J.L., and Bataille, R. (1998). High incidence of translocations t(11;14)(q13;q32) and t(4;14)(p16;q32) in patients with plasma cell malignancies. Cancer Res *58*, 5640-5645.

Bairoch, A., Bucher, P., and Hofmann, K. (1997). The PROSITE database, its status in 1997. Nucleic Acids Res *25*, 217-221.

Balczon, R., and West, K. (1991). The identification of mammalian centrosomal antigens using human autoimmune anticentrosome antisera. Cell Motil Cytoskeleton *20*, 121-135.

Bayliss, R., Sardon, T., Vernos, I., and Conti, E. (2003). Structural basis of Aurora-A activation by TPX2 at the mitotic spindle. Mol Cell *12*, 851-862.

Ben-Dor, S., Esterman, N., Rubin, E., and Sharon, N. (2004). Biases and complex patterns in the residues flanking protein N-glycosylation sites. Glycobiology *14*, 95-101.

Berger, B., Wilson, D.B., Wolf, E., Tonchev, T., Milla, M., and Kim, P.S. (1995). Predicting coiled coils by use of pairwise residue correlations. Proc Natl Acad Sci U S A *92*, 8259-8263.

Bergsagel, P.L., and Kuehl, W.M. (2001). Chromosome translocations in multiple myeloma. Oncogene *20*, 5611-5622.

Bershadsky, A., Chausovsky, A., Becker, E., Lyubimova, A., and Geiger, B. (1996). Involvement of microtubules in the control of adhesion-dependent signal transduction. Curr Biol *6*, 1279-1289.

Bhattacharya, N., Wang, Z., Davitt, C., McKenzie, I.F., Xing, P.X., and Magnuson, N.S. (2002). Pim-1 associates with protein complexes necessary for mitosis. Chromosoma *111*, 80-95.

Blagden, S.P., and Glover, D.M. (2003). Polar expeditions--provisioning the centrosome for mitosis. Nat Cell Biol *5*, 505-511.

Boisson, B., and Meinnel, T. (2003). A continuous assay of myristoyl-CoA:protein N-myristoyltransferase for proteomic analysis. Anal Biochem *322*, 116-123.

Boland, C.R., Thibodeau, S.N., Hamilton, S.R., Sidransky, D., Eshleman, J.R., Burt, R.W., Meltzer, S.J., Rodriguez-Bigas, M.A., Fodde, R., Ranzani, G.N., and Srivastava, S. (1998). A National Cancer Institute Workshop on Microsatellite Instability for cancer detection and familial predisposition: development of international criteria for the determination of microsatellite instability in colorectal cancer. Cancer Res *58*, 5248-5257.

Boleti, H., Karsenti, E., and Vernos, I. (1996). Xklp2, a novel Xenopus centrosomal kinesin-like protein required for centrosome separation during mitosis. Cell *84*, 49-59.

Brigati, C., Giacca, M., Noonan, D.M., and Albini, A. (2003). HIV Tat, its TARgets and the control of viral gene expression. FEMS Microbiol Lett *220*, 57-65.

Cao, Q., and Richter, J.D. (2002). Dissolution of the maskin-eIF4E complex by cytoplasmic polyadenylation and poly(A)-binding protein controls cyclin B1 mRNA translation and oocyte maturation. Embo J *21*, 3852-3862.

Cao, K., Nakajima, R., Meyer, H.H., and Zheng, Y. (2003). The AAA-ATPase Cdc48/p97 regulates spindle disassembly at the end of mitosis. Cell *115*, 355-367.

Carroll, P.E., Okuda, M., Horn, H.F., Biddinger, P., Stambrook, P.J., Gleich, L.L., Li, Y.Q., Tarapore, P., and Fukasawa, K. (1999). Centrosome hyperamplification in human cancer: chromosome instability induced by p53 mutation and/or Mdm2 overexpression. Oncogene *18*, 1935-1944.

Chakravarty, A., Howard, L., and Compton, D.A. (2004). A mechanistic model for the organization of microtubule asters by motor and non-motor proteins in a Mammalian mitotic extract. Mol Biol Cell *15*, 2116-2132.

Chang, D.C., Xu, N., and Luo, K.Q. (2003). Degradation of cyclin B is required for the onset of anaphase in Mammalian cells. J Biol Chem *278*, 37865-37873.

Cheeseman, I.M., and Desai, A. (2004). Cell division: AAAtacking the mitotic spindle. Curr Biol *14*, R70-72.

Chen, J.G., Yang, C.P., Cammer, M., and Horwitz, S.B. (2003). Gene expression and mitotic exit induced by microtubule-stabilizing drugs. Cancer Res *63*, 7891-7899.

Chesi, M., Bergsagel, P.L., Brents, L.A., Smith, C.M., Gerhard, D.S., and Kuehl, W.M. (1996). Dysregulation of cyclin D1 by translocation into an IgH gamma switch region in two multiple myeloma cell lines. Blood *88*, 674-681.

Chesi, M., Bergsagel, P.L., Shonukan, O.O., Martelli, M.L., Brents, L.A., Chen, T., Schrock, E., Ried, T., and Kuehl, W.M. (1998). Frequent dysregulation of the c-maf proto-oncogene at 16q23 by translocation to an Ig locus in multiple myeloma. Blood *91*, 4457-4463.

Cho, R.J., Huang, M., Campbell, M.J., Dong, H., Steinmetz, L., Sapinoso, L., Hampton, G., Elledge, S.J., Davis, R.W., and Lockhart, D.J. (2001). Transcriptional regulation and function during the human cell cycle. Nature Genetics *27,* 48-54.

Collis, L., Hall, C., Lange, L., Ziebell, M., Prestwich, R., Turley, E.A. (1998) Rapid hyaluronan uptake is associated with enhanced motility: implications for an intracellular mode of action. FEBS Lett. *440*, 444-9.

Conte, N., Delaval, B., Ginestier, C., Ferrand, A., Isnardon, D., Larroque, C., Prigent, C., Seraphin, B., Jacquemier, J., and Birnbaum, D. (2003). TACC1-chTOG-Aurora A protein complex in breast cancer. Oncogene *22*, 8102-8116.

Crainie, M., Belch, A.R., Mant, M.J., and Pilarski, L.M. (1999). Overexpression of the receptor for hyaluronan-mediated motility (RHAMM) characterizes the malignant clone

in multiple myeloma: identification of three distinct RHAMM variants. Blood *93*, 1684-1696.

David-Pfeuty, T., and Nouvian-Dooghe, Y. (1990). Immunolocalization of the cellular src protein in interphase and mitotic NIH c-src overexpresser cells. J Cell Biol *111*, 3097-3116.

De Smet, C., Martelange, V., Lucas, S., Brasseur, F., Lurquin, C., and Boon, T. (1997). Identification of human testis-specific transcripts and analysis of their expression in tumor cells. Biochem Biophys Res Commun *241*, 653-657.

Dekker, P.B., Kuipers-Dijkshoorn, N., Hogendoorn, P.C., van der Mey, A.G., and Cornelisse, C.J. (2003). G2M arrest, blocked apoptosis, and low growth fraction may explain indolent behavior of head and neck paragangliomas. Hum Pathol *34*, 690-698.

Desai, A., and Mitchison, T.J. (1997). Microtubule polymerization dynamics. Annu Rev Cell Dev Biol *13*, 83-117.

Dictenberg, J.B., Zimmerman, W., Sparks, C.A., Young, A., Vidair, C., Zheng, Y., Carrington, W., Fay, F.S., and Doxsey, S.J. (1998). Pericentrin and gamma-tubulin form a protein complex and are organized into a novel lattice at the centrosome. J Cell Biol *141*, 163-174.

Duval, A., Rolland, S., Compoint, A., Tubacher, E., Iacopetta, B., Thomas, G., and Hamelin, R. (2001). Evolution of instability at coding and non-coding repeat sequences in human MSI-H colorectal cancers. Hum Mol Genet *10*, 513-518.

Elbashir, S.M., Harborth, J., Lendeckel, W., Yalcin, A., Weber, K., and Tuschl, T. (2001). Duplexes of 21-nucleotide RNAs mediate RNA interference in cultured mammalian cells. Nature *411*, 494-498.

Ensoli, B., Buonaguro, L., Barillari, G., Fiorelli, V., Gendelman, R., Morgan, R.A., Wingfield, P., and Gallo, R.C. (1993). Release, uptake, and effects of extracellular human immunodeficiency virus type 1 Tat protein on cell growth and viral transactivation. J Virol *67*, 277-287.

Evans, T., Rosenthal, E.T., Youngblom, J., Distel, D., and Hunt, T. (1983). Cyclin: a protein specified by maternal mRNA in sea urchin eggs that is destroyed at each cleavage division. Cell *33*, 389-396.

Eyers, P.A., and Maller, J.L. (2004). Regulation of Xenopus Aurora A activation by TPX2. J Biol Chem *279*, 9008-9015.

Fonseca, R., Barlogie, B., Bataille, R., Bastard, C., Bergsagel, P.L., Chesi, M., Davies, F.E., Drach, J., Greipp, P.R., Kirsch, I.R., Kuehl, W.M., Hernandez, J.M., Minvielle, S., Pilarski, L.M., Shaughnessy, J.D., Jr., Stewart, A.K., and Avet-Loiseau, H. (2004). Genetics and cytogenetics of multiple myeloma: a workshop report. Cancer Res *64*, 1546-1558.

Fonseca, R., Blood, E., Rue, M., Harrington, D., Oken, M.M., Kyle, R.A., Dewald, G.W., Van Ness, B., Van Wier, S.A., Henderson, K.J., Bailey, R.J., and Greipp, P.R. (2003a). Clinical and biologic implications of recurrent genomic aberrations in myeloma. Blood *101*, 4569-4575.

Fonseca, R., Debes-Marun, C.S., Picken, E.B., Dewald, G.W., Bryant, S.C., Winkler, J.M., Blood, E., Oken, M.M., Santana-Davila, R., Gonzalez-Paz, N., Kyle, R.A., Gertz, M.A., Dispenzieri, A., Lacy, M.Q., and Greipp, P.R. (2003b). The recurrent IgH translocations are highly associated with nonhyperdiploid variant multiple myeloma. Blood *102*, 2562-2567.

Fukasawa, K., Choi, T., Kuriyama, R., Rulong, S., and Vande Woude, G.F. (1996). Abnormal centrosome amplification in the absence of p53. Science *271*, 1744-1747.

Gaglio, T., Saredi, A., Bingham, J.B., Hasbani, M.J., Gill, S.R., Schroer, T.A., and Compton, D.A. (1996). Opposing motor activities are required for the organization of the mammalian mitotic spindle pole. J Cell Biol *135*, 399-414.

Garrett, S., Auer, K., Compton, D.A., and Kapoor, T.M. (2002). hTPX2 is required for normal spindle morphology and centrosome integrity during vertebrate cell division. Curr Biol *12*, 2055-2059.

Gavanescu, I., Vazquez-Abad, D., McCauley, J., Senecal, J.L., and Doxsey, S. (1999). Centrosome proteins: a major class of autoantigens in scleroderma. J Clin Immunol *19*, 166-171.

Gergely, F., Karlsson, C., Still, I., Cowell, J., Kilmartin, J., and Raff, J.W. (2000). The TACC domain identifies a family of centrosomal proteins that can interact with microtubules. Proc Natl Acad Sci U S A *97*, 14352-14357.

Ghadimi, B.M., Sackett, D.L., Difilippantonio, M.J., Schrock, E., Neumann, T., Jauho, A., Auer, G., and Ried, T. (2000). Centrosome amplification and instability occurs exclusively in aneuploid, but not in diploid colorectal cancer cell lines, and correlates with numerical chromosomal aberrations. Genes Chromosomes Cancer *27*, 183-190.

Gordon, M.B., Howard, L., and Compton, D.A. (2001). Chromosome movement in mitosis requires microtubule anchorage at spindle poles. J Cell Biol *152*, 425-434.

Greiner, J., Ringhoffer, M., Taniguchi, M., Li, L., Schmitt, A., Shiku, H., Dohner, H., and Schmitt, M. (2004). mRNA expression of leukemia-associated antigens in patients with

acute myeloid leukemia for the development of specific immunotherapies. Int J Cancer *108*, 704-711.

Greiner, J., Ringhoffer, M., Taniguchi, M., Schmitt, A., Kirchner, D., Krahn, G., Heilmann, V., Gschwend, J., Bergmann, L., Dohner, H., and Schmitt, M. (2002). Receptor for hyaluronan acid-mediated motility (RHAMM) is a new immunogenic leukemia-associated antigen in acute and chronic myeloid leukemia. Exp Hematol *30*, 1029-1035.

Groisman, I., Huang, Y.S., Mendez, R., Cao, Q., Theurkauf, W., and Richter, J.D. (2000). CPEB, maskin, and cyclin B1 mRNA at the mitotic apparatus: implications for local translational control of cell division. Cell *103*, 435-447.

Groisman, I., Jung, M.Y., Sarkissian, M., Cao, Q., and Richter, J.D. (2002). Translational control of the embryonic cell cycle. Cell *109*, 473-483.

Groen, A.C., Coughlin, M.L., Mitchison, T.J., and Ohi, R. (2002). Organization of the spindle pole by the Xenopus laevis human homologue RHAMM. Mol Biol Cell Suppl *13*, Abstract L108.

Groen, A.C., Mitchison, T.J., and Ohi, R. (2003). The role of XMAP150 in spindle morphogenesis. Mol Biol Cell Suppl *14*, Abstract 2399.

Gruss, O.J., Wittmann, M., Yokoyama, H., Pepperkok, R., Kufer, T., Sillje, H., Karsenti, E., Mattaj, I.W., and Vernos, I. (2002). Chromosome-induced microtubule assembly mediated by TPX2 is required for spindle formation in HeLa cells. Nat Cell Biol *4*, 871-879.

Guinn, B.A., Bland, E.A., Lodi, U., Banham, A.H., and Mufti, G.J. (2004). Humoral detection of presentation acute myeloid leukaemia antigens in a testes cDNA library. Proceedings of the American Association of Cancer Research, Abstract 5452.

Hall, C.L., Wang, C., Lange, L.A., and Turley, E.A. (1994). Hyaluronan and the hyaluronan receptor RHAMM promote focal adhesion turnover and transient tyrosine kinase activity. J Cell Biol *126*, 575-588.

Hall, C.L., Yang, B., Yang, X., Zhang, S., Turley, M., Samuel, S., Lange, L.A., Wang, C., Curpen, G.D., Savani, R.C., and et al. (1995). Overexpression of the hyaluronan receptor RHAMM is transforming and is also required for H-ras transformation. Cell *82*, 19-26.

Hanamura, I., Iida, S., Akano, Y., Hayami, Y., Kato, M., Miura, K., Harada, S., Banno, S., Wakita, A., Kiyoi, H., Naoe, T., Shimizu, S., Sonta, S.I., Nitta, M., Taniwaki, M., and Ueda, R. (2001). Ectopic expression of MAFB gene in human myeloma cells carrying (14;20)(q32;q11) chromosomal translocations. Jpn J Cancer Res *92*, 638-644.

Hardwick, C., Hoare, K., Owens, R., Hohn, H.P., Hook, M., Moore, D., Cripps, V., Austen, L., Nance, D.M., and Turley, E.A. (1992). Molecular cloning of a novel hyaluronan receptor that mediates tumor cell motility. J Cell Biol *117*, 1343-1350.

Haren, L., and Merdes, A. (2002). Direct binding of NuMA to tubulin is mediated by a novel sequence motif in the tail domain that bundles and stabilizes microtubules. J Cell Sci *115*, 1815-1824.

Hascall, V.C., Majors, A.K., De La Motte, C.A., Evanko, S.P., Wang, A., Drazba, J.A., Strong, S.A., Wight, T.N. (2004) Intracellular hyaluronan: a new frontier for inflammation? Biochim Biophys Acta *1673*, 3-12.

Hideshima, T., Bergsagel, P.L., Kuehl, W.M., and Anderson, K.C. (2004). Advances in Biology of Multiple Myeloma: Clinical Applications. Blood.

Hirota, T., Kunitoku, N., Sasayama, T., Marumoto, T., Zhang, D., Nitta, M., Hatakeyama, K., and Saya, H. (2003). Aurora-A and an interacting activator, the LIM protein Ajuba, are required for mitotic commitment in human cells. Cell *114*, 585-598.

Ho, P.J., Campbell, L.J., Gibson, J., Brown, R., and Joshua, D. (2002). The biology and cytogenetics of multiple myeloma. Rev Clin Exp Hematol *6*, 276-300.

Hofmann, M., Assmann, V., Fieber, C., Sleeman, J.P., Moll, J., Ponta, H., Hart, I.R., and Herrlich, P. (1998). Problems with RHAMM: a new link between surface adhesion and oncogenesis? Cell *95*, 591-592; author reply 592-593.

Hoshi, M., Ohta, K., Gotoh, Y., Mori, A., Murofushi, H., Sakai, H., and Nishida, E. (1992). Mitogen-activated-protein-kinase-catalyzed phosphorylation of microtubule-associated proteins, microtubule-associated protein 2 and microtubule-associated protein 4, induces an alteration in their function. Eur J Biochem *203*, 43-52.

Hurt, E.M., Wiestner, A., Rosenwald, A., Shaffer, A.L., Campo, E., Grogan, T., Bergsagel, P.L., Kuehl, W.M., and Staudt, L.M. (2004). Overexpression of c-maf is a frequent oncogenic event in multiple myeloma that promotes proliferation and pathological interactions with bone marrow stroma. Cancer Cell *5*, 191-199.

Intini, D., Baldini, L., Fabris, S., Lombardi, L., Ciceri, G., Maiolo, A.T., and Neri, A. (2001). Analysis of FGFR3 gene mutations in multiple myeloma patients with t(4;14). Br J Haematol *114*, 362-364.

Jiang, J., Yu, L., Huang, X., Chen, X., Li, D., Zhang, Y., Tang, L., and Zhao, S. (2001). Identification of two novel human dynein light chain genes, DNLC2A and DNLC2B, and their expression changes in hepatocellular carcinoma tissues from 68 Chinese patients. Gene *281*, 103-113.

Joliot, A., Maizel, A., Rosenberg, D., Trembleau, A., Dupas, S., Volovitch, M., and Prochiantz, A. (1998). Identification of a signal sequence necessary for the unconventional secretion of Engrailed homeoprotein. Curr Biol *8*, 856-863.

Karoui, M., Hofmann-Radvanyi, H., Zimmermann, U., Couvelard, A., Degott, C., Faridoni-Laurens, L., Ahomadegbe, J.C., Gazzeri, S., Brambilla, E., Clerici, T., Charbonnier, P., Tresallet, C., Mitry, E., Penna, C., Rougier, P., Boileau, C., Thiery, J.P., Nordlinger, B., Franc, B., and Radvanyi, F. (2001). No evidence of somatic FGFR3 mutation in various types of carcinoma. Oncogene *20*, 5059-5061.

Karsenti, E., and Vernos, I. (2001). The mitotic spindle: a self-made machine. Science *294*, 543-547.

Katayama, H., Sasai, K., Kawai, H., Yuan, Z.M., Bondaruk, J., Suzuki, F., Fujii, S., Arlinghaus, R.B., Czerniak, B.A., and Sen, S. (2004). Phosphorylation by aurora kinase A induces Mdm2-mediated destabilization and inhibition of p53. Nat Genet *36*, 55-62.

Keats, J.J., Reiman, T., Maxwell, C.A., Taylor, B.J., Larratt, L.M., Mant, M.J., Belch, A.R., and Pilarski, L.M. (2003). In multiple myeloma, t(4;14)(p16;q32) is an adverse prognostic factor irrespective of FGFR3 expression. Blood *101*, 1520-1529.

Kellogg, D.R., Moritz, M., and Alberts, B.M. (1994). The centrosome and cellular organization. Annu Rev Biochem *63*, 639-674.

Khodjakov, A., Cole, R.W., Oakley, B.R., and Rieder, C.L. (2000). Centrosome-independent mitotic spindle formation in vertebrates. Curr Biol *10*, 59-67.

Khodjakov, A., Copenagle, L., Gordon, M.B., Compton, D.A., and Kapoor, T.M. (2003). Minus-end capture of preformed kinetochore fibers contributes to spindle morphogenesis. J Cell Biol *160*, 671-683.

Kilmartin, J.V., and Goh, P.Y. (1996). Spc110p: assembly properties and role in the connection of nuclear microtubules to the yeast spindle pole body. Embo J *15*, 4592-4602.

Knop, M., and Schiebel, E. (1997). Spc98p and Spc97p of the yeast gamma-tubulin complex mediate binding to the spindle pole body via their interaction with Spc110p. Embo J *16*, 6985-6995.

Kornovski, B.S., McCoshen, J., Kredentser, J., and Turley, E. (1994). The regulation of sperm motility by a novel hyaluronan receptor. Fertil Steril *61*, 935-940.

Kuehl, W.M., and Bergsagel, P.L. (2002). Multiple myeloma: evolving genetic events and host interactions. Nat Rev Cancer *2*, 175-187.

Lamb, J., Ramaswamy, S., Ford, H.L., Contreras, B., Martinez, R.V., Kittrell, F.S., Zahnow, C.A., Patterson, N., Golub, T.R., and Ewen, M.E. (2003). A mechanism of cyclin D1 action encoded in the patterns of gene expression in human cancer. Cell *114*, 323-34.

Lee, M.G., and Nurse, P. (1987). Complementation used to clone a human homologue of the fission yeast cell cycle control gene cdc2. Nature *327*, 31-35.

Lee, M.J., Gergely, F., Jeffers, K., Peak-Chew, S.Y., and Raff, J.W. (2001). Msps/XMAP215 interacts with the centrosomal protein D-TACC to regulate microtubule behaviour. Nat Cell Biol *3*, 643-649.

Li, H., Guo, L., Li, J.W., Liu, N., Qi, R., and Liu, J. (2000). Expression of hyaluronan receptors CD44 and RHAMM in stomach cancers: relevance with tumor progression. Int J Oncol *17*, 927-932.

Line, A., Slucka, Z., Stengrevics, A., Silina, K., Li, G., and Rees, R.C. (2002). Characterisation of tumour-associated antigens in colon cancer. Cancer Immunol Immunother *51*, 574-582.

Lingle, W.L., Barrett, S.L., Negron, V.C., D'Assoro, A.B., Boeneman, K., Liu, W., Whitehead, C.M., Reynolds, C., and Salisbury, J.L. (2002). Centrosome amplification drives chromosomal instability in breast tumor development. Proc Natl Acad Sci U S A *99*, 1978-1983.

Lingle, W.L., and Salisbury, J.L. (1999). Altered centrosome structure is associated with abnormal mitoses in human breast tumors. Am J Pathol *155*, 1941-1951.

Liu, X., Yan, S., Zhou, T., Terada, Y., and Erikson, R.L. (2004). The MAP kinase pathway is required for entry into mitosis and cell survival. Oncogene *23*, 763-776.

Lupas, A., Van Dyke, M., and Stock, J. (1991). Predicting coiled coils from protein sequences. Science *252*, 1162-1164.

Lynn, B.D., Li, X., Cattini, P.A., Turley, E.A., and Nagy, J.I. (2001a). Identification of sequence, protein isoforms, and distribution of the hyaluronan-binding protein RHAMM in adult and developing rat brain. J Comp Neurol *439*, 315-330.

Lynn, B.D., Turley, E.A., and Nagy, J.I. (2001b). Subcellular distribution, calmodulin interaction, and mitochondrial association of the hyaluronan-binding protein RHAMM in rat brain. J Neurosci Res *65*, 6-16.

Mack, G.J., Rees, J., Sandblom, O., Balczon, R., Fritzler, M.J., and Rattner, J.B. (1998). Autoantibodies to a group of centrosomal proteins in human autoimmune sera reactive with the centrosome. Arthritis Rheum *41*, 551-558.

Maizel, A., Tassetto, M., Filhol, O., Cochet, C., Prochiantz, A., and Joliot, A. (2002). Engrailed homeoprotein secretion is a regulated process. Development *129*, 3545-3553.

Maller, J.L. (1985). Regulation of amphibian oocyte maturation. Cell Differ *16*, 211-221.

Marumoto, T., Hirota, T., Morisaki, T., Kunitoku, N., Zhang, D., Ichikawa, Y., Sasayama, T., Kuninaka, S., Mimori, T., Tamaki, N., Kimura, M., Okano, Y., and Saya, H. (2002). Roles of aurora-A kinase in mitotic entry and G2 checkpoint in mammalian cells. Genes Cells *7*, 1173-1182.

Masellis-Smith, A., Belch, A.R., Mant, M.J., Turley, E.A., and Pilarski, L.M. (1996). Hyaluronan-dependent motility of B cells and leukemic plasma cells in blood, but not of bone marrow plasma cells, in multiple myeloma: alternate use of receptor for hyaluronan-mediated motility (RHAMM) and CD44. Blood *87*, 1891-1899.

Maton, G., Thibier, C., Castro, A., Lorca, T., Prigent, C., and Jessus, C. (2003). Cdc2-cyclin B triggers H3 kinase activation of Aurora-A in Xenopus oocytes. J Biol Chem *278*, 21439-21449.

Matsumoto, Y., and Maller, J.L. (2002). Calcium, calmodulin, and CaMKII requirement for initiation of centrosome duplication in Xenopus egg extracts. Science *295*, 499-502.

Maurer-Stroh, S., Eisenhaber, B., and Eisenhaber, F. (2002). N-terminal N-myristoylation of proteins: refinement of the sequence motif and its taxon-specific differences. J Mol Biol *317*, 523-540.

Maxwell, C.A., Hendzel, M., Chan, G., Sun, X., Belch, A.R., and Pilarski, L.M. (2001). The RHAMM oncogene may promote chromosomal instability in multiple myeloma. BLOOD *98*, 773-774a.

Maxwell, C.A., Keats, J.J., Crainie, M., Sun, X., Yen, T., Shibuya, E., Hendzel, M., Chan, G., and Pilarski, L.M. (2003). RHAMM is a centrosomal protein that interacts with dynein and maintains spindle pole stability. Mol Biol Cell *14*, 2262-2276.

Mayor, S., and Riezman, H. (2004). Sorting GPI-anchored proteins. Nat Rev Mol Cell Biol *5*, 110-120.

Meraldi, P., Honda, R., and Nigg, E.A. (2002). Aurora-A overexpression reveals tetraploidization as a major route to centrosome amplification in p53-/- cells. Embo J *21*, 483-492.

Meraldi, P., Honda, R., and Nigg, E.A. (2004). Aurora kinases link chromosome segregation and cell division to cancer susceptibility. Curr Opin Genet Dev *14*, 29-36.

Merdes, A., Ramyar, K., Vechio, J.D., and Cleveland, D.W. (1996). A complex of NuMA and cytoplasmic dynein is essential for mitotic spindle assembly. Cell *87*, 447-458.

Mitchison, T., Evans, L., Schulze, E., and Kirschner, M. (1986). Sites of microtubule assembly and disassembly in the mitotic spindle. Cell *45*, 515-527.

Mohapatra, S., Yang, X., Wright, J.A., Turley, E.A., and Greenberg, A.H. (1996). Soluble hyaluronan receptor RHAMM induces mitotic arrest by suppressing Cdc2 and cyclin B1 expression. J Exp Med *183*, 1663-1668.

Neben, K., Giesecke, C., Schweizer, S., Ho, A.D., and Kramer, A. (2003). Centrosome aberrations in acute myeloid leukemia are correlated with cytogenetic risk profile. Blood *101*, 289-291.

Neben, K., Tews, B., Wrobel, G., Hahn, M., Kokocinski, F., Giesecke, C., Krause, U., Ho, A.D., Kramer, A., and Lichter, P. (2004). Gene expression patterns in acute myeloid leukemia correlate with centrosome aberrations and numerical chromosome changes. Oncogene *23*, 2379-2384.

Nickel, W. (2003). The mystery of nonclassical protein secretion. A current view on cargo proteins and potential export routes. Eur J Biochem *270*, 2109-2119.

Nigg, E.A. (2002). Centrosome aberrations: cause or consequence of cancer progression? Nat Rev Cancer *2*, 815-825.

Ookata, K., Hisanaga, S., Bulinski, J.C., Murofushi, H., Aizawa, H., Itoh, T.J., Hotani, H., Okumura, E., Tachibana, K., and Kishimoto, T. (1995). Cyclin B interaction with microtubule-associated protein 4 (MAP4) targets p34cdc2 kinase to microtubules and is a potential regulator of M-phase microtubule dynamics. J Cell Biol *128*, 849-862.

Ota, J., Yamashita, Y., Okawa, K., Kisanuki, H., Fujiwara, S., Ishikawa, M., Lim Choi, Y., Ueno, S., Ohki, R., Koinuma, K., Wada, T., Compton, D., Kadoya, T., and Mano, H. (2003). Proteomic analysis of hematopoietic stem cell-like fractions in leukemic disorders. Oncogene *22*, 5720-5728.

Ouchi, M., Fujiuchi, N., Sasai, K., Katayama, H., Minamishima, Y.A., Ongusaha, P.P., Deng, C., Sen, S., Lee, S.W., and Ouchi, T. (2004). BRCA1 Phosphorylation by Aurora-A in the Regulation of G2 to M Transition. J Biol Chem *279*, 19643-19648.

Patel, R., Holt, M., Philipova, R., Moss, S., Schulman, H., Hidaka, H., and Whitaker, M. (1999). Calcium/calmodulin-dependent phosphorylation and activation of human Cdc25-C at the G2/M phase transition in HeLa cells. J Biol Chem *274*, 7958-7968.

Piekorz, R.P., Hoffmeyer, A., Duntsch, C.D., McKay, C., Nakajima, H., Sexl, V., Snyder, L., Rehg, J., and Ihle, J.N. (2002). The centrosomal protein TACC3 is essential for hematopoietic stem cell function and genetically interfaces with p53-regulated apoptosis. Embo J *21*, 653-664.

Pihan, G.A., Purohit, A., Wallace, J., Knecht, H., Woda, B., Quesenberry, P., and Doxsey, S.J. (1998). Centrosome defects and genetic instability in malignant tumors. Cancer Res *58*, 3974-3985.

Pihan, G.A., Purohit, A., Wallace, J., Malhotra, R., Liotta, L., and Doxsey, S.J. (2001). Centrosome defects can account for cellular and genetic changes that characterize prostate cancer progression. Cancer Res *61*, 2212-2219.

Pihan, G.A., Wallace, J., Zhou, Y., and Doxsey, S.J. (2003). Centrosome abnormalities and chromosome instability occur together in pre-invasive carcinomas. Cancer Res *63*, 1398-1404.

Prudovsky, I., Mandinova, A., Soldi, R., Bagala, C., Graziani, I., Landriscina, M., Tarantini, F., Duarte, M., Bellum, S., Doherty, H., and Maciag, T. (2003). The non-classical export routes: FGF1 and IL-1alpha point the way. J Cell Sci *116*, 4871-4881.

Raff, J.W. (2002). Centrosomes and cancer: lessons from a TACC. Trends Cell Biol *12*, 222-225.

Reszka, A.A., Seger, R., Diltz, C.D., Krebs, E.G., and Fischer, E.H. (1995). Association of mitogen-activated protein kinase with the microtubule cytoskeleton. Proc Natl Acad Sci U S A *92*, 8881-8885.

Roh, M., Gary, B., Song, C., Said-Al-Naief, N., Tousson, A., Kraft, A., Eltoum, I.E., and Abdulkadir, S.A. (2003). Overexpression of the oncogenic kinase Pim-1 leads to genomic instability. Cancer Res *63*, 8079-8084.

Ronchetti, D., Finelli, P., Richelda, R., Baldini, L., Rocchi, M., Viggiano, L., Cuneo, A., Bogni, S., Fabris, S., Lombardi, L., Maiolo, A.T., and Neri, A. (1999). Molecular analysis of 11q13 breakpoints in multiple myeloma. Blood *93*, 1330-1337.

Sadek, C.M., Pelto-Huikko, M., Tujague, M., Steffensen, K.R., Wennerholm, M., and Gustafsson, J.A. (2003). TACC3 expression is tightly regulated during early differentiation. Gene Expr Patterns *3*, 203-211.

Sahin, U., Tureci, O., and Pfreundschuh, M. (1997). Serological identification of human tumor antigens. Curr Opin Immunol *9*, 709-716.

Salisbury, J.L. (2003). Centrosomes: coiled-coils organize the cell center. Curr Biol *13*, R88-90.

Salisbury, J.L. (2004). Centrosomes: Sfi1p and centrin unravel a structural riddle. Curr Biol *14*, R27-29.

Santella, L. (1998). The role of calcium in the cell cycle: facts and hypotheses. Biochem Biophys Res Commun *244*, 317-324.

Santra, M., Zhan, F., Tian, E., Barlogie, B., and Shaughnessy, J., Jr. (2003). A subset of multiple myeloma harboring the t(4;14)(p16;q32) translocation lacks FGFR3 expression but maintains an IGH/MMSET fusion transcript. Blood *101*, 2374-2376.

Sato, N., Mizumoto, K., Nakamura, M., Nakamura, K., Kusumoto, M., Niiyama, H., Ogawa, T., and Tanaka, M. (1999). Centrosome abnormalities in pancreatic ductal carcinoma. Clin Cancer Res *5*, 963-970.

Savani, R.C., Wang, C., Yang, B., Zhang, S., Kinsella, M.G., Wight, T.N., Stern, R., Nance, D.M., and Turley, E.A. (1995). Migration of bovine aortic smooth muscle cells after wounding injury. The role of hyaluronan and RHAMM. J Clin Invest *95*, 1158-1168.

Sawyer, J.R., Waldron, J.A., Jagannath, S., and Barlogie, B. (1995). Cytogenetic findings in 200 patients with multiple myeloma. Cancer Genet Cytogenet *82*, 41-49.

Scanlan, M.J., Simpson, A.J., and Old, L.J. (2004). The cancer/testis genes: review, standardization, and commentary. Cancer Immun *4*, 1.

Schnackenberg, B.J., Khodjakov, A., Rieder, C.L., and Palazzo, R.E. (1998). The disassembly and reassembly of functional centrosomes in vitro. Proc Natl Acad Sci U S A *95*, 9295-9300.

Shaughnessy, J., Jr., Gabrea, A., Qi, Y., Brents, L., Zhan, F., Tian, E., Sawyer, J., Barlogie, B., Bergsagel, P.L., and Kuehl, M. (2001). Cyclin D3 at 6p21 is dysregulated by recurrent chromosomal translocations to immunoglobulin loci in multiple myeloma. Blood *98*, 217-223.

Simanis, V. (2003). Events at the end of mitosis in the budding and fission yeasts. J Cell Sci *116*, 4263-4275.

Smadja, N.V., Bastard, C., Brigaudeau, C., Leroux, D., and Fruchart, C. (2001). Hypodiploidy is a major prognostic factor in multiple myeloma. Blood *98*, 2229-2238.

Smadja, N.V., Fruchart, C., Isnard, F., Louvet, C., Dutel, J.L., Cheron, N., Grange, M.J., Monconduit, M., and Bastard, C. (1998). Chromosomal analysis in multiple myeloma: cytogenetic evidence of two different diseases. Leukemia *12*, 960-969.

Soverini, S., Cavo, M., Cellini, C., Terragna, C., Zamagni, E., Ruggeri, D., Testoni, N., Tosi, P., De Vivo, A., Amabile, M., Grafone, T., Ottaviani, E., Giannini, B., Cangini, D., Bonifazi, F., Neri, A., Fabris, S., Tura, S., Baccarani, M., and Martinelli, G. (2003). Cyclin D1 overexpression is a favorable prognostic variable for newly diagnosed multiple myeloma patients treated with high-dose chemotherapy and single or double autologous transplantation. Blood *102*, 1588-1594.

Spruck, C.H., Won, K.A., and Reed, S.I. (1999). Deregulated cyclin E induces chromosome instability. Nature *401*, 297-300.

Steadman, B.T., Schmidt, P.H., Shanks, R.A., Lapierre, L.A., and Goldenring, J.R. (2002). Transforming acidic coiled-coil-containing protein 4 interacts with centrosomal AKAP350 and the mitotic spindle apparatus. J Biol Chem *277*, 30165-30176.

Stenoien, D.L., Sen, S., Mancini, M.A., and Brinkley, B.R. (2003). Dynamic association of a tumor amplified kinase, Aurora-A, with the centrosome and mitotic spindle. Cell Motil Cytoskeleton *55*, 134-146.

Still, I.H., Vettaikkorumakankauv, A.K., DiMatteo, A., and Liang, P. (2004). Structure-function evolution of the Transforming acidic coiled coil genes revealed by analysis of phylogenetically diverse organisms. BMC Evol Biol *4*, 16.

Still, I.H., Vince, P., and Cowell, J.K. (1999). The third member of the transforming acidic coiled coil-containing gene family, TACC3, maps in 4p16, close to translocation breakpoints in multiple myeloma, and is upregulated in various cancer cell lines. Genomics *58*, 165-170.

Stirling, D.A., Rayner, T.F., Prescott, A.R., and Stark, M.J. (1996). Mutations which block the binding of calmodulin to Spc110p cause multiple mitotic defects. J Cell Sci *109 (Pt 6)*, 1297-1310.

Sundberg, H.A., Goetsch, L., Byers, B., and Davis, T.N. (1996). Role of calmodulin and Spc110p interaction in the proper assembly of spindle pole body compenents. J Cell Biol *133*, 111-124.

Taimen, P., Viljamaa, M., and Kallajoki, M. (2000). Preferential expression of NuMA in the nuclei of proliferating cells. Exp Cell Res *256*, 140-149.

Takahashi, M., Yamagiwa, A., Nishimura, T., Mukai, H., and Ono, Y. (2002). Centrosomal proteins CG-NAP and kendrin provide microtubule nucleation sites by anchoring gamma-tubulin ring complex. Mol Biol Cell *13*, 3235-3245.

Tanaka, M., Ueda, A., Kanamori, H., Ideguchi, H., Yang, J., Kitajima, S., and Ishigatsubo, Y. (2002). Cell-cycle-dependent regulation of human aurora A transcription is mediated by periodic repression of E4TF1. J Biol Chem *277*, 10719-10726.

Theis-Febvre, N., Filhol, O., Froment, C., Cazales, M., Cochet, C., Monsarrat, B., Ducommun, B., and Baldin, V. (2003). Protein kinase CK2 regulates CDC25B phosphatase activity. Oncogene *22*, 220-232.

Toole, B.P. (2004) Hyaluronan: from extracellular glue to pericellular cue. Nat Rev Cancer *4*, 528-39.

Tsai, M.Y., Wiese, C., Cao, K., Martin, O., Donovan, P., Ruderman, J., Prigent, C., and Zheng, Y. (2003). A Ran signalling pathway mediated by the mitotic kinase Aurora A in spindle assembly. Nat Cell Biol *5*, 242-248.

Turley, E.A., Belch, A.J., Poppema, S., and Pilarski, L.M. (1993). Expression and function of a receptor for hyaluronan-mediated motility on normal and malignant B lymphocytes. Blood *81*, 446-453.

Turley, E.A., and Harrison. (1999). RHAMM, a member of the hyaladherins. In: Science of Hyaluronan Today, eds. V.C. Hascall and M. Yanagishita: http://www.glycoforum.gr.jp/science/hyaluronan/HA11/HA11E.html.

Turley, E.A., Hossain, M.Z., Sorokan, T., Jordan, L.M., and Nagy, J.I. (1994). Astrocyte and microglial motility in vitro is functionally dependent on the hyaluronan receptor RHAMM. Glia *12*, 68-80.

Turley, E.A., Noble, P.W., and Bourguignon, L.Y. (2002). Signaling properties of hyaluronan receptors. J Biol Chem *277*, 4589-4592.

Verlhac, M.H., de Pennart, H., Maro, B., Cobb, M.H., and Clarke, H.J. (1993). MAP kinase becomes stably activated at metaphase and is associated with microtubule-organizing centers during meiotic maturation of mouse oocytes. Dev Biol *158*, 330-340.

Verschuren, E.W., Klefstrom, J., Evan, G.I., and Jones, N. (2002). The oncogenic potential of Kaposi's sarcoma-associated herpesvirus cyclin is exposed by p53 loss in vitro and in vivo. Cancer Cell *2*, 229-241.

Wang, C., Thor, A.D., Moore, D.H., 2nd, Zhao, Y., Kerschmann, R., Stern, R., Watson, P.H., and Turley, E.A. (1998). The overexpression of RHAMM, a hyaluronan-binding protein that regulates ras signaling, correlates with overexpression of mitogen-activated protein kinase and is a significant parameter in breast cancer progression. Clin Cancer Res *4*, 567-576.

Weiser, T.S., Guo, Z.S., Ohnmacht, G.A., Parkhurst, M.L., Tong-On, P., Marincola, F.M., Fischette, M.R., Yu, X., Chen, G.A., Hong, J.A., Stewart, J.H., Nguyen, D.M.,

Rosenberg, S.A., and Schrump, D.S. (2001). Sequential 5-Aza-2 deoxycytidine-depsipeptide FR901228 treatment induces apoptosis preferentially in cancer cells and facilitates their recognition by cytolytic T lymphocytes specific for NY-ESO-1. J Immunother *24*, 151-161.

Whitaker, M. (1996). Control of meiotic arrest. Rev Reprod *1*, 127-135.

Yamashita, Y.M., Jones, D.L., and Fuller, M.T. (2003). Orientation of asymmetric stem cell division by the APC tumor suppressor and centrosome. Science *301*, 1547-1550.

Zaman, A., and Savani, R.C. (2003). A 70kDa RHAMM is GPI-modified and associates with caveolins in lipid rafts. Molecular Biology of the Cell Suppl *13*, B334.

Zhan, F., Hardin, J., Kordsmeier, B., Bumm, K., Zheng, M., Tian, E., Sanderson, R., Yang, Y., Wilson, C., Zangari, M., Anaissie, E., Morris, C., Muwalla, F., van Rhee, F., Fassas, A., Crowley, J., Tricot, G., Barlogie, B., and Shaughnessy, J., Jr. (2002). Global gene expression profiling of multiple myeloma, monoclonal gammopathy of undetermined significance, and normal bone marrow plasma cells. Blood *99*, 1745-1757.

Zhang, S., Chang, M.C., Zylka, D., Turley, S., Harrison, R., and Turley, E.A. (1998). The hyaluronan receptor RHAMM regulates extracellular-regulated kinase. J Biol Chem *273*, 11342-11348.

Zhou, H., Kuang, J., Zhong, L., Kuo, W.L., Gray, J.W., Sahin, A., Brinkley, B.R., and Sen, S. (1998). Tumour amplified kinase STK15/BTAK induces centrosome amplification, aneuploidy and transformation. Nat Genet *20*, 189-193.